Chirag Joshi

Experimental Investigations of Adsorption Chiller Cycle Using Stratified Thermal Storage for Heat Recovery

Karlsruhe 2016

Experimental Investigations of Adsorption Chiller Cycle Using Stratified Thermal Storage for Heat Recovery

Zur Erlangung des akademischen Grades
Doktor der Ingenieurwissenschaften
der Fakultät für Maschinenbau
Karlsruher Institut für Technologie (KIT)

genehmigte
Dissertation
von
M.Sc. Chirag Joshi
aus Pune, Indien

Tag der mündlichen Prüfung: 28. Januar 2016
Hauptreferent: Prof. Dr.-Ing. Martin Gabi
Korreferent: Prof. Dr. rer. nat. Hans-Martin Henning
Korreferent: Dr. rer. nat. Ferdinand Schmidt

Acknowledgement

The work presented here was developed during my occupation as scientific researcher at the Institute of Fluid Machinery of Karlsruhe Institute of Technology (KIT).
I would like to thank Prof. Dr.-Ing. Martin Gabi for giving me this great opportunity and for taking over the role of the main Ph.D supervisor. I would also like to thank Prof. Dr. rer. nat. Hans-Martin Henning for becoming the second supervisor on short notice and giving me valuable inputs in the thesis.
I would like to express my gratitude towards Dr. rer. nat. Ferdinand Schmidt for the technical discussions and helpful recommendations which led to improve the quality of work.
I take this opportunity to thank all my wonderful colleagues who have maintained a joyful work atmosphere which was essential during rather tough phases of the work. I hereby thank the students who have also contributed to successful completion of this thesis.
My family and friends have been very supportive and motivating which has helped me to achieve my goal. A very special thanks goes to my loving wife Gauri who has always stood behind me through thick and thin, especially during the writing phase of the thesis.

Karlsruhe, January 2016 *Chirag Joshi*

Nomenclature

Latin symbols

a	[m]	Distance between the camera and the background
A_c	[m^2]	Internal cross sectional area of the tank
A_i	[m^2]	Surface area of different zones of the tank
A_{ends}	[m^2]	Surface are of the tank end zones
$A_{surface}$	[m^2]	Surface area of the tank per tank zone
A_{top}	[m^2]	Cross sectional area of the tank with insulation
A_{total}	[m^2]	Total surface area of the tank
b	[m]	Distance between the camera and the density field
COP		Coefficient of performance
COP_{cool}		Coefficient of performance for cooling
COP_{cool}^{ideal},COP_{cool}^{Carnot}		Ideal coefficient of performance for cooling
COP_{cool}^{real}		Real coefficient of performance for cooling
COP_{heat}^{ideal},COP_{heat}^{Carnot}		Ideal coefficient of performance for heating
COP_{heat}^{real}		Real coefficient of performance for heating
$COP_{cool}^{stratisorp}$		Cooling COP for stratisorp cycle
$COP_{heat}^{stratisorp}$		Heating COP for stratisorp cycle
COP_{cool}^{max}		Maximum cooling COP available for stratisorp cycle
c_p	[J/kgK]	Specific heat at constant pressure
D	[m]	Diameter of the tube
Fr		Froude number
Fr_m		Modified Froude number
g	[m/s^2]	Acceleration due to gravity
$G(\lambda)$		Gladstone dale constant
H_{min}	[m]	Position of the first sensor
H_{max}	[m]	Position of the last sensor
l_r	[m]	Characteristic Length
L	[m]	Length of the tube
$\dot{m}_{ads}$,$\dot{m}_{ad}$	[kg/s]	Mass flow rate of adsorber
$\dot{m}_c$	[kg/s]	Mass flow rate of cooling module flowing through the tank
$\dot{m}_{cond}$	[kg/s]	Mass flow rate of condenser
$\dot{m}_{ev}$	[kg/s]	Mass flow rate of evaporator
$\dot{m}_h$	[kg/s]	Mass flow rate of heating module
m_{tank}	[kg]	Mass of the water contained in the tank
m_{zone}	[kg]	Mass of water in each zone
n,n_0		Refractive index
N		Total number segments between the temperature sensors
N_{cycles}		Number of cycles
p^{ratio}		Thermal conductivity multiplier
Pr		Prandtl number

Pe		Peclet number
P_c	[mbar]	Condenser pressure
P_e,$P_{evaporator}$	[mbar]	Evaporator pressure
$\dot{Q}_{ads}$	[W]	Adsorber power during adsorption half cycle
$\dot{Q}_{des}$	[W]	Adsorber power during desorption half cycle
$\dot{Q}_c$	[W]	Cooler power
$\dot{Q}_h$	[W]	Heater power
$\dot{Q}_{ev}$	[W]	Evaporator power
$\dot{Q}_{cond}$	[W]	Condenser power
$\dot{Q}_{cooling}$	[W]	Cooling power
$\dot{Q}_{heating}$	[W]	Heating power
Q_{ads},$Q_{adsorber}$,$Q_{adsorption}$	[J]	Heat of adsorption
Q_{des},$Q_{desorption}$	[J]	Heat supplied to adsorber during desorption
Q_{cooler} Q_c	[J]	Heat rejected in the cooling module from the tank
Q_{cond}	[J]	Heat rejected by the condenser in the cooling module
Q_{ev},$Q_{evaporator}$	[J]	Heat absorbed in the evaporator
Q_h,Q_{heater}	[J]	Heat supplied by the heating module
Q_C,Q_A	[J]	Heat rejected to the medium temperature heat sink
Q_H	[J]	Heat supplied by the high temperature heat source
Q_L,Q_e	[J]	Heat supplied by the low temperature heat source
Q_{cs}	[J]	Heat supplied by the medium temperature heat source
Q_{tank}	[J]	Total energy contained in the tank
$Q_{tank_{end}}$	[J]	Energy contained in the tank at the end of the cycle
$Q_{tank_{start}}$	[J]	Energy contained in the tank at the start of the cycle
ΔQ_{tank}	[J]	Difference in $Q_{tank_{start}}$ and $Q_{tank_{end}}$
Q_{bottom}	[J]	Energy contained in the bottom zone of the tank
Q_{top}	[J]	Energy contained in the top zone of the tank
$Q_{loss_{6hr}}$	[J]	Energy lost to the surroundings from each zone in 6 hours
$Q_{loss_{total}}$	[J]	Total energy lost to the surroundings during the cool down test
Ri		Richardson number
Ri_{crit}		Critical Richardson number
$R_1 \cdots R_6$		Stratification rings from 1 to 6
$\dot{S}_{adsorber,in}$	[W/K]	Rate of change of entropy of adsorber flow entering the tank
$\dot{S}_{adsorber,out}$	[W/K]	Rate of change of entropy of adsorber flow leaving the tank
$\dot{S}_{cooler,in}$	[W/K]	Rate of change of entropy of cooler flow entering the tank

$\dot{S}_{cooler,out}$	[W/K]	Rate of change of entropy of cooler flow leaving the tank
$\dot{S}_{heater,in}$	[W/K]	Rate of change of entropy of heater flow entering the tank
$s_{heater,in}$	[J/kgK]	Specific entropy of the heater flow entering the tank
$s_{heater,out}$	[J/kgK]	Specific entropy of the heater flow leaving the tank
$\dot{S}_{heater,out}$	[W/K]	Rate of change of entropy of heater flow leaving the tank
$\dot{S}_{hl}$	[W/K]	Rate of change of entropy due to heat loss from the tank
$\dot{S}_{irr,int}$	[W/K]	Rate of internal entropy generation
$\dot{S}_{tank}$	[W/K]	Rate of change of entropy in the tank
ΔT_{ad}	[K]	Temperature spread across the adsorption chiller
$\overline{T_{amb_{6hr}}}$	[K]	Average ambient temperature over 6 hours
$T_{amb_{initial}}$	[K]	Initial ambient temperature
T_A,T_C,T_c	[K]	Medium temperature
T_H,T_h	[K]	High temperature
T_L,T_e,T_l	[K]	Low temperature
$T_{ad,i}$,$T_{ad,o}$	[K]	Temperature of the supply and return flow from adsorption chiller
$T_{c,i}$,$T_{c,o}$	[K]	Temperature of the supply and return flow from cooling module
$T_{ev,i}$,$T_{ev,o}$	[K]	Temperature of the supply and return flow from evaporator
$T_{h,i}$,$T_{h,o}$	[K]	Temperature of the supply and return flow from heating module
ΔT_c,ΔT_h	[K]	Temperature spread across the cooling and heating module
$TH_1 \cdots TH_9$	[K]	Temperature recorded by the horizontal lance
t_{end}	[s]	Duration of the complete cycle
$t_{halfcycle}$	[s]	Duration of the half cycle
T_{inlet}	[K]	Temperature of the inlet flow to the plexiglas tank
$T_{R_1} \cdots T_{R_6}$	[K]	Temperature recorded by sensors inside the rings
$T_{setpoint}$	[K]	Temperature setpoint
t_{total}	[s]	Duration of the cool down test
$\overline{T_{tank}}$	[K]	Temperature of water in the plexiglas tank
$\overline{T_{tank_{init}}}$	[K]	Average tank temperature at the start of the cool down test
$\overline{T_{tank_{final}}}$	[K]	Average tank temperature at the end of the cool down test
T_{zone}	[K]	Temperature of different tank zones
$\Delta T_{zone_{6hr}}$	[K]	Temperature change of the tank zone after 6 hours
$T_1 \cdots T_{15}$	[K]	Tank temperature recorded by sensors from the bottom to the top of the tank

u_r	[m/s]	Velocity of flow
U_{tank}	[W/m^2°C]	Overall heat transfer coefficient based on real time measurement method
$U_{tank_{avg}}$	[W/m^2°C]	Area weighted average overall heat transfer coefficient of the tank
$U_{tank_{LMTD}}$	[W/m^2°C]	Overall heat transfer coefficient based on LMTD method
$U_{Z_1} \cdots U_{Z_{15}}$	[W/m^2°C]	Overall heat transfer coefficient of the tank zones
$\dot{V}$	[lph]	Flow rate through the plexiglas tank
$\dot{V}_{ad}$	[lph]	Adsorber flow rate
$\dot{V}_{ad_{adsorption}}$	[lph]	Adsorber flow rate during adsorption half cycle
$\dot{V}_{ad_{desorption}}$	[lph]	Adsorber flow rate during desorption half cycle
$\dot{V}_c$	[lph]	Cooling module rate circulating through the tank
$\dot{V}_{c_{tot}}$	[lph]	Total flow rate of cooling module
$\dot{V}_{cond}$	[lph]	Condenser flow rate
$\dot{V}_{evap}$	[lph]	Evaporator flow rate
$\dot{V}_h$	[lph]	Heating module flow rate
V_1,V_2		3-Way valves
W	[W]	Work done
Δx	[mm]	Pixel displacement in x direction
Δy	[mm]	Pixel displacement in y direction
z	[m]	Vertical distance between two adjacent sensors mounted in the tank
Z_D	[m]	Distance of the density field from background
ΔZ_D	[m]	Width the density field
$Z_1 \cdots Z_5$		Tank zones between the stratification rings

Greek symbols

β	[1/K]	coefficient of thermal expansion
η		Carnot efficiency
ρ	[kg/m^3]	density
ε	[°]	angle of deviation
ϕ		diameter

Miscellaneous

BOS	Background Oriented Schlieren
CHP	Combined Heat and Power
CCHP	Combined Cooling, Heating and Power
LIF	Laser Induced Fluorescence
PIV	Particle Image Velocimetry
TES	Thermal Energy Storage

Contents

Abstract

The heat driven chillers offer a promising option in light of the world's global warming problem. The adsorption chiller based on a silica gel-water pair are suited for heat sources like waste heat due to a lower regeneration temperature required. However, the adsorption chillers do not offer a high COP of cooling as compared to the absorption chillers or the air conditioners. Improvement in the adsorption chiller's cooling COP has been a topic of research for many years. This thesis is aimed at the experimental investigations of a silica gel-water adsorption module used for a commercial adsorption chiller based on a novel heat recovery system (stratisorp) by the use of a stratified thermal storage tank. According to the stratisorp concept of heat recovery, the heat of adsorption released during the adsorption half cycle is stored in a stratified thermal storage tank for later use in the desorption half cycle thereby achieving internal heat recovery. The adsorber module is cooled and heated by extracting water from the stratified thermal storage tank. The mixing taking place in the tank during the extraction and insertion of the fluid adversely affects the performance of the adsorption chiller cycle. In this work, a stratification system is constructed which is aimed at introducing the water in the tank with minimal mixing in a rotationally symmetric fashion. The qualitative assessment of the stratification system is carried out using a flow visualisation technique (Background Oriented Schlieren). An experimental set-up consisting of the stratification system and different components of the adsorption chiller hydraulic circuit was constructed. The performance of the stratisorp system was assessed through various experiments. The major factors which affect the COP_{cool} of the cycle were identified and based on the initial experiments further control strategies were proposed. The stratisorp cycle was operated using the new control strategies and the improvement in the COP_{cool} of the stratisorp cycle was demonstrated.

Chapter 1

Introduction

The issue of global warming and protection of the ozone layer has been intensively addressed in the last few decades and stringent regulations on the use of chlorofluorocarbons as refrigerants have been implemented since the Montreal protocol in 1989. As per these regulations the conventional vapour compression systems are operated by using hydrofluorocarbons as refrigerants. However, use of these refrigerants is also restricted due to limitation of the emission of some greenhouse gases. The mechanical moving parts (e.g. compressor) are prone to wear with time and hence regular maintenance becomes essential. As a consequence of these facts the thermally driven heat pumps have gained popularity in the recent years. Moreover, the environmental impact of these heat pumps is far less than the conventional electrically driven heat pumps [18]. In countries like Germany where the energy utilised for heating applications by the industrial and domestic consumers is significant (ca. 40% and ca. 60% respectively [4]), the choice of thermally driven heat pumps for heating applications in the light of environmental protection becomes attractive. Thermally driven heat pumps also have the potential to improve primary energy efficiency in air conditioning applications in countries like the USA. Around 87% of U.S. households are now equipped with air conditioners for cooling application. There has been a steady rise in air conditioned homes in all regions in the united states [3]. The thermally driven sorption heat pumps (absorption and adsorption) have gained popularity not only due to their better primary energy efficiency but also due to other advantages such as a lack of moving parts, lack of noise and vibrations and less maintenance to name a few.

The adsorption heat pumps, for heating and cooling applications, can be operated using a low temperature driving energy e.g. waste heat. The adsorption heat pumps not only recover the heat which is rejected to the environment but also offer a cost effective operational system. Other sustainable heat sources like solar and geothermal energies can also be utilised. Even though the adsorption heat pump is operated using these heat sources, a small amount of input energy is required to drive the cycle (e.g. auxiliary pumps). However, less frequently, the adsorption heat pumps have to be evacuated to remove the inert gases which leaked into the vacuum chamber. This adds to the maintenance cost. The adsorption heat pumps incorporate adsorbent-adsorbate pairs like zeolite-water, active carbon-methanol, silica gel-water and carbon-ammonia. Silica gel can regenerate at lower temperatures, achievable with a simple flat plate or evacuated tube collector and waste heat. Since water is used as a refrigerant with silica gel, this pair is unable to produce cooling below 0 °C. Activated carbon-methanol

can be operated with a low temperature heat source and can be used for refrigeration below 0 °C. However, latent heat of vaporisation of methanol is only half of that of water [14]. Water is a very attractive refrigerant as it is non toxic and with theoretically no environmental impact. It is also available in abundance. One of the main disadvantages of adsorption technology as compared to the conventional vapour compression system is lower coefficients of performance (COP) values. Many research works have been focussed at improving the COP of the adsorption heat pumps in order to make this technology competitive and make it technically and economically an alternative to the conventional system.

The focus of this work is exclusively on experimental investigation of an adsorption chiller operated using silica gel-water pair for cooling applications. In this work, experimental proof of the concept of internal heat recovery for improving the COP of adsorption chiller using a stratified thermal storage is presented. This system concept has been termed as "stratisorp" and was originally proposed by Schmidt *et al.* [51]. At the research group "Energy and Building Technology" dedicated research has been carried out based on the stratisorp concept as a part of which a detailed simulation study was carried out [53]. The simulation study was based on a zeolite-water pair and mainly focussed on improving the COP_{heat} of the cycle. An experimental follow up project based on the outcomes of the simulation work was undertaken with industrial partner SorTech AG and academic partner University of Stuttgart. A silica gel module manufactured by SorTech AG for the adsorption chiller eCOO 2.0 was used for this work. The main aim of the experimental study was to investigate the thermodynamic cycle based on the stratisorp concept and the assessment of the operating parameters which efficiently utilise the potential of this system concept. The adsorber chiller is cooled during the adsorption half cycle by extracting cooler water from continuously decreasing heights of a thermally stratified storage tank. The action is reversed during the desorption half cycle. The heat of adsorption released during the adsorption half cycle is stored in the tank which is later used in the desorption half cycle. This recovers a major part of the heat of adsorption. The energy expended in the heater for driving the cycle is hence reduced. Thus the stratified storage tank plays a very vital role in the performance improvement. A very well stratified tank makes sure that the adsorber is cooled and heated with small driving temperatures and thereby decreases the entropy generation in the adsorber. The stratification system with which the insertion and extraction from the tank is carried out should not cause major perturbations in the tank. The mixing in the tank is primarily caused by momentum of flow entering the tank. Additionally it was essential that the flow entered into the tank or left the tank with rotational symmetry i.e. simultaneously along the inside perimeter of the tank. This condition was necessary for numerical modelling. Such rotational symmetry reduces the model to a 2-D axisymmetrical model that is computationally less costly. Hence designing of inlet distributors that fulfil this requirement is a crucial part of this work. Before these inlet distributors were mounted into the tank to execute the heat pump cycles based on the stratisorp system concept, it was vital to check if the inlet distributors fulfilled their function. This is possible using one of the non invasive flow visualisation techniques. In this work, the Background Oriented Schlieren (common short form "BOS") method which is generally used in the field of aerodynamics, is adapted to be used for flow visualisation. The tank that is thermally stratified due to different densities of warm and cold water, has a significant density gradient. The density gradient for a very well stratified tank is predominantly in the vertical direction rather than in the horizontal direction. The presence of such a density

gradient field makes the BOS method a suitable tool for qualitative assessment of the inlet flow distributors. After carrying out preliminary investigations with the BOS method on a small scaled tank, the method was implemented on a full scaled tank with windows on opposite sides along with the inlet flow diffusers (called "stratification rings" in this work). The experimental set-up consisting of a closed stratification tank with the stratification rings mounted at different heights of the tank, the silica gel-water adsorption module, a high temperature energy source (heating module), a recooler for rejecting heat at medium temperature level (cooling module) and a low temperature energy source (emulator) was built. The modules and the emulator were available through the cooperation with the academic partners. The stratisorp system concept was experimentally investigated where different operating points based on the variations in supply temperature and medium temperature were tested and the COP_{cool} and cooling power was estimated. In this thesis, the operating point with cycle conditions 72/27/18 °C is analysed in depth. One of the important goals of this work was to understand various effects occurring during the stratisorp cycle and to identify different operational modes which demonstrate the ways in which the basic stratisorp cycle can further be improved.

Chapter 2 provides the basics of the adsorption chiller technology. The different methods of heat recovery found in literature are also discussed in this chapter. The background to the stratisorp system concept is also discussed here. Moreover, the significance of the stratified thermal storage tank with a thorough literature review is presented. The methods used for thermodynamic analysis and flow visualisation are narrated.

In chapter 3, various experimental set-ups are discussed in detail by explaining different components and the construction steps. The preliminary investigations using the ink test for flow visualisation on a small scaled tank followed by BOS measurements on this tank are documented. Different stratification systems used in this work are explained in detail with the necessary figures. The flow visualisation using the constructed inlet flow distributors is shown in this chapter.

The various results obtained from the experiments carried out on the stratisorp cycle with the test set-up are documented and discussed in chapter 4. In the first half of this chapter the BOS measurements carried out on the full scaled tank with the stratification rings are described in detail. The stratification mechanism observed using the BOS technique and the temperature measurements is explained. In the second half of the chapter the stratisorp experiments with different cycle conditions and their thermodynamic analysis is presented.

Concluding remarks with an outlook based on the results achieved in this work constitutes chapter 5.

Chapter 2

Theory and Methods

2.1 Adsorption heat pump technology

2.1.1 Thermally driven heat pumps

Heat pumps are devices that extract heat from a low temperature level (T_L) and give off this heat at a higher temperature level (T_C or T_A). If the extracted heat region i.e. the low temperature region is the main concern, then the device is called a chiller or refrigerator which is essentially the case for this thesis. The second law of thermodynamics states that the heat transfer from a low temperature to a high temperature is only possible with the existence of a third energy source. This energy may be available in the form of mechanical or electrical energy as in the case of mechanically driven compression heat pumps or in the form of heat as in the case of thermally driven sorption (adsorption and absorption) heat pumps. Thermal heat pumps operate on the principle of sorption [66]. In the sorption process, an evaporative substance (sorbate) and an absorbing material (the sorbent) are involved. Liquid absorption concerns the sorption of the refrigerant by a liquid, while solid sorption deals with the sorption of the refrigerant by a solid [41]. Liquid absorption is a volume phenomenon whereas solid adsorption is a surface phenomenon. In the case of an adsorption heat pump, the refrigerant vapour i.e. the adsorbate is held in a solid material i.e an adsorbent at low temperature T_L and is given off at a higher temperature when the temperature of the adsorbent is raised. The adsorption of adsorbate molecules (e.g. water vapour) into a porous solid adsorbent (e.g. zeolite, silica gel), results in the release of the heat of adsorption [15]. For the operation of this heat pump, a third heat source available at a temperature T_H, higher than T_A and T_L, is essential. Heating is provided at medium temperature levels T_A and T_C and cooling is provided at the lowest temperature level T_L. A thermodynamic representation of the adsorption heat pump is shown in Fig. 2.1.

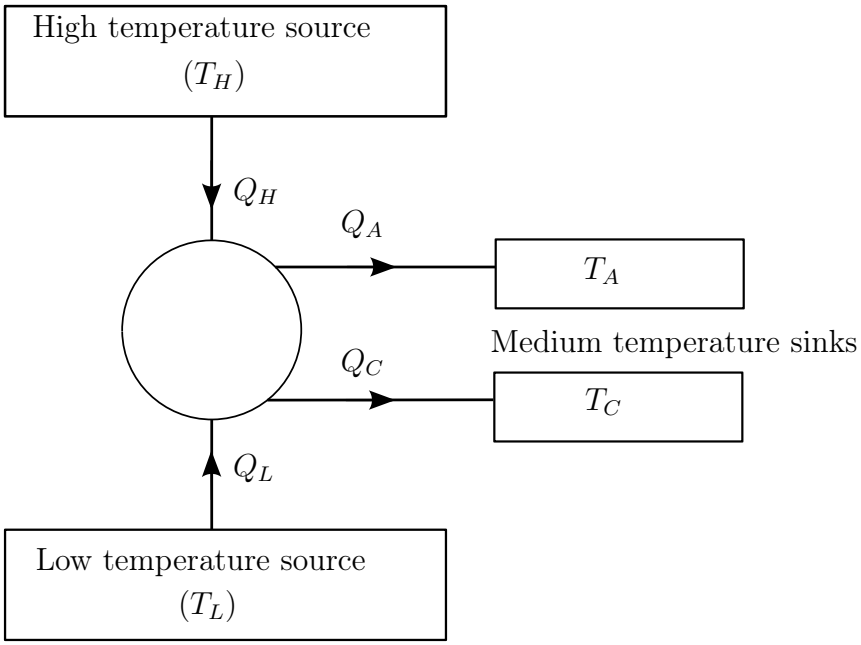

Figure 2.1: Thermodynamic representation of an adsorption heat pump [66]

This adsorption heat pump working according to Carnot cycle, can be divided into two systems; operating between T_H - T_C and between T_A - T_L temperatures as shown in Fig. 2.2. Any thermodynamic cycle operating according to Carnot cycle is reversible and has a maximum efficiency.

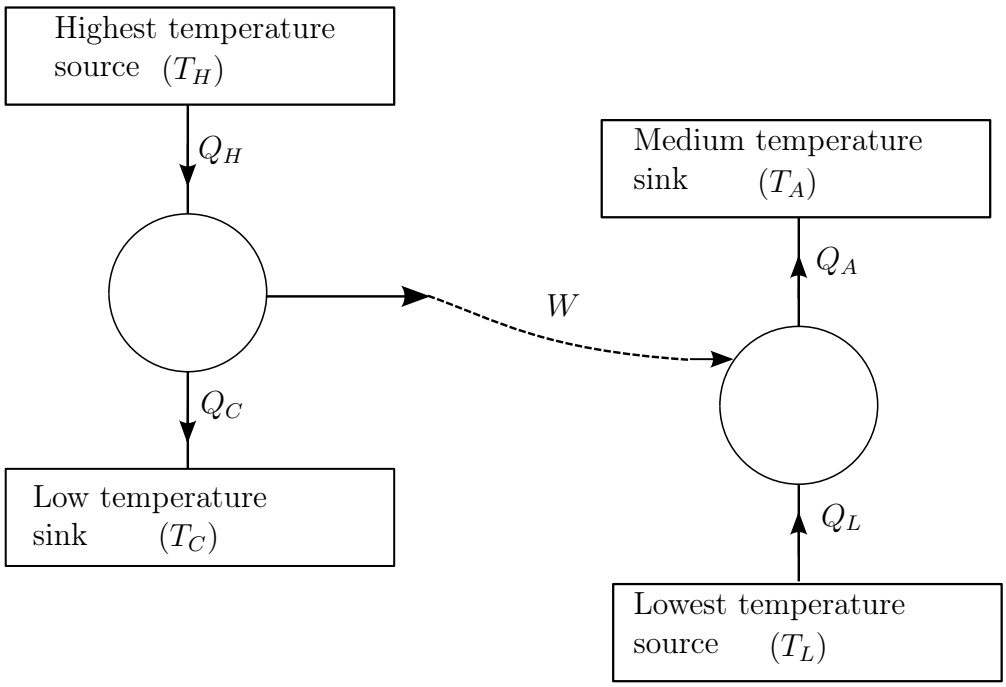

Figure 2.2: A heat pump as two systems

The first system operates as a heat engine which receives Q_H amount of heat from the highest temperature source (T_H) and rejects Q_C amount of heat at a lower temperature

(T_C). In the second system, Q_L is transferred from the lowest temperature source (T_L) to the medium temperature sink (T_A) using the work produced in the first system. The temperatures of the intermediate sinks (T_A and T_C) are generally close to each other [18]. If there is only one medium temperature level (T_A=T_C) then the entire heat of adsorption and condensation (Q_C) is rejected at this medium temperature level. Applying the first and the second law of thermodynamics [66] :

$$Q_L + Q_H = Q_C \qquad \text{and} \qquad -\frac{Q_L}{T_L} - \frac{Q_H}{T_H} + \frac{Q_C}{T_C} \geq 0 \tag{2.1}$$

and the maximum or ideal performance coefficient i.e. the Carnot coefficient of performance (Carnot COP) comes out as :

$$COP_{cool}^{ideal} = \frac{1 - \frac{T_C}{T_H}}{\frac{T_C}{T_L} - 1} \qquad \text{and} \qquad COP_{heat}^{ideal} = 1 + \frac{1 - \frac{T_C}{T_H}}{\frac{T_C}{T_L} - 1} \tag{2.2}$$

The COP values obtained for the real adsorption refrigeration cycle are lower than the ideal COP values. Since it is not possible to operate a heat pump according to the Carnot cycle, the ratio of the COP of the actual heat pump to that of a Carnot heat pump operating between the same temperature levels is defined [66] which is also known as the thermodynamic efficiency [56].

$$\eta = \frac{COP_{actual}}{COP_{Carnot}} \tag{2.3}$$

The entropy production or the irreversibilities due to external and internal thermal coupling are the main cause for the difference in COP values of the sorption heat pumps. The internal coupling arises in the case of heat recovery between the adsorbers. In the case of a finite number of adsorbers (cascading cycles) the heat recovered from one adsorber is used to heat another adsorber at a lower temperature. This driving temperature at the adsorber gives rise to the internal thermal coupling responsible for the internal entropy generation. The internal entropy generation does not exist for a single adsorber cycle. The external entropy production comes from the fact that the temperature of the components varies while the temperatures of the reservoir are constant [41], [42]. The adsorber temperature varies during the whole thermodynamic cycle whereas the temperatures of the heat sink and heat sources are constant. This temperature inequality leads to the external entropy generation. In the case of the absorption cooling machines, the regenerated absorbent leaves the generator at a high temperature and is cooled to a lower absorber temperature. The rich solution leaving the absorber is heated to the level of the generator temperature. These temperature variations are analogous to the temperature variations observed during the adsorption refrigeration cycle. The temperature mismatch between the heat sources and the fluid causes the external thermal coupling entropy generation. There are however more sources of entropy generation in the absorption and adsorption refrigeration cycle. The non uniformity of the solution temperature in the generator and absorber caused due to the variation in solution concentration from inlet to outlet causes heat-transfer irreversibilities. There are also irreversibilities caused during the internal heat recovery in the solution heat exchanger and due to the throttling of the refrigerant and solution. Desuperheating in the condenser is also another source of irreversibility. Meunier *et al.* [41] have comprehensively documented the effect of both external and internal thermal coupling entropy production on the degradation of the COP

for adsorption and absorption refrigeration cycles.
Thus, the need of very low driving temperatures to reduce the entropy production due to external thermal coupling is necessary. The stratisorp system concept exactly addresses this issue. The core idea behind this concept is to cool or heat the adsorber with low driving temperatures to reduce the irreversibilities and improve the COP of the system.

As per definition of COP, the real values of COP for any heat pump are :

$$COP_{cool}^{real} = \frac{Q_{evaporator}}{Q_{heater}} \qquad \text{and} \qquad COP_{heat}^{real} = \frac{Q_{condenser} + Q_{adsorber}}{Q_{heater}} \tag{2.4}$$

2.1.2 Elements of adsorption heat pump

The working principle of the adsorption cycle can be explained from Fig. 2.3. The adsorption cycle, like any sorption cycle is based on three (or four) temperature levels. The adsorption refrigerator is a closed system and is implemented such that only the heat is exchanged with the surroundings (heat source and sink) but not the working fluid. The environmental heat is transferred via a heat exchanger (evaporator) from a low temperature heat source and is rejected at the medium temperature heat sink using another heat exchanger (condenser). The heat and mass transfer in the adsorber is governed totally by the working fluid atmosphere. The thermodynamic cycle (Fig. 2.3 (a)) consists of four periods. In the first period, AB, the adsorber is isosterically heated by the high temperature source at T_h while being closed. Hence the temperature of the adsorbent rises accompanied by a rise in the vapour pressure of the adsorbent from the evaporator pressure (P_e) to the condenser pressure (P_c). At the end of the first period, the adsorber pressure matches the condenser pressure. Hence in the second period, BD, the adsorber is connected with the condenser. The adsorber continues receiving heat, the adsorbate is desorbed and condenses in the condenser (point C in Fig. 2.3) by releasing the heat of condensation (Q_c). The liquid refrigerant (water in the case of silica gel-water adsorbers) enters the evaporator (point E).

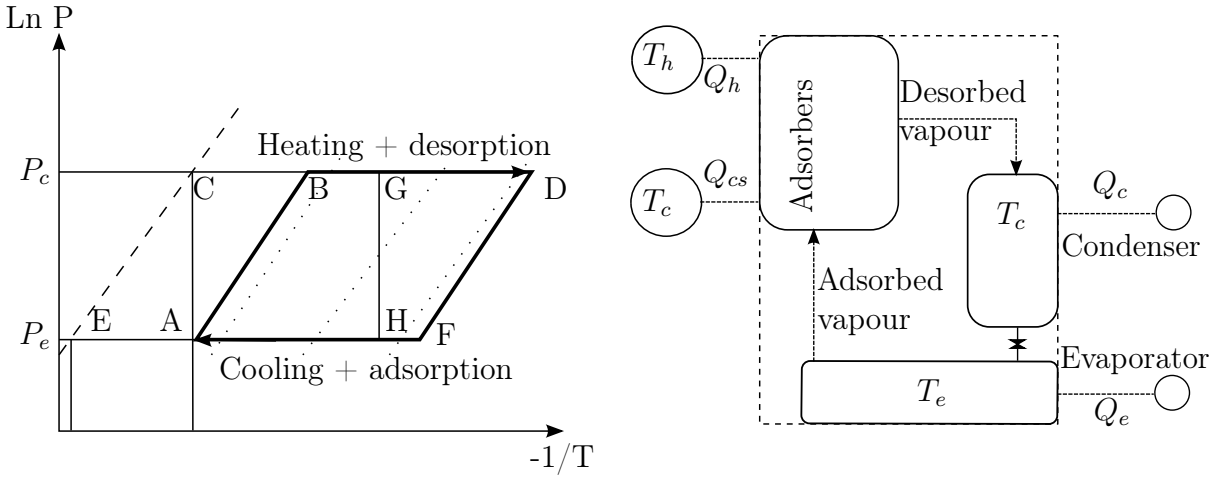

(a) Clapeyron diagram (ln$P$ Vs. -1/T)

(b) Schematic description of an adsorption heat pump

Figure 2.3: Principle of the adsorption refrigeration cycle and schematic arrangement of different components in an adsorption heat pump [56]

At the end of the desorption/condensation period, isosteric cooling (period DF) of the

adsorber is commenced. The adsorber is cooled by a medium temperature sink at T_c. Therefore, the vapour pressure drops down to the evaporator pressure while the adsorber is being closed. When the adsorber and the evaporator pressure matches, they are connected with each other and the fourth period of the cycle starts. During this period (period FA), water vaporises in the evaporator by taking the environmental heat from a low temperature source at T_e (analogous to T_L from Fig.2.2). This vapour gets adsorbed by the adsorber thereby releasing the heat of adsorption. The temperature of the adsorbent particles rises due to the heat of adsorption. The rise in temperature of the adsorbent particles shifts the adsorption equilibrium to low adsorber loading. Therefore the heat of adsorption has to be removed before further vapour mass transfer into the adsorbent particles may take place [50]. When all the energy received by the adsorber during the heating period (ABD) is supplied by the heating system, the cycle is termed as a single effect cycle. The cooling effect caused due to the evaporation of refrigerant during such cycles is only intermittently available. The thermodynamic efficiency (η) of a single effect cycle is usually quite low. Therefore, measures have to be taken to enhance performance e.g. heat recovery processes.

2.1.3 Methods of heat recovery for adsorption heat pump

The basic idea behind the heat recovery for adsorption heat pump is that of utilising the heat released during the adsorption half cycle (isosteric cooling (DF) and isobaric adsorption (FA) in Fig. 2.3 (a)) for desorption of the same or another adsorber. This reduces the heat input to the adsorber during the desorption half cycle and thereby improves the COP of the cycle.

Heat recovery cycle: One of the simplest approaches used by few researchers and some machines available on the market is deployment of another adsorber in the system which is working out of phase with respect to the first adsorber [22], [56], [12], [33]. Due to the out of phase operation of the adsorbers, one adsorber is hot at the end of its desorption half cycle (point D) where as the other adsorber is cold at the end of its adsorption half cycle (point A). The cold adsorber can then be heated by removing the heat from the hot adsorber using a heat transfer fluid until their temperatures match i.e. the cold adsorber reaches point G after heating by the hot adsorber while the hot adsorber reaches point H after the heat transfer. After this sub-period of heat recovery, the heat source heats up one adsorber (GD) while the other adsorber is cooled down by the heat sink (HA). In this way part of the sorption latent heat can be recovered from the path FH to the path BG, depending on the temperature of the heat source. Although each adsorber follows exactly the same cycle as the basic adsorption heat pump cycle, the heat supplied to the total system decreases. A COP enhancement of 25% was found by Wang [60] and 50% by Szarzynski *et al.* [56]. Wang used activated carbon-methanol as a working pair and varied the regeneration temperature (T_h) between 85-120 °C whilst the medium and low temperature were kept constant at 30 °C and 5 °C respectively. The documented rise in COP_{cool} was found to have occurred at 100 °C and above. Szarzynski *et al.* incorporated a zeolite-NaX+water pair. The documented improvement in COP_{cool} was found using a regeneration temperature of 120 °C. Here the heat balance corresponds to that of a double effect cycle.
The cycle used by Douss *et al.* [22] is also called as a cascading cycle. They proposed a modified adsorption cycle, which consists of two cycles. A zeolite-water cycle for the high temperature stage (T_h = 220 °C) and an active carbon-methanol cycle for the low

temperature stage ($T_h = 100$ °C). The heat required by the active carbon-methanol cycle for isosteric heating and isobaric desorption is completely obtained from the zeolite-water cycle. The experimental cooling COP was found to be 1.06. They showed that using an infinite number of adsorbers, with ideal heat recovery between adsorbers, a maximum cooling COP of about 68% of the theoretical maximum cooling COP (Carnot COP) corresponding to those operating temperatures could be achieved. However, a higher number of adsorbers would naturally increase the complexity of the hydraulic circuit and it would be very expensive to build.
SorTech AG, an adsorption chiller manufacturer from Germany, has patented their invention of heat recovery [46]. In principle it is similar to the heat recovery cycle. In the standard heat recovery cycle, an additional circulation pump is required to circulate the heat transfer fluid from the hot adsorber to the cold adsorber. SorTech AG removes the need for this pump as the heat recovery takes place solely with valves and the pumps which are required for the sorption phases anyway. Due to this reduction of the number of necessary pumps, the current consumption and the generation of noise is drastically reduced and the electrical efficiency is improved. The heat recovery phase according to this invention works as follows: The valves in the supply flow to both adsorbers at the beginning of the heat recovery phase are positioned such that the adsorber in the desorption phase receives heat transfer fluid from the high temperature heat source and hence it is heated up. The return flow of this "new" desorber is still cold and it continues to be connected to the medium temperature circuit until the temperature level increases significantly. The threshold of this temperature is generally the temperature of the return flow of the adsorber in adsorption phase or the "old" desorber. Similarly the adsorber in the adsorption phase i.e. the "new" adsorber is supplied with heat transfer fluid from the medium temperature circuit. The return flow of this adsorber is still hot as it had previously been desorbing. This hot return flow is continued to be connected with the high temperature source until the return flow temperature level decreases down to the return flow of the "new" desorber. This delayed adsorption or desorption is claimed to improve the COP of the adsorption chiller.

Heat and mass recovery cycle: After normal adsorption/desorption half cycle in two adsorber system with heat recovery, if the adsorbers are connected to each other, refrigerant flows from the high pressure adsorber to the low pressure one. The desorber desorbs further by pressure reduction while the adsorber further adsorbs due to the increase in pressure. This operation is called mass recovery [14]. Generally heat and mass recovery are used together with heat recovery process following the mass recovery process. Wang [60] found that by using both of these measures, the COP of the adsorption cooling cycle could be increased by more than 10% when compared with the basic cycle using two adsorbers without heat and mass recovery.

Thermal wave cycle: The percentage of internally recovered energy, and thereby the COP, can be improved when the principle of heat storage with heat regeneration is implemented. The concept of the adsorption heat pump with heat regeneration was first proposed by Shelton *et al.* [54]. The heat regeneration process is commonly termed as 'temperature front' or 'thermal wave' in the field of adsorption refrigeration cycles [56]. The system with heat generation is essentially composed of two adsorbers connected in series which are out of phase i.e. when one adsorber is in adsorption phase, the other adsorber is in desorption

phase (Fig. 2.4).

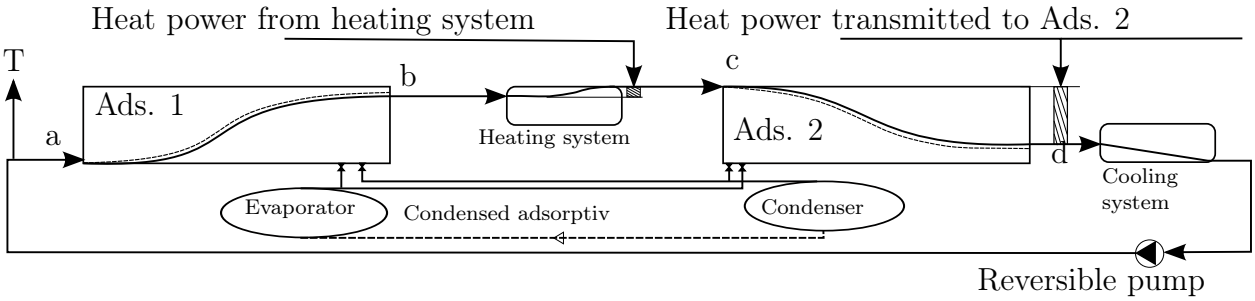

Figure 2.4: Principle of the adsorption cycle with the thermal wave effect [56]

The heat transfer fluid is circulated using a reversible pump successively through the first adsorber (Ads. 1) in its adsorption phase and then through the second adsorber (Ads. 2) in its desorption phase. Naturally the first adsorber produces a cooling effect at the evaporator while the second adsorber produces a heating effect at the condenser. The heat transfer fluid is significantly heated from T_c close to heat source temperature T_h in the first adsorber. The heat transfer fluid is then heated to T_h in the heating system. Hence desorption can take place in adsorber 2. In this way the heat transfer fluid serves to transmit heat recovered from the adsorbing bed being cooled to the desorbing bed being heated [14]. It can also be seen that the heat power supplied by the heating system is much lower than the heat power transmitted to adsorber 2 as long as the fluid temperature at the exit of adsorber 1 is close enough to T_h. It was shown by calculations that around 80% of the heat required by the second adsorber was available from adsorber 1. The working pair of ammonia-zeolite was assumed with the following values: $T_h = 316$ °C, $T_c = 38$ °C, $T_l = 5$ °C. An experimental COP of 0.9 using a consolidated zeolite and graphite adsorbent bed was achieved although with limited power [48]. However, the cycle can be efficiently run provided that a large temperature drop/lift is available in the desorber/adsorber. Good heat transfer properties of the adsorbent bed are required by the cycle, which is difficult to achieve from low thermal conductivity adsorbent materials. It was shown by Amar *et al.* [5] that not only the thermal conductivity of the adsorbent bed but also good mass transfer properties are essential for the success of a thermal wave cycle. Poor mass transfer can become a cause for very large pressure fluctuations in the bed, especially when the operating pressure is low, as in the case of water. A further modification of the thermal wave cycle was proposed by Christoph [16]. The author used forced convection in the thermal wave cycle where the refrigerant itself acted as the heat transfer fluid. This approach is only suitable for high pressure refrigerants like ammonia but not suitable for water.

2.2 Heat recovery using stratisorp cycle

2.2.1 Principle of working

The methods of heat recovery discussed above have been developed mostly in the 90's and early 2000. A relatively new concept for internal heat recovery using a stratified thermal storage was introduced by Schmidt *et al.* [51]. Silica gel-water is one of the commonly

used adsorbent-adsorbate pair in adsorption technology. Silica gel can be regenerated at low temperature making it an attractive choice for waste heat recovery and solar cooling. Fig. 2.5 shows a typical differential heat curve for silica gel-water pair working under three temperatures[1].

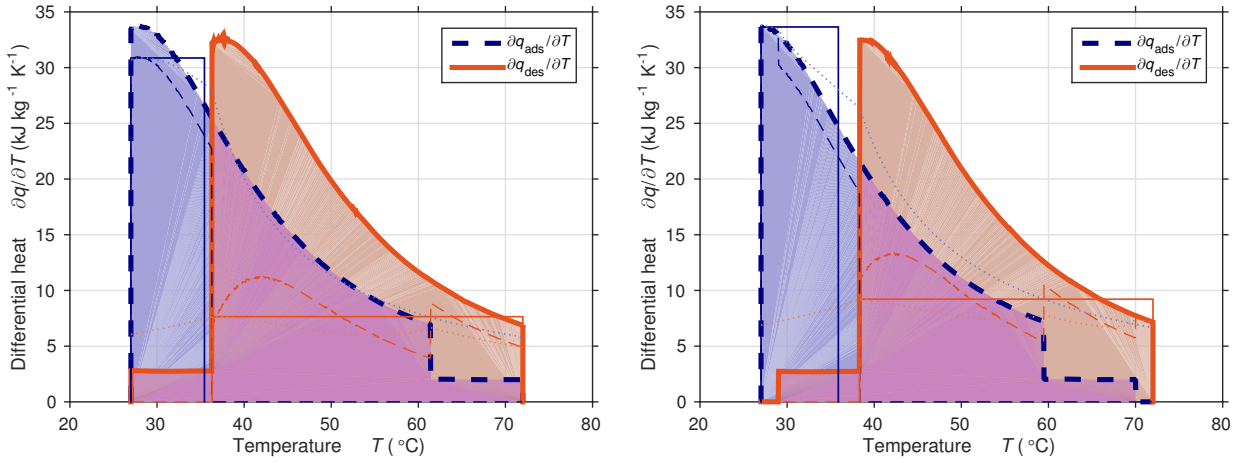

(a) $\Delta T \approx 0$ K
$COP^{max}_{cool} = 1.91$, $COP^{Carnot}_{cool} = 4.21$
$\eta = 45\%$

(b) $\Delta T = 1$ K
$COP^{max}_{cool} = 1.57$, $COP^{Carnot}_{cool} = 4.21$
$\eta = 37\%$

Figure 2.5: Differential heat curve for silica gel 127B-water pair working under $T_h = 72$ °C, $T_c = 27$ °C and $T_e = 18$ °C condition [52]

A large amount of heat is released during the adsorption half cycle as adsorption being an exothermic process. In addition to this energy, some energy is available due to the sensible cooling of the adsorber. The total energy released during the adsorption half cycle equals the area under the thick dotted blue curve. This energy also equals the energy demand of the adsorber during the desorption half cycle which is the area under the curve bounded by the thick orange line. It can be observed that these two areas have a significant overlap (light pink area in Fig. 2.5(a)). This means, a large fraction of the heat of adsorption can be utilised in the desorption half cycle and thus the heat recovery can be achieved. The remaining heat demand during desorption is covered using an external heat source (light orange area in Fig. 2.5 (a)). The non-recoverable portion of the heat needs to be rejected in a re-cooler (light blue area in Fig. 2.5 (a)). Hence, a heater and a re-cooler are integral part of this system. It can be observed that the amount of heat of adsorption released is different at different temperatures. Hence a cylindrical stratified thermal storage tank is deployed in order to store the heat of adsorption at each temperature level until it can be used for desorbing the adsorber in the next half cycle.

[1]The shape of the differential heat curve is different for different adsorbent-adsorbate pairs. In this thesis, the differential heat curve of only silica gel-water has been considered. For the differential heat curves of other material pairs refer [52]

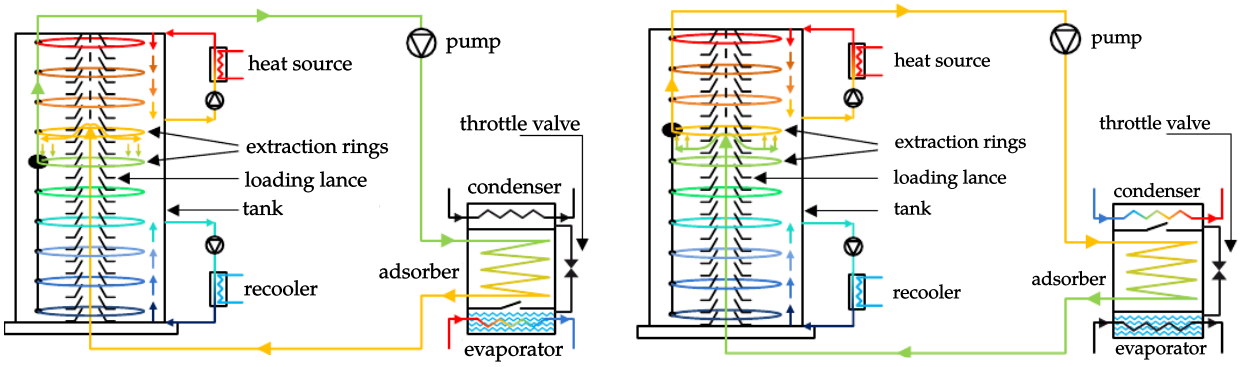

(a) Adsorption half cycle (b) Desorption half cycle

Figure 2.6: Working of the stratisorp system [53]

The top of the tank is maintained at the maximum desorption temperature by the heater (e.g 72 °C) while the bottom of the tank is maintained at the medium temperature of the cycle (e.g 27 °C) by the cooler. The heater and cooler extract water from a fixed height of the tank and reinsert the flow into the tank at the top and at the bottom of the tank respectively. The adsorber can be supplied by the heat transfer fluid (here water) extracted from the tank whose temperature is close to the adsorber temperature. During the adsorption half cycle the adsorber is cooled by taking water from decreasing heights of the tank. The adsorber receives water at medium temperature from the bottom of the tank towards the end of the adsorption half cycle. The water returning to the tank is warm due to the heat of adsorption. The tank is loaded with this warm return flow by using a suitable stratification system (active or passive). Conversely, the adsorber is heated during the desorption half cycle by extracting water initially from the lower part of the stratified tank and then with increasing adsorber temperature from increasing heights of the tank. The adsorber is desorbed by extracting water at maximum desorption temperature at the end of the desorption half cycle. Due to the use of stratified thermal storage for the sorption cycle, this cycle has been termed as 'stratisorp' cycle (stratified sorption). This term will be used here after in this thesis. The heater and cooler circulate water with the tank at a low flow rate compared to the adsorber flow rate.

2.2.2 Role of the stratified thermal storage

The overlapping area of the two heat curves in Fig. 2.5 (a) is the theoretical maximum recoverable heat for silica gel-water, working under the mentioned temperature limits. The maximum heat recovery is only possible when the adsorber is cooled (during adsorption) or heated (during desorption) with infinitesimally small temperature difference ($\Delta T \approx 0$). For this ideal case the theoretical maximum COP can be achieved (COP_{cool}^{max} =1.91). However, it is not practically possible to achieve ideal heat recovery. A finite ΔT is always needed at the adsorber to get useful heating or cooling power. Fig. 2.5 (b) shows the effect of the driving temperature difference on the overlapping area of the heat curves. In this case, the recoverable heat reduces significantly merely by introducing a very small temperature difference ($\Delta T = 1$ K) and the maximum achievable COP is reduced to 1.57. The driving temperature difference is the cause of irreversibilities. Consequently, the heater has to supply and the cooler has to reject more heat. The COP_{cool} and COP_{heat} of the cycle would reduce considerably owing to

Eq. 2.4[2]. The driving temperature difference should be kept as low as possible to push the real COP towards the ideal COP. Moreover,the maximum COP corresponding to the heat curves is only then achieved when the stratisorp cycle is operated exactly along the curve bounding the overlapping area is Fig. 2.5. In other words, the heat of adsorption released at different temperature levels should be stored in the tank in ideal manner i.e. the temperature at which the heat is stored in a fluid slice should remain constant until the same amount of heat is required by the adsorber in the desorption half cycle. The mixing in the tank tends to change the temperature of this fluid slice. This is the main reason why the real COP of the stratisorp cycle deviates from the maximum achievable COP. The stratified thermal storage plays a vital role in maintaining ΔT as low as possible. A detailed simulation study on the stratisorp system was carried out by the authors [53]. The effect of mixing in the stratified thermal storage on the COP of the stratisorp cycle was investigated. It was observed that more mixed tank led to degradation of the COP values for all adsorber chiller designs under consideration (Fig. 2.7(a)). Zeolite 13X-water was used as adsorbent-adsorbate pair. The effect of varying number of extraction/insertion heights on the COP was also investigated (Fig. 2.7(b)). It was observed that the COP of the stratisorp system increased with increase in the number of extraction heights. For 8 or more extraction heights the change in COP was not significant and the COP against extraction height curve reached a plateau[3]. The degradation of the COP at lower number of extraction heights is attributed to higher driving temperature difference at the adsorber and higher mixing in the tank. As seen before, during the adsorption half cycle the adsorber is cooled by extracting fluid from the tank. With the progress of the cycle the fluid is progressively taken from the lower part of the tank. As soon as the criterion for switching to the next level is reached the fluid is extracted from the next available lower level. The plot of the supply temperature to the adsorber against time takes form of saw tooth profile. Higher number of extraction levels reduce the height of each saw tooth and thereby reducing the driving temperature difference at the adsorber. This phenomenon reverses during the desorption half cycle.

[2]The effect of driving temperature difference on the differential heat curves and the associated irreversibilities has been documented by Schwamberger [52]

[3]The experimental investigations discussed further in this work were carried out using 6 extraction rings in order to keep the test set-up simple and not too intricate

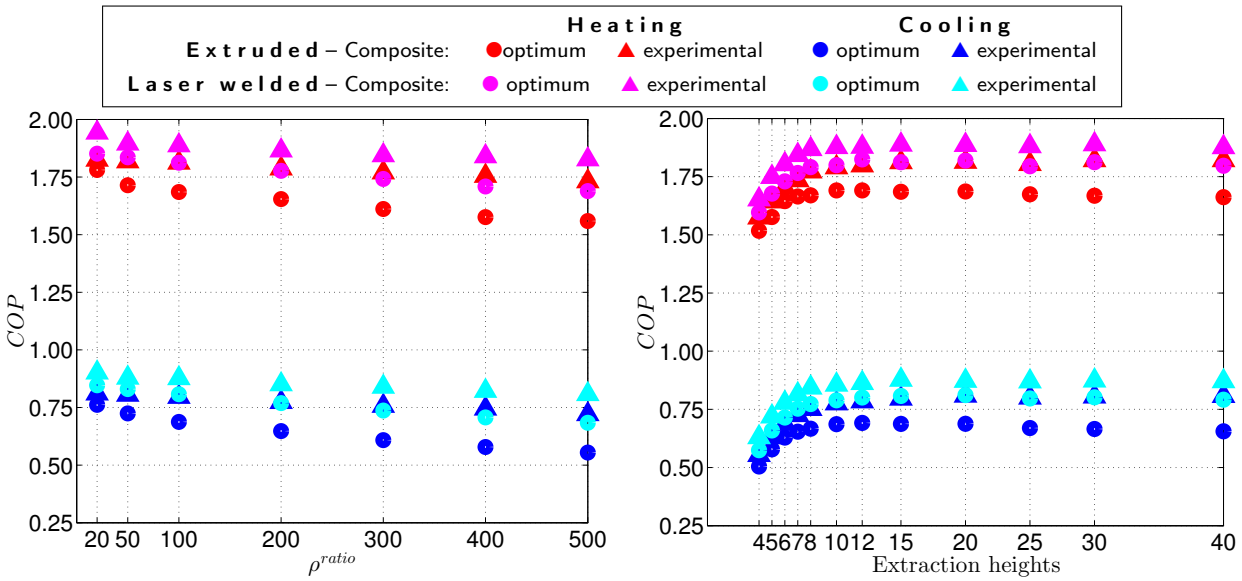

(a) Effect of mixing

(b) Effect of varying extraction heights

Figure 2.7: Degradation of COP attributed to the mixing in the storage and dependency on number of extraction levels. The mixing in the tank was modelled by artificially increasing the thermal conductivity of the fluid layers in the region of fluid extraction or insertion by a factor (p^{ratio}) [53].

2.3 Design aspects of stratified thermal storage

2.3.1 Classification of stratified thermal storage tanks

In most of the solar energy collection systems water is heated during the day and stored for use during the night. This extends the use of solar energy over a large part of the day. Chilled water storage stores cool water and assists the air conditioning systems. Chilled water storage can shift part of the cooling load to off-peak hours. This allows the chiller to operate during the cooler night temperatures, which results in better coefficient of performance. All existing thermal storage tank systems have the same goal of maintaining the thermodynamic availability of stored energy so that it can be extracted at the same temperature at which it was stored [20]. Stratified thermal storage plays a key role in storing energy efficiently in order to assist the solar heating systems or air conditioning systems. Maintaining stratification on storage tanks is important for better performance of energy systems with which these tanks are integrated.
The principle of operation of stratified thermal storage is based on natural process of stratification. Therefore the fluid flow in these storage tanks involves both natural and forced convection. The stratified thermal energy storage tanks (TES) are generally of two types.

- Thermocline TES
- Stratified TES

These definitions are based on the temperature of the flow entering the tank. The flow coming into a thermocline TES has constant temperature where as for a stratified TES, the inlet temperature is variable. The thermocline TES has another important characteristic difference

compared to stratified TES. Consider a thermal energy storage coupled to a heat source in a heat storage application in which the cold fluid is extracted from the bottom of the tank, heated at the heat source e.g. heat pump, solar collector, gas fired heater and returning hot fluid is stored at the top of the tank. Let us assume that the returning hot fluid has constant temperature. In that case, the incoming flow entering with certain momentum will tend to mix with the fluid in the tank. Owing to the buoyancy force which directed upwards as the fluid being hot, would restrict the motion the incoming stream to the surface region. As more and more fluid enters the tank, the region of initial mixing would grow and would be pushed down. This leaves behind a region of uniform temperature which equals the inlet flow temperature. The region of intermediate temperature which separates this regions of uniform temperature from that initially in the tank is termed as thermocline. Thermocline is the region of steepest temperature gradient in the tank. It acts as a physical barrier which separates the hot and the cold fluid regions in the tank. The thickness of the thermocline region is the important indicator for quality of stratification as seen from Fig. 2.8. A solar energy collection system with controlled output temperature is a typical example where a thermocline TES could be deployed.

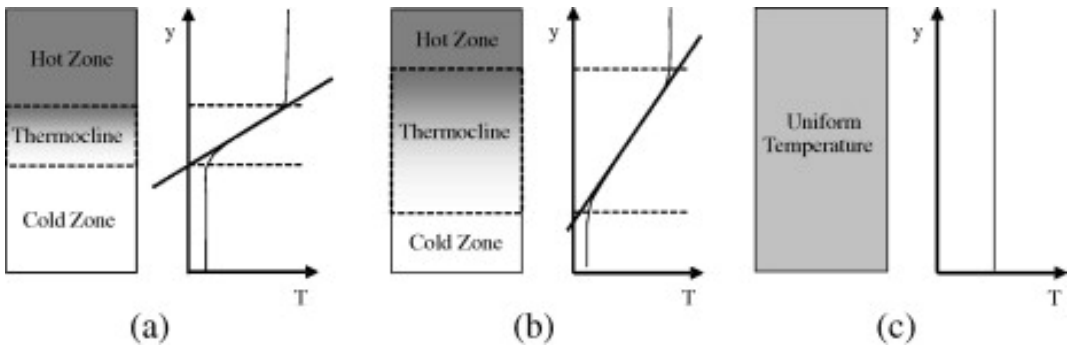

Figure 2.8: Different degrees of stratification within a storage tank with the same amount of stored heat [27], (a) highly stratified,(b) moderately stratified,(c) fully mixed (unstratified)

On the contrary, if the output temperature of the solar collector is not controlled the flow returning to the thermal storage tank varies in temperature which generally is the case. The buoyant flow entering the tank constantly seeks equilibrium with fluid in the tank enhancing mixing. This prohibits the formation of the thermocline region and it is never formed. In such scenarios, the thermal energy storage is called stratified TES. The term thermocline is exclusively used for thermocline TES.
stratisorp cycle implementing stratified storage tank is a case of stratified TES. The flow returning from the adsorber to the tank is constantly varying in temperature. Hence no clear thermocline region can be formed inside the tank. To avoid excessive mixing in the tank the return flow should be inserted at proper level either using passive or active stratification device[4].

[4]Different stratification mechanisms implemented in this work have been discussed in the next chapter

2.3.2 Dimensionless numbers

The discussions concerning thermally stratified tanks are incomplete without introduction of some dimensionless number. The dimensionless numbers facilitate the designer to analyse the stratified tank problem irrespective of the dimensions of different physical quantities involved in a process. As mentioned earlier the flow in the thermal storage tank is of mixed convection type. Hence relative magnitudes of the buoyancy and inertia forces play a major role in the flow development. Richardson number (Ri) puts these two forces in relation with each other. The Richardson number is derived from dimensionless analysis. It is the ratio of buoyancy force to inertia force exerted by the fluid. The mathematical expression for Richardson number reads :

$$Ri = \frac{g\beta\Delta T l_r}{{u_r}^2} \tag{2.5}$$

The subscript r denotes a reference quantity. The Richardson number is one of the most important dimensionless numbers in case of the convective flows for the topic of this work. The goal of design of the stratified thermal storage should be to increase the Richardson number.
When the design of flow diffuser is the prime goal of the designer then very often the Froude number (Fr) is used. The effect of Froude number on the stratification has been a central topic of research [35], [64], [61]. Froude number is defined as the square root of the ratio of the inertia and gravity forces. However, frequently, another form of Froude number is used which is called modified Froude number, Fr_m, which is based on buoyant force per unit mass, $g\beta\Delta T$.

$$Fr_m = \frac{u_r}{\sqrt{g\beta\Delta T l_r}} \tag{2.6}$$

Some research works use Peclet number (Pe) to characterize the relative magnitudes of the thermal energy transported by fluid motion to that transported by molecular diffusion. It is expressed in terms of Reynolds number and Prandtl number as :

$$Pe = RePr \tag{2.7}$$

2.3.3 Factors affecting stratification

The stratification in thermal storage tank is prone to degradation. The factors that are responsible for degradation can be roughly categorised into two types : **mixing caused by the inlet stream during charging or discharging of the tank** and **heat transfer from the fluid in the tank**.
The mixing caused by the kinetic energy of flow entering the tank is by far the most influential factor which degrades stratification. Design of inlet diffusers play a vital role in controlling the inlet velocity of the flow. Efficient design of inlet diffuser which reduces the flow inertia and thereby reduces mixing in the tank and improves stratification has hence been an important research agenda. Karim [35] experimentally investigated a stratified chilled water storage tank in which the influence of flow diffuser[5] design onto the stratification quality was analysed.

[5]Flow diffusers designed for variable inlet temperature case are termed as inlet distributors [20]

It was concluded that low Froude numbers cause unequal pressure drop in the diffusers which leads to unequal flow from different openings. This study claims that opening area and distribution of holes are important factors for stratification. However, a study by Wildin [61] for different diffusers with same inlet Froude number, revealed that inlet Reynolds number has a strong influence on thermocline development [20].
Cabelli [11] investigated stratified TES based on his 2-D numerical model. This model was found to be stable for $Re < 200$ where Re and Ri were based on the inlet port velocity and tank height. Within the limited scope of this model due to its instability at higher Re, it concluded that increasing Ri beyond unity has negligible effect on stratification. Ghajar *et al.*[65] numerically investigated the conditions under which the effect of the inlet geometry on stratification vanishes in case of thermocline TES. It was found that the inlet geometry has significant effect on stratification for $Ri < 5$ and a negligible effect for $Ri > 10$. Ri was based on height of the tank and the tank bulk fluid velocity. Cai *et al.* [13] also reached similar conclusion with their modelling approach. Guo *et al.* [26] also identified Ri as a significant parameter for characterization of flow pattern and temperature distribution inside the storage tank. They removed the limitation on Reynolds number values in Cabelli's work. For a single-flow circuits(charge or discharge), values of $Ri > 1$ were found to provide better stratification while for the case of two-flow circuits (charge and discharge), poor stratification was obtained at $Ri = 1$. The stratisorp cycle is a case of a two-flow circuit. Mo *et al.* [43] also underlined the importance of achieving higher Richardson numbers. They noted that at high Ri values one dimensional plug flow in the stratified storage tank can be justified. At very low Ri values ($Ri = 0.005$) severe mixing and short circuiting of hot fluid directly to the outlet takes place. A critical value of Richardson number ($Ri_{crit} = 0.244$) was documented by Sliwinski *et al.* [9] below which no stratification was observed in case of thermocline TES. It is clear from this discussion that higher Richardson number is favourable to higher stratification, both in thermocline TES and stratified TES. Favourable conditions for higher Ri can be created by reducing inertia of the inlet flow. Naturally, increase in flow rate has negative effect on stratification.
The loss of stratification quality can also be caused due to heat transfer from the fluid in the tank. Heat transfer to the surroundings through the tank wall and insulation, heat diffusion across the thermocline region and axial heat conduction through the wall of tank are the main ways in which the heat transfer can take place. These heat transfer routes can hamper the quality of stratification and lead to degradation. Due to low thermal conductivity of water, conduction across the thermocline was found to be a minor factor as compared to other factors [20]. The ratio of fluid to wall thermal conductivity is a governing parameter. Higher values of this ratio are essential for better stratification. These findings regarding the effect of conducting wall are based on static tests with partially charged tank. Lightstone *et al.* [39] showed that in the dynamic mode of operation, heat transfer through the tank wall has negligible effect on the stratification.
Among other parameters, aspect ratio of the tank (height to diameter ratio) also influences the stratification. The stratification was generally seen to improve with increase in aspect ratio. Nelson *et al.* [45] concluded that only negligible improvements are observed beyond aspect ratio of 3.0. It was pointed out by other researchers that a reasonable trade off between performance and cost can be made for aspect ratio between 3 and 4 [37].

2.4 Methods for thermodynamic analysis

2.4.1 Determination of the COP of stratisorp cycle

The COP of an adsorption heat pump working between 3 temperature levels can be given by Eq. 2.4. This equation can not be directly used to estimate the COP of the stratisorp cycle. As seen from Fig. 2.9 the stratified thermal storage is within the system borders and hence the energy contained in the tank has also to be accounted for calculation of COP.

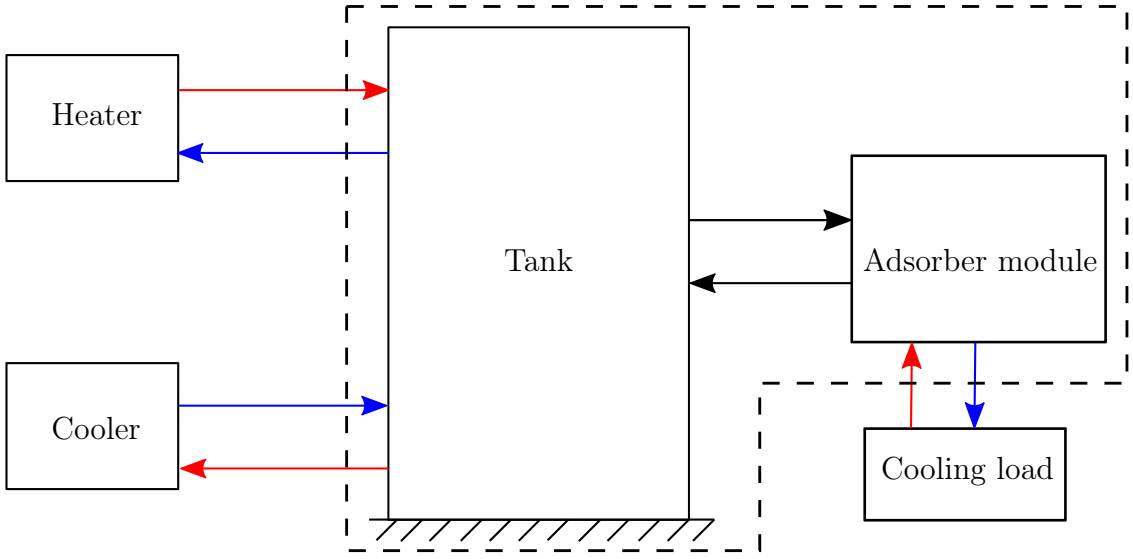

Figure 2.9: System borders for the stratisorp system

During one complete adsorption cycle, the tank receives heating energy Q_{heater} from the heater. Total cooling energy rejected at the cooler from the tank is Q_{cooler}. The tank receives heat of adsorption $Q_{adsorption}$ from the adsorber during the adsorption half cycle and supplies $Q_{desorption}$ during the desorption half cycle. As a result of these different energy exchanges with the tank during each cycle, net energy is stored in the tank. The energy stored in the tank assists the adsorption heat pump cycle by reducing the demand for the total driving energy required. If $Q_{tank_{end}}$ and $Q_{tank_{start}}$ is the energy contained in the tank at the end and at the start of the adsorption cycle respectively, then the total change in the energy contained in the tank would be:

$$\Delta Q_{tank} = Q_{tank_{end}} - Q_{tank_{start}} \tag{2.8}$$

Considering the term ΔQ_{tank} for the COP estimation, the Eq. 2.4 would modify to :

$$\begin{aligned} COP_{cool}^{stratisorp} &= \frac{Q_{evaporator}}{Q_{heater} - \Delta Q_{tank}} \\ COP_{heat}^{stratisorp} &= \frac{Q_{condenser} + Q_{cooler}}{Q_{heater} - \Delta Q_{tank}} \end{aligned} \tag{2.9}$$

These equations serve as an estimate for COP of the stationary stratisorp cycle. The cycle is termed stationary only when the energy content of the tank at the start and at the

end of the cycle is exactly equal ($\Delta Q_{tank} = 0$). However it is also possible that the system oscillates between two states and no definite stationary cycle exists. Consequently ΔQ_{tank} would oscillate between two finite values and it does not diminish with increasing number of cycles. If the magnitude of ΔQ_{tank} is of diminishing nature from cycle to cycle then it can be assumed that the system is close to a stationary cycle. A stationary cycle condition is said to have reached when $\Delta Q_{tank} \approx 0$. Under laboratory conditions this condition is practically not possible to achieve as :

$$\lim_{N_{cycles} \to \infty} \Delta Q_{tank} = 0 \tag{2.10}$$

Hence the approximate stationary state achieved in practice after finite number of cycle is termed as quasi stationary state [6]. When the tank reaches quasi stationary state then it is possible to carry out the energy balance of the system on the tank.
Here, theoretically for the last cycle :

$$Q_{heater} - Q_{cooler} + Q_{adsorption} - Q_{desorption} + \Delta Q_{tank} \approx 0 \tag{2.11}$$

The resultant term is the heat loss to the environment from the tank.
In the experiments described in chapter 4, the terms $Q_{tank_{end}}$ and $Q_{tank_{start}}$ are computed from the temperature measured by the temperature sensors placed along the vertical axis of the tank. The spatial resolution of the temperature sensors is the limiting criterion for approximation of the temperature profiles between two sensors. Here, a piecewise linear temperature distribution between the adjacent temperature sensors was assumed. Fig. 2.10 shows a typical temperature profile in a stratified thermal storage tank used for the stratisorp cycle. It was also assumed that the temperature of the tank did not have gradient in the radial direction. The temperature recorded by the sensors hence represented the temperature of the complete fluid layer at that position.

[6] In real case, after 10 cycles it was observed that term ΔQ_{tank} starts to oscillate around 0 and the magnitude of oscillations was less than 100 kJ. For detailed results see Chapter "Results and Discussions"

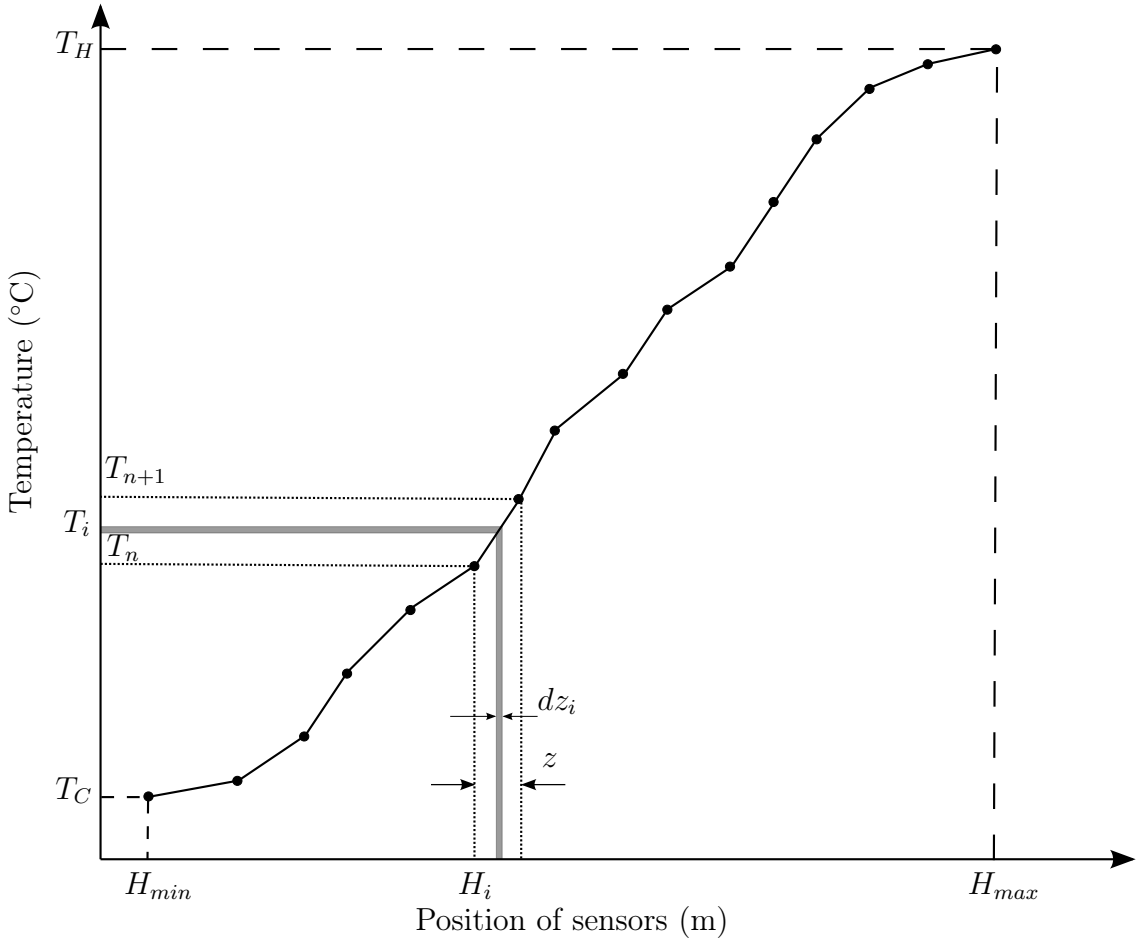

Figure 2.10: Estimation of energy contained in the stratified storage tank

The top of the tank is maintained at the maximum temperature of desorption T_H while the bottom of the tank is maintained at the minimum adsorption temperature or the temperature of heat rejection T_C. Let an arbitrary number of temperature sensors be equally placed at distance z along the height of the tank starting from H_{min} to H_{max}. Consider an infinitesimally small horizontal slice of thickness dz_i at temperature T_i which lies between temperature sensors T_n and T_{n+1}. The energy contained in this fluid layer is :

$$dQ_i = A_c \cdot \rho \cdot c_p \cdot dz_i \cdot T_i \tag{2.12}$$

where $A_c \cdot \rho \cdot dz_i$ is mass (m_i) of the fluid layer. Therefore the energy contained in the complete fluid layer between sensors T_n and T_{n+1} is :

$$Q_i = A_c \cdot \rho \cdot c_p \cdot \int_{H_i}^{H_i+z} T_i(z) \cdot dz_i \tag{2.13}$$

The solution of integral is the area under the curve bounded by T_n, T_{n+1}, H_i and $H_i + z$ where $T_i(z)$ is the position dependent temperature of the fluid layer. Likewise the energy for all segments between adjacent temperature sensors can be computed. The total energy contained in the tank will then be :

$$Q_{tank} = \sum_{i=1}^{N} Q_i \tag{2.14}$$

where N is total number of segments between the temperature sensors. Eq. 2.14 is only valid if there exists a temperature sensor each at the bottom of the tank and at the top of the tank very close to the tank lid. However, in practice due to constructional limitations this condition can not be always achieved. In such case the Eq. 2.14 is modified to :

$$Q_{tank} = Q_{bottom} + \sum_{i=1}^{N} Q_i + Q_{top} \tag{2.15}$$

where Q_{bottom} and Q_{top} are the energies of the fluid layers below the first sensor at the bottom and above the last sensor at the top respectively.

2.4.2 Characterisation of stratification

Many methods have been proposed for characterization of thermal stratification in water storages. For the development of components of thermal energy storage and comparison of different storages an index is sought after. Such index can be used to determine the ability of a thermal energy storage to promote and maintain stratification during charging, storing and discharging. Haller *et al.* [27] have made a comprehensive review of all methods available in literature that propose to characterize thermal stratification in a water storage. The authors note that only few methods allow for full flexibility in variability of temperature and flow rates applied during the process. In a typical stratisorp cycle, the inlet temperature to the tank is not constant. Moreover, for future development of the stratisorp cycle a need might arise to vary the flow rate at different stages of the cycle. In the light of these two facts, the role of the stratified TES in the stratisorp cycle is identical to a stratified TES used for solar thermal application. It was concluded by the authors that only the method proposed by Huhn [34] was in qualitative agreement with the internal rate of entropy generation. However, the shortcoming of this method is that it does not separate the entropy changes due to heat losses from entropy generation due to internal mixing and heat conduction. Hence with the method of Huhn different stratification efficiencies will be obtained for two TES with the same stratification behaviour, but different heat losses. In a following article by the same authors [28] efforts were made to further develop the method of Huhn by separating the external entropy production caused by heat losses from the internal entropy generation caused by mixing. The method developed by the authors, in its current form, is able to determine stratification efficiency for constant inlet temperature and flow rate cases only. The authors note that the stratification not only depends on the TES itself, but also on the temperature and mass flow rate profile of the experiment. These profiles are necessary in order to estimate the stratification efficiency.

The stratification efficiency mentioned above is calculated based on the internal entropy generation of the experimental TES relative to the internal entropy generation of the fully mixed TES. In a thermal energy storage entropy may be generated not only by mixing but also by heat conduction and diffusion. Thus entropy generation is an unwanted but unavoidable phenomenon [28]. One way of comparing the amount of mixing that is taking

place in a storage is to show the absolute values of entropy generation of the storage tank. As shown in the Fig. 2.11, the entropy change in the TES may be caused by mass transfer across the system boundaries [7] as indicated by $\dot{S}_{in}$ and $\dot{S}_{out}$ respectively as well as by heat transfer across the system boundary $\dot{S}_{hl}$ or by internal entropy generation $\dot{S}_{irr,int}$.

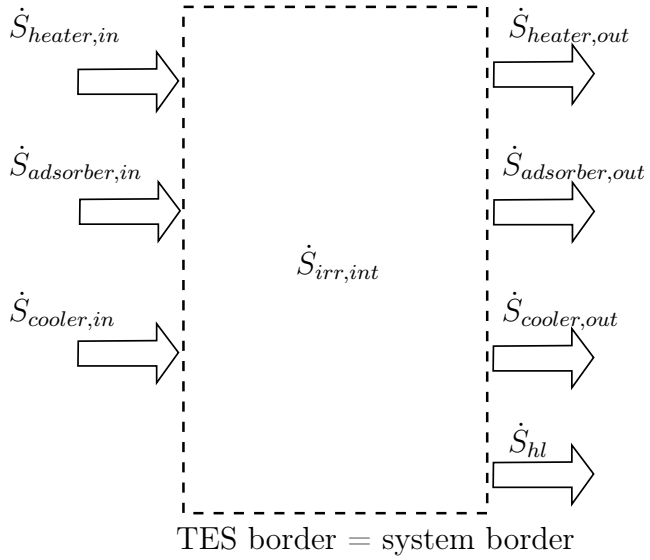

Figure 2.11: Internal entropy generation in the storage [28]. The system border here is at the outer surface of the tank insulation

The entropy change rate of a thermal energy storage process $\dot{S}_{tank}$ is,

$$\dot{S}_{tank} = \dot{S}_{in} - \dot{S}_{out} - \dot{S}_{hl} + \dot{S}_{irr,int} \tag{2.16}$$

where,

$$\dot{S}_{in} = \dot{S}_{heater,in} + \dot{S}_{adsorber,in} + \dot{S}_{cooler,in} \tag{2.17}$$

$$\dot{S}_{out} = \dot{S}_{heater,out} + \dot{S}_{adsorber,out} + \dot{S}_{cooler,out} \tag{2.18}$$

The rate of internal entropy generation is:

$$\dot{S}_{irr,int} = \dot{S}_{tank} - (\dot{S}_{in} - \dot{S}_{out}) + \dot{S}_{hl} \geq 0 \tag{2.19}$$

The Eq.2.19 when applied to the stratisorp cycle changes to:

$$\dot{S}_{irr,int} = \dot{S}_{tank} - (\underbrace{\dot{S}_{heater,flow} + \dot{S}_{adsorber,flow} + \dot{S}_{cooler,flow}}_{\dot{S}_{flow}}) + \dot{S}_{hl} \geq 0 \tag{2.20}$$

Now, let us derive the expression for the terms constituting $\dot{S}_{flow}$. The net rate of change of entropy flow into the tank associated with the heater flow is expressed as:

$$\dot{S}_{heater,flow} = \dot{S}_{heater,in} - \dot{S}_{heater,out} \tag{2.21}$$

[7] This system border should not to be confused with the stratisorp system border shown in Fig. 2.9. Here, the system border is only relevant for calculation of internal entropy generation in the TES

If the flow enters the tank from the heater with $T_{h,i}$ and leaves the with $T_{h,o}$ with mass flow rate $\dot{m}_h$, then the Eq. 2.21 can be modified as [55]:

$$\dot{S}_{heater,flow} = \dot{m}_h \cdot (s_{heater,in}(t) - s_{heater,out}(t)) = \dot{m}_h \cdot c_p \cdot \ln \frac{T_{h,i}(t)}{T_{h,o}(t)} \tag{2.22}$$

Similarly, the expressions for $\dot{S}_{adsorber,flow}$ and $\dot{S}_{cooler,flow}$ can be written as:

$$\begin{aligned} \dot{S}_{adsorber,flow} &= \dot{m}_{ads} \cdot c_p \cdot \ln \frac{T_{ad,i}(t)}{T_{ad,o}(t)} \\ \dot{S}_{cooler,flow} &= \dot{m}_c \cdot c_p \cdot \ln \frac{T_{c,i}(t)}{T_{c,o}(t)} \end{aligned} \tag{2.23}$$

The rate of change of entropy due the heat loss to the surroundings through the tank wall and the insulation can be etimated as [55], [28]:

$$\dot{S}_{hl} \approx \sum_{zone=1}^{N+1} \frac{\dot{Q}}{T_{amb}(t)} = \sum_{zone=1}^{N+1} U \cdot A_{zone} \cdot \frac{T_{zone}(t) - T_{amb}(t)}{T_{amb}(t)} \tag{2.24}$$

The rate of change of entropy in the tank is:

$$\dot{S}_{tank} = \lim_{\tau \to 0} \sum_{zone=1}^{N+1} m_{zone} \cdot c_p \cdot \ln \frac{T_{zone}(t)}{T_{zone}(t-\tau)} \tag{2.25}$$

The tank temperature is approximated by using finite number of temperature sensors. It is also assumed that the temperature of each tank zone is uniform across the diameter of the tank. Hence $\dot{S}_{hl}$ and $\dot{S}_{tank}$ are estimates for the real values. The rate of internal entropy generation in the tank during the stratisorp process can be computed by substituting Eq. 2.22, Eq. 2.23, Eq. 2.24, Eq. 2.25 into Eq. 2.20.

The mixing in the tank can be quantified based on the rate of entropy change of different tank zones. The tank can be considered to be made up of 15 cylindrical slices stacked on top of each other. Each slice has the mass m_{zone}. The entropy change rate of each zone can be computed according to Eq. 2.25. This entropy change rate does not directly infer the rate of internal entropy generation in the tank ($\dot{S}_{irr,int}$). The entropy change due to the mass flows crossing the system border ($\dot{S}_{flow}$) and the entropy change due to the plug flow across the zone boundaries should be subtracted to achieve the internal entropy generated in the stratisorp cycle. The later term is however very difficult to compute. The fluid in the tank is extracted from different locations at different times in one cycle as per the stratisorp system concept. It means that the flow scenario across any control volume in which the entropy balance is carried out also changes as the cycle progresses. The entropy generated in any zone between two adjacent rings is governed by the flow entering and leaving the tank from the adsorber and the temperature change of that zone[8]. As soon as the fluid is exchanged with another zone[9], the entropy generated in the previous zone is governed by only the temperature change due to mixing and heat loss to the environment. The temperature

[8] the heater and the cooler flow should be considered when calculating the entropy generated in the top and the bottom zones

[9] the next lower zone in case of adsorption half cycle or next upper zone in case of desorption half cycle

change as a result of mixing and the temperature change as a result of plug flow can be differentiated by comparison with the results obtained from a detailed numerical model of the system. For this reason, a more detailed analysis can be found in the thesis of Schwamberger [52]. The discussion regarding entropy change in this thesis are to be considered as a first step towards dynamic entropy analysis over the cycle and going further will require comparison with simulation data, which is beyond the scope of this work. Few representative results regarding the rate of change of entropy of different zones of the tank for the experiments discussed in this thesis can be found in appendix A.9.

2.5 Method for flow visualisation

The need to visualise and analyse the flow field in the stratified thermal storage is very important as mentioned in the previous chapter. There are number of classical flow visualisation methods available. In particular for the stratisorp system, the large scale flow phenomenon in the stratified thermal storage are of more significance than the velocity of flow in a small fluid volume.
Interferometry is one of such methods. However, a complex experimental set up using different lenses is required which makes this method expensive as well.
Laser Induced Fluorescence (LIF) is a laser optical method which uses the fluorescence images of a fluid with dye. The measured fluorescence intensity is proportional to the concentration of the dye and depending on the choice of the dye, proportional to the temperature. This method also has some drawbacks. The fluctuations in the laser intensity lead to directly proportional fluctuations in the fluorescence signal and the derived temperature from there. Moreover, for measurements over a longer period, the dye loses the fluorescence properties [29]. Apart from these technical drawback there are some practical issues. The LIF method needs a laser optical system and a special software. Due to unavailability of these resources the LIF method was not selected.
Background Oriented Schlieren or BOS (a common short form) [49], was a very attractive choice due to various reasons. The construction of the test set up is relatively simple. BOS method allows larger fields of views than traditional schlieren equipment [30]. The details of the test set-up and the theory of BOS are described in the following sections.

2.5.1 Principle of Background Oriented Schlieren method

The Background Oriented Schlieren method is a non intrusive flow diagnostic method. It is based on the principle that the light rays bend when passing through a field of variable refractive indices owing to density gradients. When these light rays coming from a background picture through the density field are captured in a camera, the image produced shows a virtual displacement of the background pixels as compared to the background picture without the density gradients. Figure 2.12 illustrates this principle.

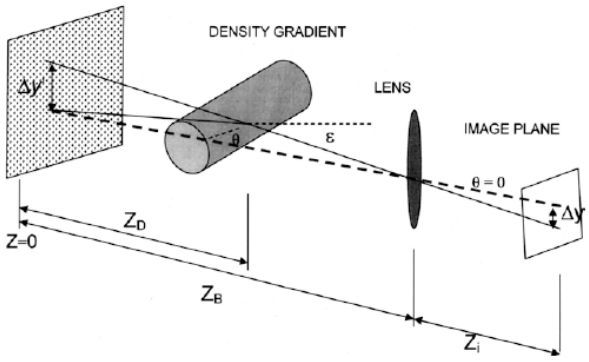

Figure 2.12: Principle of the BOS method [58]

Two images of a deliberately structured background are obtained. The first is through the undisturbed transfer channel and the second is through the phase object of interest. The

"difference" between these two images provide information about the phase object. The field gradients in the path of the imaging rays cause deflection of the light rays, leading to shifts in the image details. If Z is the line-of-sight direction in Fig. 2.12, then cross-correlation of these two images would yield the displacements of the background pixels in the x and y directions. The obtained displacements are the density gradients at each point in the field. The gradients of this density field yield an elliptical partial differential equation also known as Poisson equation which reads:

$$\frac{\partial^2}{\partial x^2}\rho(x,y) + \frac{\partial^2}{\partial y^2}\rho(x,y) = S(x,y) \tag{2.26}$$

where $S(x,y)$ is the source term calculated at each mesh point from the displacements obtained through correlation. The solution of Eq. 2.26 yields the line-of-sight integrated density distribution, which is a projection of the three-dimensional density field in the direction of viewing. The density distribution in a given plane is then calculated by means of a transformation from this projection [58].
BOS technique is very common in the experiments involved with air. It is a very attractive choice for determining the density field in the shock wave, the analysis of free jets and the analysis of wing tip vortices etc. Since the deflection of a single beam contains information about the spatial gradient of the refractive index integrated along the axial path, the image deflection ε is defined as :

$$\varepsilon = \frac{1}{n_0}\int_{Z_D-\Delta Z_D}^{Z_D+\Delta Z_D}\frac{\delta n}{\delta y}dz \tag{2.27}$$

Eq. 2.27 is only valid with the assumption that the half-width of the region of the density gradient $\Delta Z_D \ll Z_D$. Furthermore, the relation between the refractive index n and the density ρ is given by the Gladstone-Dale equation [40].

$$\frac{n-1}{\rho} = G(\lambda) \tag{2.28}$$

where $G(\lambda)$ is called the Gladstone-Dale constant and depends on the characteristic of the medium and frequency of the light used. Values for $G(\lambda)$ can be found in the handbook of physical chemistry. Using the mathematical treatment explained before and the equations (2.27) and (2.28), the density of the object of interest can be determined. For phase objects having axial symmetry, quantitative results can be derived from one projection using Abel inversion technique [24]. Similarly, fluid properties can be successfully measured for two-dimensional planar flows. As seen before, schlieren is an integrating optical method. Therefore its use as a quantitative method in unknown three-dimensional flows requires tomographic reconstruction [30]. For objects with higher complexity more projections are needed. Atcheson *et.al.* [6] used 16 high definition camcorders to analyse non-stationary gas flows. Goldhahn *et.al.* [25] incorporated 8 cameras to measure density of air behind straight blades placed in the flow.
In this work with the goal of visualisation of the density gradients in a stratified thermal storage, multiple projections of the flow field would be required in order to reconstruct the 3-D density field. As the flow is neither axisymmmetric nor planar, only one projection would yield

a qualitative information about the density gradients which leads to qualitative information about the temperature gradients. Moreover, the flow in the tank is highly unsteady. The tomographic reconstruction is out of the scope of the present work. Qualitative BOS combined with a reasonable spatial resolution of temperature sensors along the axis of the tank will provide quantitative information about the flow in the tank.
The literature survey for BOS revealed that this technique has mostly been used to analyse flow phenomenon involving air. The investigations of flow properties with water as the medium using BOS has been carried out by very few research groups. Moreover, the know-how about this technique was also not available at FSM. Therefore, a very simple test set-up was built for understanding the basics of BOS which would eventually help for implementation on the stratified storage tank.

2.5.2 Experimental set-up to demonstrate the Background Oriented Schlieren method

Hampel M. investigated the mixing of two flows at different temperatures using flow visualisation techniques, such as LIF, PIV and dye ink tests [29]. Theoretically, similar investigations, however qualitative, can be carried out using BOS technique. Hence a plexiglas tank with the same dimensions as used by Hampel was built. Figure 2.13 shows the schematic of this test set-up.

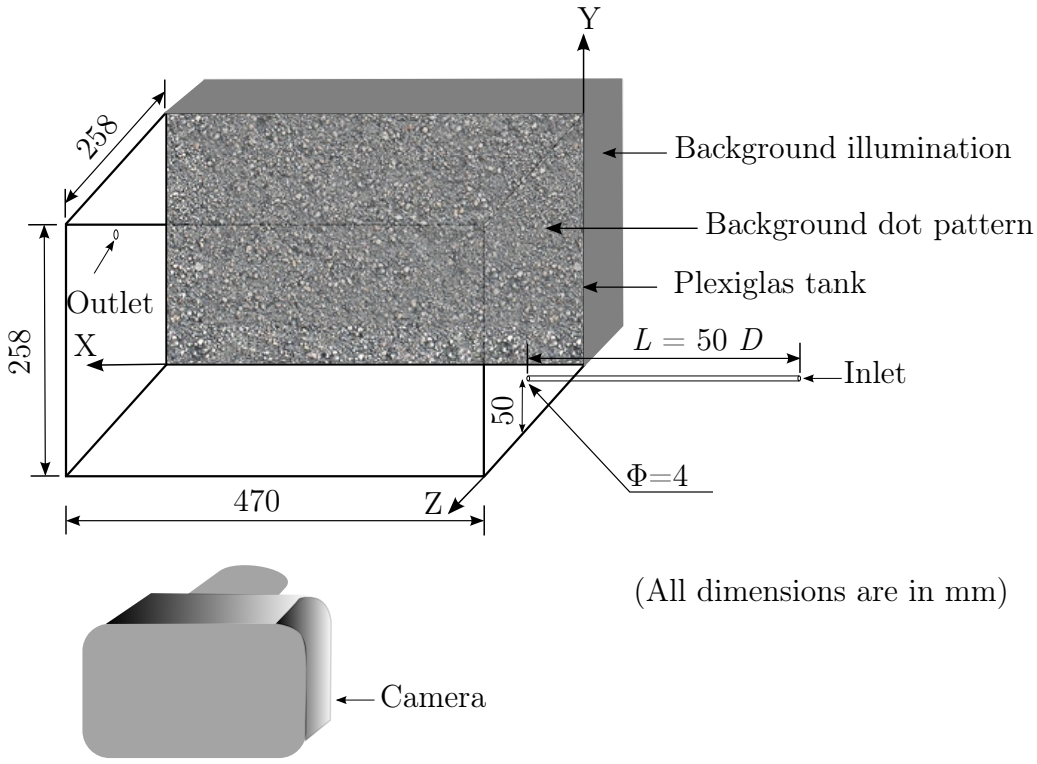

Figure 2.13: Test set-up to demonstrate the BOS technique

The test measurements were carried out in co-operation with the colleagues from French-German Research Institute of Saint-Louis (ISL). A slightly different method than the conventional BOS technique had been used. In order to increase the performance of the conventional Background Oriented Schlieren technique (BOS) the monochromatic background is replaced by a coloured dot pattern [38]. Canon EOS-1Ds Mark II with 16 megapixel was placed as shown and focussed on the background placed on the other side of the tank. This background was illuminated by a matrix of filament bulbs integrated in a wooden box. The inlet section of the flow was kept at $50 \cdot D$ so that a fully developed flow field could be achieved at the inlet. Using this set up, two different measurements were carried out. Table 2.1 lists the relevant experimental boundary conditions.

	measurement 1	measurement 2
Initial temperature	25 °C	20 °C
Inlet temperature	30 °C	40 °C
ΔT	5	20
Flow rate	3 lph	12 lph
Velocity	6.6 cm/s	26.5 cm/s
Reynold's number	264	1060

Table 2.1: BOS test set up parameters

For both the measurements, at first an initial picture of the illuminated background was recorded with undisturbed water. The flow was then started and sequence of the background pictures was recorded by the camera. These pictures, when compared with the original background picture using cross-correlation algorithm, produce images showing apparent shift in the background pixels within the flow field. Figure 2.14 depicts the results of the cross-correlation applied on these two measurements.

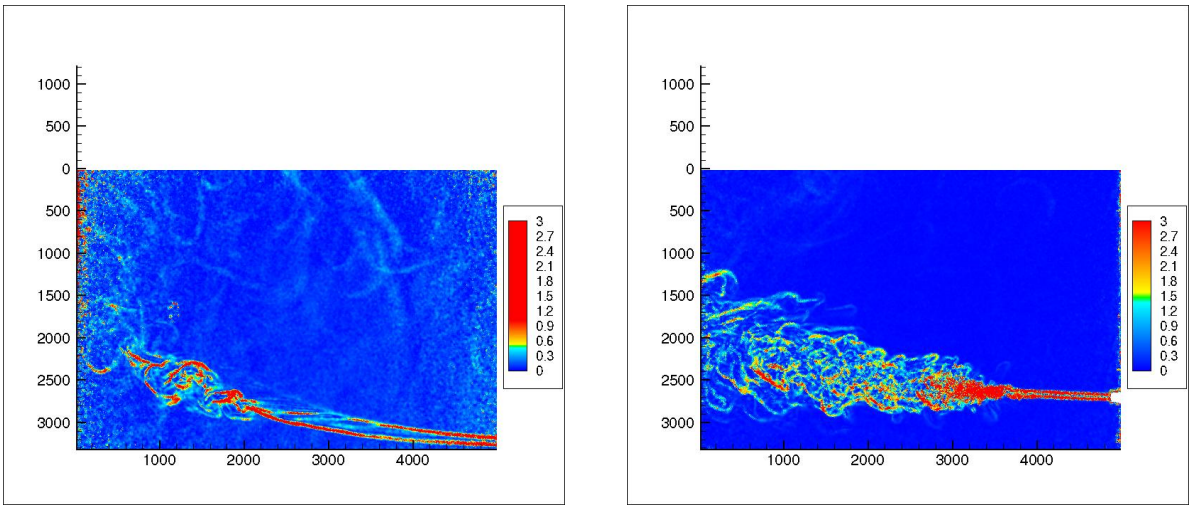

(a) Measurement 1

(b) Measurement 2

Figure 2.14: BOS evaluation of jet of warm water entering a tank containing cooler water after (a) 60 seconds and (b) 15 seconds. The scale indicates pixel shift computed from cross-correlation.

The virtual pixel shift can only be observed in the directions perpendicular to the direction of viewing. As the direction of viewing here is Z direction, the density gradients can only be observed and analysed for the X and the Y directions. Figure 2.15 explains schematically the procedure of cross-correlating. A standard PIV (**P**article **I**mage **V**elocimetry) algorithm subdivides the images into interrogation windows the size of which can be preselected by the user.e.g. 32 pixels x 32 pixels, 16 pixels x 16 pixels. The background image captured with undisturbed water is compared window by window with each subsequent image captured with the flow already started. The probability distribution of the shift in the pixels is computed using the auto correlation function.

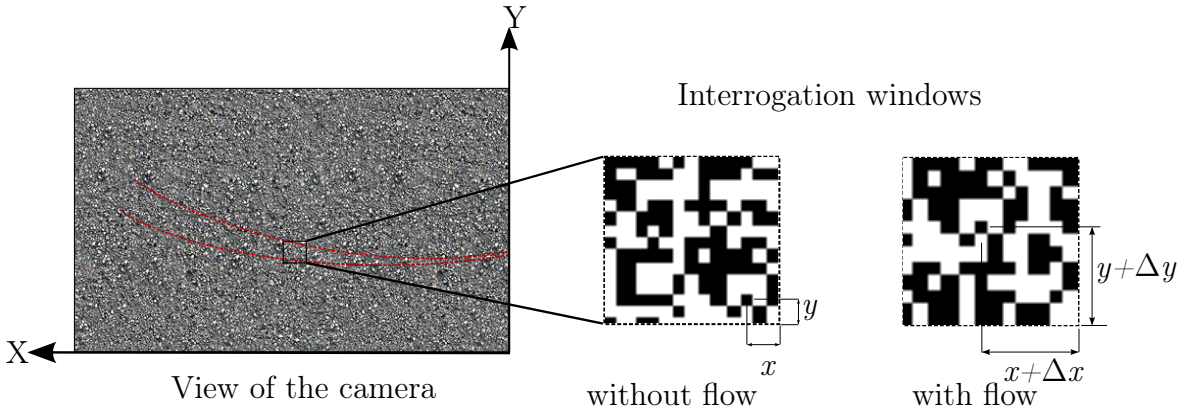

Figure 2.15: Computation of pixel displacement using cross correlation

In Fig. 2.15, one of the pixels in the interrogation window is shifted by Δx in the X direction and by Δy in the Y direction.The displacement of this pixel in X and in Y directions can be represented as :

$$pixel\ shift = \sqrt{\Delta x^2 + \Delta y^2} \tag{2.29}$$

Thus, the contours in Fig. 2.14 depict the resultant of the virtual pixel shifts in X and in Y direction.The sequence of the images for measurement 1 were converted into a film. It is observed that the jet of warm water slowly inclines towards the top of the tank with time. This happens due to the upwardly acting buoyancy force.
It can be seen that even for a very small temperature difference between the entering water and the water in the tank, a considerable pixel shift is observed. It is a very important result as it proves that the BOS technique can be used for qualitative visualising of the mixing of two liquids at two different temperatures. Later it will be shown that this technique is effective even at smaller temperature differences than considered in this experiment.

Chapter 3

Preliminary Investigations

3.1 Experimental investigations

3.1.1 Experimental set-up to visualise density gradients in a cylindrical tank

The facts about the BOS technique were tested and established with the experiment described in the previous chapter. This technique would eventually be used to visualise the temperature gradients in a cylindrical tank. It was necessary to test the functionality of this technique on a smaller cylindrical tank before applying it on a larger tank (volume $\approx$ 500 litres). The study of the mixing of two fluids at different temperatures in a cylindrical tank arrangement, the study of the thermal stratification behaviour at different temperatures and the study of stratification based on dimensionless numbers was also important. These investigations would be very challenging to carry out on a tank which is simultaneously a part of the adsorption cooling system. Therefore, a much smaller tank (approx. 10 L) was selected to carry out these studies. These investigations of flow in this tank can be carried out independent of the adsorption chiller. Moreover, a smaller tank with rotationally symmetric fluid entry would eliminate the need of complicated and expensive three dimensional CFD models. The experimental results obtained from this test set-up can be used for qualitative validation of CFD models. A rotationally symmetric flow condition would additionally improve the stratification in the tank by creating and maintaining the thermocline [35].

Design and construction of the tank

By far, the most important criterion for the design of the tank was the optical access to the fluid. The material of the tank should be able to transmit light through the walls without much loss of intensity. For the reasons of workability and robustness, polymethyl methacrylate (PMMA) which is commonly known as plexiglas, was chosen as the material of the tank.

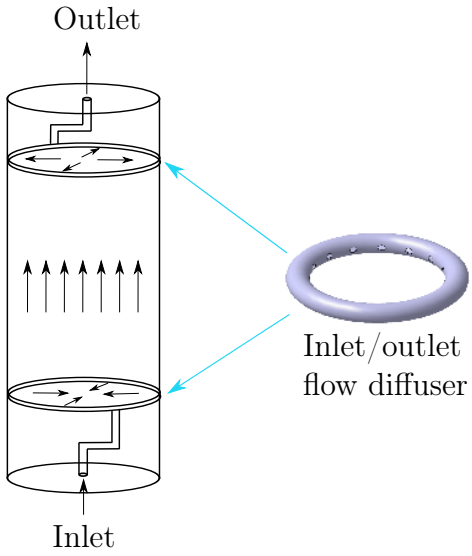

Figure 3.1: Plexiglas pipe and flow diffusers

As the first obvious choice, a simple plexiglas pipe was chosen for this experiment (Fig. 3.1). Flow diffusers made of plastic tubes in ring shape and holes for radial entry of water were initially used. The black arrows schematically show the direction of water flow in the tank. The radial entry of water in the tank was sought after due to the reasons explained before. However the curved surface of the tank caused problems for the BOS evaluation. Different experimental arrangements are shown in Fig. 3.2. The background image appeared mirrored as the tank filled with water worked as a magnifying lens for the arrangement A. To avoid this effect, a relatively wider background was needed. In case of the arrangement B, only the centre of the background image was correctly focussed which obviously was a huge drawback. In addition to the problem of correctly focussing the background, the pixels of the background image were extremely distorted for arrangement C.

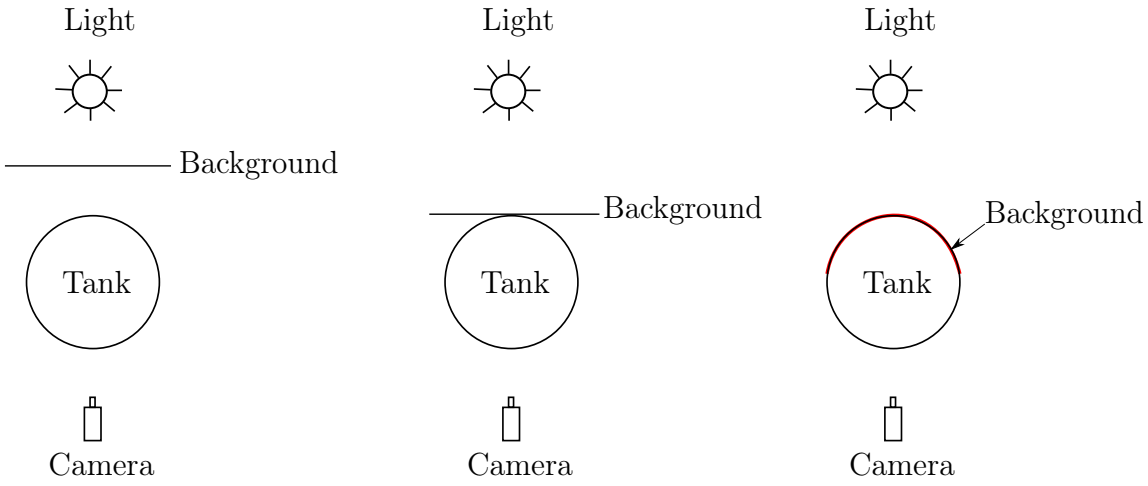

A) background at a distance B) tangential background C) wrapped background

Figure 3.2: Different positions of the background with respect to the the tank

Owing to these drawbacks, it was clear that the tank should be built in such a way that it offered a flat surface in the front and at the rear of the tank but still maintained the cylindrical

shape of the tank. This was achieved by machining cylindrical cavity in rectangular plexiglas blocks and plates and stacking them on top of each other. Fig. 3.3 elaborates this set-up.

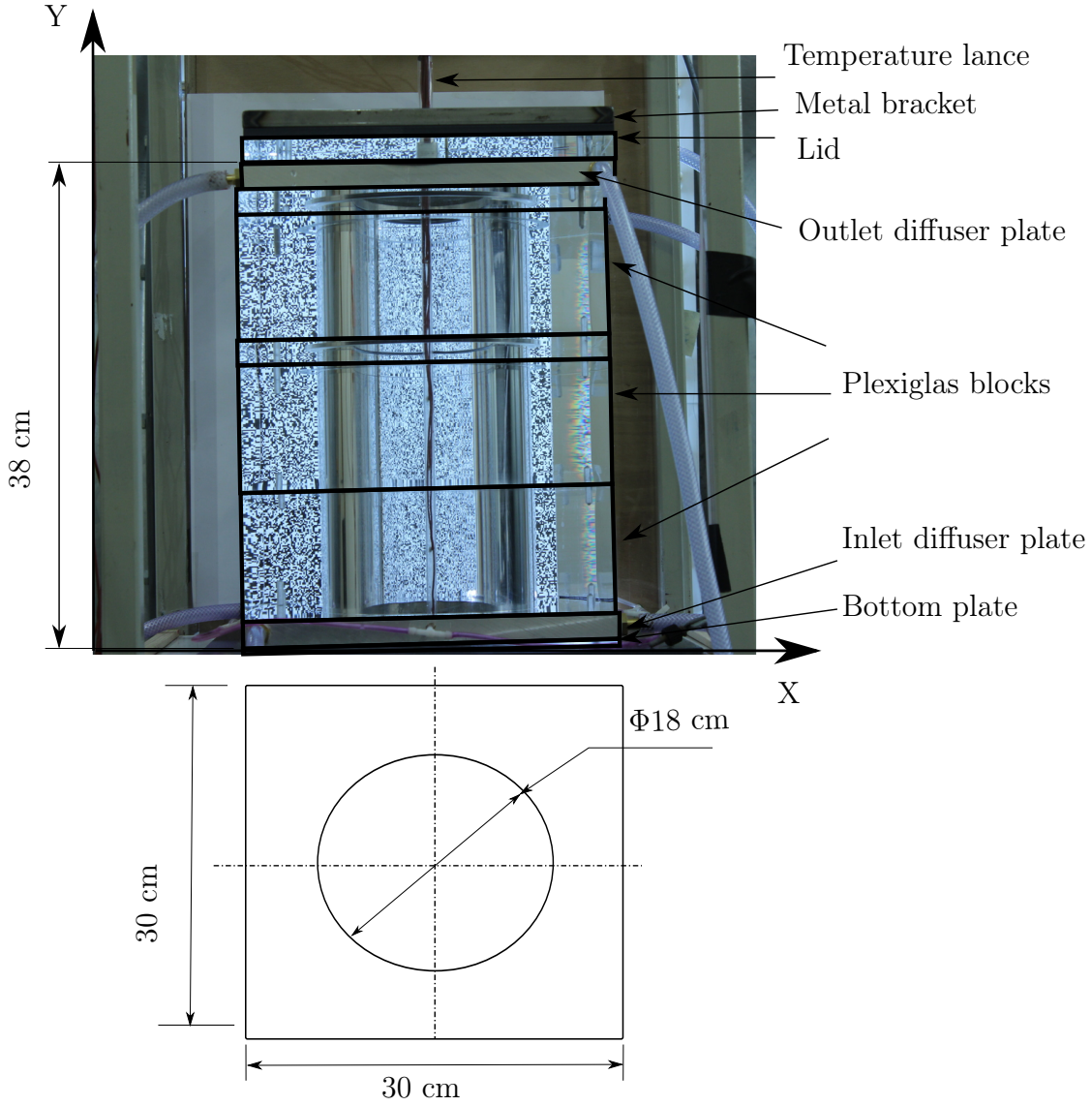

Top view of a plexiglas block

Figure 3.3: Plexiglas blocks and plates forming the tank

Window sealing was used to seal the interfaces between two adjacent blocks or the interfaces between the blocks and the plates. Dowel pins were used to guide the plates and the blocks to coincide the cylindrical cavities of adjacent components. The whole stack of the blocks and the plates was clamped using big iron clamps. A square metal bracket and a PVC plate were instrumental in distributing the load uniformly on the sides and thus holding the whole stack in place. This stack thus forms a cylindrical tank which can contain approximately 10 litres of water. The entry of water to the tank was achieved through a inlet diffuser plate made of aluminium. The steps leading to the final design of this plate are discussed in the next section. A plexiglas plate was fixed at the back of the tank few centimetres away from the tank surface. A background pattern consisting of randomly

distributed black squares on a white background was stuck at the back of the plexiglas plate. This background was illuminated by six neon tube lights (14 W each) contained in a wooden box. Fig. 3.4 schematically shows the side view of this whole construction.

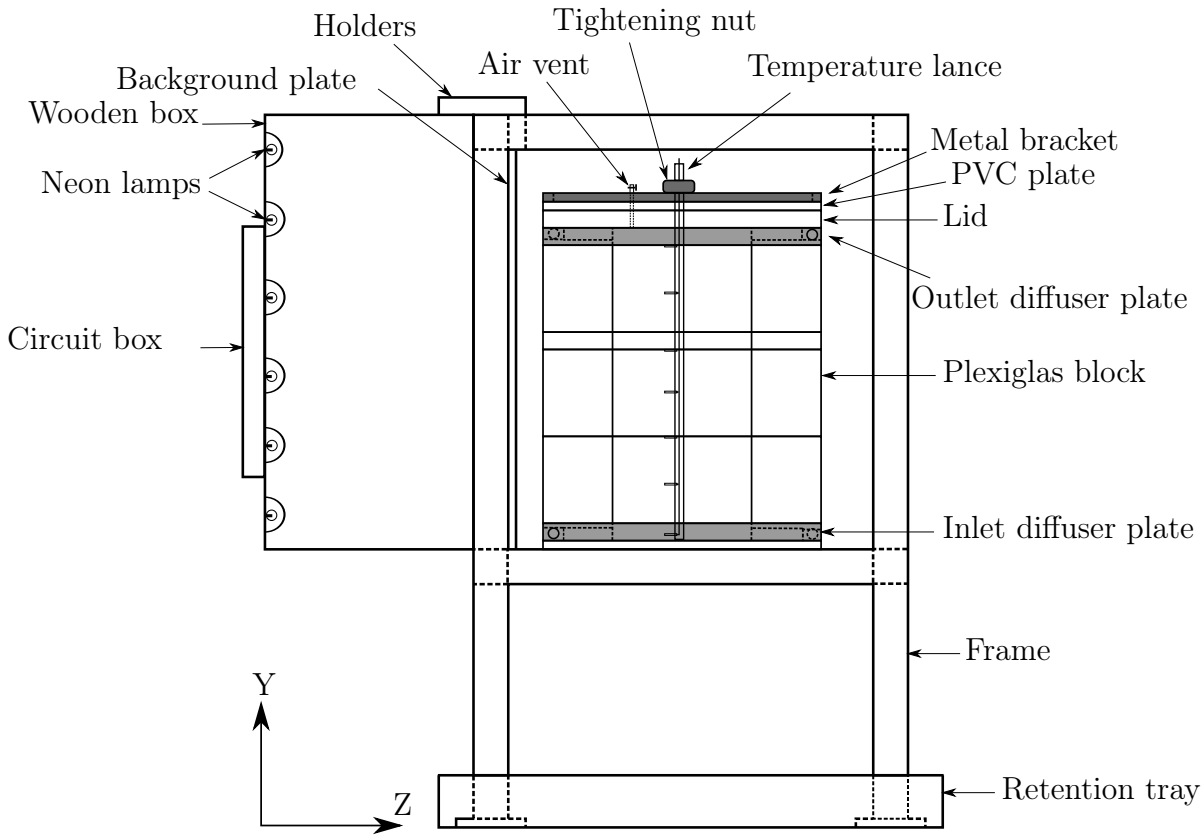

Figure 3.4: Side view of background illumination fixture and the plexiglas blocks

Measures to achieve rotationally symmetric inflow condition

The necessity of rotationally symmetric fluid entry has already been stressed in the previous section. The design of the inlet diffuser plate is the deciding factor in achieving it. The design goal of the inlet diffuser plate was to find very simple construction of the plate which leads to a rotationally symmetric fluid flow condition. Therefore, a single entry approach was initially used in which the water entered a ring-channel machined in a plexiglas plate through a single entry hole of 8 mm diameter drilled at the side and tangential to the ring channel. The fluid would flow towards the tank cavity through semicircular grooves before passing through a gap 1 mm. This construction is explained in Fig. 3.5.

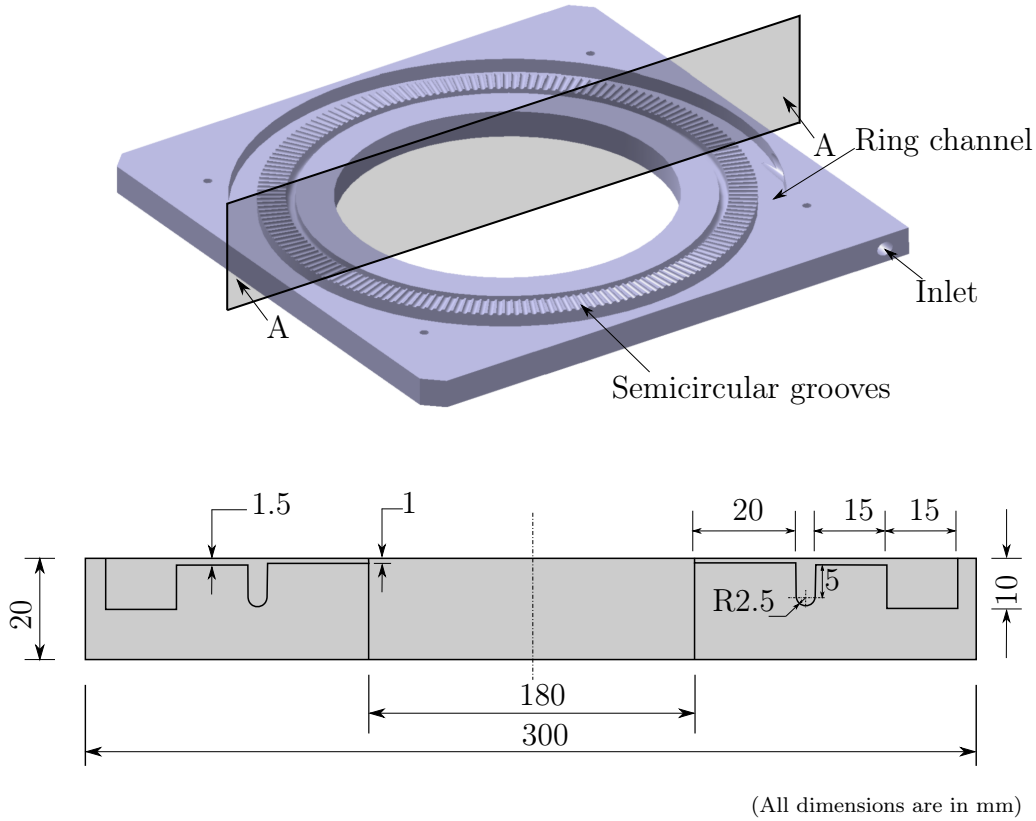

Figure 3.5: Sectional view of the inlet diffuser plate

The semicircular grooves were directed towards the centre of the tank. The idea behind this kind of construction was to introduce water into the tank cavity in radial direction only. Moreover, a 9 mm deep circumferential groove to homogenise the flow leaving the semicircular grooves. The performance of this design was tested using dye ink test at 180 lph.

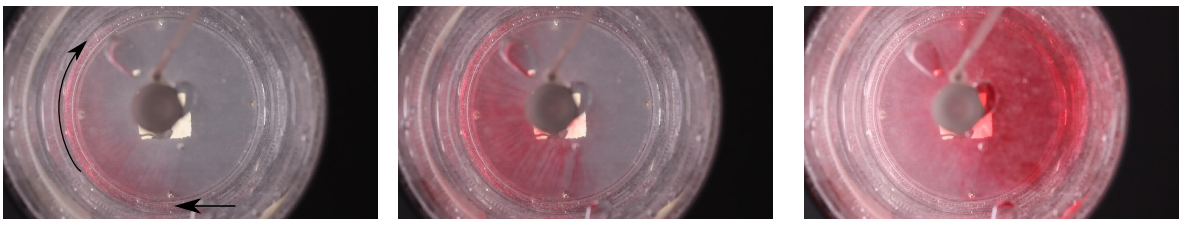

(a) after 2 sec. (b) after 4 sec. (c) after 12 sec.

Figure 3.6: Dye ink test of the inlet diffuser plate

Fig.3.6 shows the top view of this test. The arrows indicate the direction of the flow in the ring channel. It can be seen that the flow development is non uniform. A significant part of the flow has already entered the tank before the flow makes one complete rotation around the axis. Jets are formed in spite of using the circumferential groove. These jets collide against the opposite side and after 12 seconds it is clear that the upward flow has an

offset from the axis. However, the flow has almost no circumferential component.

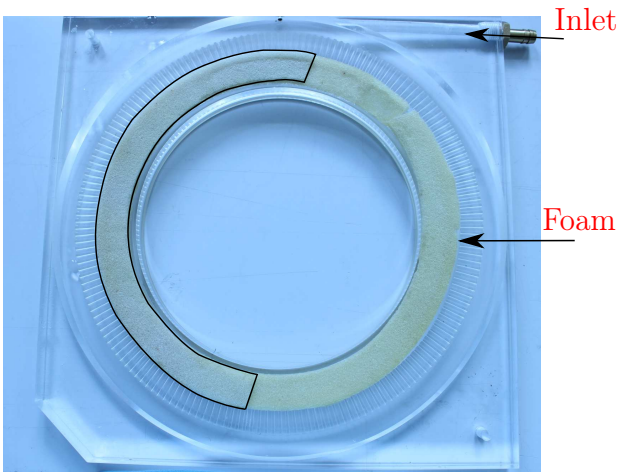

Figure 3.7: Selective damping using foam

If the flow enters the tank cavity with high velocity, it proves detrimental to the stratification in the tank. Hence it was essential to reduce the velocity of incoming water. Foam stripes of 2 mm thickness were used to cover the gap of 1 mm (refer Fig. 3.5) to test the effect of damping on the flow distribution. From Fig. 3.6 it can be seen that the flow enters in the tank through the initial semicircular section of the ring channel. Therefore an additional layer of foam was used in this region to provide more damping against the flow. Fig. 3.8 shows the development of the flow distribution using this configuration. However, this new measure did not show any significant improvement over the previous design of the inlet diffuser plate. The flow distribution shows a similar pattern like seen in Fig. 3.6.

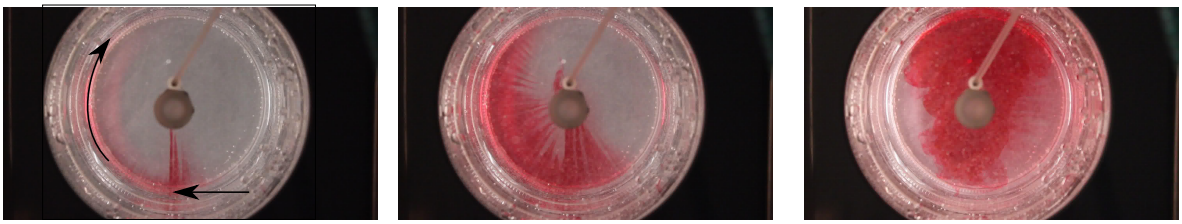

(a) after 2 sec. (b) after 4 sec. (c) after 12 sec.

Figure 3.8: Effect of selective damping on flow distribution

After carrying out intensive dye ink tests on these two different configurations, it was inferred that the flow should enter the ring channel from at least one more location. It could lead to better uniformity in the flow distribution. Occurrence of one more inlet could be eliminated by widening the inlet port into a triangular cavity as shown in Fig. 3.9. Such cavity would lead the flow into the ring channel equally on both sides. Additionally, a piece of reticulated foam of 20 ppi was placed in the triangular cavity. This piece of foam would help to reduce the inlet flow velocity. The velocity of the incoming flow was further reduced due to increase in the inlet cross section by approximately 18 fold. The semicircular grooves (shown in Fig. 3.5) caused the flow to exit with small jets into the tank. Hence these grooves were removed by CNC machining and flattened to form a gap of 1.5 mm. A steel mesh manufactured from 0.26 mm thick steel wires forming a mesh size of 0.5 mm and open mesh area of 46 % according to ISO 9044 was placed.

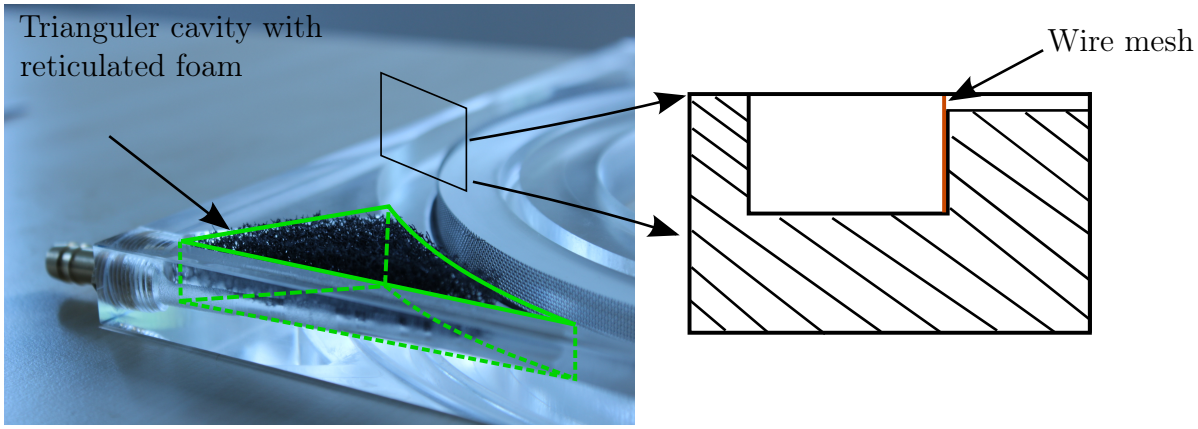

Figure 3.9: Inlet diffuser plate with triangular cavity and reticulated foam. The wire mesh in the ring channel works as flow equaliser

The effect of the above mentioned measure is depicted in Fig. 3.10. The flow starts to distribute in the directions of the arrows. This time the flow is able to enter on the both sides of ring channel. After 4 seconds it seems as if the flow has achieved the rotationally axisymmmetric condition. However, it is clear after 12 seconds that the flow has drifted on one side more than the other.

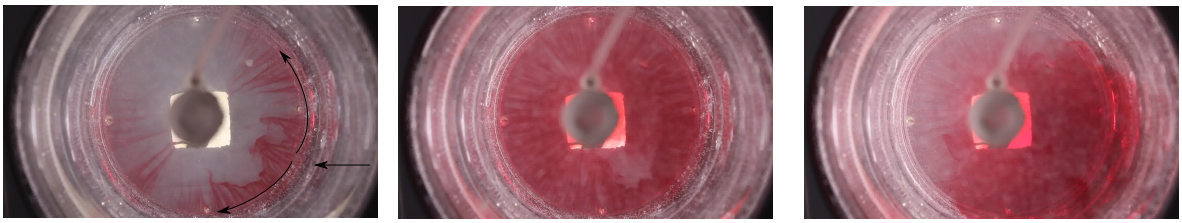

(a) after 2 sec. (b) after 4 sec. (c) after 12 sec.

Figure 3.10: Effect of flow equaliser (steel mesh) and triangular inlet cavity on flow distribution

Hence it was inevitable to provide one opening on each side of the plate i.e. total 4 openings. It was also observed that the thickness of the readily available plexiglas plates varied over the length and the breadth of the plates. However small, these variations were responsible for varying the gap available for the flow, inducing more non uniformity. Hence a new plate with 4 openings was made from aluminium. The velocity of the flow was further reduced by removing the material between the edge of the ring channel and the edge of the tank cavity. Here again, the wire meshes were placed where the edge of the ring channel existed and just before the tank cavity. This construction is elaborated in Fig. 3.11.

The idea behind using wire mesh at two locations in the plate before the tank cavity was to change the direction of the flow gradually from circumferential to radial. To achieve the entry of the water exactly at the bottom of the tank, the inlet aluminium plate was mounted as shown in Fig. 3.12. During the initial tests using this plate configuration, it was noticed that the air bubbles accumulated in the ring channel as the plate is placed in an up side down position with respect to the previous configurations. This remaining air significantly affected the uniformity of the flow and hence it was essential to remove it thoroughly. Therefore

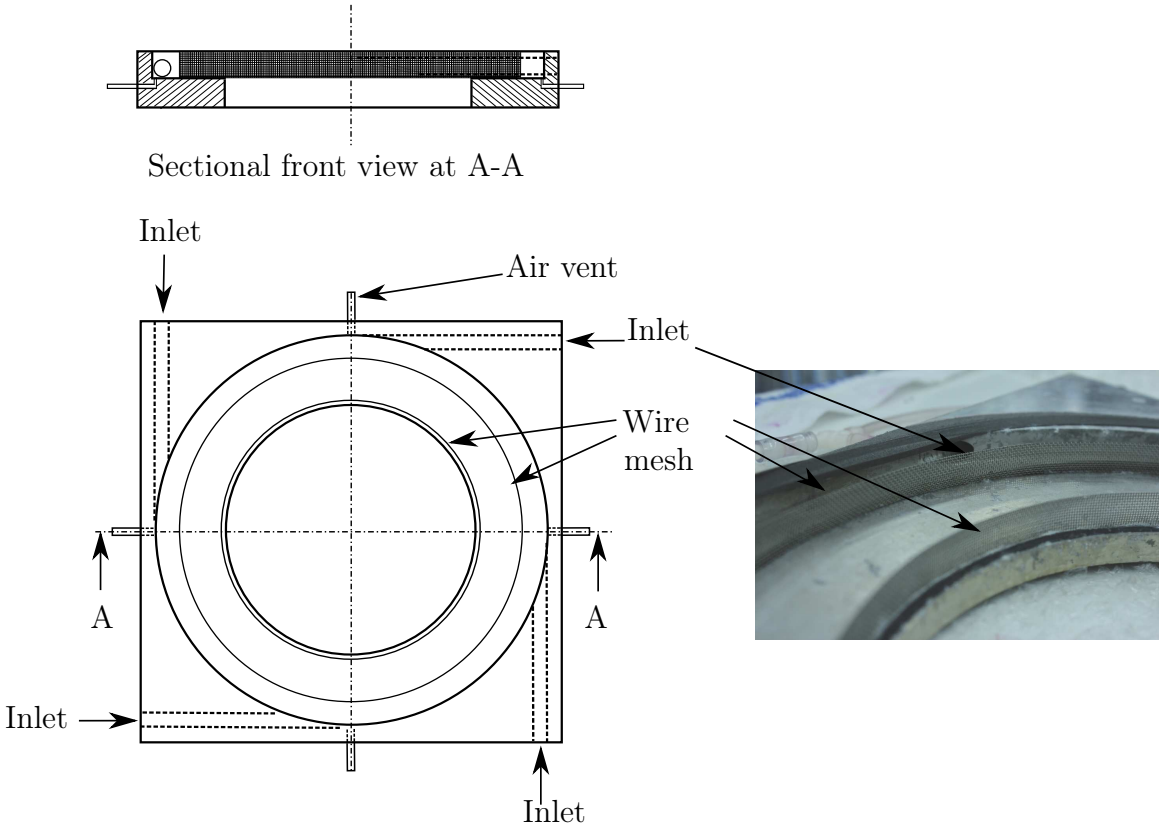

Figure 3.11: Aluminium plate with four tangential inlets and wire meshes for flow equalisation

four air vents, one on each side of the plate were drilled as shown. All four vents were interconnected with plastic tubes from out side of the plate to form a common deaeration port. At the start of each experiment, the deaeration was carried out from this port and for rest of the experiment the port was sealed using a clamp.

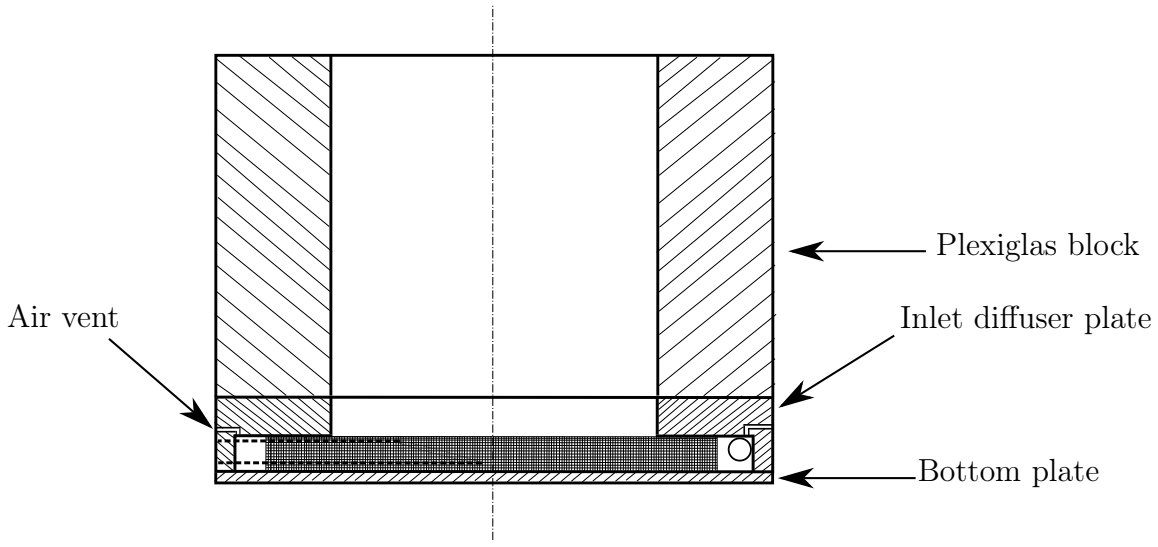

Figure 3.12: Assembly of the aluminium plate and first plexiglas block

The remaining plates and blocks were stacked on top of the stack formed (Fig. 3.12) which resulted in the complete tank set-up (Fig. 3.3 and Fig. 3.4). A plexiglas tube of 10 mm internal diameter was used to hold seven Pt-1000 temperature sensors placed at every 5 cm. This tube was fixed vertically at the centre of the tank forming the axis of the tank [1]. Similar to the previous case, an ink test was carried out for this experimental arrangement. The results of this test are shown in the Fig. 3.13. The arrows indicate the direction of the flow in the inlet and in the ring channel. It can be clearly seen that the wire meshes successfully change the direction of the flow. The flow is very symmetric as well as the velocity of the flow is considerably reduced.

(a) after 2 sec. (b) after 4 sec. (c) after 12 sec.

Figure 3.13: Flow distribution in the tank using aluminium plate with steel wire meshes.

Consequently this configuration of the inlet diffuser plate was used for the following BOS measurements. A second aluminium plate was placed under the lid of the tank. It functioned as the outlet diffuser plate.

3.1.2 Experimental set-up

The condition of rotationally symmetric flow was achieved after the steps were carried out in section 3.1.1. The tank was then integrated in the test set-up shown in Fig. 3.14. The main purpose of this test set-up was to be able to condition the water in the tank at an initial temperature and then to be able to introduce water at a different temperature in the tank at a defined flow rate. It was achieved using two containers for warm and cold water, two circulation pumps, a volume flow meter, an electric heater and two 4-way valves. A detailed documentation of the functioning of this test set-up can be found in [23]. Canon EOS 600D with 18-55 mm zoom lens was chosen for taking the pictures for BOS analysis. The temperature measured by the Pt-1000 sensors and the volume flow measured by the magnetic inductive flow meter was stored using a data acquisition program developed in LabView (refer appendix A.2). The camera was placed in front of the tank so that the centre of the lens coincided with the axis of the tank (the temperature lance).

[1] refer appendix A.1 for the data related to the calibration of these sensors

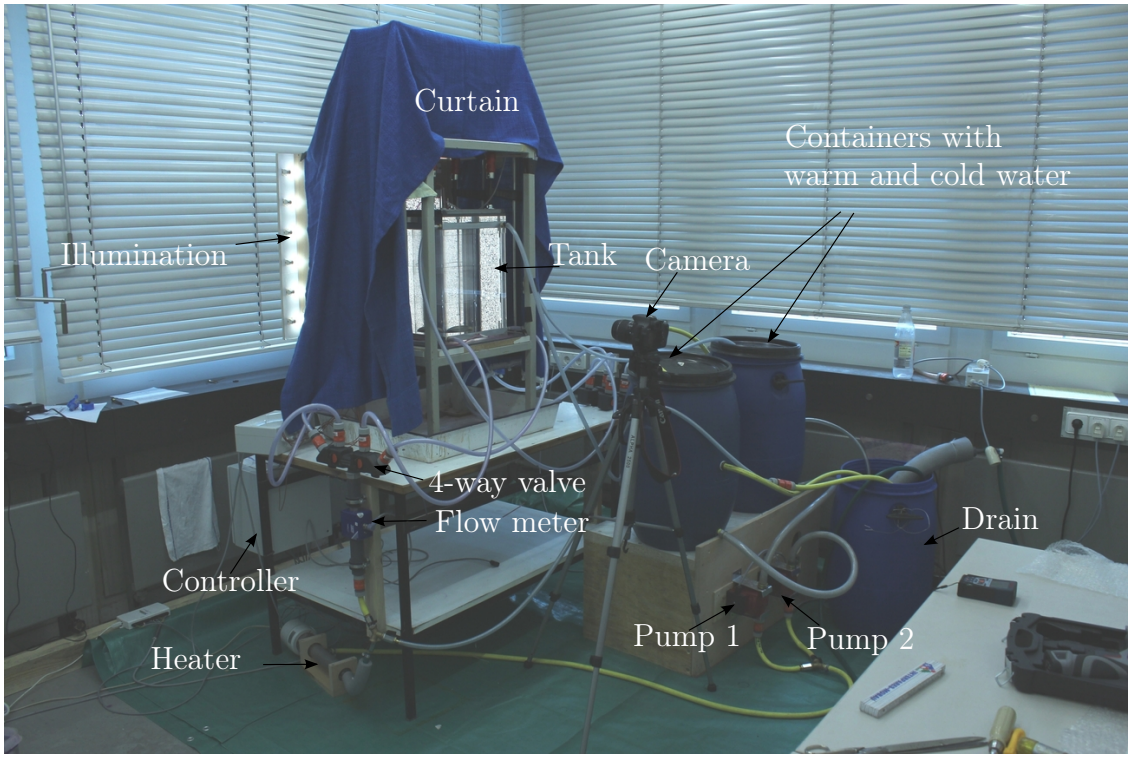

Figure 3.14: Experimental test set-up to visualise the density gradients in the plexiglas tank

For a non stationary case discussed in the following section, the video mode of the camera used to record videos of the flow in the tank at 25 fps. The recorded video was then broken into images (25 images/second) resulting in the image resolution of 2 megapixels. The resolution of the background picture was so selected that even in the upright position of the camera and picture resolution of 2 megapixels, the BOS evaluation would lead to reasonable quality of the results. Backgrounds of different resolutions were printed and tested in a test experiment. The background was printed on poster paper and the image was scaled (height/width = 1.5) in order to fit exactly in the area behind the plexiglas tank. Due to the use of video mode of the camera no lossless recording was possible (video codec: .mov). Hence a coarse resolution of the background picture was necessary. It was found that resolution of 100000 points was sufficient for the experiment. This resolution meant that each point of the background image was resolved by up to 20 pixels of the camera chip. The results of the flow visualisation experiments using this set-up are discussed in section 3.2.

3.2 Flow visualisation experiments

The experimental test set-up was used to investigate two different flow phenomena in order to demonstrate the BOS technique on a thermally stratified tank namely

1. Transient flow field
2. Stationary flow field

3.2.1 Transient flow field

A transient flow field is generated when a flowing fluid at a certain temperature mixes with another fluid, (either moving or stationary) at a different temperature resulting into a zone of mixed fluid. The discharging process of a storage of a solar heating system is a practical example of a transient flow field. Such condition can be achieved when the water in the plexiglas tank is conditioned at 40 °C (stationary fluid) and the water at a different temperature (moving fluid) is introduced into the tank. At the start of the charging process of the storage tank, a gravity current of the cooler fluid flows across the bottom of the tank [32]. A thermal transition layer called a thermocline, forms between the warm fluid contained in the tank and the cool fluid entering into the tank near the inlet diffuser. The first pass of the current across the tank is responsible to form most of the thermocline [7]. As the bottom plate of the plexiglas block-plates stack is made non-transparent material (aluminium), the gravity current was optically inaccessible.

Canon EOS 600D captures images with maximum frequency of only 3.7 fps at maximum resolution of 18 megapixels. The classical BOS technique had to be adapted for capturing this highly transient flow field. The background image was adapted accordingly as explained earlier. The first image from the sequence of the images obtained was considered as the background image. It was assured that the video and the data acquisition started simultaneously after which the flow of water through the tank was switched on. The frequency of the data acquisition was matched with the frame rate (25 Hz). The drop in the temperature recorded by the first sensor was considered as starting point of the experiment. The recorded video was edited and analysed during the same time interval. The sequence of the images obtained from the video was compared with the background image using cross-correlation to obtain a flow film.

The tank was pre-conditioned at 40 °C. The inlet temperature and the flow rate was varied between 20 °C (i.e. $|T_{tank} - T_{inlet}| = 20$ K) and 35 °C (i.e. $|T_{tank} - T_{inlet}| = 5$ K) and 360 lph and 180 lph respectively. An additional measurement was carried out in which only the inlet temperature was set to 38 °C keeping the flow rate constant at 180 lph. Fig. 3.15 depicts the comparison between the measurements after 1 minute. Here both inlet temperature and the flow rate were varied. Fig. 3.15(a) shows the temperature profile in the tank after 1 minute of measurement in which the inlet temperature was varied between 20 °C and 35 °C while the flow rate was constant at 360 lph. Likewise, Fig. 3.15(b) shows the experimental result for the same combination of inlet temperatures. Here the flow rate was set to 180 lph.

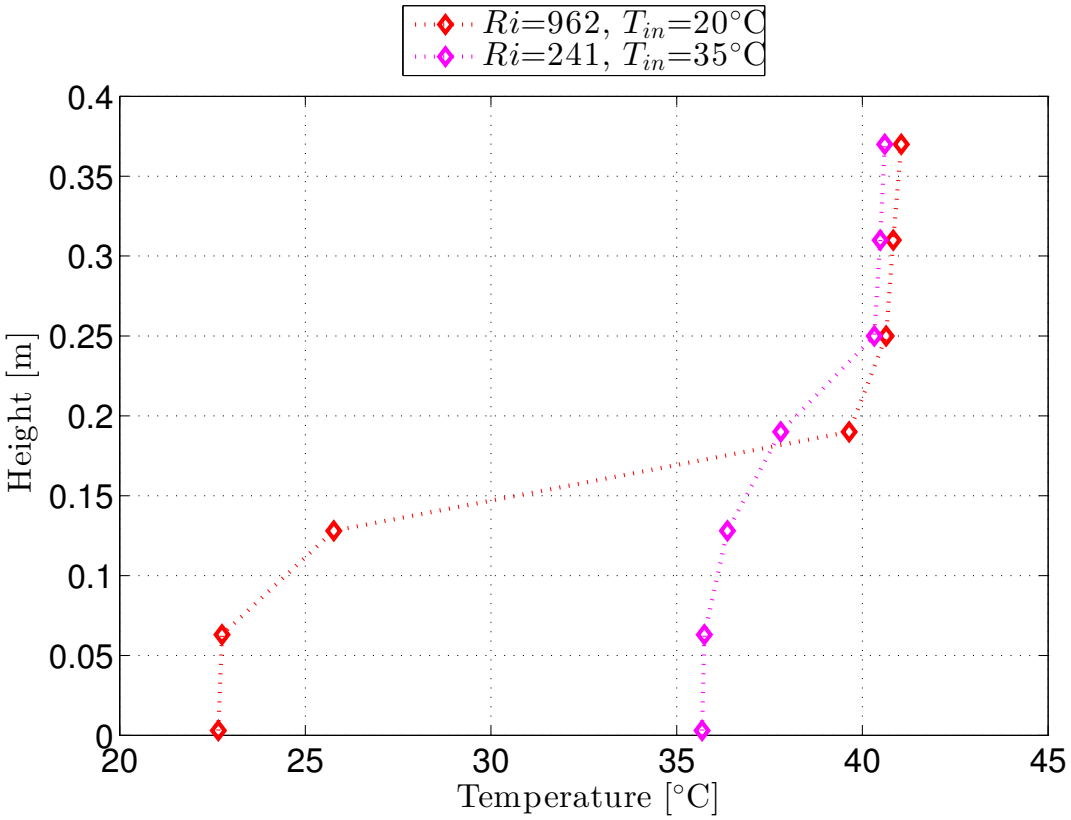

(a) $\dot{V}$=360 lph

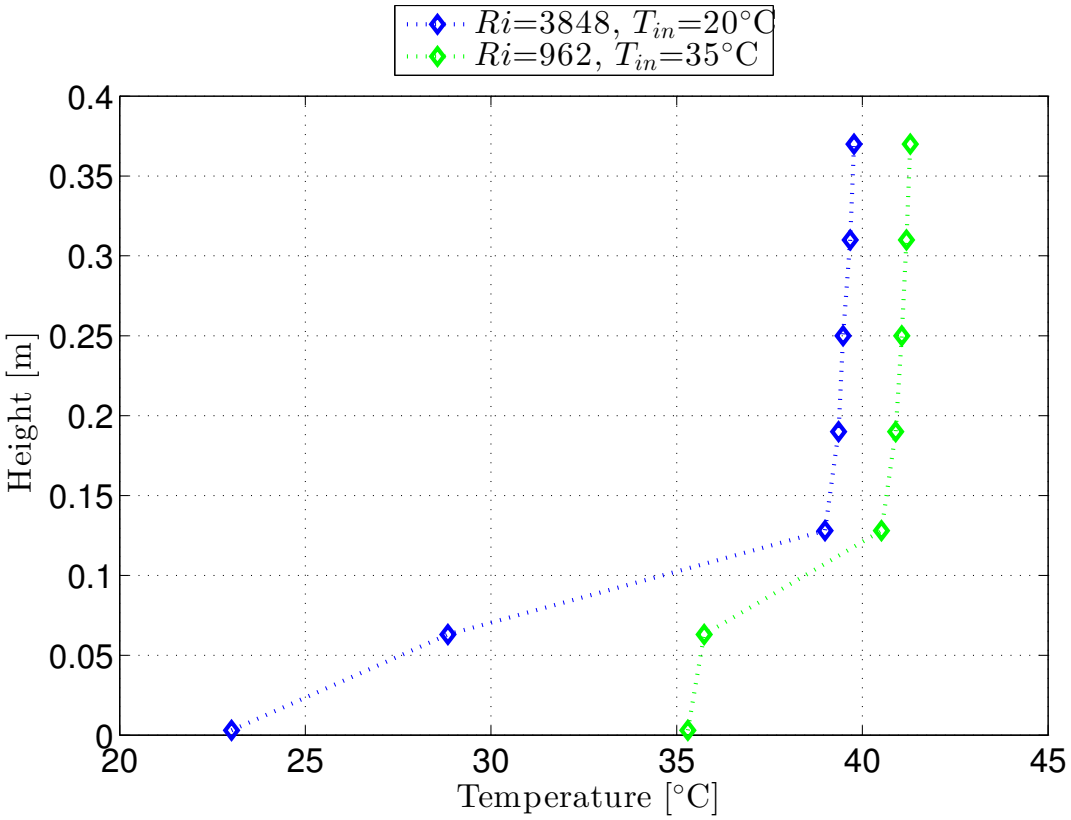

(b) $\dot{V}$=180 lph

Figure 3.15: Effect of Ri number on stratification

The initial temperature profile near the top of the tank after conditioning did not match exactly for all cases. Therefore a deviation of the order of 0.5–1 K can be observed in each experiment. The Richardson number considered here is based on the height of the tank. As discussed earlier in chapter 2, the Richardson number has a decisive effect on the formation of thermal stratification. Many research works have concluded that higher values of the Richardson number are beneficial to the thermal stratification [63]. This fact can be observed in the diagram as well. In both the diagrams it can be observed that for higher Ri numbers, the change from cold region to the warmer region is rather sharper than for the lower Ri numbers. In Fig. 3.15(a) the first four temperature sensors and in Fig. 3.15(b) the first three sensors near the bottom of the tank are relevant for this discussion. The first two sensors in Fig. 3.15 (a) qualitatively show similar trend of temperature change. The third sensor and the fourth sensor show considerably higher change in temperature for higher Ri number (Ri=962) than for lower Ri number (Ri=241). A steeper trend till the fourth sensor in case of a lower Ri number suggests that the incoming water in the tank has mixed well with the water in the tank in this region. In other words, the tank is in more stratified state for higher Ri numbers while it is in a more mixed state for lower Ri numbers. A similar effect is observed in Fig. 3.15(b). The temperature difference between the first and the second sensor in case of higher Ri number (Ri=3848) is greater (around 5 K) than in case of lower Ri number (Ri=962) which is merely 1 K. The positive effect of Ri number on the thermal stratification is significant at $Ri > 1000$. At lower Ri numbers the stratification is only marginally improved.

Once the flow with constant inlet temperature enters the tank, the flow momentum tends to mix the incoming flow with the fluid in the tank while the buoyancy tends to make the incoming stream to flow in a gravity current below the warmer tank fluid. The inlet temperature is constant throughout the experiment. This condition helps to build a stable thermocline in the tank. If the inlet temperature does not remain constant e.g. return flow of a solar collector, it would enhance the mixing in the tank and the thermocline region would be no longer clearly visible. Once the thermocline is formed at the bottom of the tank during the discharging process, it travels up as the discharging continues [20]. The thickness of the thermocline region is an important indicator of how well the stratified tank is designed. This thickness is function of several variables like geometry of the tank and the inlets, hydrodynamic and thermal characteristics of the flow in the tank. Yoo et. al (1986) estimated the thickness of the thermocline. According to their definition of the thermocline, the thermocline thickness was found to decrease with increasing Fr_i *number* (or with decrease in the Ri number). Smaller thicknesses are measured at lower Ri number whereas the thickness of the thermocline increases with increase in Ri number [62]. This phenomenon can be observed in Fig. 3.16. The thickness of the thermocline is significantly reduced for lower Ri number values. Here the variations in Ri number were achieved by varying the inlet temperature to the tank.

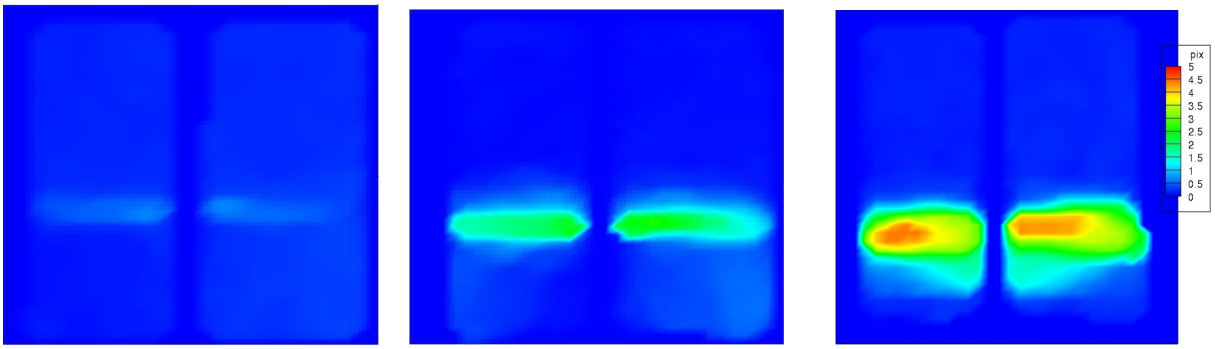

(a) $\Delta T = 2$ K (b) $\Delta T = 5$ K (c) $\Delta T = 20$ K

Figure 3.16: Thickness and position of the thermocline from low Ri number (for $\Delta T = 2$ K) to higher values of Ri number (for $\Delta T = 20$ K) after 30 seconds

As the thermocline region moves upwards, an equal amount of fluid at a constant temperature fills the tank. The thermocline acts as a physical barrier between the warm and the cool fluids and thus prevents mixing. Hence the cooler fluid entering underneath the thermocline has no temperature gradient. Hence the BOS evaluation shows almost no pixel shift in this region. However a small pixel displacement is observed near the walls of the tank. This happens due to the fact that the background image was captured when the tank had been conditioned at 40 °C. Therefore as the fluid with lower temperature fills the tank the background dots in the curvature region of the tank show a major distortion. Had the image been taken with the tank conditioned at T_{inlet} there would be no pixel displacement in the curvature region below the thermocline, however in the region above the thermocline where the tank fluid temperature would still be close to the initial temperature (40 °C), pixel displacement near the wall would be observed. To rectify this effect, two background images were captured: when the tank was conditioned at T_{inlet} and when the tank was conditioned at 40 °C. Using these images the BOS results were rectified and images without any artefacts near the tank wall were generated. This procedure has been documented in detail by Feuerstein F. [23]. In Fig. 3.16, this method is implemented for the experiment with $\Delta T = 20$ K. Due to presence of the temperature measurement lance, the region around the axis of the tank could not be evaluated. Hence a mask with width equal to the diameter of the temperature lance was used while evaluating the flow field using BOS analysis software.

3.2.2 Stationary flow field

A Stationary flow field can be achieved when the tank is charged with warmer fluid through the top diffuser plate and cooler fluid is charged through the bottom diffuser plate at very low flow rates. Additionally, fluid at an intermediate temperature flowing at a different flow rate, is introduced into the tank through a porous manifold placed in the middle of the tank. The fluid is discharged from the tank at about 30% height from the bottom of the tank. These modifications in the plexiglas tank are shown in Fig. 3.17. A porous manifold in thermal storage tanks has been used by many researchers and is a standard means of achieving stratification [63] [10].

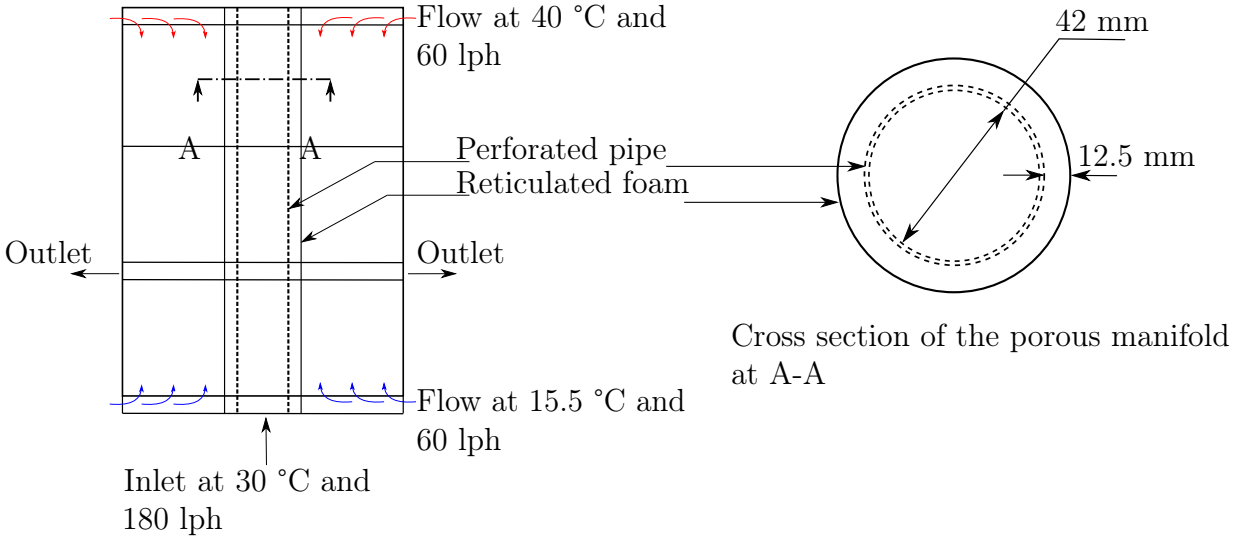

Figure 3.17: Modifications in the plexiglas tank to achieve stationary flow field

An additional temperature sensor was placed in the discharge plate. As soon as the temperature recorded by this sensor reached a stationary value, a stationary flow field was achieved. Detailed experiments were carried out on this set-up during the diploma thesis by Feuerstein F. [23]. The goal of the diploma thesis was to perform BOS measurements on the stationary flow field in the thermally stratified tank and qualitative comparison with ink tests and CFD simulations. The CFD simulations were part of a Masters thesis [8]. Feuerstein F. investigated the effect of change in the inlet flow temperature and flow rate on the stratification behaviour in the plexiglas tank. Some of these results are shown in Fig. 3.18.

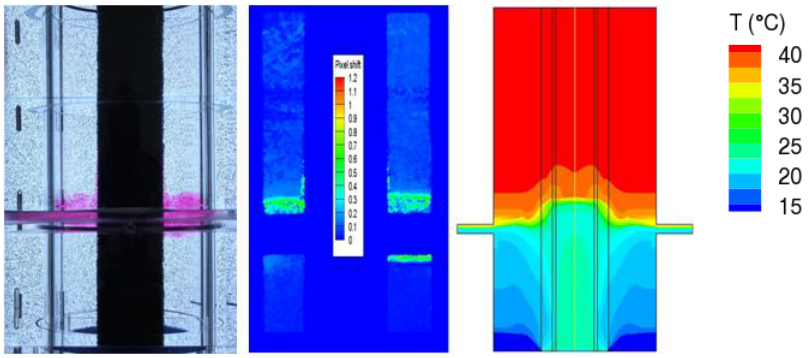

(a) $\dot{V}_{inlet}$ = 180 lph, T_{inlet} = 25 °C, Ri = 12.1

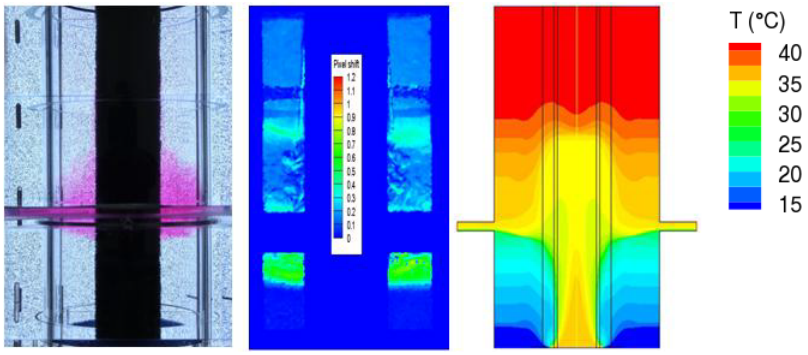

(b) $\dot{V}_{inlet}$ = 180 lph, T_{inlet} = 35 °C, Ri = 6.1

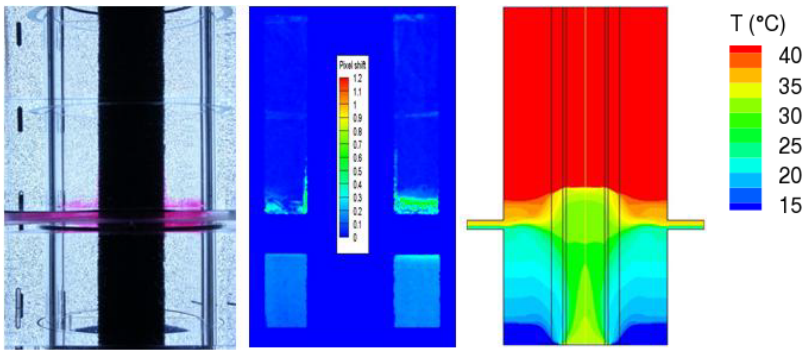

(c) $\dot{V}_{inlet}$ = 120 lph, T_{inlet} = 30 °C, Ri = 13.6

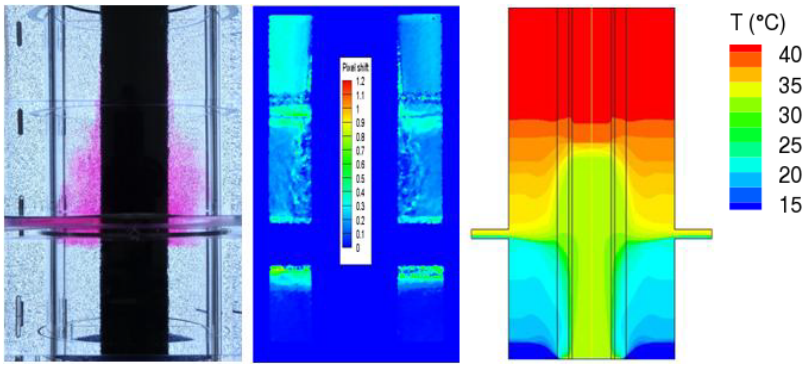

(d) $\dot{V}_{inlet}$ = 240 lph, T_{inlet} = 30 °C, Ri = 5.7

Figure 3.18: Effect of variations of the inlet flow temperature and flow rate on the thermal stratification

The results are to be identified as results of ink test, BOS measurement and numerical simulation from left to right for each experimental setting. These results were obtained using a foam thickness of 12.5 mm mounted on a perforated pipe with internal diameter of 42 mm. The height at which the flow is inserted into the tank through the perforated pipe and foam is affected by the inlet temperature and the flow rate. The Richardson number of the flow leaving the porous manifold is inversely proportional to the square of the velocity of the flow and directly proportional to the temperature difference between the inlet flow and the water in the tank. The buoyancy forces are more significant than the inertia forces for higher temperature differences and low flow velocities resulting in higher values of the Richardson number. The inlet flow tends to rise in the porous manifold to a height which corresponds the matching temperature of the fluid surrounding the manifold. This reduces mixing in the tank as the path of the fluid after leaving the manifold till the outlet is short which is beneficial to the stratification. This effect can be seen in Fig. 3.18, a & c.
On the other hand, the inertia forces are more significant than the buoyancy forces for higher inlet velocities and lower temperature differences which results in lower Richardson numbers. The inlet flow tends to overshoot the height corresponding to the matching temperature of the fluid surrounding the manifold. This enhances the mixing in the tank as the fluid leaving the manifold takes a longer path to the outlet which is detrimental to the stratification. This effect can be seen in Fig. 3.18, b & d.
Here the Ri number is based on the tank radius and the velocity of flow leaving the surface of the foam. The area for calculation of velocity was estimated from the observations made in the ink test. The height at which the flow left the foam surface was noted and the temperature recorded by the sensor at this height was considered for building the temperature difference term in Ri number estimation.

Thus it can be concluded that the Background Oriented Schlieren technique can be effectively used for qualitative visualisation of temperature gradients in transient as well as stationary flow fields. This method of flow visualisation can be made semi quantitative by inclusion of temperature sensors in the flow field.

3.3 Experimental set-up for investigation of adsorption heat pump cycle

A stratified thermal storage is capable of recovering a part of the adsorptive heat released during adsorption half cycle. For demonstration of the potential of the thermally stratified storage as an agent for internal heat recovery and its effect on the performance of the adsorption heat chiller's cycle, an experimental set-up was designed and built during this work. This set-up consists of the following essential components.

1. Heating module (Heat source)
2. Cooling module (Heat sink)
3. Adsorber emulator module
4. Adsorption chiller aggregate (Adsorbent: Silica gel)
5. Stratified thermal storage tank

In this work, the experimental investigations were carried out using two main experimental set-ups using the components listed above. Fig. 3.19 shows the experimental set-up used for emulation and flow visualisation of the heat pump cycle.

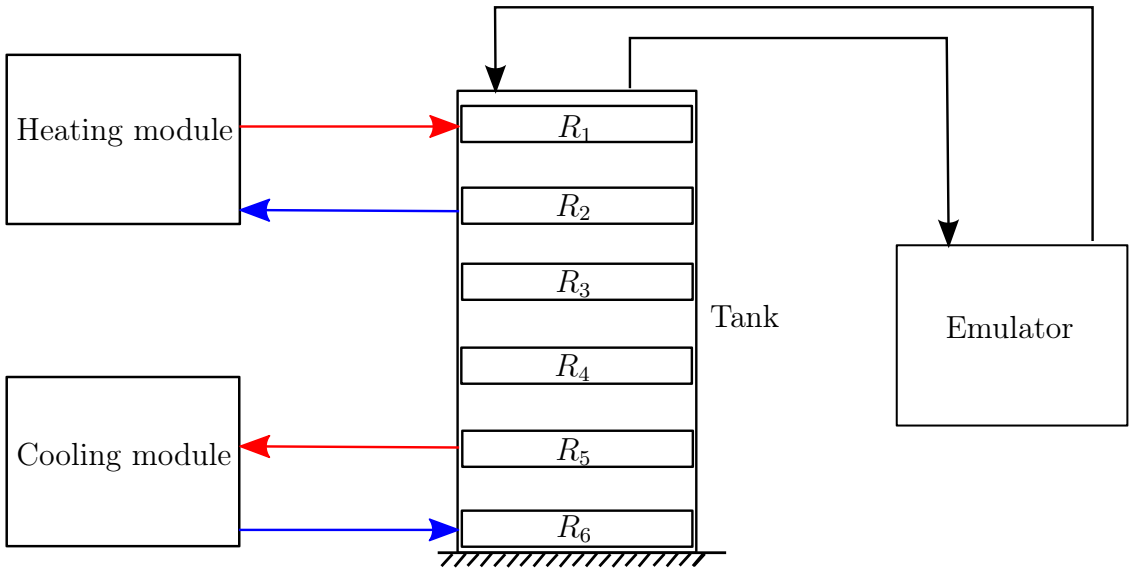

Figure 3.19: Experimental set-up used for the emulation and the flow visualisation of the heat pump cycle

Fig. 3.20 depicts the set-up used for the investigation of the stratisorp cycle. The emulator used in the flow visualisation experiments was operated as the cooling load (i.e., as low temperature heat source for the evaporator) for this experimental investigation. Initially, experiments were carried out in which the emulator fulfilled the role of a medium temperature heat sink for the condenser during desorption and a low temperature heat source for the evaporator load during adsorption. It was necessary to operate the emulator in this fashion as the adsorption chiller contained a common heat exchanger for condensation and evaporation.

However, it was observed that after switching from desorption to adsorption, the supply temperature to the evaporator was significantly higher than the setpoint of the emulator (18 °C). This was caused by the thermal mass of the emulator which had also heated up during the desorption phase. Hence it became necessary to use different devices for the adsorption and the desorption half cycles. Two 3-way valves (V_1 and V_2) were deployed which did the task of switching the flow between the two half cycles. These valves were so positioned that the evaporator circulated water with $\dot{V}_{evap}$ only with the emulator during the adsorption half cycle. The emulator heated the returning chilled water from the evaporator to the setpoint of 18 °C while the condenser pump remained off. The cooling module cooled the bottom part of the tank with $\dot{V}_{c_{tot}}$. An external trigger programmed with LabView and linked with a relay, switched the condenser pump, V_1 and V_2 at the same time in order to switch to desorption half cycle. Simultaneously the emulator stopped circulating water with the evaporator as the solenoid valve was closed. A bypass mounted in the emulator was opened at the same time in order to keep the water circulating at 18 °C and to protect the pump. Here, the evaporator heat exchanger works as condenser. The heat of condensation is rejected in the cooling module. The cooling module has to cool both the condenser and the bottom of the tank during the desorption half cycle. $\dot{V}_{c_{tot}}$ was always set higher than $\dot{V}_{cond}$ thereby assuring that always some flow was circulated through the tank. The cooling module receives flow at $\dot{V}_{cond}$ from the condenser and the difference i.e. $\dot{V}_c$ flows through the tank. Fig. 3.21 and Fig. 3.22 show the hydraulic connections during the desorption and the adsorption half cycles. In the following sections, the working and the significance of the devices or components used as shown in Fig. 3.20 is discussed. These components were borrowed (partly purchased) from the project partners. Important changes and repairs were carried out so that these components could be adapted for the current work. The results obtained using this experimental set-up are discussed in Chapter 4.

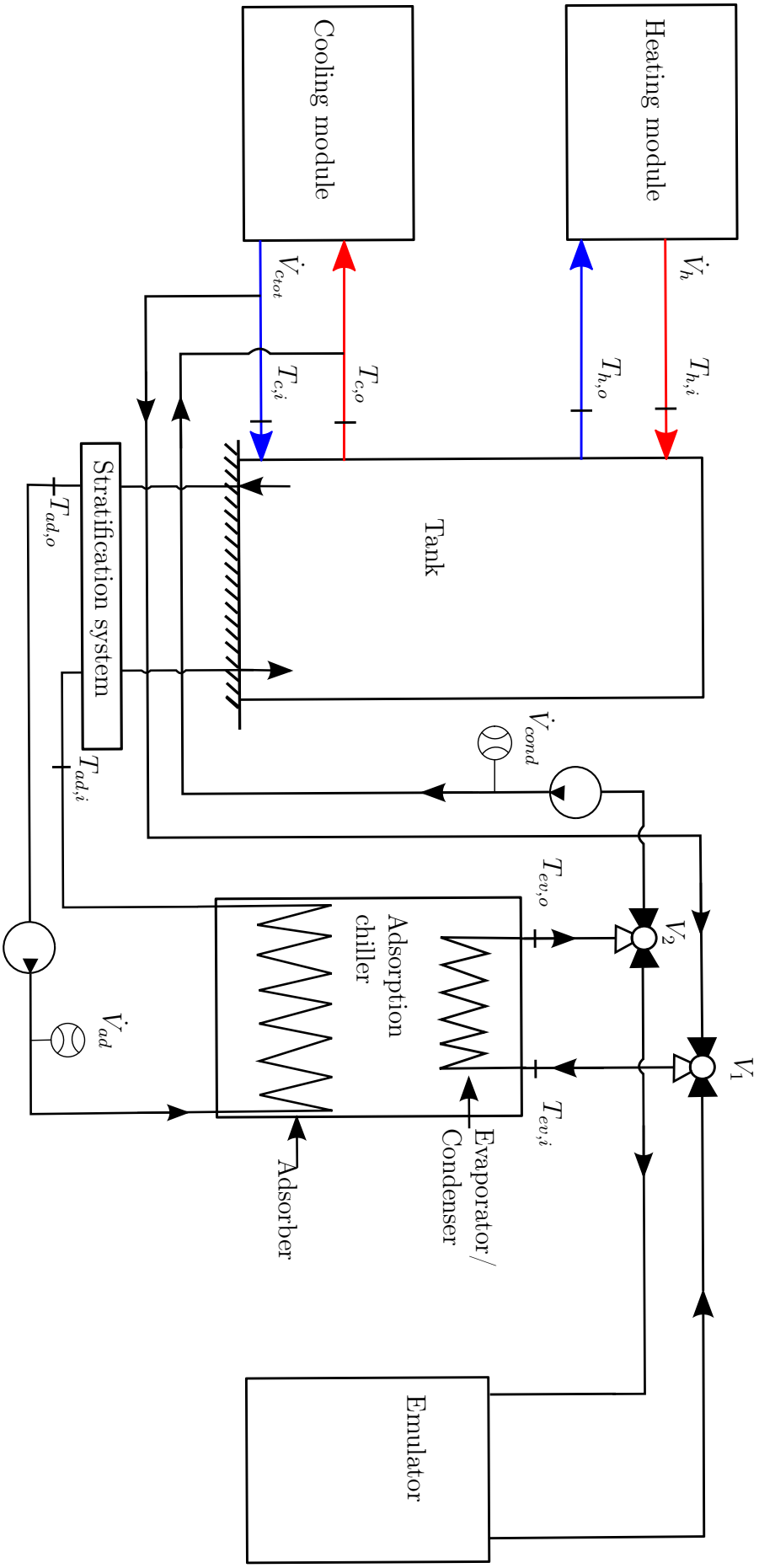

Figure 3.20: Experimental set-up used for investigation of the stratisorp cycle

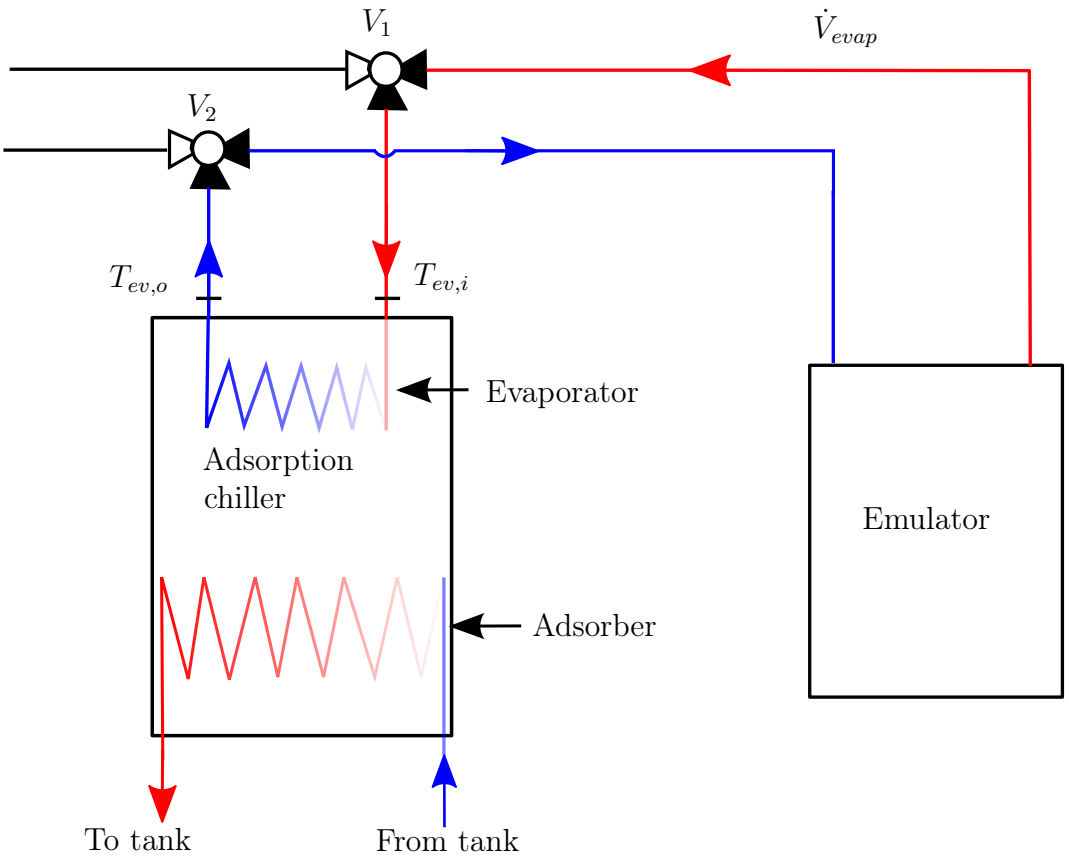

Figure 3.21: Hydraulic connections during adsorption half cycle

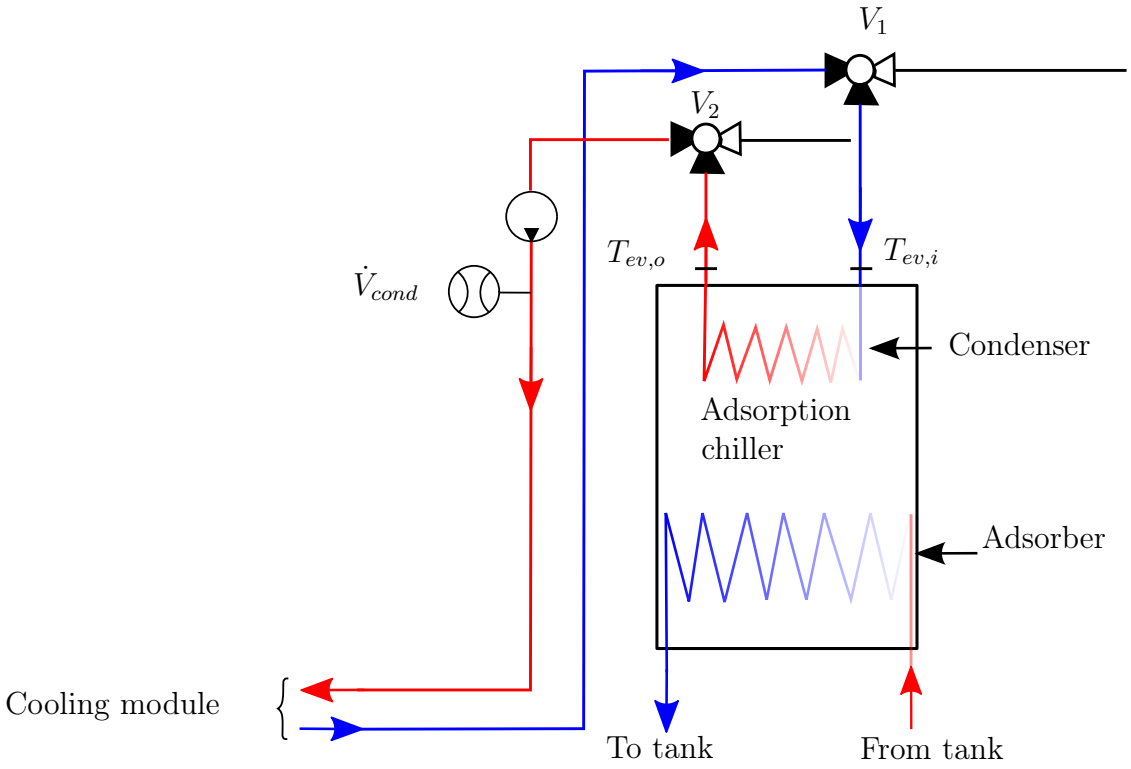

Figure 3.22: Hydraulic connections during desorption half cycle

3.3.1 Heating module

The necessary thermal energy required by the chiller to drive the cycle is provided by the heating module. In practice, the hot water available from a CHP unit or a gas burner or solar collectors can be used for this purpose. For the laboratory experiments an electric heater is preferred. The schematic diagram shown below in Fig. 3.23 reflects on the construction of the heating module used for this work. A LabView [2] interface was used for the data acquisition, the temperature and flow rate control and the data visualisation of the different physical quantities measured by these components.

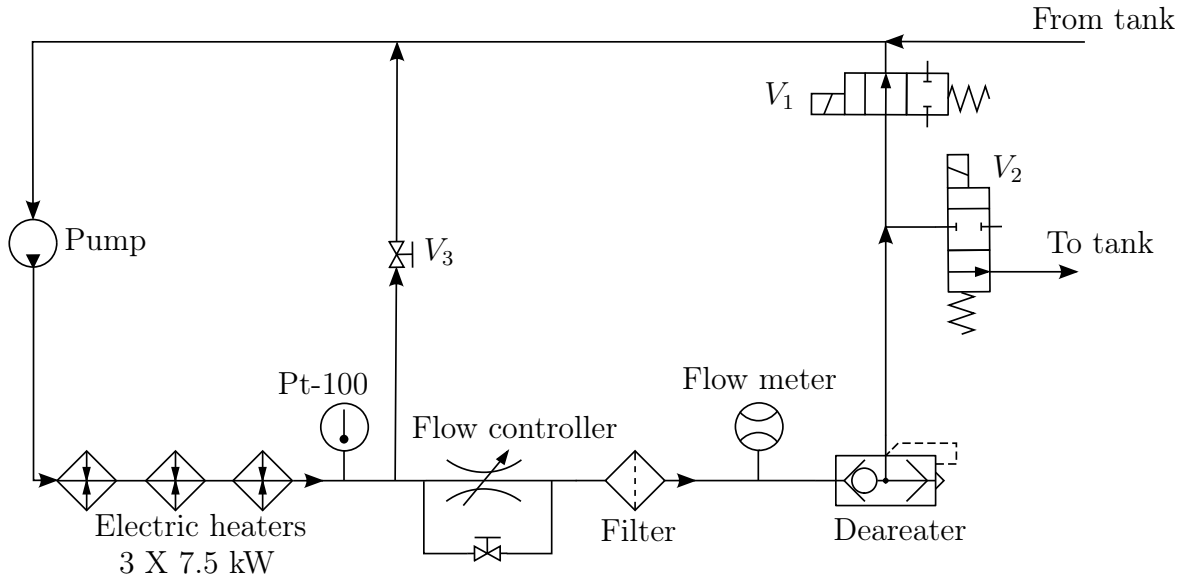

Figure 3.23: Schematic hydraulic circuit diagram of the heating module

Each of the electric heaters has a heating power of 7.5 kW. The electric heaters are connected in series which makes the maximum heating power of the module to be 22.5 kW. The temperature of the water leaving the 3^{rd} electric heater is measured by a Pt-100 temperature sensor. The temperature control is achieved by a Eurotherm controller which compares this measured temperature with the setpoint and switches the electric heaters ON or OFF. The flow rate of the module can be set and regulated by the flow controller (a proportional controller). As the flow rate of the heating module is kept constant during the measurements, it was not necessary to regulate the flow rate. Hence the flow rate for the experiments was set using the bypass valve V_3. Closing of the valve V_3 would increase the flow rate of the heating module being circulated through the tank and vice versa. The maximum volume flow rate is limited by the measurement range of the flow sensor which is 0-840 lph.

3.3.2 Cooling module

The cooling module is necessary for keeping the bottom section of the tank close to the temperature of the medium temperature heat sink. Additionally, it is used for heat rejection from the condenser during the desorption half cycle due to absence of a cooling tower. A

[2]The LabView code was developed by the project partners ITW. In this work, this code was further adapted to accommodate the changes made in the experimental set-up e.g. the inclusion of additional flow and temperature sensors, solenoid valves

cooling module of cooling capacity of approximately 20 kW and accuracy of +/− 0.5 K was designed and built by project partner SWT Technologie, Stuttgart. The temperature setpoint was controlled using a Eurotherm 3216 controller. The controller parameters had to be tuned in order to ensure fast response and accurate control of the cooler output temperature. The controller tuning is documented in the appendix A.5.

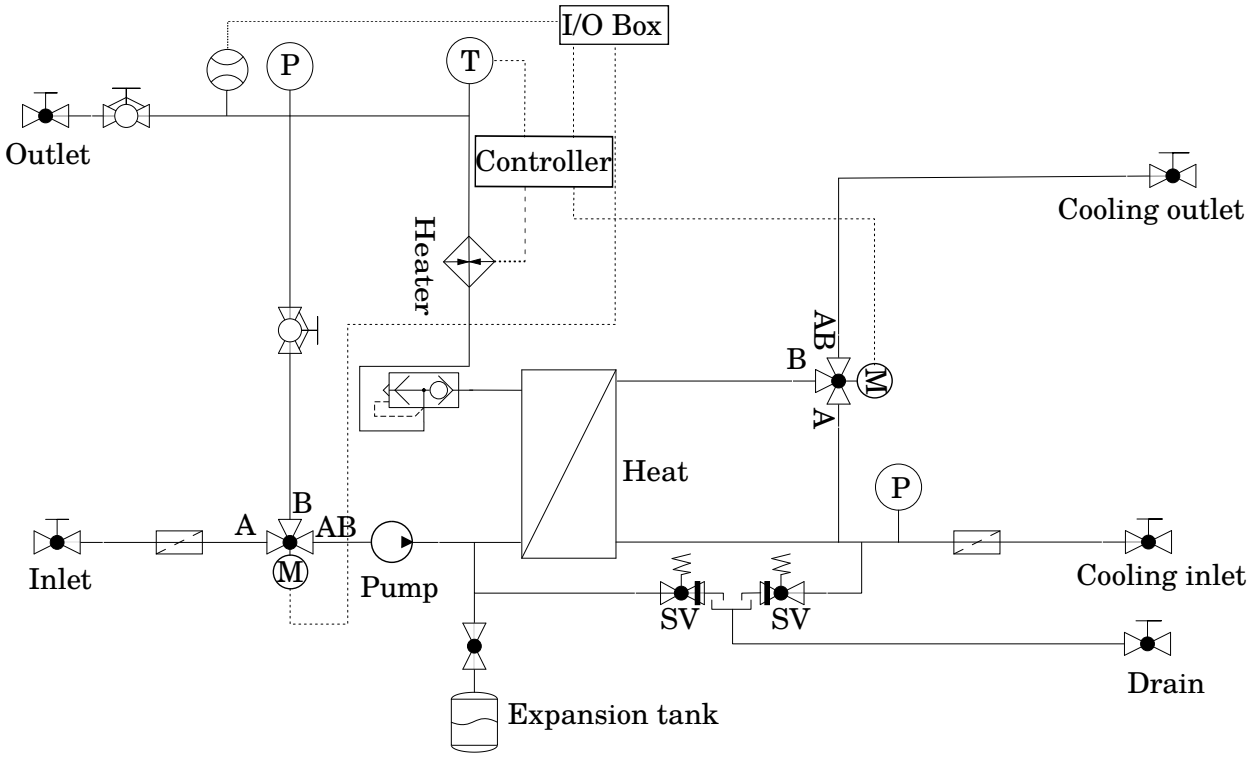

Figure 3.24: Schematic hydraulic circuit diagram of the cooling module (SV: **S**olenoid **V**alve)

The heat exchanger of the cooling module is connected with the cooling network of the building. The cooling network has supply temperature of 15 °C and volume flow of 500 lph is available.

3.3.3 Adsorber emulator module

One of the important goals of this thesis was to investigate the different flow phenomena in the stratified thermal storage independent of the adsorption chiller used. The adsorber emulator module (or emulator) allows good control over the flow conditions. The emulator is able to cool and heat the flow streams and control the flow rate as well. The construction of the emulator is shown in the Fig. 3.25.

Similar to the heater module, the flow rate and the temperature setpoints can be set and controlled. The return flow from the tank is first sent through a cross flow heat exchanger and cooled with the maximum cooling power available[3].

[3]This posed a problem during the emulation of the adsorption half cycle. At the start of the half cycle when the return flow was relatively warm, less cooling power was needed. However, due to the maximum cooling power available at the heat exchanger the temperature of the flow leaving the heat exchanger was too low for the heaters to heat it back to the given setpoint at the set flow rate. On the contrary, towards

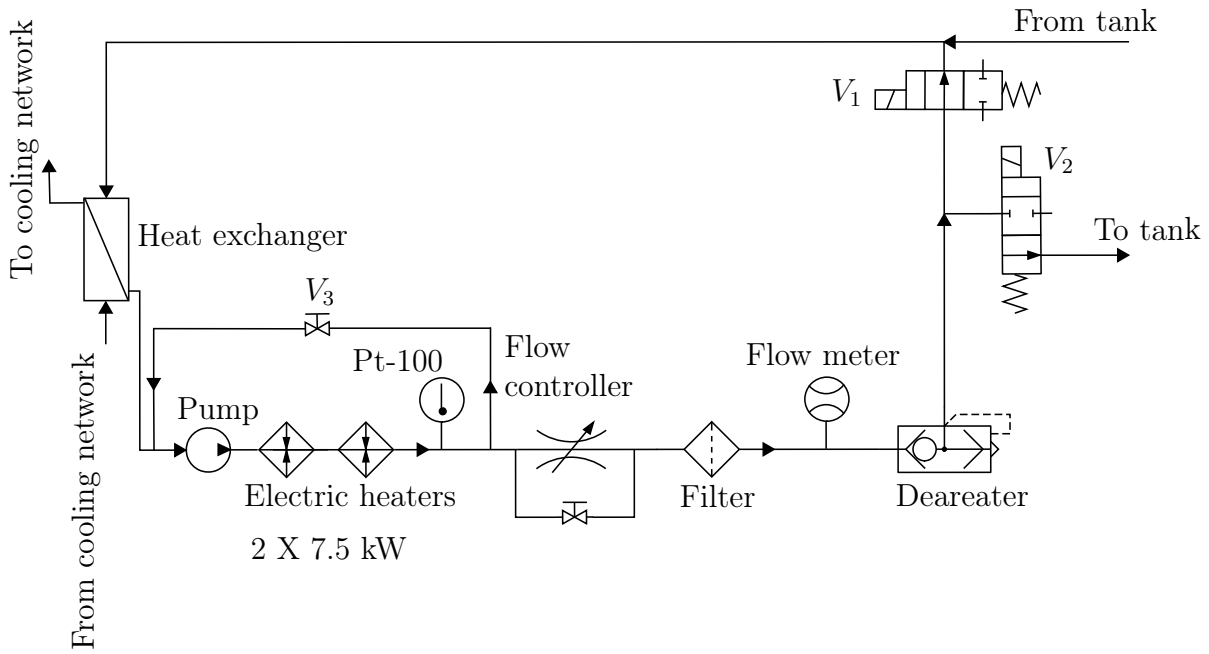

Figure 3.25: Schematic hydraulic circuit diagram of the adsorber emulator module

The cooled flow is then pumped through the two electric heaters connected in series. The electric heaters have total power of 15 kW. The Eurotherm controller controls the temperature of the water entering the tank by intermittently switching the heaters ON or OFF.

3.3.4 Adsorption chiller aggregate

The adsorption chiller aggregate used in this study was manufactured by SorTech AG, a leading manufacturer of silica gel adsorption chillers. Fig. 3.26 shows the image of the adsorber integrated in the test set-up and the schematic of internal arrangement of the adsorber and the evaporator/condenser heat exchangers.

The same heat exchanger which works as the condenser during the desorption half cycle, works as the evaporator during the adsorption half cycle. The adsorber and the evaporator/condenser heat exchangers are mounted in the same vacuum chamber with spacers in between. The water pool at the bottom of the chamber contains approximately 7 litres of water. The adsorber is connected with the tank while the evaporator/condenser heat exchanger is connected with the medium temperature heat sink (heating load) or low temperature heat source (cooling load). The emulator can also be programmed to work as a heating or cooling load. The designed cooling power of this adsorption chiller is around 4 kW. The adsorber heat exchanger is a finned tube heat exchanger. The fins are covered with silica gel granules. A special glue assures that the granules are appropriately attached with the metallic body of the adsorber heat exchanger. This is extremely important to achieve a good thermal coupling between the granules and the body of the heat exchanger.

the end of the adsorption half cycle, the maximum cooling power was required owing to higher temperature difference across the emulator. The control over the cooling power was achieved by throttling the cooling flow to the heat exchanger. Detailed documentation can be in found in [19]

(a) Image of the adsorption chiller

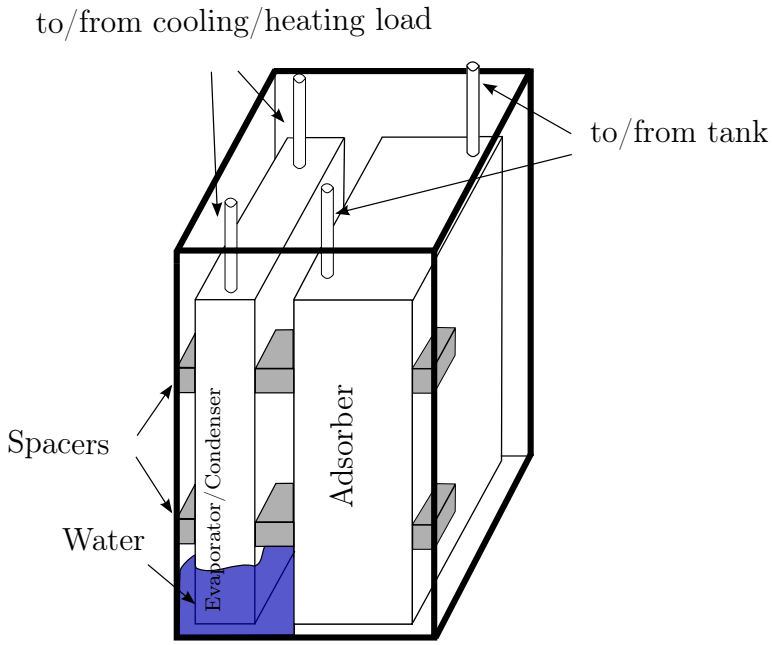

(b) Schematic internal LHS view of the adsorption chiller

Figure 3.26: Adsorption chiller based on silica gel-water pair

3.3.5 Stratified thermal storage tank

The stratified thermal tank is very important component of the experimental set-up relevant for the internal heat recovery of the adsorption chiller's cycle. Two different designs of the tank were considered for this work.

3.3.6 Tank for flow visualisation

The flow visualisation in the thermal storage was very important to investigate the stratification mechanism and performance of the stratification system. Hence a tank with windows on opposite sides was used for this purpose. The windows provided the necessary optical access for the implementation of the BOS method. A background illumination system similar to Fig. 3.4 was mounted on the outside of one of the windows. The camera was positioned such that it focussed on the background image stuck on the outside of this window through the window on the opposite side. This storage tank contained approximately 500 litres of water. The tank is made of steel with anti corrosion coating from the inside. Glass wool laminated with aluminium foil was used to insulate the tank. The details regarding the construction of the tank and the BOS set-up can be found later in this chapter. This tank was used by Hampel M. [29] for his research activities. Owing to the limited modifications allowed in the

original construction of the storage tank, the stratification system had to be inserted from the top into the tank. This made it almost impossible to close the tank using a lid. Therefore the tank when filled with water, had a free water surface making the system a pressure-less (open) system. The fact that the system pressure could not be increased more than 1 bar had certain shortcomings (discussed in 4.1). The design of this stratification system consisting of rings is discussed later in this chapter. Figure 3.27 shows the CAD model and the vertical cross section of this tank along with the stratification system. Here the tank without the insulation is shown. It was necessary to keep some safety margin (3 cm) from the top edge of the tank to avoid the danger of water spilling over. One ring was placed just below the free water surface while another ring was placed at the bottom of the tank. The remaining four rings were placed equidistantly along the height of the tank. Hence when the tank was completely filled, the space between adjacent rings contained approximately 100 litres of water. Each ring could be used for charging or discharging from the tank. This was achieved by means of a solenoid valve bank shown in Fig. 3.28. This valve bank was placed on the lid of the tank.

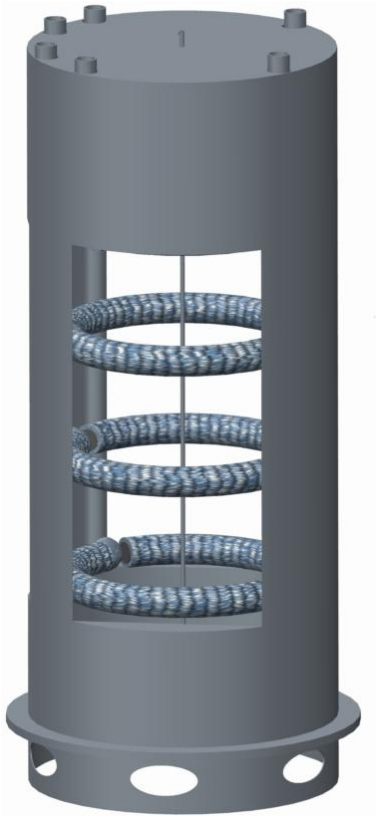

(a) CAD model of the tank

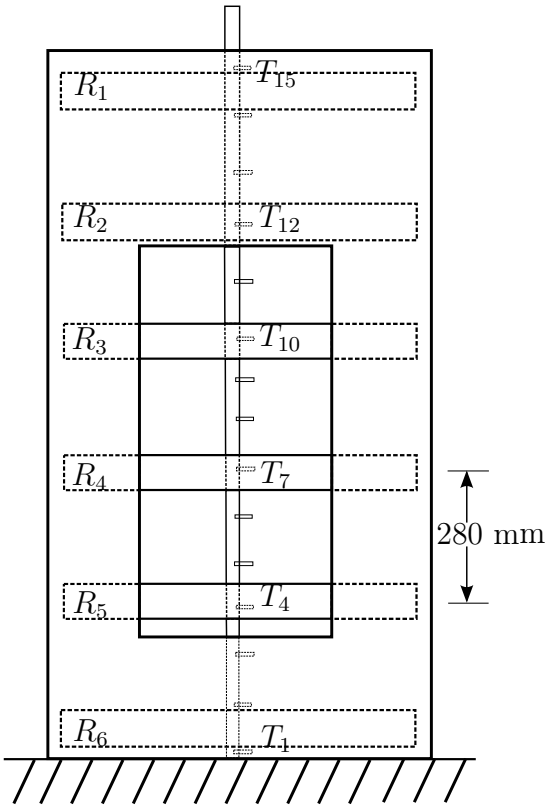

(b) Arrangement of the rings and the temperature sensors

Figure 3.27: Tank used for flow visualisation: components and their position

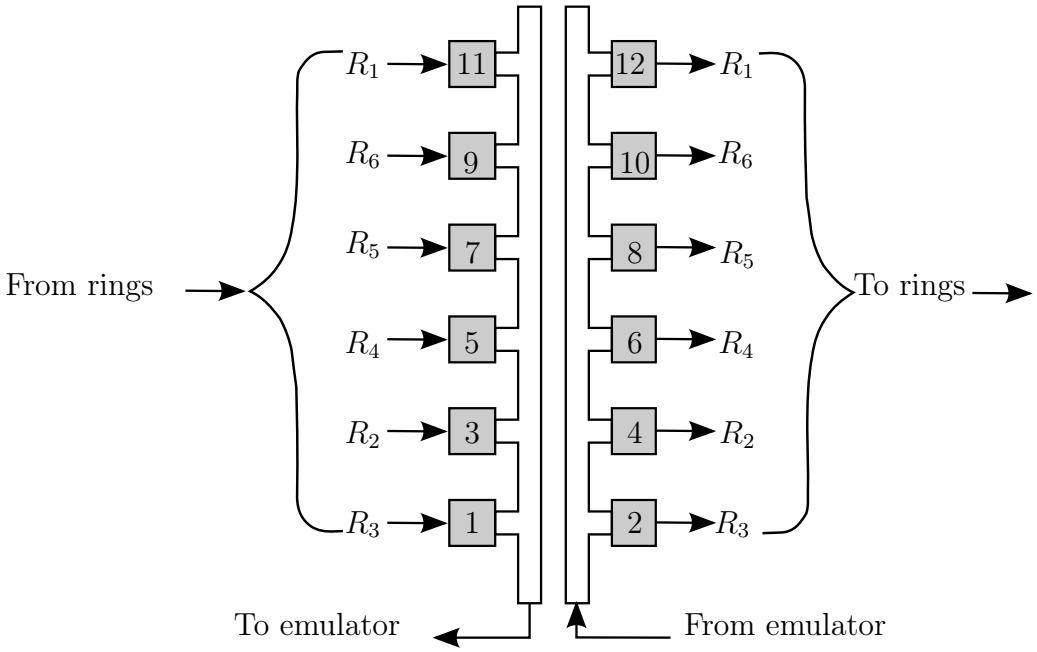

Figure 3.28: Solenoid valve bank

Figure 3.29 elaborates the hydraulic connections between the valve bank and the stratification rings.

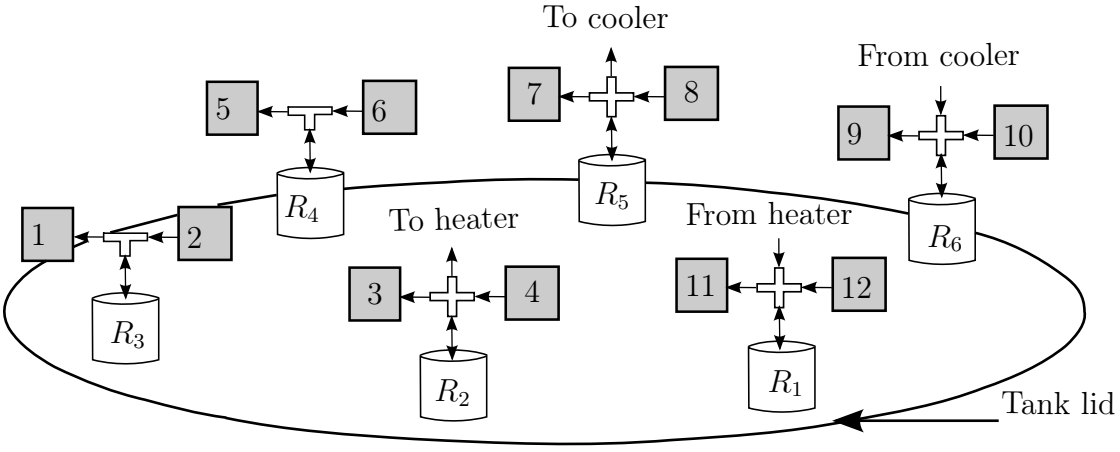

Figure 3.29: Schematic view of the hydraulic connections between the solenoid valve bank and the rings through the lid of the tank

The switches with even numbers were used to activate the charging flow to the tank whereas the switches with odd numbers were used to activate the discharging flow from the tank. As far as the stratisorp cycle was concerned, only adjacent rings were used at any given point in time for charging or discharging. The heating module was attached to the tank through ring 1 and ring 2 bypassing the valve bank. Similarly, the cooling module was attached to the tank through ring 5 and ring 6. Each ring was connected with the corresponding valves using straight pipe sections through the tank lid. The working of this stratification system can be understood from Fig. 3.30.

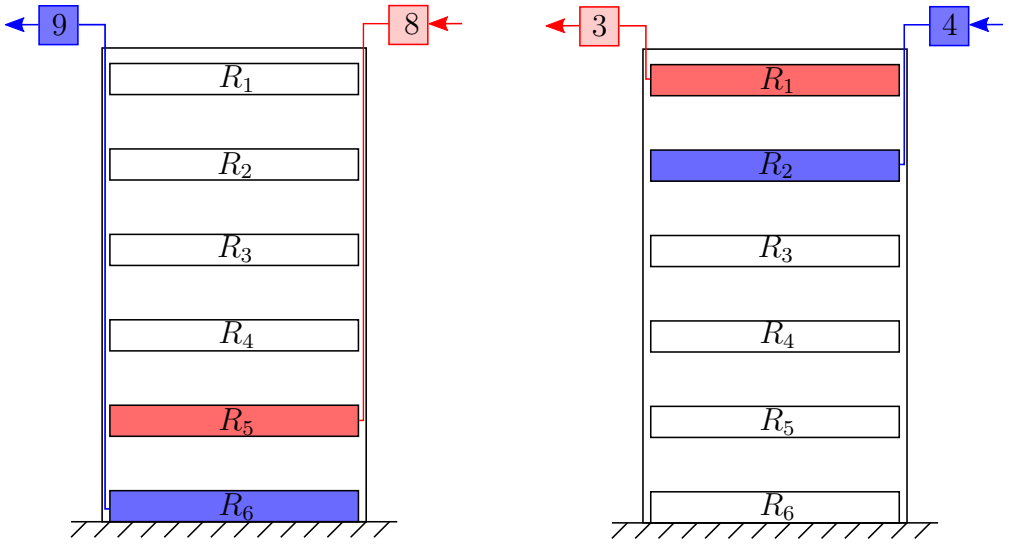

(a) Adsorption (b) Desorption

Figure 3.30: Working of the stratification system using rings

Fig. 3.30(a) shows the situation at the end of the adsorption half cycle. During the adsorption half cycle, the emulator discharges cooler water from the tank using lower positioned rings (here from R_6) and inserts warmer water returning to the tank in the next higher positioned ring (here in R_5). On the contrary, during the desorption half cycle, the warmer water is discharged from the tank using the rings positioned higher in the tank (here from ring R_1) and cooler water returning to the tank is inserted in the next lower positioned ring (here into R_2). Fig. 3.30(b) shows the charging and the discharging process at the end of the desorption half cycle.

3.3.7 Tank for investigation of stratisorp concept

A separate tank was used for the experimental investigation of the adsorption chiller's cycle based on the stratisorp cycle. For the investigation of the stratisorp concept, the tank was connected with the adsorption chiller explained in 3.3.4. This tank differed the tank used for flow visualisation in some aspects. This tank could be closed with a pressure tight lid as the supply and return pipes for the stratification system were designed through the walls of the tank. Moreover, this tank had no glass windows for flow visualisation further improving the pressure tightness of the tank. Hence it was possible to build a pressurised system with maximum 3 bar pressure. The details of the design of this tank can be found in appendix A.4.

Stratification system based on charging lance: As differed to the ring based stratification system, this system makes use of state of the art charging lance manufactured by SOLVIS (SL96, max.1900 lph, diameter 80 mm, height 1.59 m). Fig. 3.31 shows the stratified injection by this lance [47]. The charging process of the tank using this charging lance is buoyancy driven. The water entering the tank rises in the lance to a level determined by the buoyancy and the inertia of the flow. Hence the charging process is passive. For the discharging process the solenoid valve bank was used. Fig. 3.32 depicts this stratification system.

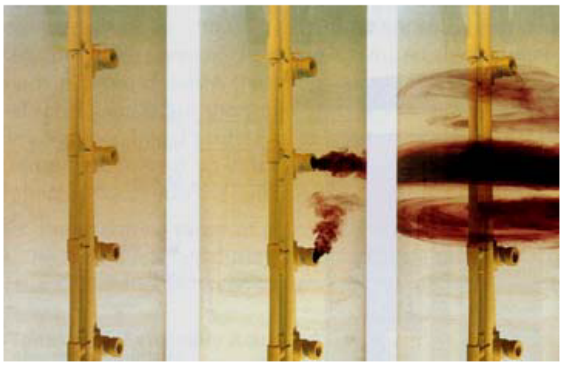

Figure 3.31: A stratified injection using charging lance by SOLVIS

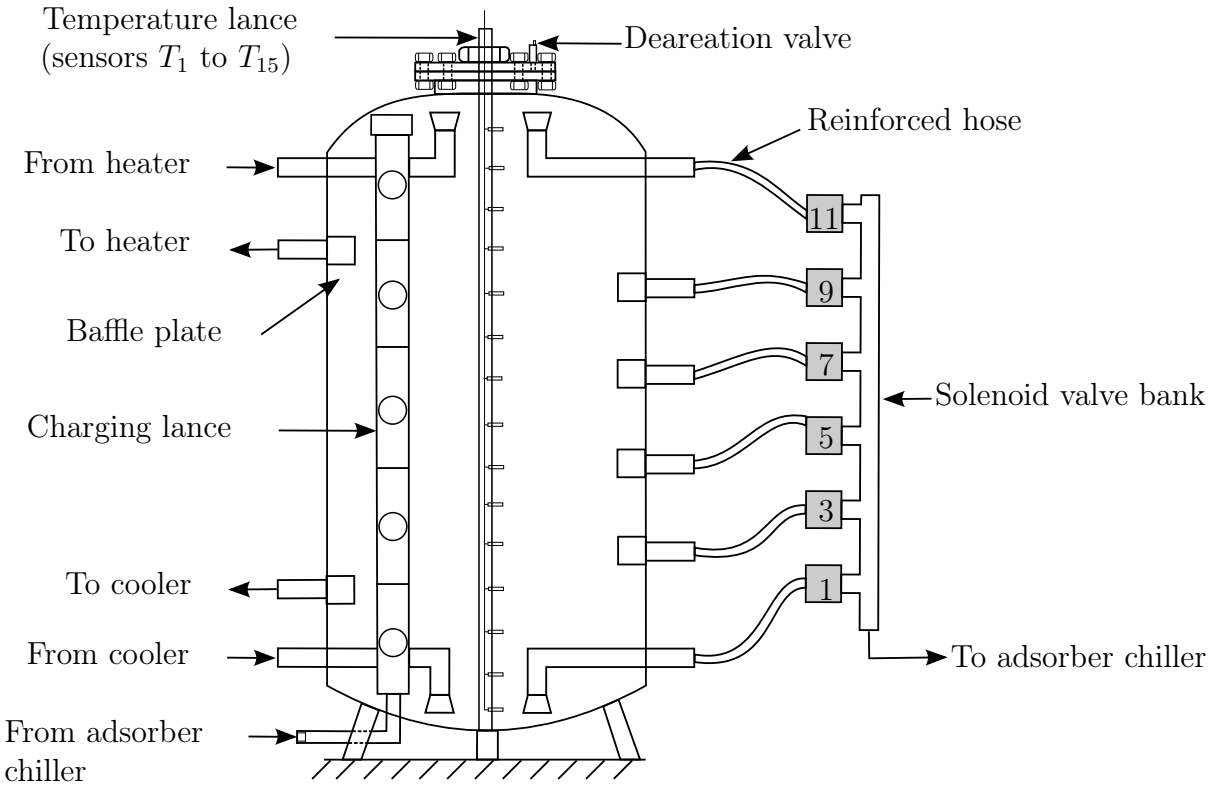

Figure 3.32: Working of the stratification system using charging lance [47]

The tank was equipped with a temperature lance made of multi layer composite pipe carrying Pt-1000 temperature sensors is placed at the axis. These 15 sensors were placed equidistantly at 11 cm each. The sensors were numbered beginning from the bottom of the tank. The heating and the cooling module were attached to the tank using separate connections. Hence the flow rates of the adsorber chiller and heating or cooling modules did not interact with each other. The outlets were attached with baffle plates in order to reduce the inertia of the flow leaving the tank thereby reducing the mixing near the outlet region in the tank. As the charging process was passive, it was relatively difficult to precondition the tank.

The working of this stratification system is similar to the previous system, the only difference

being that the position of the water being inserted into the tank is temperature dependent. Additionally, the area available for the flow to exit from the lance is much smaller than the rings which causes lower Ri numbers. The adsorption half cycle sees the adsorber chiller being supplied with water extracted from the tank starting with extraction from the valve 9. The flow returning to the tank rises above the extraction level as it is at higher temperature than the flow leaving the tank due to the heat of adsorption. As the adsorption half cycle continues, the adsorber chiller is supplied with cooler water from the next lower level. The criteria for switching to the next lower level in the case of adsorption or to the next higher level in the case desorption half cycle will be discussed in the coming sections. At the end of the adsorption half cycle, the adsorber chiller receives water stored at the bottom of the tank through valve 1.
The desorption half cycle starts with extraction of water from valve 3. The flow returning to the tank during the desorption half cycle is cooler than the flow being extracted from the tank. Hence the flow entering the tank can rise only to a level lower than the extraction level. The desorption half cycle continues by extracting warmer water available at the next higher extraction level. At the end of the desorption half cycle the adsorber chiller receives the warmest water stored in the tank thereby completing the adsorption chiller's thermal cycle. In this work this tank and the stratification system is used to demonstrate an adsorption heat pump cycle without heat recovery i.e. desorbing the adsorber with maximum desorption temperature and adsorbing with the lowest adsorption temperature.

Stratification system based on rings: As the name suggests, this system makes use of stratification rings for charging and discharging the tank. The stratification rings used in section 3.3.6 had been fitted in the tank shown in Fig. 3.32. The insertion and the extraction of the flow from the tank is achieved identically as explained before in section 3.3.6. The only difference here is that the pipes leading to each stratification ring were connected through the tank wall. Consequently, the valve bank responsible for loading and unloading of the tank was attached to the tank wall on the outside as shown in Fig. 3.33. Two way valves with electric drive were used for this valve bank[4]. The figure also shows the charging and the discharging during the adsorption and the desorption half cycles.

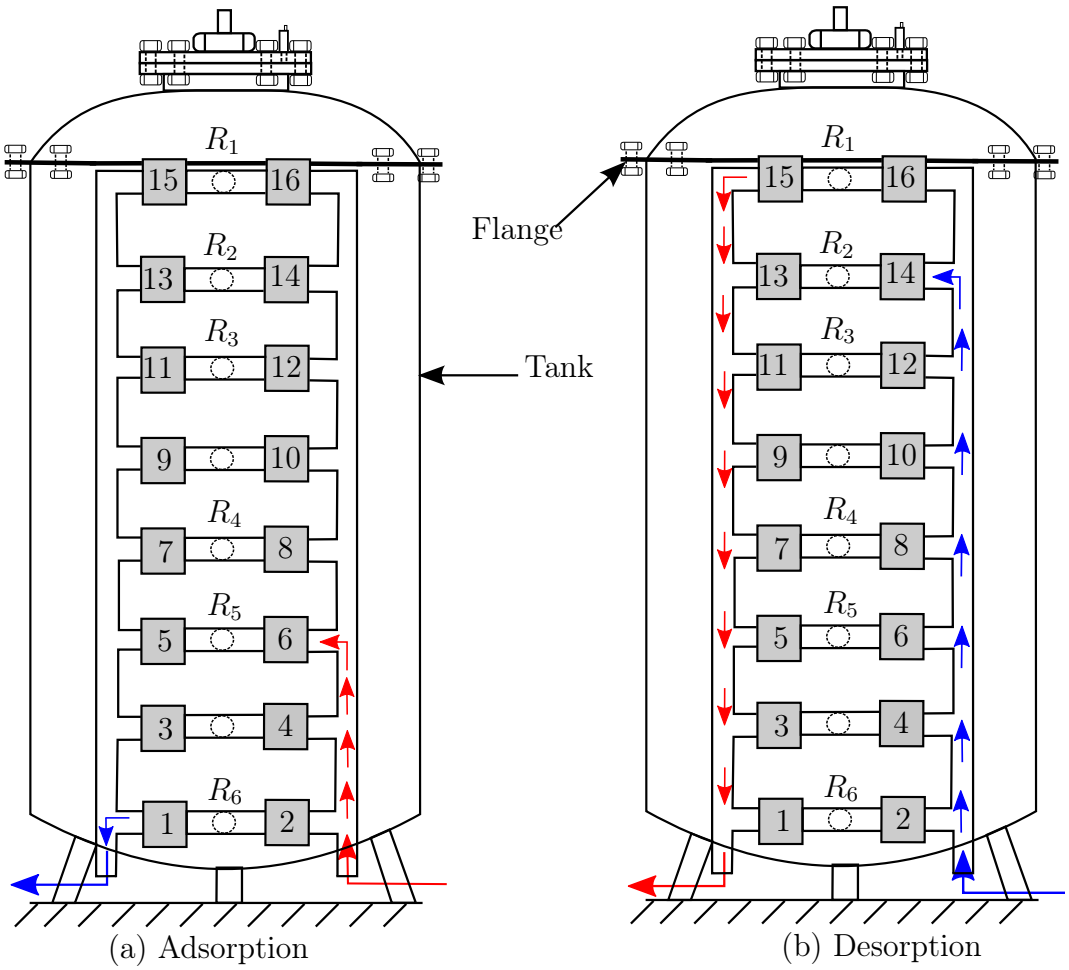

Figure 3.33: Working of the stratification system using rings

The tank was provided with an additional flange coupling to provide access to the inside of the tank during mounting of the rings. The number of insertion and extraction level in the tank also have influence on the performance of the adsorption heat pump's cycle. However, this effect has not yet been experimentally investigated. Hence, two additional ports for mounting more rings or flow diffusers were provided for investigation in near future. For this study, however, the experiments were carried out using six stratification rings. All investigations on the stratisorp system are performed using this tank and stratification system.

[4]manufacturer: Belimo, valve type: R425, DN 25, kvs 26, electric drive: LRA-D60 007 T0G, switching time = 2.5 sec.

3.4 Design and construction of flow diffusers

The most important requirement of the stratification system is to insert or extract the water from the tank causing minimum perturbation. Hence the flow diffusers should offer outlet area as large as possible however still maintaining the plug flow inside the tank fluid volume. With reference to the stratisorp system, the stratification system should be able to insert or extract from different levels of the tank. The vertical components of the insertion or the extraction flow velocities are detrimental to the thermal stratification [5]. Hence the flow diffuser should insert the flow as far as possible parallel to the bottom of the tank. Additionally, the flow diffuser should insert or extract the flow symmetrically from the inner perimeter of the tank [6]. These requirements could be fulfilled using a ring shaped flow diffuser. Various research works on stratified thermal storage have deployed ring shaped or octagonal shaped flow diffusers [35]. The maximum diameter of the ring was limited by the window to window distance of the tank. Multi-layer composite pipe with aluminium layer was used as it provided good flexibility for bending the pipe.
The momentum of the flow entering the tank is the most important factor which is responsible for destruction of the thermal stratification. The flow diffuser should introduce water to the tank uniformly and inhibit mixing so that the buoyancy forces create and maintain the thermal stratification. Various research works, both experimental and numerical, underlined the positive impact of using porous material on the thermal stratification, such as [10], [63] and [8]. Reticulated foam stripes of 5 cm width and 3 cm thickness were wrapped around the rings and the adjacent passes of the foam stripes were sewn to each other for stability (refer A.6 for the data).
The number of openings (holes of 5 mm diameter at 10 mm spacing) on the surface of the diffuser rings and their orientation directly affect the velocity of flow entering the tank. The dimension and the spacing of the holes was selected such that homogenisation of the individual jets through the foam layer could be assumed. A simple test was necessary to approximate the velocity of flow leaving the foam surface. The Richardson number derived from this velocity could be used to determine the functional effectiveness of the rings. It was also important to investigate the flow homogenisation offered by the use of foam. Hence a short study was carried out on small sections of the multi-layer composite pipe in an aquarium (2.5.2) filled with clear water. Coloured water was introduced through the flow diffusers for flow visualisation. Fig. 3.34 shows the experimental set-up for this study. The test was carried out using flow rate of 300 lph (or 6 cm/s) per pipe section. The perforated pipe sections were mounted in the aquarium such that the drilled sides of the pipes faced each other. Any vertical temperature gradient inside the aquarium were avoided because the focus of the experiment was to investigate the flow pattern of flow escaping the foam surface in absence of buoyancy effects. A short temperature lance mounted with Pt-1000 sensors was used to monitor the temperature of the water inside the aquarium. The experiment was carried out with the tap water in the laboratory at 20 °C. A floating plexiglas plate was placed on the surface of water to suppress any waves generated inside the aquarium. Here it is worthwhile to mention that the flow entered into the perforated pipe of diameter 42 mm

[5] Under certain flow conditions occurrence of flow veils was later confirmed. The flow veils, although having predominantly vertical component of velocity, did not destroy the stratification. Hence this assumption of detrimental effect of vertical jets is not a general phenomena

[6] The tank explained in 3.3.6 was used for the flow visualisation experiments with rings

from the inlet pipe sections of 10 mm internal diameter. This abrupt increase in the cross section was absent in the stratification system using rings. Hence a small cylindrical piece of reticulated foam was fitted at the inlet to the perforated pipe section inside the pipe to homogenise the inlet flow and suppress any secondary flow which might arise.

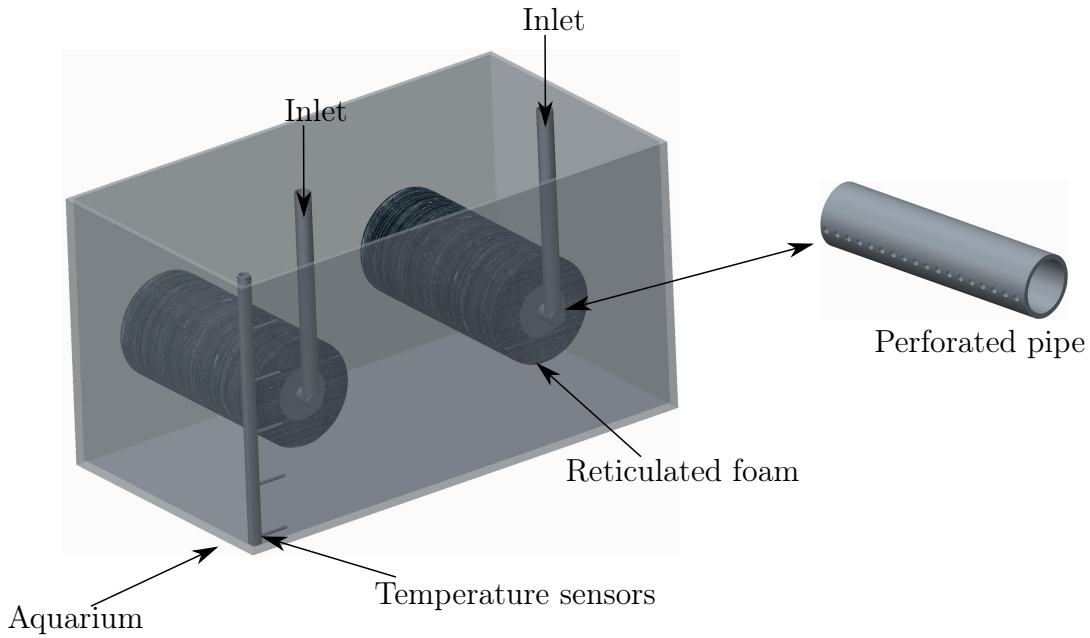

Figure 3.34: Experimental set-up to investigate the performance of flow diffuser

Three different types of the perforated pipe sections were tested, namely

I. single row of holes

II. three rows of holes

III. multiple rows of holes (covering whole circumference)

Fig.3.35 and Fig. 3.36 show the snapshots of the front view and the top view of the ink test after 5 seconds. The air trapped underneath the plexiglas plate can be seen in the top views (the horizontal line in Fig. 3.36(a)).

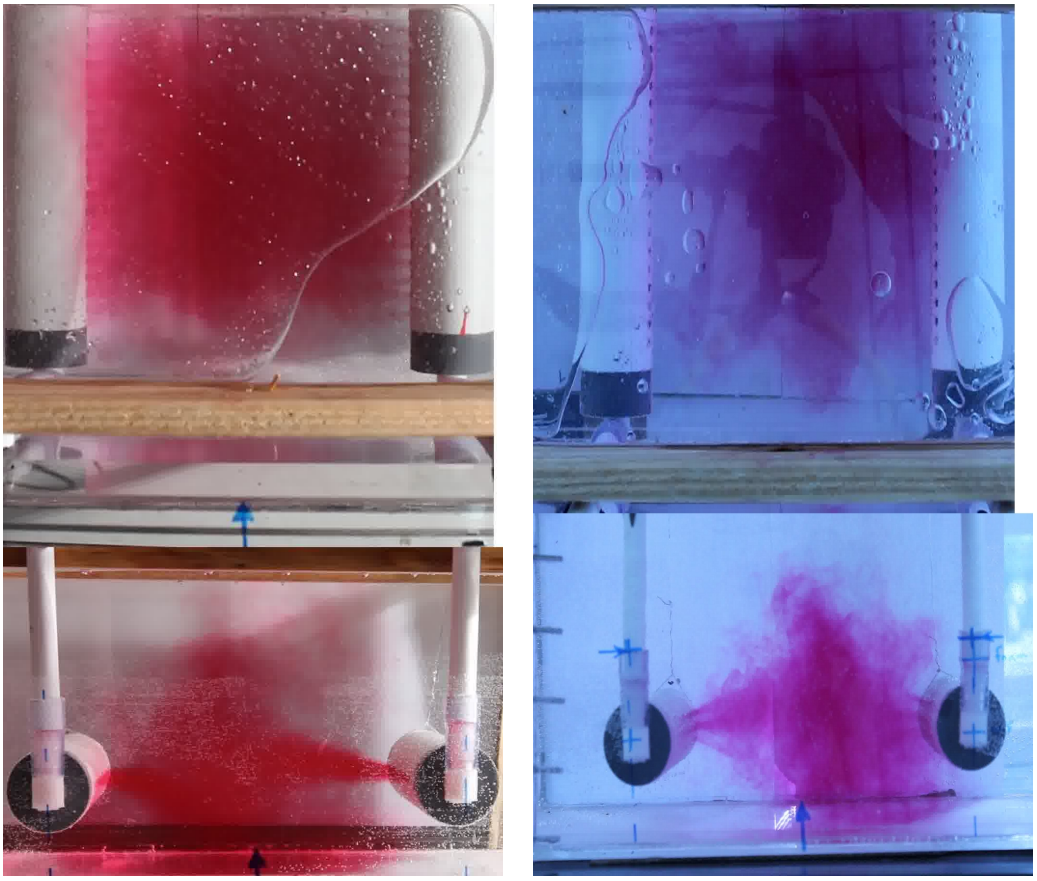

(a) Diffuser I (b) Diffuser II

Figure 3.35: Dye ink test on the perforated pipes without foam

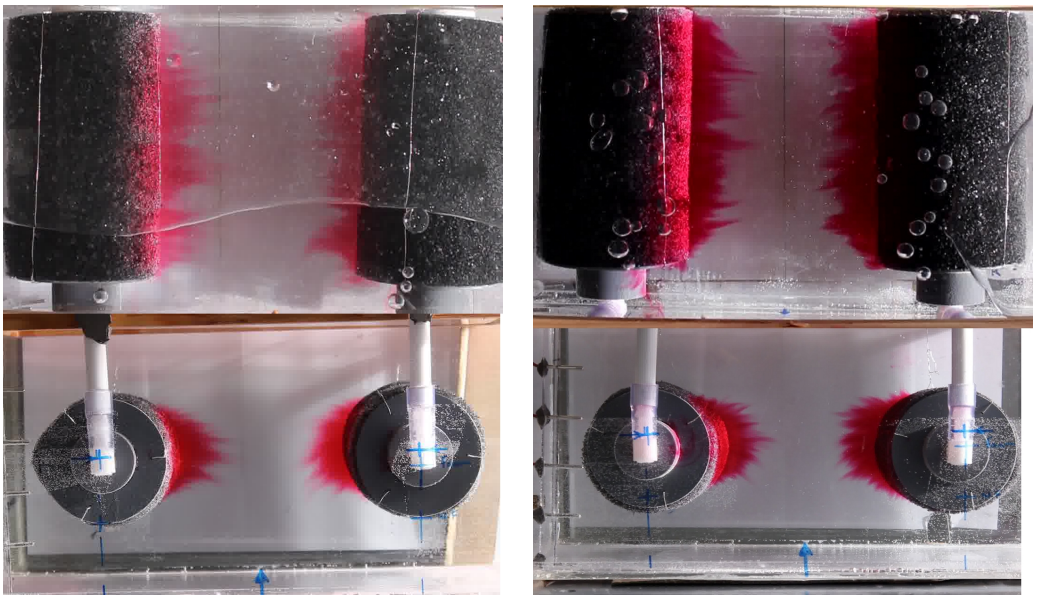

(a) Diffuser I (b) Diffuser II

Figure 3.36: Dye ink test on the perforated pipes with foam

Initially the experiment was conducted without using the reticulated foam. It was evident that only after few seconds that the water in the aquarium was significantly mixed. More number of holes in diffuser II lead to a smaller flow velocity, however due to more number of jets more surrounding fluid is entrained causing higher mixing as seen in Fig. 3.35(b).
From Fig. 3.36 the effect of using the reticulated foam stripes on the flow pattern is noticeable. It is evident by comparison that the flow front in the Fig. 3.36 has not even reached the half distance between the diffusers. This proves that the reticulated foam strips successfully reduce the inertia of the incoming flow and homogenise the flow such that no individual jets occur. If the static pressure inside the diffuser piping is uniform, uniform discharge velocity from the diffuser can be expected. Absolute uniformity is difficult to achieve, however it can be approximated by making the total opening area in the diffuser branch half the cross sectional area of the pipe. This approach has been recommended for distributed type diffusers (linear and radial) [61], [21]. Karim [35] applied this design criterion for two octagonal diffusers with slots oriented in vertically downward, radially inward and outward directions. Such diffuser has similarities to a ring shaped diffuser. He concluded that for a diffuser with higher ratio of flow opening area to pipe cross-sectional area the pressure drop along the diffuser length is non-uniform. Increasing the opening area would significantly lower the exit velocity of fluid. However, on the other hand it would lead to unequal pressure drop causing non-uniform flow velocities leaving the diffuser. In case of a ring diffuser system, where this ratio is much higher, it would mean a rotationally symmetric fluid entry into the tank would be difficult to achieve. This was the main motivation behind using the reticulated foam. The foam layer wrapped around the pipe sections is hence used to homogenise the exiting flow. The total opening area for the diffuser with single row of holes accounted for 28 % and for three rows of holes accounted for 84% of the pipe cross sectional area. The significantly increased opening area caused by the perforated pipe wall reduced the velocity of flow whereas the foam layer was beneficial towards the homogenisation of the flow. It was observed during the test that the velocity of the flow along the foam surface was uniform. The coloured water entered the tank almost at the same time from the whole length of the pipe sections. On the contrary, when no foam was used, the coloured water entered first through the holes situated near the fluid entry section and later through the holes further away. Hence it can be stated that the reticulated foam strips homogenise the flow.
An in depth investigation on exactly how much increase in the total opening area was offered by the foam is out of the scope of this work. However, efforts were made to approximate the area of the foam surface from where the flow entered the aquarium. The shape of the flow front defined by the coloured water was closely observed from the videos recorded. It was observed that the flow front of the diffuser I had a pointed shape while the flow front of the diffuser II was much wider as shown in Fig. 3.37. Here only the left sides of the diffusers are shown. The flow leaving the foam surface of diffuser II covered approximately 10% more surface area than the flow leaving surface of diffuser I. Consequently the velocity of the flow in case of diffuser II would be 10% lower.

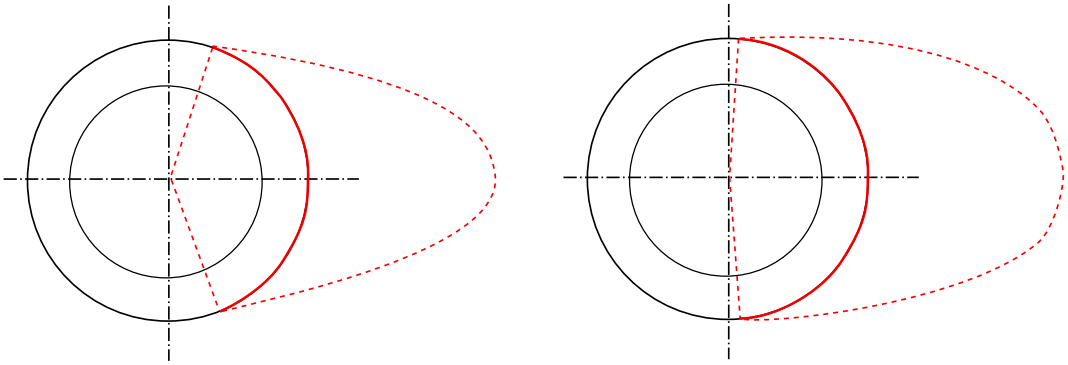

(a) Diffuser I (b) Diffuser II

Figure 3.37: Shape and span of flow velocity profiles observed from the ink test

Richardson number would then increase by 21 % for diffuser II as it is inversely proportional to the square of the flow velocity. Thus the diffuser II would provide favourable conditions for stable stratification in the tank.
Similar to the diffuser I and diffuser II, the third diffuser was tested in the aquarium. Fig. 3.38 shows the snapshot of the front view after 20 seconds.

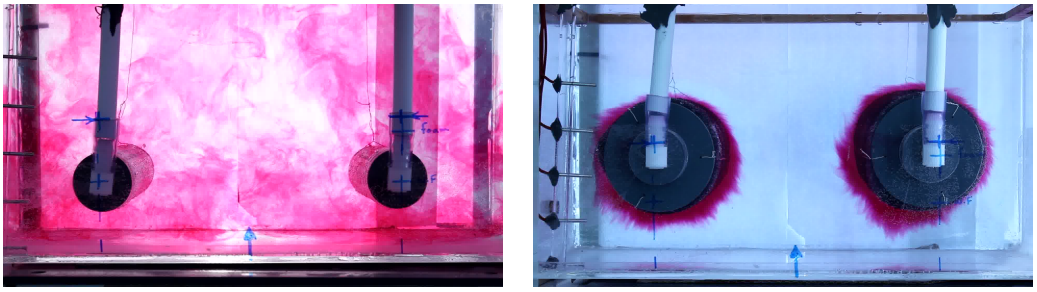

(a) Without foam cladding (b) With foam cladding

Figure 3.38: Dye ink test on diffuser III

The flow homogenisation by the foam layer is evident from this result. However, it was noted that construction of this diffuser was more time consuming and the improvement over the diffuser II was not significantly high. Hence the design of diffuser II was chosen for the construction of the stratification rings.

Chapter 4

Results and Discussion

4.1 Emulation of adsorption heat pump cycle and flow visualisation

The flow diffusers in the shape of rings were constructed based on the results obtained from the ink tests. The construction steps are documented in appendix A.3. These diffusers were mounted in the tank (Fig.3.27). The tank was hydraulically connected with the heating module (Fig.3.23), cooling module (Fig.3.24) and the adsorber emulator module (Fig.3.25) where the connecting interface being the solenoid valve bank placed on the lid of the tank (Fig.3.28, Fig.3.29). The schematic of this experimental set-up along with the temperature sensors relevant for further discussions is shown in Fig.4.1.

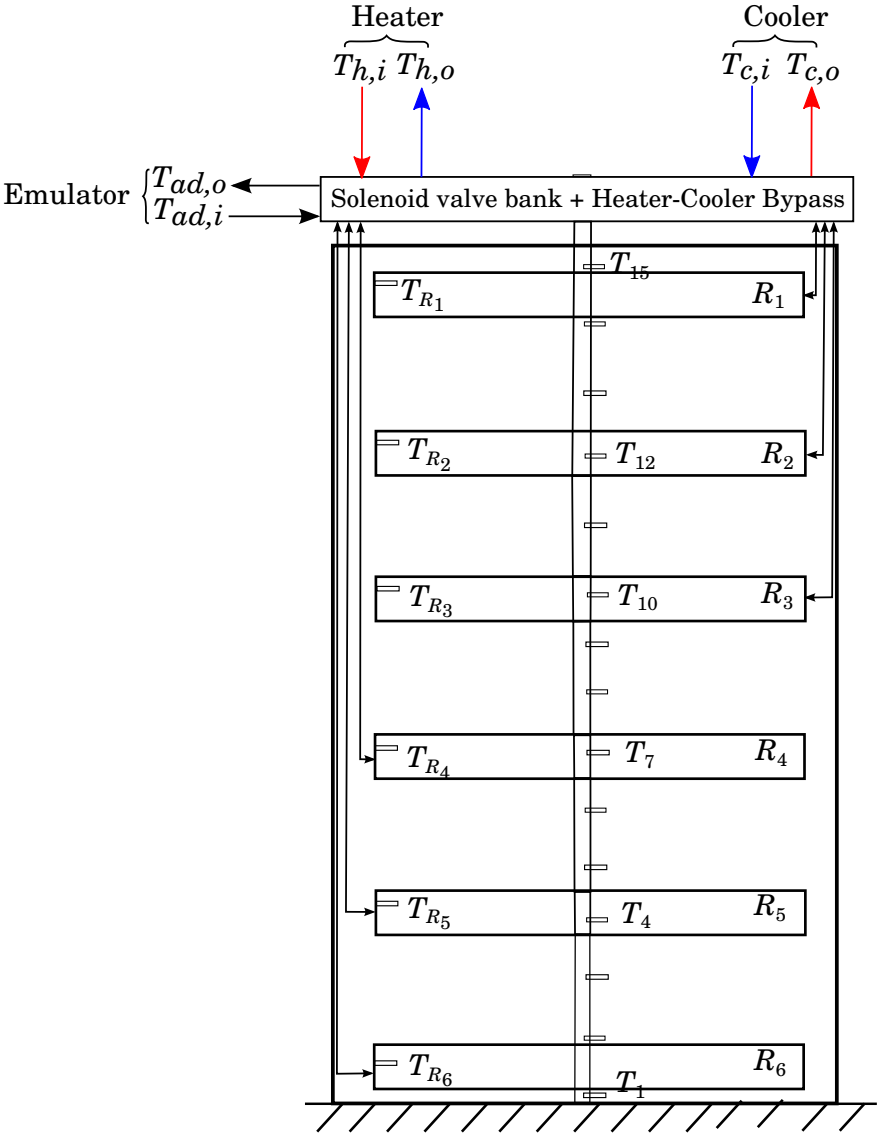

Figure 4.1: Experimental set-up for emulation and flow visualisation of the stratisorp cycle

The goal of this experimental set-up was investigation of the performance of the flow diffuser rings during a complete stratisorp cycle using BOS technique and various temperature measurements. The temperature of the flows leaving and entering the tank from different modules was measured by Pt-100 sensors ($T_{ad,i}$,$T_{ad,o}$ etc.). The tank temperature was measured using the Pt-1000 sensors (T_1,T_2,... etc.) mounted in middle of the tank on a plexiglas pipe. The sensors were stuck using a water and heat resistant adhesive fluid in holes drilled on the surface of the pipe and the connecting sensor cables were sewn through. Such measure assured that the cables remained dry during the experiment and did not affect the temperature measurement. Moreover, at the entry of each ring diffuser Pt-1000 sensor was mounted.
The emulator was programmed so that a pseudo stratisorp cycle could be run. Pseudo adsorption half cycle was carried out by extracting cooler water from the tank, heating it up to the defined set-point and inserting it back into the tank. Warm water was extracted by the emulator and inserted back into the tank at lower temperature to demonstrate a

pseudo desorption half cycle. The emulator extracted or inserted water in the tank using the stratification mechanism explained previously. The stratisorp cycle based on the silica gel-water pair offers a good overlap between the differential heats of adsorption and desorption for the selected temperature conditions (72/27/18 °C, cooling with low temperature lift), thereby offers a good potential for heat recovery. Only a small amount of heat remains unrecoverable. A part of the unrecoverable heat is deficit and a part is excess. The heat deficit should be supplied by the heater whereas the excess heat should be rejected by the cooler. The integral of the heating and the cooling energies during one adsorption cycle can be expressed as fraction of the recoverable heat. For the emulation of the thermodynamic cycle this fraction is set to 3. Hence the flow rates of the heater and the cooling module were scaled by the same factor with the flow rate of the emulator. The flow rate of the emulator was set to 300 lph [1]. Consequently the flow rate of the heater and the cooling module was set to 100 lph each. The highest temperature of the cycle was set to 60 °C rather than the originally planned 70 °C [2]. Therefore the lowest temperature in the tank was reduced to 20 °C. The water volume between the adjacent rings was approximately 100 litres. The emulator circulated water with 300 lph i.e. within 20 minutes the water between two ring would be completely circulated. Therefore switching time of 15 minutes was chosen. The various set-points and the time intervals are tabulated in Tab. 4.1. The temperature set-point of the emulator for the first adsorption step and of the heater for the complete duration of the cycle was set higher than 60 °C to compensate for the heat loss of both modules.

[1] The selection of this flow rate was dependent mainly on the test conditions from section 3.4. The flow diffusers were tested at 300 lph per diffuser. Therefore it was essential to evaluate working of the rings at this flow rate

[2] Initial tests with 70 °C highlighted the drawback of using open hydraulic system. The maximum pressure of this system was little over 1 bar (Atmospheric pressure plus the hydrostatic pressure of the water column inside the tank) because of the open water surface in the tank. The circulation pumps in the emulator and the heater were fitted with single lip radial seals. These seals offer sealing action from inside of the pump to the outside with the prerequisite of pressurised system. That meant any local pressure drop near the pump shaft sucked air in the pump therefore in the module which obviously led to flow rate fluctuations. This effect was even graver at higher temperatures as the sealing material gets softer with increase in temperature

Module	Time (min)	$T_{setpoint}$ (°C)	$\dot{V}$ (lph)	Extraction	Insertion
Heater	150	63	100	R_2	R_1
Cooler	150	20	100	R_5	R_6
Emulator (Adsorption)	15	63	300	R_2	R_1
		55		R_3	R_2
		53		R_4	R_3
		43		R_5	R_4
		33		R_6	R_5
Emulator (Desorption)	15	20	300	R_5	R_6
		30		R_4	R_5
		40		R_3	R_4
		50		R_2	R_3
		55		R_1	R_2

Table 4.1: Set-points and time intervals of various modules during emulation

Water was extracted from next lower or next upper ring after every 15 minutes during the adsorption or the desorption half cycles respectively. Naturally the duration of both half cycles was 75 minutes each. Initially the water in the tank was at uniform temperature. It has been hypothesised that a quasi stationary stratisorp cycle has a linear temperature profile in the tank. Such profile leads to low mixing [53]. It would take very long to reach a quasi stationary linear temperature profile in the tank. Hence, it was crucial to precondition the tank before the actual measurement started. The preconditioning of the tank was aimed at achieving a linear temperature profile.

A temperature profile between the warmest zone at the top (at 60 °C) and lowest temperature at the bottom (20 °C) would be an ideal preconditioned tank for the stratisorp application. The first zone (Z_1) shown in Fig. 4.2 was preconditioned using the heater. The heater extracted water from the tank through R_2 and inserted heated water through R_1. Similarly the last zone (Z_5) was preconditioned using the cooling module. It extracted water from the tank through R_5 and inserted it back through R_6 after cooling it to the set-point. The emulator was deployed for preconditioning of the remaining zones after Z_1 and Z_5 were completely conditioned. Each zone is bordered by two rings. The water from lower lying ring was extracted and the conditioned water at the set-point was reinserted in the next upper ring. The zones from Z_2 to Z_4 were sequentially preconditioned starting with Z_2 after Z_1 had reached the set-point. The tank temperature was constantly monitored over the LabView interface. The preconditioning of each zone lasted 20 minutes with 300 lph.

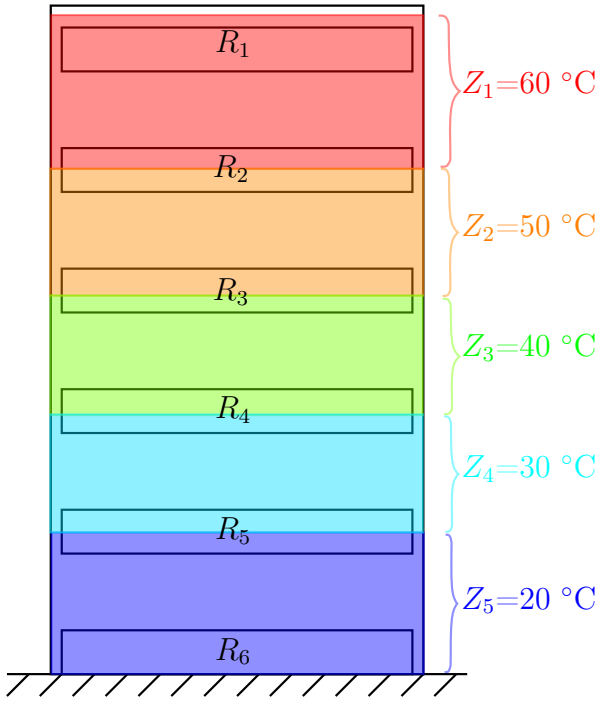

Figure 4.2: Preconditioning of the tank zones

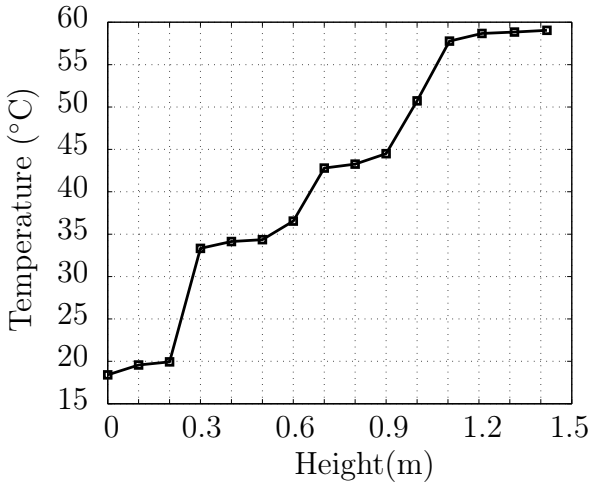

Figure 4.3: Temperature profile after the conditioning sequence

At the end of the preconditioning sequence i.e. when the zone Z_4 was completely preconditioned, the adsorption half cycle could be initiated. The sequence of switching between different rings during the adsorption and the desorption half cycle is shown in the Tab. 4.1. The temperature at different positions along the height of the tank immediately after preconditioning of the tank is shown in Fig. 4.3. It can be seen that the temperature profile along the height of the tank is nearly linear. The flat plateaus in the profiles show that an approximately uniform temperature had been reached in different zones between the rings.

4.1.1 Results of the thermodynamic cycle

Fig. 4.4 depicts temperatures in the heating, cooling and emulator loops as well as the temperatures of flows entering or exiting the tank from the stratification rings.

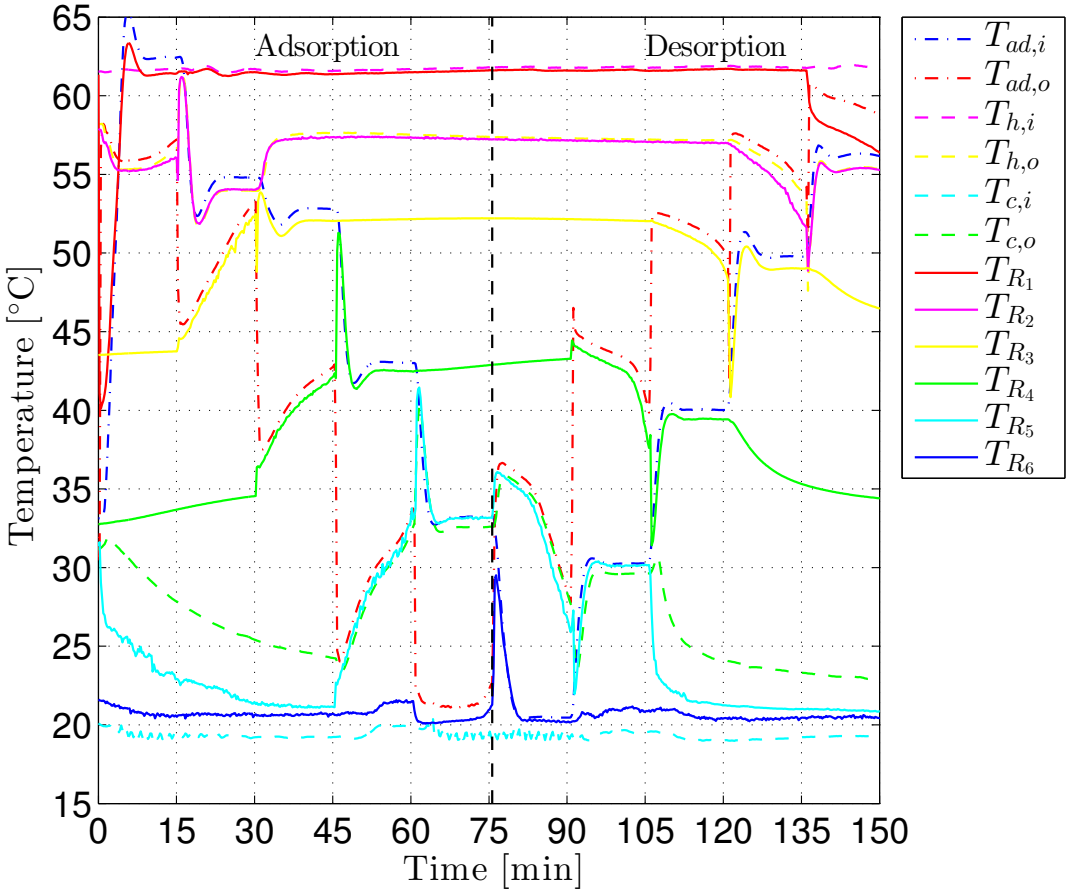

Figure 4.4: Emulated stratisorp cycle: temperatures in the heating, cooling and emulator loops

As seen before from Fig. 4.1, the temperature sensors $T_{ad,i}$, $T_{ad,o}$, $T_{h,i}$, $T_{h,o}$, $T_{c,i}$, $T_{c,o}$ are on the outside of the tank while the sensors T_{R_1},...,T_{R_6} are located inside the tank. Before the adsorption half cycle started, the emulator had been preconditioning Z_4. Hence at the start of the adsorption cycle, the sensor $T_{ad,o}$ recorded the temperature of the water in the tubes between the tank and the emulator. The emulator then heats the extracted water to set-point of 63 °C with maximum available power. The control loop of the emulator overshoots the set-point by 2 °C. However the steady state is immediately achieved and the supply water temperature $T_{ad,i}$ reaches the set-point. Thus the heated water being inserted into the tank at temperature $T_{ad,i}$ emulates the return flow from the adsorber chiller after it had absorbed the heat of adsorption. However, during the real adsorption half cycle, $T_{ad,i}$ would continuously drop as $T_{ad,o}$ i.e. supply temperature to the chiller, would gradually increase causing a drop in the heat of adsorption released. Hence $T_{ad,i}$ would not remain constant in case of a real adsorption chiller like seen in Fig. 4.4. The rise in $T_{ad,o}$ is caused by the plug flow moving in the zones from the upper rings to the lower rings e.g. from R_2 to R_3 in Z_2. More and more warmer water returning to the tank is pushed down after initial mixing causing rise in $T_{ad,o}$. Exactly opposite effects are observed during the desorption half cycle. The water returning to tank is cooler. During each desorption step between the adjacent rings, the cooler water returning to the tank is pushed upwards in a plug flow after initial mixing and formation of thermocline. Hence $T_{ad,o}$ gradually drops. In case of the real desorption half cycle, $T_{ad,i}$ would gradually increase during each desorption step. This experiment is basically aimed

at evaluating the functional effectiveness of the ring stratification system and not at exact reproduction of the adsorber chiller-stratified tank system behaviour. Hence these functional differences are not crucial in this experiment.
The adsorption half cycle continues by extracting water from the lower rings and inserting heated water into the upper rings. After every 15 minutes, the water is extracted from the next lower ring as explained earlier. The straight pipe sections connecting the solenoid valve bank with the rings pass through the thermally stratified field. Hence the water being extracted from the tank at temperature T_{R_i} warms up continuously till it reaches to the sensor $T_{ad,o}$. It can be noticed that $T_{ad,o}$ is always higher than the temperature of water leaving the corresponding ring. This effect was observed even though the straight pipe sections were insulated. The identical effect is seen during the desorption half cycle. After the switching to the next lower ring takes place, the warm water in the tubes between the emulator and the tank is still at the previous temperature set-point which is higher than the new set-point. This warmer water enters the new ring at elevated temperature causing a peak in T_{R_i}. The sharp rise in T_{R_6} immediately after switching to the desorption half cycle after 75 minutes happens due to the same reason. On the contrary, during the desorption half cycle after switching to the next upper ring, the water at temperature lower than the new set-point first enters the ring causing sharp fall in T_{R_i}. Another important effect can also be observed namely $T_{c,o}$ and T_{R_5} differ considerably ($\sim$ 5 K) although the temperature of the water being extracted from R_5 is measured by the sensor $T_{c,o}$. The cooling module extracts water from R_5 with 100 lph. Heating power of 584 W is delivered by the warmer fluid layers situated above as the residence time is significantly long ($\sim$ 1 min). This effect is observed until the start of the fourth adsorption step. During the fourth adsorption step the flow rates of the emulator and the cooling module overlap and as a consequence, the water is extracted through R_5 at 400 lph. The higher flow-rate reduces the residence time and the difference $T_{c,o} - T_{R_5}$ reduces. A similar effect is identified during the desorption half cycle. The flow returning to the tank from the cooler is at $T_{c,i}$ which is seen slightly fluctuating. These fluctuations were completely removed by properly tuning the controller as explained in appendix A.5.

Fig.4.5 shows the temperatures along the axis of the tank during the emulated thermodynamic cycle. The temperature near the water surface (T_{15}) does not seem to remain constant for the duration of the cycle. The cause for this effect being the uninsulated tank lid leading to significant heat loss through the lid. The level in the tank where the flow from the heater and the cooler enter and leave the tank is also shown[3].

It can be easily noticed that during each adsorption step, only the temperature sensors located in the corresponding zones show rise in temperature while the temperature outside of this zone remains relatively unaffected e.g. during the second adsorption step which takes place in Z_2, only T_{12}, T_{11} and T_{10} increase while T_{13} and T_9 remain relatively unaffected. The slight drop in T_{13} is due to cooling of Z_1. An opposite effect is seen during the desorption half cycle owing to the change in the direction of flow insertion and extraction. Here the sensors in the corresponding zones show drop in temperature as plug of cooler water entering the tank moves from lower ring to the upper ring. These flow phenomena were closely investigated using flow visualisation based on BOS technique.

[3]FH-**F**rom **H**eater,TH-**T**o **H**eater, TC-**T**o **C**ooler,FC-**F**rom **C**ooler

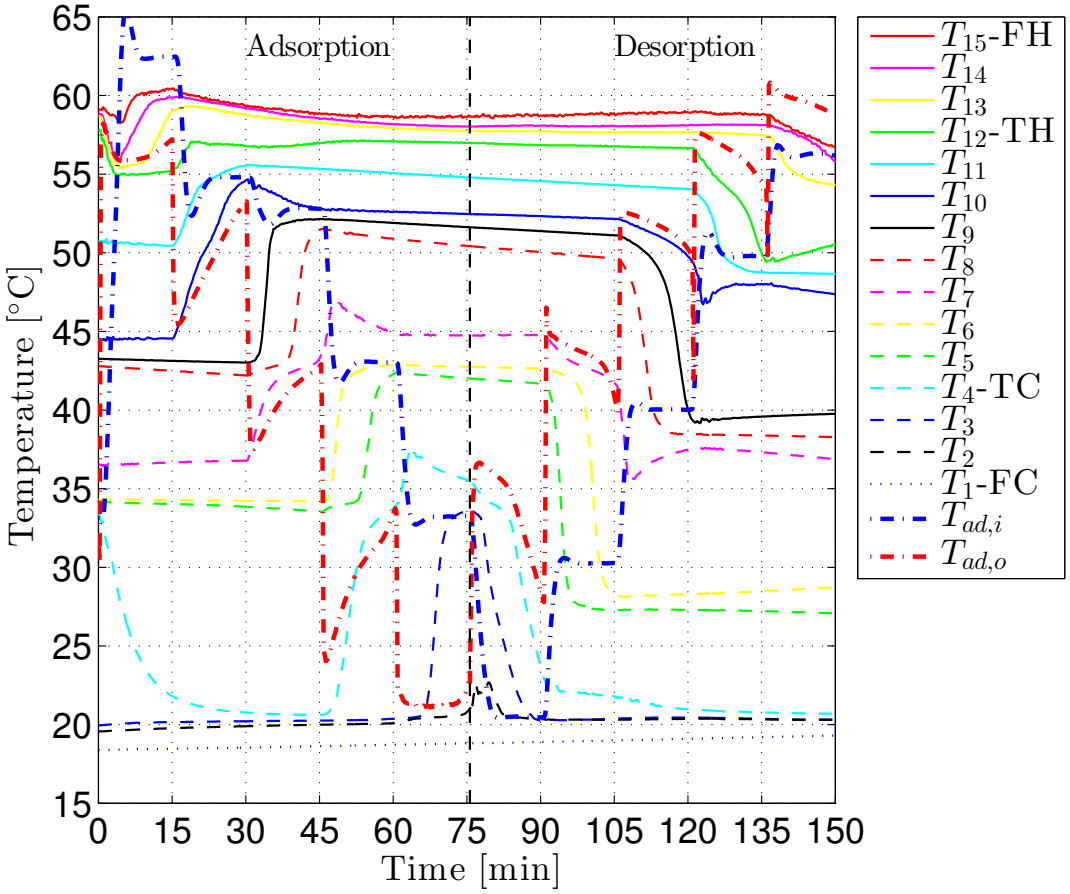

Figure 4.5: Temperatures along the height of the tank

4.1.2 Flow visualisation for investigation of stratification mechanism

Fig. 4.6 shows the experimental set-up used for this study.

The sensitivity of this experiment could be increased by decreasing the ratio of the distance of camera to the density field (b) and to the background (a) (i.e. the density field moves closer to the camera and away from the background) [30]. As the background was stuck to the rear window on the outside, any change in distance b (i.e. moving camera closer or farther from the tank) would change a and thereby the sensitivity of the measurement. The distance a was limited by the dimension of the room. For this experiment, $b/a = 0.82$ was used. The background used in the present experiment was composed of randomly distributed black squares on a white background of 0.34 x 0.8 m. The resolution of the image was kept the same as used in the other experiment (i.e. 20 pixel/dot for the video mode). This resolution resulted in very high resolution (180 pixels/dot) for the photo mode of the camera which recorded images at every 3 seconds with external trigger at full resolution of 18 megapixels. This resolution was chosen as for some experiments two cameras were simultaneously deployed: one camera operating in video mode and the other operating in photo mode with external trigger.

Fig. 4.7 shows the unmasked and the masked image of the background. The region covered by the rings and the temperature lance has been masked and excluded from the BOS analysis.

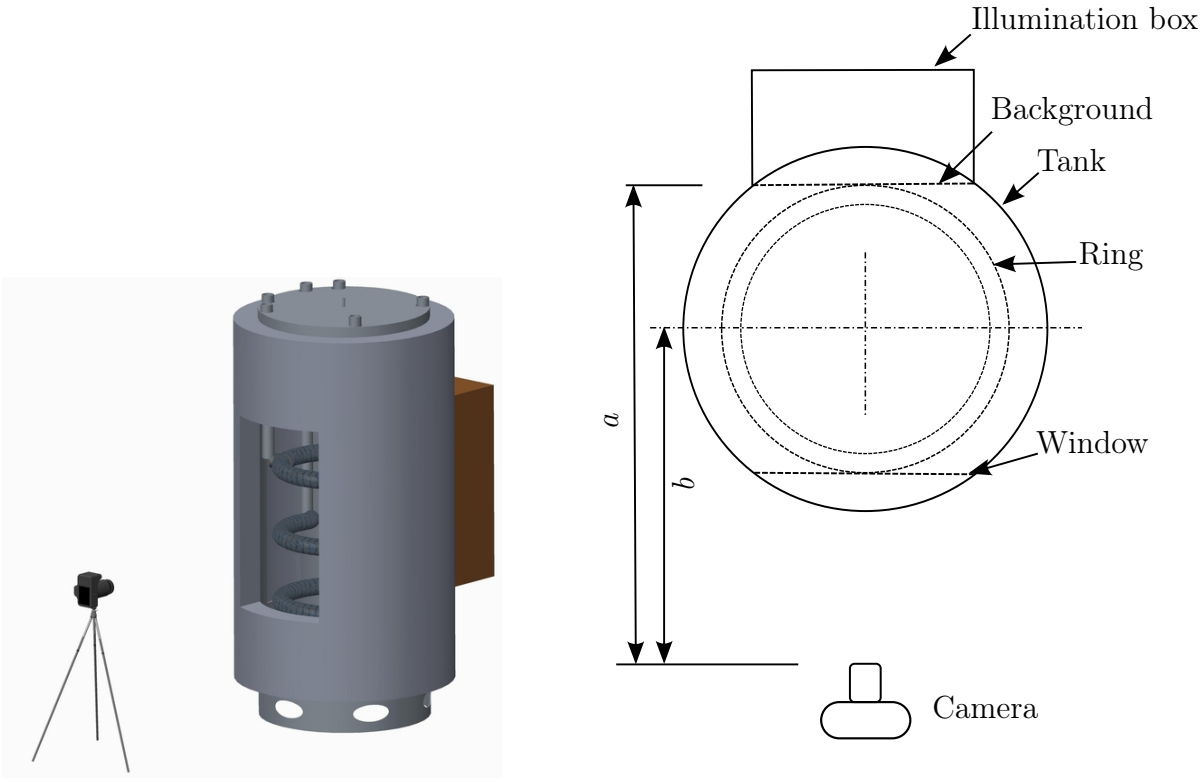

(a) Experimental arrangement (b) Optical arrangement

Figure 4.6: BOS set-up for evaluating the performance of the ring stratification system

Additionally a horizontal temperature lance was installed between R_3 and R_4 for evaluating the horizontal temperature field. The sensors on this lance were numbered from TH_1 near the front window to TH_9 near the rear window. From Fig. 4.7 it is clear that the flow visualisation was carried out in Z_3 and Z_4. The observable section of the adsorption half cycle is between 30 and 60 minutes and for the desorption half cycle is between 90 and 120 minutes.

The temperature sensors T_5, T_6, T_8 and T_9 lying in these zones can be seen while the sensors T_{10}, T_7 and T_4 are concealed by the rings R_3, R_4 and R_5 respectively. The background picture was recorded at the start of the experiment i.e. immediately after the tank was preconditioned to a nearly linear temperature profile as explained before.[4] The data acquisition running under LabView and recording of the images using external trigger was simultaneously commenced.

Fig.4.8 shows the contour plot of the resultant pixel displacements during the adsorption half cycle and the downward movement of the thermocline through the zones Z_3 and Z_4. The position of the thermocline at various points in time is shown. The warmer water entering the rings mixes with the water in the tank and forms this thermocline. The temperature gradient within the thermocline region is almost entirely vertical (refer appendix A.3). As

[4]In the classical BOS method, the background image is recorded when no temperature gradient in the fluid domain exist. i.e. when the tank was at a uniform temperature before the start of the conditioning process. However, it was not possible due to practical difficulties e.g. limited battery charge, camera prone to shaking during simultaneous lab activities during preconditioning process etc.

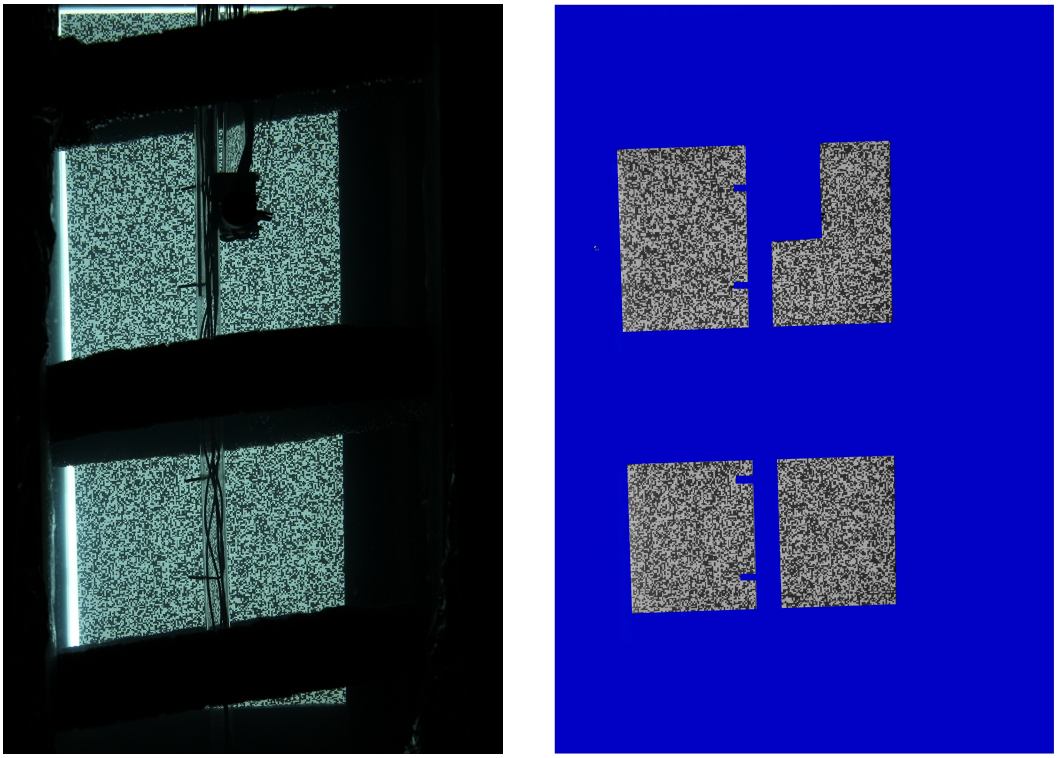

(a) Unmasked image of the background (b) Masked background image

Figure 4.7: Image preprocessing before the BOS analysis

the thermocline moves through the zones towards the ring lying below, the next plug of warm water enters the tank. The thermocline prevents the mixing of the warm water entering at the top and the cooler water leaving from below. The rings insert the flow into the tank in rotationally symmetric fashion. It can be seen that the region above the thermocline, which has higher temperature than before, has negligible temperature gradient.

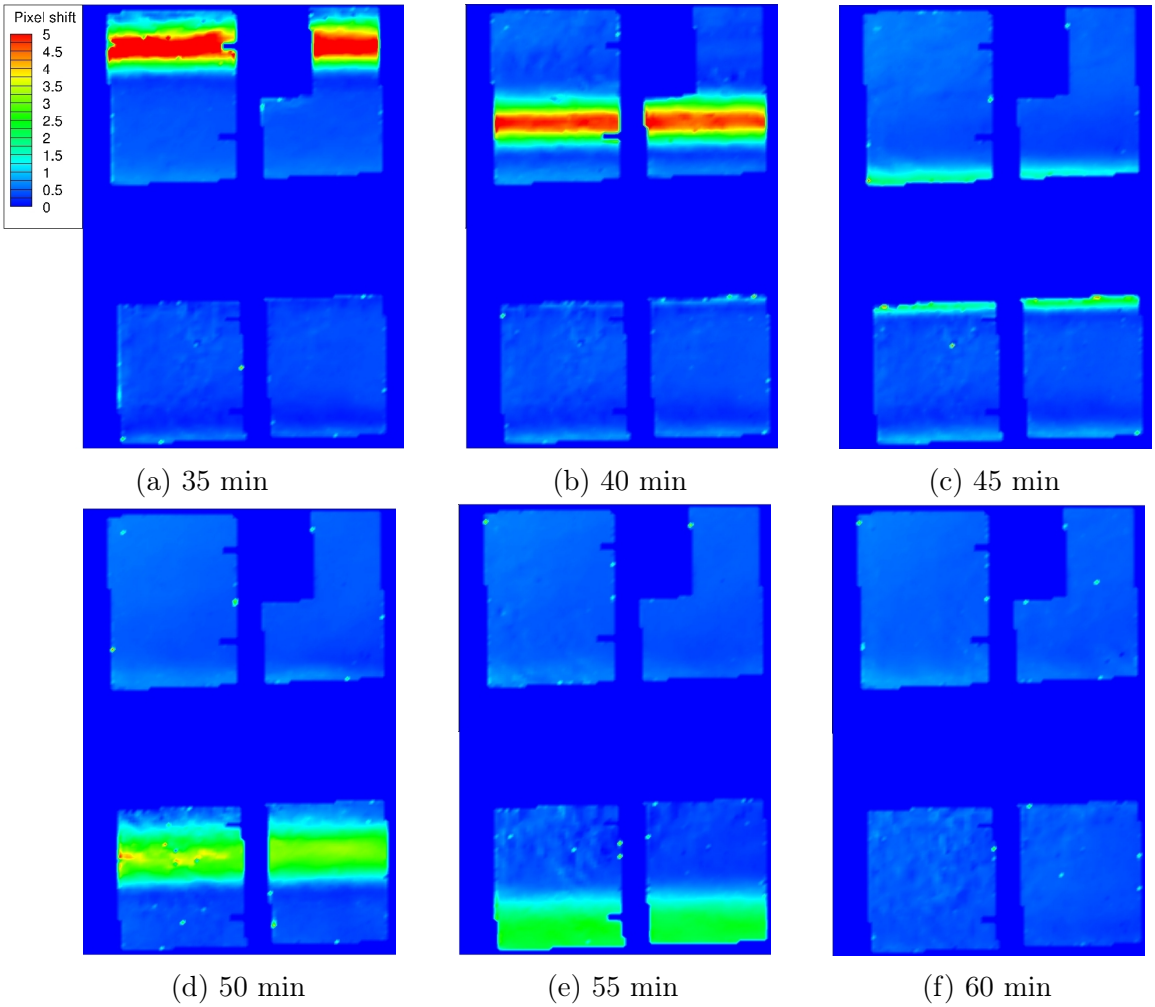

(a) 35 min (b) 40 min (c) 45 min

(d) 50 min (e) 55 min (f) 60 min

Figure 4.8: Downward movement of the thermocline through Z_3 and Z_4 during the adsorption half cycle

This effect can also be seen in Fig. 4.9. The flow enters Z_3 at temperature $T_{ad,i}$ and leaves at temperature $T_{ad,o}$. As soon as the thermocline passes by T_9 at 35 min., T_9 attains the elevated temperature close to $T_{ad,i}$ and remains approximately constant thereafter. The trend of T_8 as well is fairly parallel to $T_{ad,i}$ and T_{10} after the thermocline has passed by. The slight drop in the temperature is caused by heat lost to the ambient through the uninsulated glass windows. Similar trends are observed for the T_6, T_5 and T_4 as the adsorption half cycle continues through Z_4.

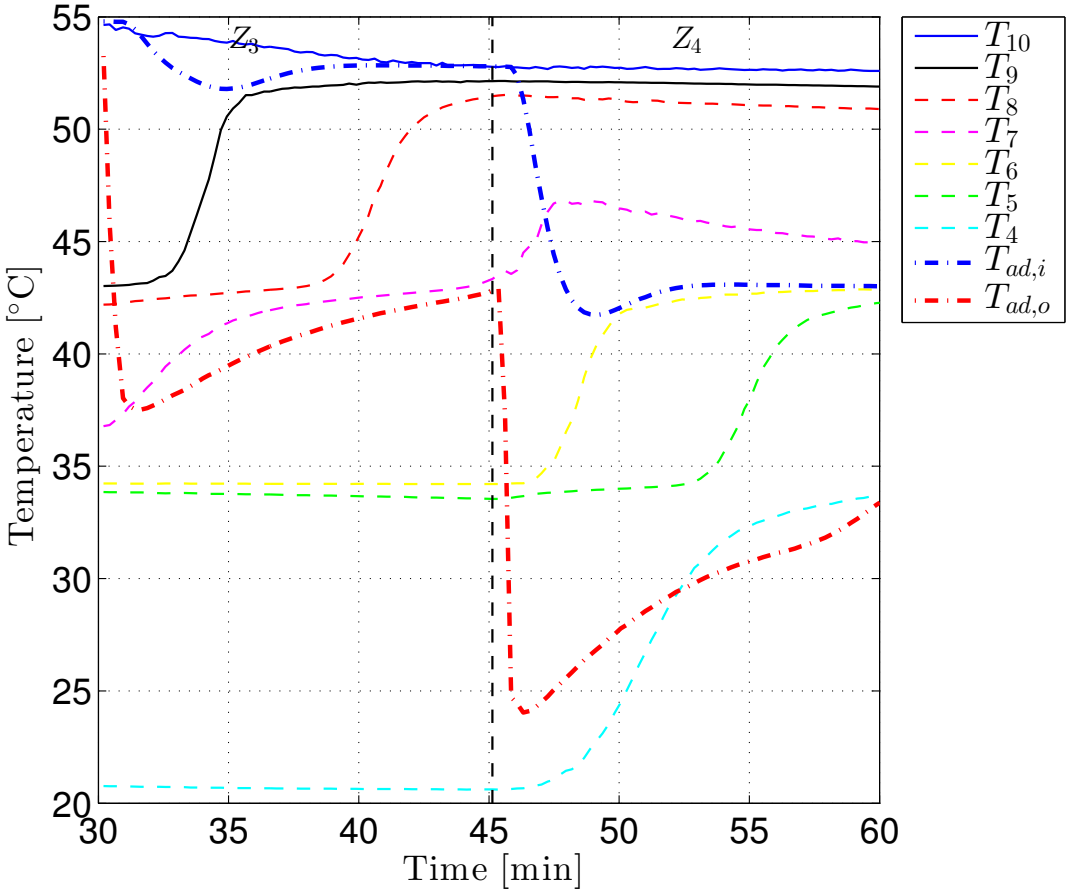

Figure 4.9: Change in the temperatures in the zones Z_3 and Z_4 during the adsorption half cycle

Fig. 4.10 shows the upward movement of the thermocline during the desorption half cycle using the contour plot of the resultant pixel displacement at various points in time.[5] The thermocline moves upwards towards the upper lying ring and passes by T_5, T_6, T_7 in Z_4 and then by T_8, T_9, T_{10} in Z_3. These sensors show drop in temperature as cooler water moves upwards after the thermocline (Fig. 4.11).[6]

[5]The bright dots in the contour plot are the residual outliers of the BOS post processing
[6]Refer appendix A.3 for additional plot

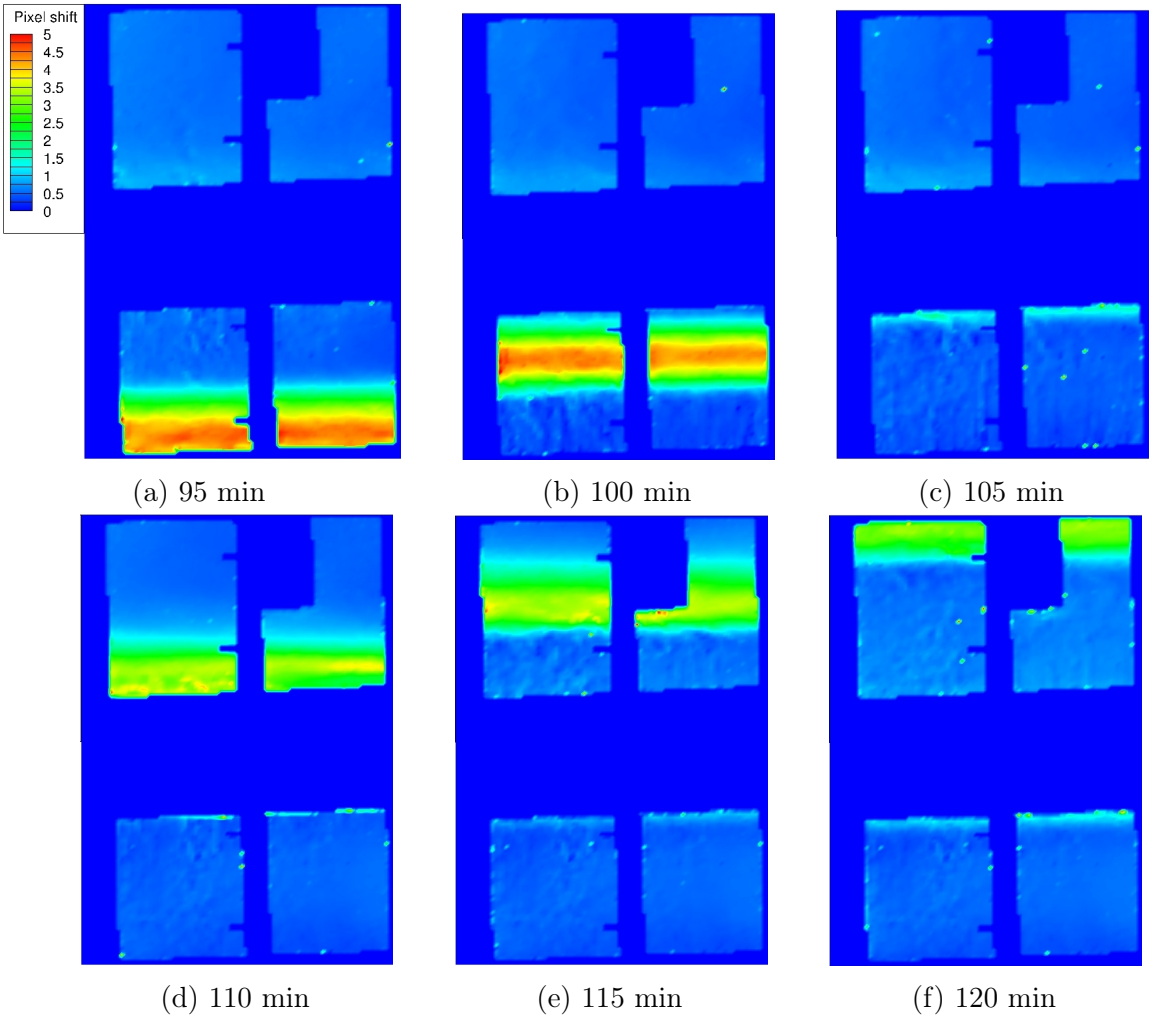

(a) 95 min (b) 100 min (c) 105 min

(d) 110 min (e) 115 min (f) 120 min

Figure 4.10: Upward movement of the thermocline through Z_4 and Z_3 during the desorption half cycle

When the thermocline region passes in front of the background image, the light rays passing through it bend differently depending upon the temperature gradient perpendicular to the direction of viewing. The temperature gradient is steeper in the middle of the thermocline and is flatter near the thermocline-hot water interface as well as thermocline-cool water interface. This gives rise to darker contours in the middle and lighter contours near the edges of the thermocline. However, the temperature gradient within each slice of the thermocline remains constant giving rise to uniform temperature contours along the thickness of the thermocline. The refractive index of water is dependent on the temperature and the wavelength of light passing through [31]. The dependence of refractive index on the wavelength of light used does not affect the quality of the BOS results significantly [23]. As the background was recorded when the tank had been linearly stratified, the contour plots of the resultant pixel displacement for the subsequent images show differences in the colour depth. These plots serve the purpose of only qualitative illustration of the thermocline. A quantitative information about the flow phenomenon in the tank can be achieved when these contour plots are considered together with the temperature plots.

The water entering the tank is nearly at the same temperature as that of the water at

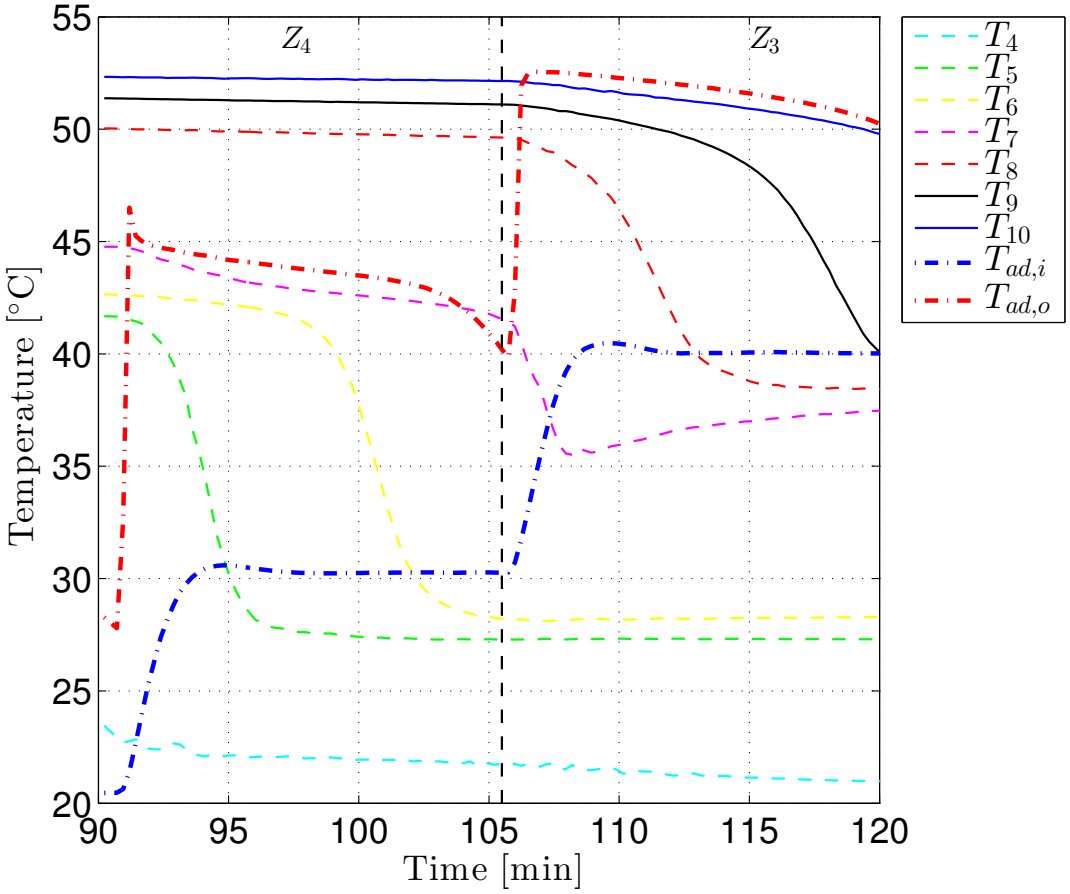

Figure 4.11: Change in the temperatures in the zones Z_4 and Z_3 during the desorption half cycle

the level of the corresponding ring. It happens due to the preconditioning of the tank as seen from Fig. 4.2. All stratified layers above this level are warmer and below this level are cooler. Hence the incoming water mixes strongly with the water in the tank at the corresponding level. Hence the plug flow movement of the thermocline is predominantly seen in this experiment. This flow phenomenon would take place during the initial adsorption heat pump cycles i.e. when the cycle has not reached the quasi steady state. After each cycle the tank temperature profile is expected to change gradually to a linear profile. The final temperature profile in the tank need not always be linear. However for this specific cycle condition a linear temperature profile has been predicted by the simulation studies. Therefore a further experiment was carried out to investigate the stratification behaviour when the tank is linearly stratified.

A linear temperature profile was achieved by preconditioning the tank using the adsorption chiller as shown in the Fig. 4.12. Instead of carrying out the complete adsorption heat pump cycle only one of the desorption steps, namely extraction at R_3 and insertion at R_4 across Z_3, was performed.

It was important to test the performance of the stratification rings at a significantly higher flow rate. Hence, the flow rate of the adsorption chiller was set to 680 lph. Consequently the duration of the experiment was reduced to 9 minutes from 15 minutes per extraction

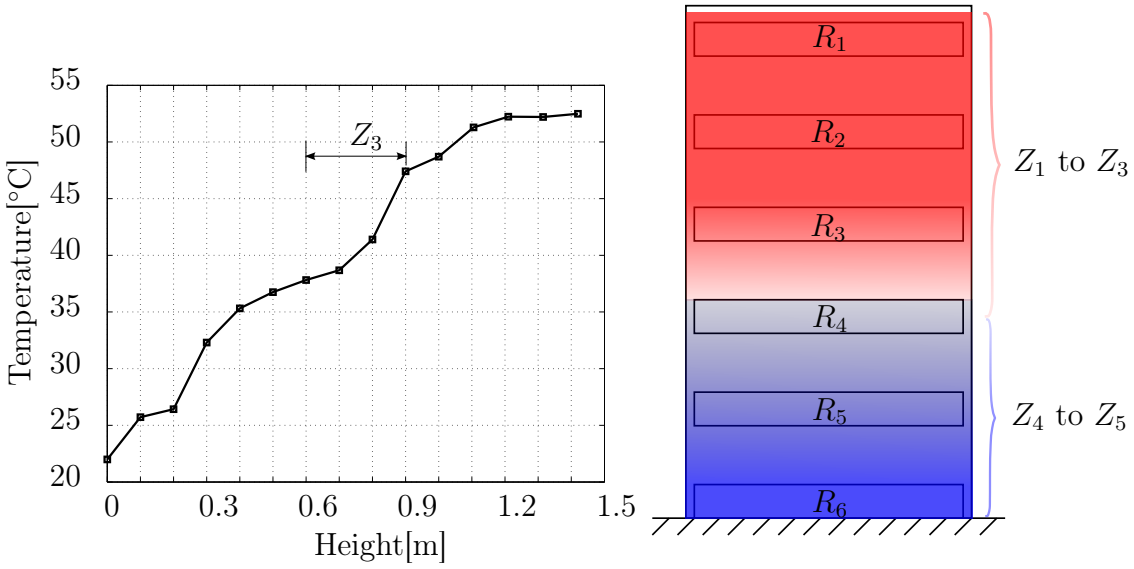

(a) Temperature profile (b) Zone temperatures

Figure 4.12: Preconditioning for the stratification test

level. The temperature of the flow returning to the tank from the adsorption chiller varied during this desorption step. This was another difference between both experiments. Due to short measurement time the video mode of the camera was used along with the photo mode. The progressive BOS analysis method was used to investigate the stratification behaviour [7]. Fig. 4.13 shows the change in the tank temperature at different levels in Z_3. The desorption step can be roughly divided into three distinctive phases. When temperature of the water entering the tank from the adsorption chiller,T_{R_4}, is :

a) $T_{R_4} < T_7$

b) $T_7 < T_{R_4} < T_{R_3}$

c) $T_{R_4} > T_{R_3}$

The state c would not appear during a real desorption half cycle as the extraction level would be switched to the next upper ring as soon as the temperature difference between the supply and the return flows ($|T_{R_3} - T_{R_4}|$) would be lower than a certain threshold. Here such switching criterion was not implemented in order to investigate the flow field.

[7]As differed to the classical BOS, the progressive BOS compares each image with each "neighbouring" image. The background image used for the analysis hence progresses forward through the sequence of images and every next image is regarded as background. Very small pixel displacements can be captured with this method. Therefore the flow front can be made visible

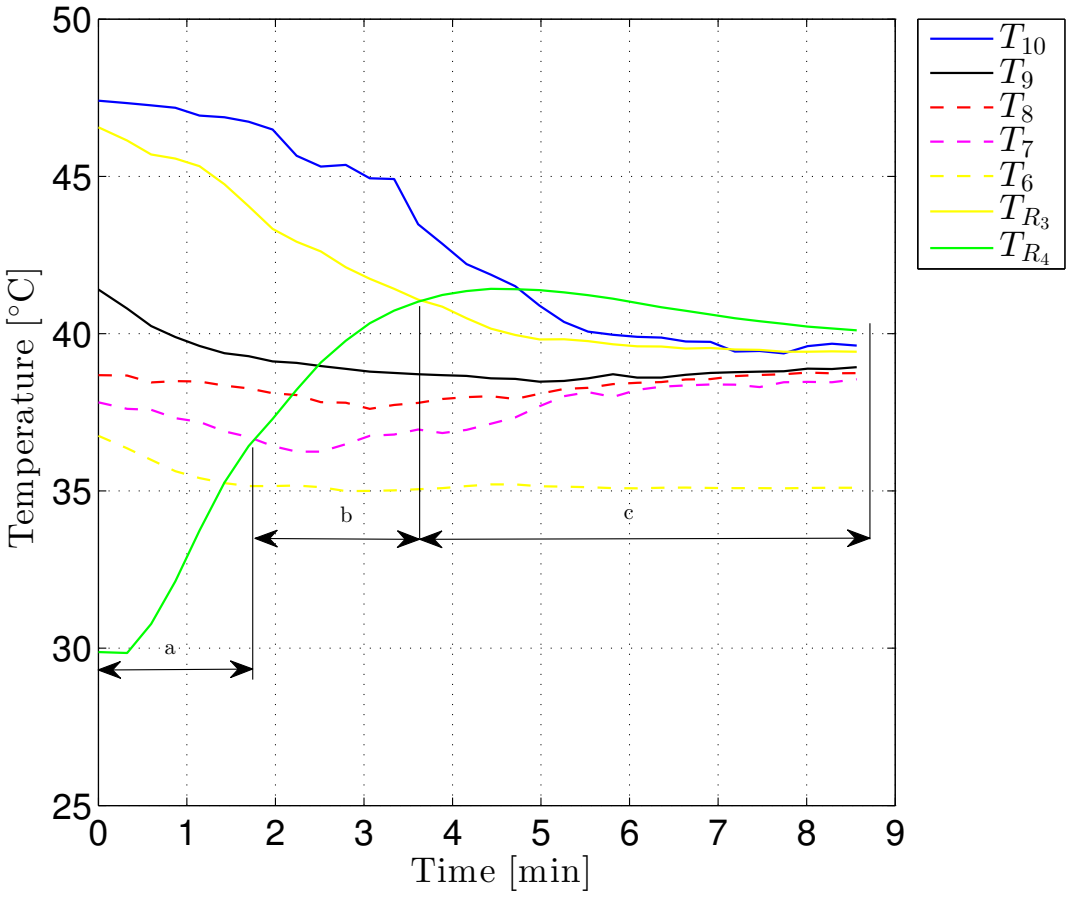

Figure 4.13: Change in the temperatures with in Z_3

Phase a : As the water entering the tank at R_4 is cooler than the surrounding water, the buoyancy force is directed downwards. It can be seen that T_6, which is located marginally below R_4 in Z_4, shows drop in temperature. This phenomenon can be observed very well in the BOS observations (Fig. 4.15(a)). The sensor T_7 which is located exactly behind the stratification ring R_4 also shows drop in temperature. The temperature drop in T_7 is relatively lower than in T_6. At the set flow rate of 680 lph, the stratification function of the rings is thus fulfilled as they cause low mixing in the tank.

Phase b : The temperature of the water being extracted from the tank gradually lowers (drop in T_{R_3}) thereby T_{R_4} gradually rises. As soon as T_{R_4} rises above T_6, the buoyancy is gradually directed upwards. It can be observed that T_6 does not change after the end of phase a. At the start of the phase b, the flow tends to stratify at the point of entry behind the ring. Hence very little pixel displacement is observed (Fig. 4.15(b)).

Phase c : The adsorber chiller receives further cooler water towards the end of the desorption step. Soon after the start of phase c, T_{R_3} drops below T_{R_4}, which means that the adsorber chiller would start adsorbing. Consequently T_{R_4} rises above T_{R_3} and the buoyancy force acting on the flow is directed upwards.

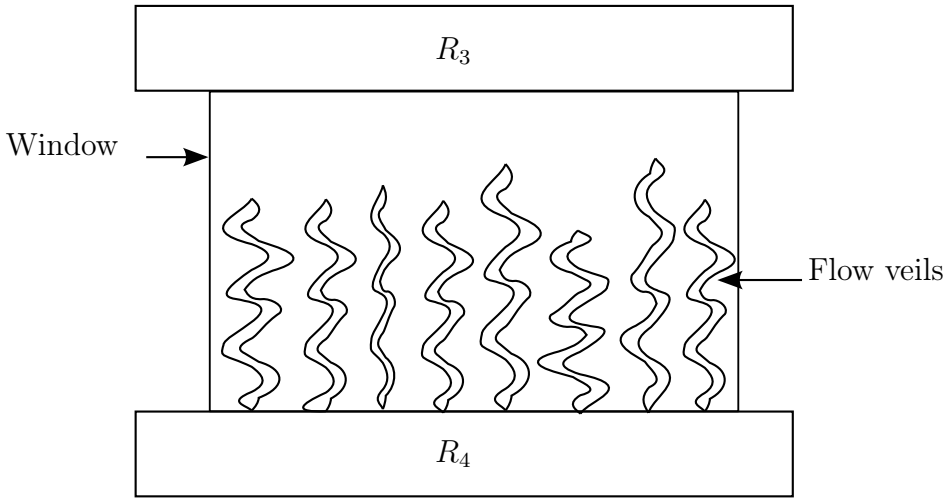

Figure 4.14: Schematic description of the flow veils

The flow entering in R_4 is warmer than the surrounding water. The flow leaves the surface of the ring diffuser in the form of veils forming a kind of curtain (Fig. 4.14 and Fig. 4.15(c)). The water in the middle of the tank remains relatively undisturbed as suggested by very slow change in T_7, T_8 and T_9. This change in temperature shows a completely different pattern than observed previously in Fig. 4.9 and Fig. 4.11.

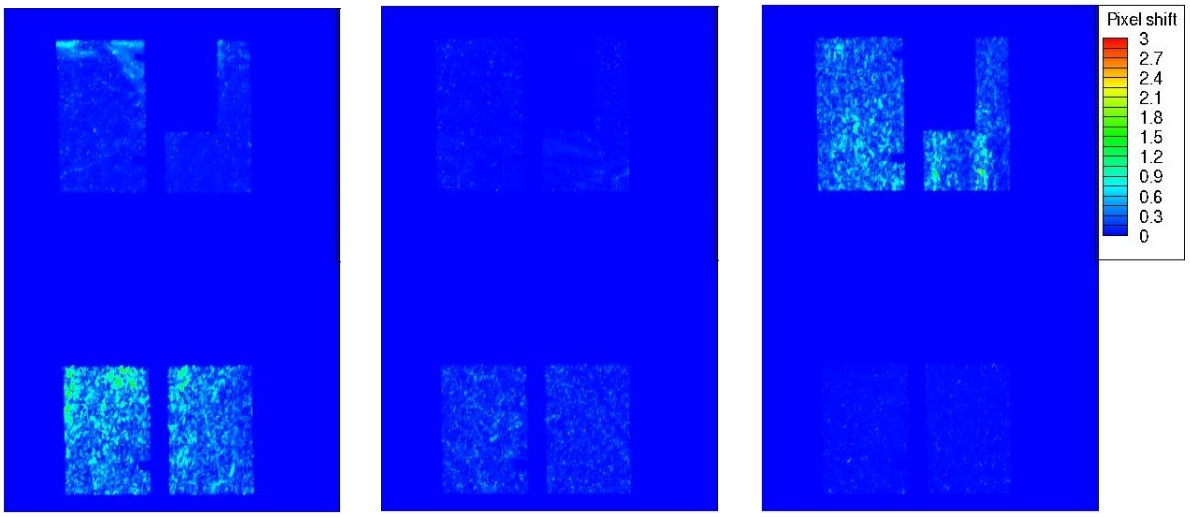

(a) 1 min (b) 3 min (c) 6 min

Figure 4.15: Stratification behaviour observed during the different phases of the desorption step

The occurrence of the veils of flow can be additionally confirmed by assessment of temperatures in the horizontal plane. Fig.4.16 shows the temperatures recorded by the sensors mounted on horizontal lance. During the phase c which starts after approximately 3.5 minutes, the sensors near the window (TH_1 and TH_2) show higher temperature than the other seven sensors (TH_3 to TH_9) lying in the same plane. Being near the window i.e. directly above the ring perimeter, TH_1 and TH_2 fall in the path of the flow veils and hence show rise in temperature.

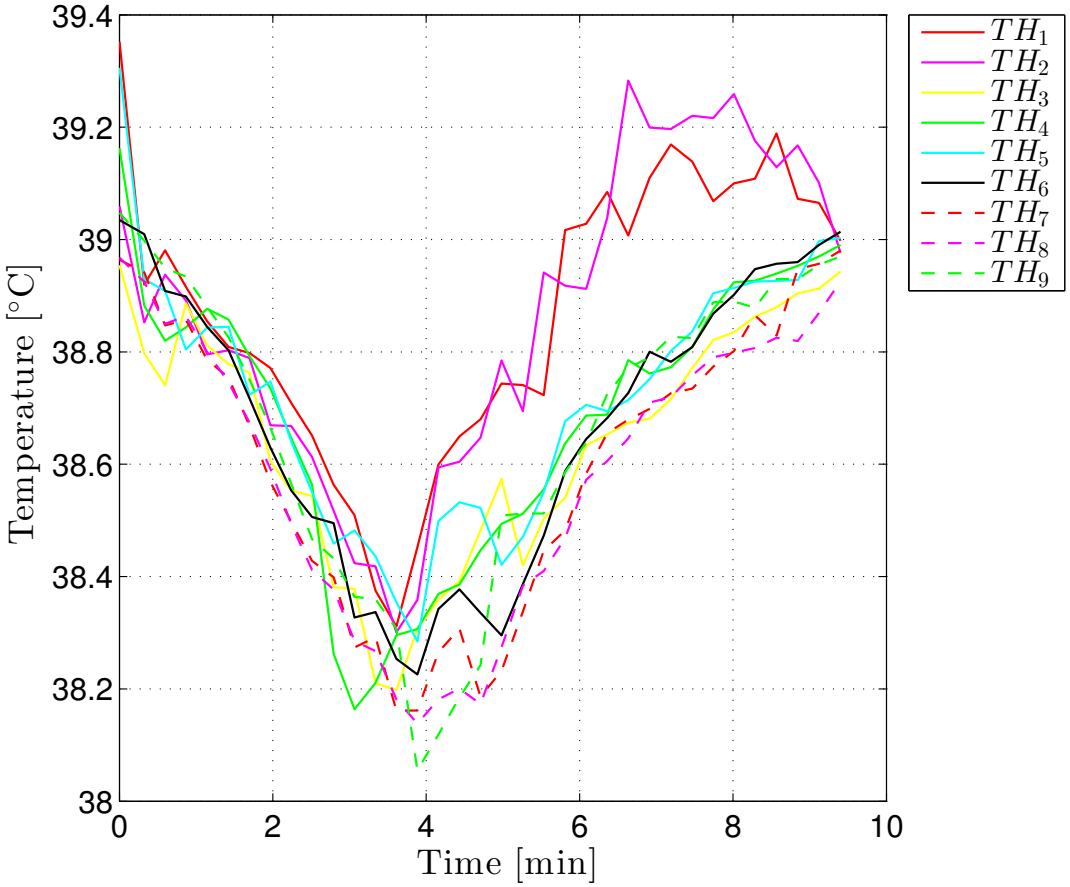

Figure 4.16: Temperature in the horizontal plane in Z_3

4.1.3 Conclusion of flow visualisation experiments

The stratification rings constructed for loading and unloading provide rotational symmetry to the flow and reduce the mixing in the tank. The rotational symmetry of the flow was confirmed by visualisation of a well defined thermocline. The reduction in mixing was however confirmed at low flow rate (300 lph). At higher flow rate (680 lph) and using the adsorption chiller it was found that the flow leaves the ring in the shape of flow veils before stratifying in the layer whose temperature is close to the temperature of the inlet flow. Although the vertical jets are generally considered detrimental to stratification, in this case their existence in the form of flow veils was proved to be beneficial to the stratification in the tank. However, this effect was not tested at higher flow rates due to the limitations on the adsorption chiller flow rate.

4.2 Experimental investigation of the stratisorp concept

In the following section a series of different experiments which demonstrate different possibilities of realising the stratisorp concept are discussed.

4.2.1 Thermal cycle without internal heat recovery

A good basis of comparison can be formed when the stratisorp cycle is compared with a cycle without heat recovery (reference cycle). The tank with SOLVIS charging lance with the experimental set-up shown in Fig. 3.20 in Chapter 3 was used. The adsorber is supplied with the lowest temperature of adsorption ($T_c = 27°C$) during the adsorption half cycle. As soon as the half cycle time is reached ($t_{halfcycle}$) water with maximum desorption temperature ($T_h = 72°C$) is pumped through the adsorber. Here the tank works only as an interface which connects the heater and the cooler with the adsorber. The water contained in the hot and the cold zones at the top and at the bottom of the tank is used for desorption and adsorption half cycles respectively. The tank is preconditioned for this experiment by heating up the top zone (between sensors T_{12} and T_{15}) to 72 °C and by cooling the bottom zone of the tank (between sensors T_1 and T_5) to 27 °C. The low temperature heat source was set to 18 °C. The experimental settings used in the reference experiment carried out by the manufacturer (SorTech AG) of the silica gel module are entered in Tab. 4.2. The tank with the position of the temperature sensors relative to different inlets and outlets of the tank is shown in Fig. 4.17.

	Component	Flow rate (lph)	$t_{halfcycle}$ (min)
Adsorber	Adsorption	2600	9.7
	Desorption	1600	
	Condenser	1600	
	Evaporator	2000	

Table 4.2: Experimental settings used by manufacturer for experiment without heat recovery (reference experiment)

Tab. 4.3 shows the maximum flow rates achievable in different hydraulic circuits.

Component	Flow rate (lph)
Adsorber	1700
Condenser	800
Evaporator	2000
Heater	1300
Cooler	866

Table 4.3: Maximum flow rates of different hydraulic circuits

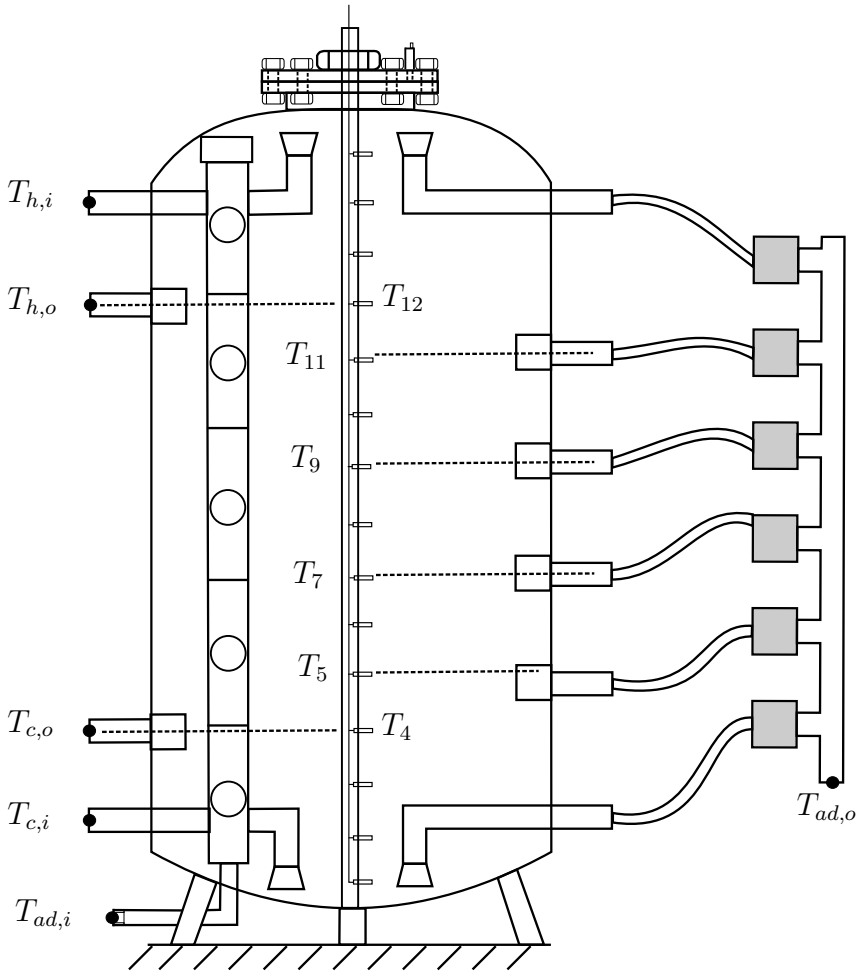

Figure 4.17: Positions of the temperature sensors in the tank with charging lance

Stationary cycle condition has to be reached for estimation of COP of the cycle. Reliable experimental results can be achieved only if many consecutive cycles are carried out as it leads to a stationary cycle condition. The experimental settings had to be selected such that for each subsequent cycle enough hot and cold water was available. It can be seen from Tab. 4.2 and Tab. 4.3 that the maximum achievable adsorber flow rate was 65% of the reference flow rate. Naturally the half cycle time could be increased by 35% (i.e. $t_{halfcycle}$=15 min) so that the equal amount of water as the reference measurement ($\approx$ 420 litres) is sent through the adsorber in each half cycle. This adoption would change the adsorber flow rate to $\dot{V}_{ad_{adsorption}}$ to 1700 lph and $\dot{V}_{ad_{desorption}}$ to 1046 lph. During desorption half cycle this change in $\dot{V}_{ad_{desorption}}$ would not cause any problem as $\dot{V}_h - \dot{V}_{ad_{desorption}} > 0$ i.e. net loading of the top zone of the tank. As a result, enough hot water would be available for the next desorption half cycle. However, as $\dot{V}_c - \dot{V}_{ad_{adsorption}} < 0$ i.e. net unloading of the bottom zone of the tank with 834 lph, within the duration of half cycle time of 15 min. approx. 200 litre water would be extracted from the cold zone. As a results, no more cool water would be available for the subsequent cycle. Hence the half cycle time had to be adapted properly[8]. From Fig. 4.18 it

[8]although the cooling module operates continuously during the desorption half cycle, only the difference ($V_{c_{tot}} - V_{cond}$ = 66 lph) could be circulated through the bottom section of the tank. This low flow rate was insufficient to refill the chilled water in the bottom zone of the tank

can be seen that the cold water volume available (140 litre corresponding to deep blue region) is less than the maximum volume which could be circulated through the adsorber (200 litre corresponding to addition of light blue and deep blue regions).

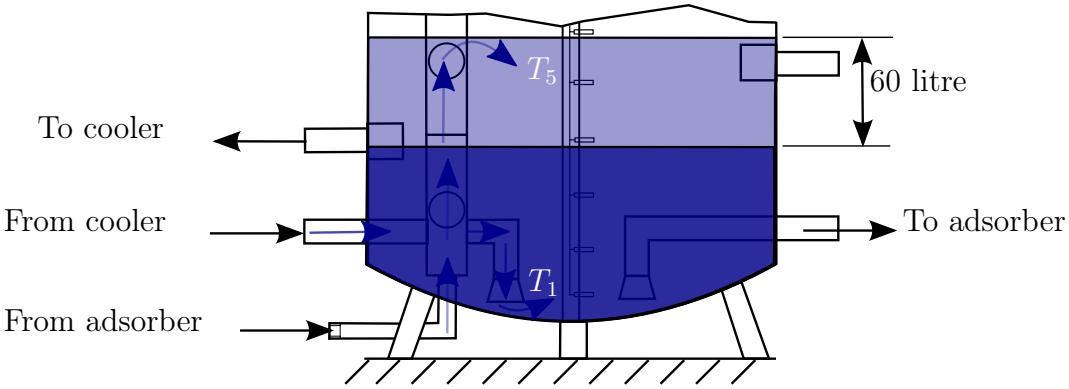

Figure 4.18: Flow scenario at the bottom of the tank during the adsorption half cycle

The half cycle time must be set such that the net volume of water ΔV, unloaded from the cold zone due to flow rate $\dot{V}_{ad_{adsorption}} - \dot{V}_c$ is not more than 140 litre. If this condition is not fulfilled then towards the end of the adsorption half cycle not enough cold water would be available for continuing the adsorption. Consequently the supply temperature to the adsorber would rise and the experiment would deviate from the reference experiment.
The following equations can be written to fulfil the above mentioned condition :

$$(\dot{V}_{ad_{adsorption}} - \dot{V}_c) \cdot t_{halfcycle} \leq \Delta V \tag{4.1}$$

Substituting values of $\dot{V}_c$ and ΔV,

$$\frac{(\dot{V}_{ad_{adsorption}} - 866)}{60} \cdot \frac{l}{min} \cdot t_{halfcycle} \cdot min \leq 140 \cdot l \tag{4.2}$$

$t_{halfcycle}$ and $\dot{V}_{ad_{adsorption}}$ should also fulfil the condition of circulating equal volume of water through the adsorber as the reference experiment. Therefore,

$$\frac{\dot{V}_{ad_{adsorption}}}{60} \cdot \frac{l}{min} \cdot t_{halfcycle} \cdot min = 420 \cdot l \tag{4.3}$$

Solving Eq. 4.2 and Eq. 4.3 : $t_{halfcycle} \geq 20$ min.

To ensure the availability of chilled water $t_{halfcycle} = 24$ min. was chosen. Consequently, $\dot{V}_{ad_{adsorption}} = 1050$ lph and $\dot{V}_{ad_{desorption}} = 640$ lph. The COP_{cool} and COP_{heat} are computed as :

$$COP_{cool} = \frac{Q_{ev}}{Q_{des}} \qquad \text{and} \qquad COP_{heat} = \frac{Q_{cond} + Q_{ads}}{Q_{des}} \tag{4.4}$$

The energy supplied or rejected in different hydraulic circuits is calculated as :

$$
\begin{aligned}
Q_{ads} &= \int_{0}^{t_{halfcycle}} dQ_{ads} = \int_{0}^{t_{halfcycle}} \dot{m}_{ad} \cdot c_p \cdot (T_{ad,i} - T_{ad,o}) \cdot dt \\
Q_h &= \int_{0}^{t_{end}} dQ_h = \int_{0}^{t_{end}} \dot{m}_h \cdot c_p \cdot (T_{h,i} - T_{h,o}) \cdot dt \\
Q_c &= \int_{0}^{t_{end}} dQ_c = \int_{0}^{t_{end}} \dot{m}_c(t) \cdot c_p \cdot (T_{c,i} - T_{c,o}) \cdot dt \\
Q_{ev} &= \int_{0}^{t_{halfcycle}} dQ_{ev} = \int_{0}^{t_{halfcycle}} \dot{m}_{ev} \cdot c_p \cdot (T_{ev,o} - T_{ev,i}) \cdot dt \\
Q_{cond} &= \int_{t_{halfcycle}}^{t_{end}} dQ_{cond} = \int_{t_{halfcycle}}^{t_{end}} \dot{m}_{cond} \cdot c_p \cdot (T_{ev,o} - T_{ev,i}) \cdot dt \\
Q_{des} &= \int_{t_{halfcycle}}^{t_{end}} dQ_{des} = \int_{t_{halfcycle}}^{t_{end}} \dot{m}_{ad} \cdot c_p \cdot (T_{ad,i} - T_{ad,o}) \cdot dt
\end{aligned}
\tag{4.5}
$$

The warm water returning to the tank during the adsorption half cycle would be extracted by the cooler. The heat of adsorption would then be rejected in the cooler which forms a part of useful energy for heating. Q_{cond} is also rejected in the cooler and hence forms the other part of the useful energy for heating. Fig. 4.19 shows the thermodynamic cycle during this experiment. This cycle was obtained after 10 consecutive adsorption-desorption cycles, hence it represents a stationary cycle.

At the start of the adsorption half cycle, it can be observed that the supply temperature to the evaporator $T_{ev,i}$ takes a while to reach the setpoint of 18 °C. As the heat exchanger was at approximately 27 °C at the end of previous desorption half cycle, the thermal mass of the heat exchanger must be first cooled to the setpoint. Hence the return flow to the emulator is warmer than the setpoint. The control loop of the emulator controls the power of the emulator and tries to achieve the setpoint. Therefore the supply temperature to the evaporator is reached after a short delay. Hence owing to Eq. 4.5, the magnitude of Q_{ev} would be reduced due to the measurements for which $T_{ev,o} > T_{ev,i}$ causing lower COP_{cool}. On the contrary, at the end of the adsorption half cycle the evaporator heat exchanger would be at approximately 18 °C. Due to the thermal mass of the evaporator exchanger the control action of the cooler temperature controller is slower. The same effect can be observed in Fig. 4.20. The positive peak in $\dot{Q}_{ev}$ till approximately 1 min. mark and the negative peak in $\dot{Q}_{cond}$ till the 25 min. mark arise due to the thermal mass of the evaporator/condenser heat exchanger. Due to these peaks in power lower cooling and heating power are computed.

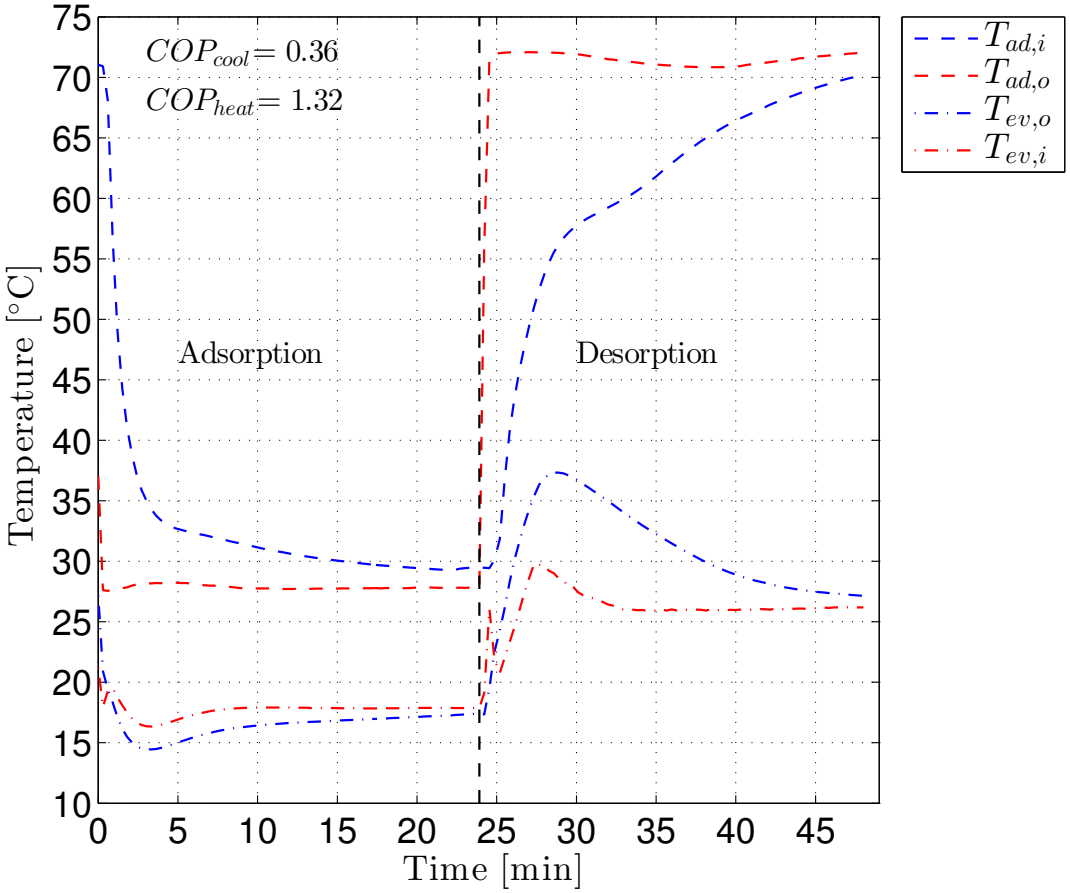

Figure 4.19: Thermodynamic cycle for the experiment without heat recovery

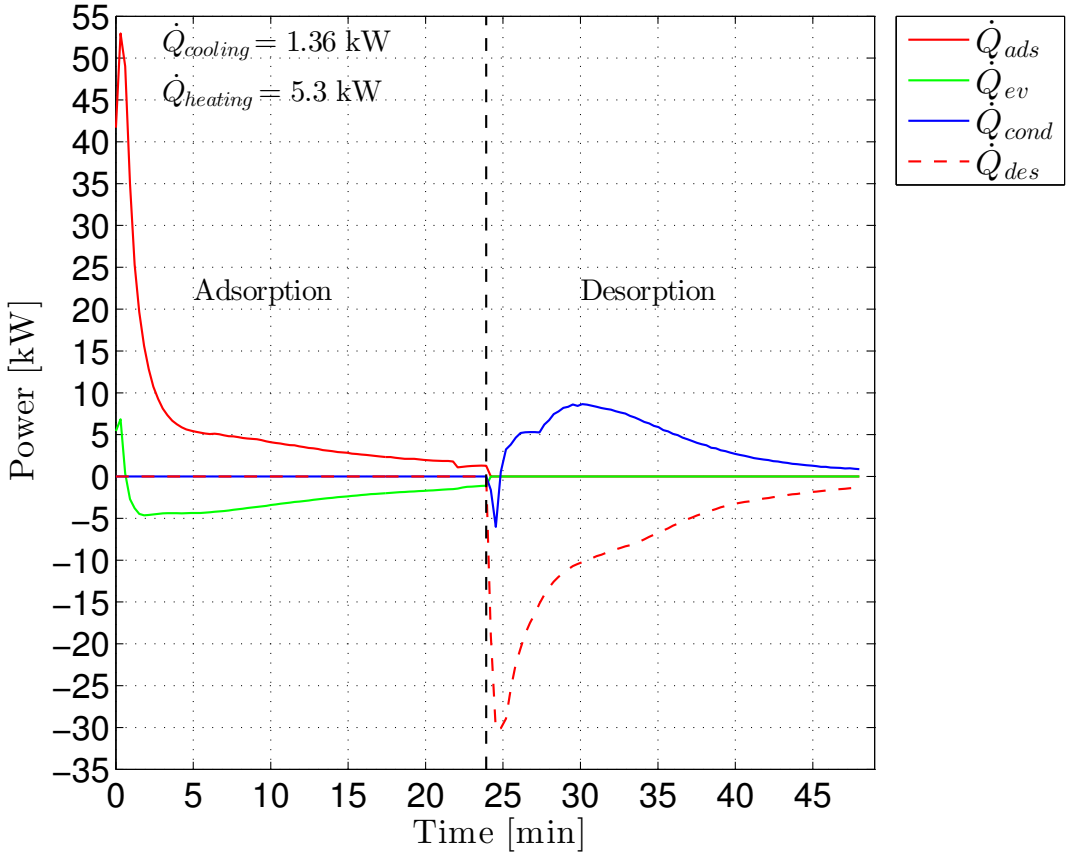

Figure 4.20: Power associated with different components during the experiment without heat recovery

The peak in the cooling power ($\dot{Q}_{ev}$) is initially on the positive side suggesting that the temperature of water returning from evaporator to be higher than the supply temperature. The condenser power ($\dot{Q}_{cond}$) has initially peak on the negative side. It means the water returning from the condenser is cooler than the supply temperature.
A $COP_{cool} = 0.36$ obtained for the experiment was lower than the $COP_{cool} = 0.41$ calculated for the reference experiment. The discrepancy in COP_{cool} is attributed to the lower flow rates of the adsorber set for the experiment. At higher flow rates (e.g. $\dot{V}_{ad_{adsorption}} = 2600$ lph) the heat transfer coefficient at the water-heat exchanger interface is higher. Therefore the heat transfer during each half cycle would be much better for the reference experiment than the adapted experiment. It also means that by keeping quantity of fluid passing through the adsorber in each half cycle the same as in the reference experiment the change in the adsorber loading would be higher and the higher ratios of Q_{ev}/Q_{des} could be expected.

4.2.2 Experiments with the stratisorp cycle

Measurement of heat loss coefficient: The evaluation of performance of the stratified TES in context of the stratisorp cycle is essential. The heat loss characteristics namely the overall heat transfer coefficient of the tank (U-value) is needed for the estimation of the entropy generation caused by the heat lost to the ambient in one cycle. Moreover, the U-value is also important for a one dimensional numerical model of the stratified TES. The cool down test was carried out according to SRCC protocol [2] mentioned by Cruickshank [17].

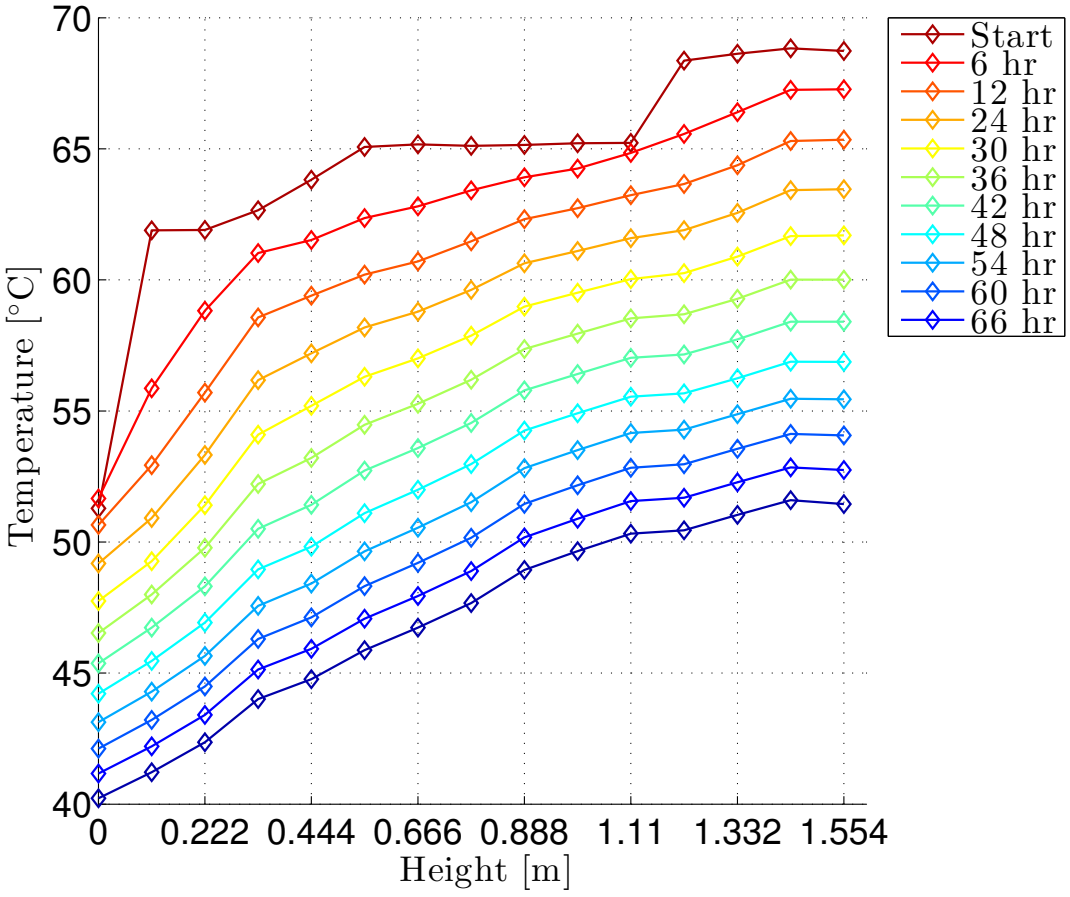

Figure 4.21: Evaluation of the tank temperature during the cool down test

Fig.4.21 shows the evaluation of the tank temperature during the timespan of the experiment. The tank with ring stratification system (Fig. 3.33) was used for this experiment. The tank was heated uniformly to above 65 °C and cooled down over a period of 66 hours. The temperature of the tank was recorded every minute using 15 equally distributed temperature sensors placed along the axis of the tank. The room temperature was simultaneously recorded.

The U-value can be calculated by different approaches. The tank can be imagined as a stack of 15 cylindrical slices. The thickness of each slice equals the spacing between the sensors. Each slice is assumed to possess the same temperature as recorded by the corresponding sensor. This assumption can be consolidated by the flow visualisation results and by referring to the cool down test results seen in Fig. 4.21. The U-value of each slice (or zone) at each 6 hour interval can be determined using energy balance as :

$$U_{zone} = \frac{Q_{loss_{6hr}}}{A \cdot (T_{zone} - \overline{T_{amb_{6hr}}}) \cdot 6 \cdot 3600} \qquad \text{where} \qquad Q_{loss_{6hr}} = m_{zone} \cdot c_p \cdot \Delta T_{zone_{6hr}} \quad (4.6)$$

Fig.4.22 shows the plot of the U_{zone} and an area weighted average, $U_{tank_{avg}}$.

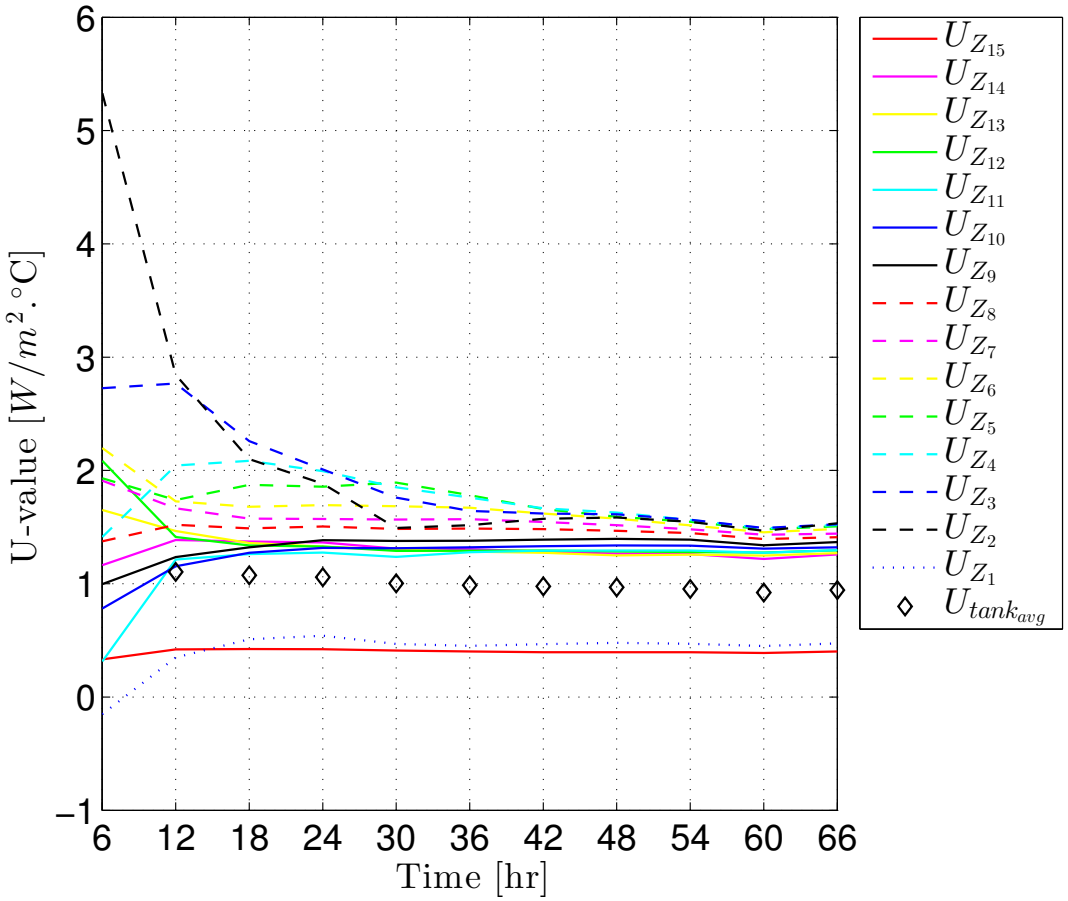

Figure 4.22: U-value of each zone and area weighted average

The area of heat transfer considered in Eq. 4.6 is different for the top and the bottom zones (A_{ends}) than other zones ($A_{surface}$). The heat transferred to the ambient from the top

and the bottom zones of the tank not only takes place through the cylindrical surface but also through the ends of the tank.

$$A_{ends} = A_{surface} + A_{top} \tag{4.7}$$

U-value can also be computed based on the a log mean temperature difference ($U_{tank_{LMTD}}$) according to SRCC [2] as:

$$U_{tank_{LMTD}} = \frac{m_{tank} \cdot c_p}{A_{total} \cdot t_{total}} \cdot ln \frac{\overline{T_{tank_{init}}} - T_{amb_{init}}}{\overline{T_{tank_{final}}} - T_{amb_{final}}} \tag{4.8}$$

The method is called as "standard decay method". This method requires an environment with nearly constant temperature. Variation of 10% in the ambient temperature is allowed in this method. This condition was not achieved in the laboratory for initial 16 hours of the experiment. In such cases, it is recommended to use an alternative test method.
The alternative test method, known by "real time measurement method", applies energy balance to the whole tank for the duration of the test. The U-value is calculated as:

$$U_{tank} = \frac{Q_{loss_{total}}}{A_{total} \cdot t_{total} \cdot (\overline{T_{tank_{init}}} - \overline{T_{amb}})} \tag{4.9}$$

where

$$Q_{loss_{total}} = m_{tank} \cdot c_p \cdot (\overline{T_{tank_{init}}} - \overline{T_{tank_{final}}}) \tag{4.10}$$

Tab. 4.4 summarises the results of the cool down test.

	U-value (W/m^2°C)
$U_{tank_{avg}}$	0.92
$U_{tank_{LMTD}}$	0.70
U_{tank}	0.72

Table 4.4: U-value computed using different approaches

The area weighted average value overestimates the U-value as compared to the "standard decay method" and the "real time measurement method". This value lies between typical U-values for hot water storage documented by Votsis *et al.* [59] (0.937 W/m^2°C) and by Kleinbach *et al.* [36] (0.59 W/m^2°C).

Description of the experiment and results: The experimental procedure and results for the stratisorp-experiment with cycle condition 72/27/18 °C using the ring stratification system are discussed in the following section. This cycle has been discussed in detail in the following section.
Fig.4.23 shows the position of different temperature sensors and the ring inside the tank. The tank was equipped with 8 possible locations for mounting the rings. The available 6 rings were placed so that the maximum potential of the stratisorp concept could be utilised.

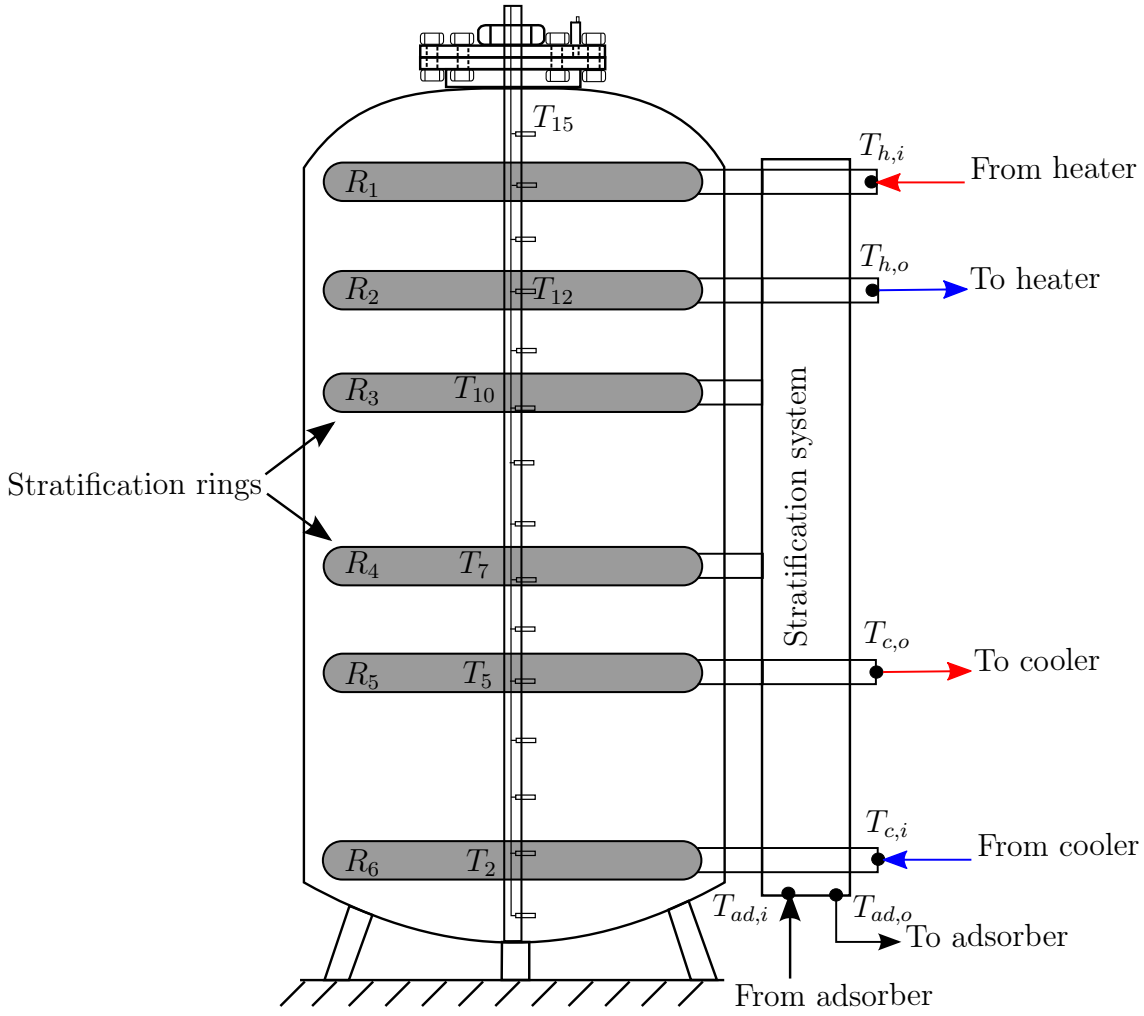

Figure 4.23: Positions of the temperature sensors in the tank with rings

Towards the end of the adsorption half cycle a major change in the loading of the adsorber takes place which causes a peak in cooling power. It is therefore beneficial for the performance of the cycle if enough cold water is available at the end of the adsorption cycle [9]. Hence the 5$^{\text{th}}$ ring was placed by skipping one mounting location. The tank temperature profile of the stationary cycle is governed by many factors such as flow rate, distribution of the rings, heating and cooling module temperature setpoints. The positioning of the rings definitely has a high impact on the final temperature profile in the tank. From the differential heat curves (Fig. 2.5) it can also be seen that the maximum overlap occurs when the adsorber temperature

[9] This is valid if $\dot{V}_{ad} > \dot{V}_c$

lies between 45-60 °C. The central section of the tank corresponds to this temperature range. In this region also one position for mounting was skipped. This measure leads to a flatter temperature profile in the corresponding zone and thereby reduces the temperature spread across the adsorber and lowers the mixing in the tank.
Tab. 4.5 shows the flow rates used in different hydraulic circuits for this experiment.

Component	Symbol	Flow rate (lph)
Adsorber	$\dot{V}_{ad}$	1000
Condenser	$\dot{V}_{cond}$	800
Evaporator	$\dot{V}_{evap}$	2000
Heater	$\dot{V}_{h}$	600
Cooler	$\dot{V}_{c_{tot}}$	866

Table 4.5: Flow rates used in different hydraulic circuits during the stratisorp experiment

The heat supplied to the adsorber during the complete cycle should only be sufficient to cover the difference of the differential heat curves (light orange area in Fig. 2.5). Similarly the heat rejected by the cooler during the cycle should only be enough to cover the unrecoverable or surplus heat of adsorption (light blue area in Fig. 2.5). The temperature spread across the heating and the cooling loop is much higher than the average temperature spread across the adsorber loop. Hence the heating and the cooling modules were operated at a much lower flow rates than the adsorber flow rate.

Selecting $\dot{V}_{c_{tot}}$ higher than $\dot{V}_{cond}$ following flow rates were achieved:

$\dot{V}_c = \dot{V}_{c_{tot}}$ (as $\dot{V}_{cond} = 0$ during adsorption half cycle)

$\dot{V}_c = \dot{V}_{c_{tot}} - \dot{V}_{cond}$ (during desorption)

$\dot{V}_c$ would always be circulated through the tank during the desorption half cycle. This assured that the bottom of the tank was cooled to T_c before the next adsorption cycle started[10].

A temperature based criterion was chosen for switching between the adsorption and desorption half cycle. As soon as the absolute value of difference between temperature of the supply and the return flow to the adsorber ($|\Delta T_{ad}|$) dropped below certain value then the water from the tank would be extracted from the next lower ring during the adsorption half cycle or the next upper ring during the desorption half cycle. The Tab. 4.6 summarizes the criterion for switching implemented for the stratisorp cycle.

The fact that the differential loading curve of the silica-gel water pair shows higher change in the loading of the adsorber at the lowest adsorption temperature, a lower temperature switching criterion was used at the end of the adsorption cycle. The last step of the adsorption was therefore prolonged which assured that the adsorber would reach a near saturation state

[10]refer appendix A.3 for the plot of the flow rates in all hydraulic circuits

Half cycle	Extraction	Insertion	while $\lvert\Delta T_{ad}\rvert$ is...
Adsorption	R_2	R_1	> 1
	R_3	R_2	> 1
	R_4	R_3	> 1
	R_5	R_4	> 1
	R_6	R_5	> 0.5
Desorption	R_5	R_6	> 1
	R_4	R_5	> 1
	R_3	R_4	> 1
	R_2	R_1	> 1
	R_1	R_2	> 1

Table 4.6: Switching criteria used during the stratisorp cycle

at the end of the adsorption half cycle.
The tank was preconditioned by heating the top zone of the tank to 72 °C and the bottom zone of the tank was cooled to 27 °C. The flow rates of different devices were set according to Tab. 4.5. When the tank top zone reached the set temperature of 72 °C the last step of desorption half cycle was carried out namely extraction from R_1 and insertion into R_2. The adsorber should be in complete desorbed state before starting the first adsorption cycle. This was ensured by achieving the criterion for switching to the next adsorption cycle i.e the last entry in Tab.4.6. Thermodynamic cycles of the silica gel-water adsorption chiller were run by repeating the switching sequence from Tab. 4.6[11]. Fig. 4.24 shows the plot of ΔQ_{tank} at the end of each cycle. Fig. 4.25 shows the temperature profile in the tank at the end of each cycle. When the tank is far from the quasi steady state at the end of the first cycle ΔQ_{tank} has a relatively higher value as compared to later cycles. As the tank approaches the quasi steady state, the magnitude of ΔQ_{tank} rapidly drops and after 5^{th} cycle ΔQ_{tank} is seen to be oscillating around 0. The magnitude of ΔQ_{tank} reached below 50 kJ for the last cycle. The same effect is seen in Fig. 4.25. The tank temperature profile changes from cycle to cycle as the central section of the tank warms up due to heat of adsorption and after the 5^{th} cycle only minor changes in the tank temperature profile are observed. The last 5 cycles were considered for the estimation of COP and power by averaging.
The region of the steepest gradient in the tank is the region between R_3 and R_4. The temperature sensors T_9 and T_{10} separated by 11 cm differ 15 °C in temperature. It is evident that the ring flow diffuser functions efficiently even at higher flow rate (1000 lph) than they had been tested for (700 lph). Other distinct temperature zones can be identified as well. The flatter temperature profiles at the bottom and at the top of the tank show that the cooler and the heater fulfil their functions as well.

[11] a Matlab code to process the results acquired from the LabView code for the calculation of COP and power and generating plots is documented in appendix A.7

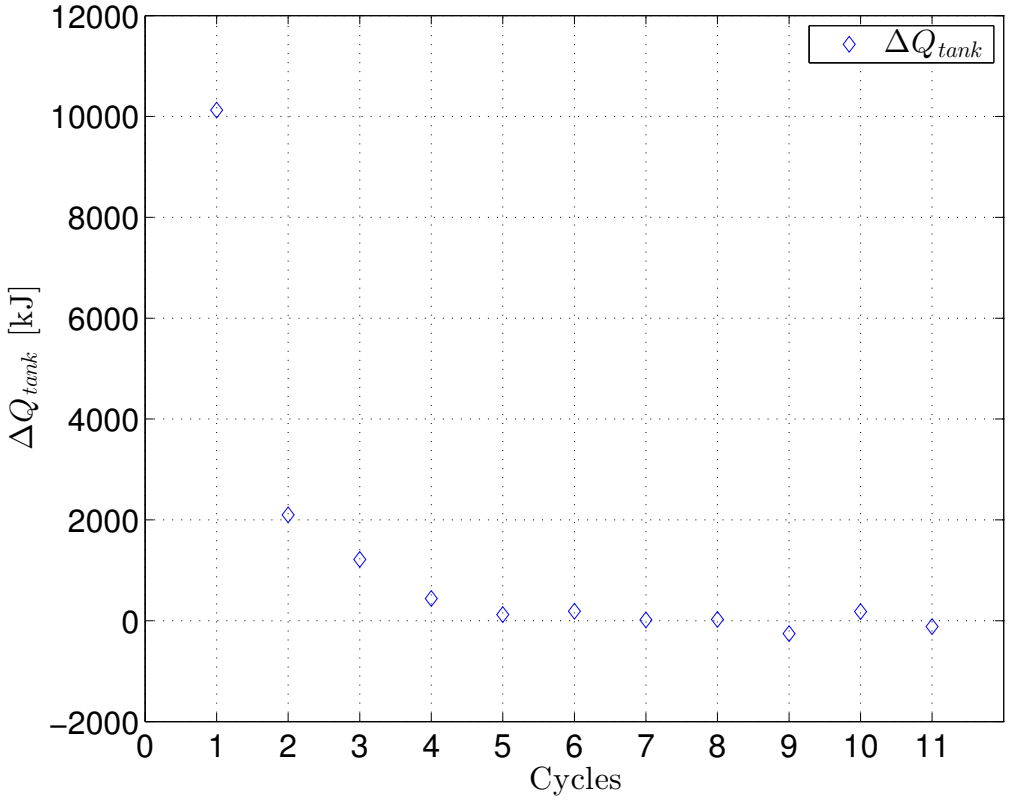

Figure 4.24: Change in tank ΔQ_{tank} at the end of each cycle

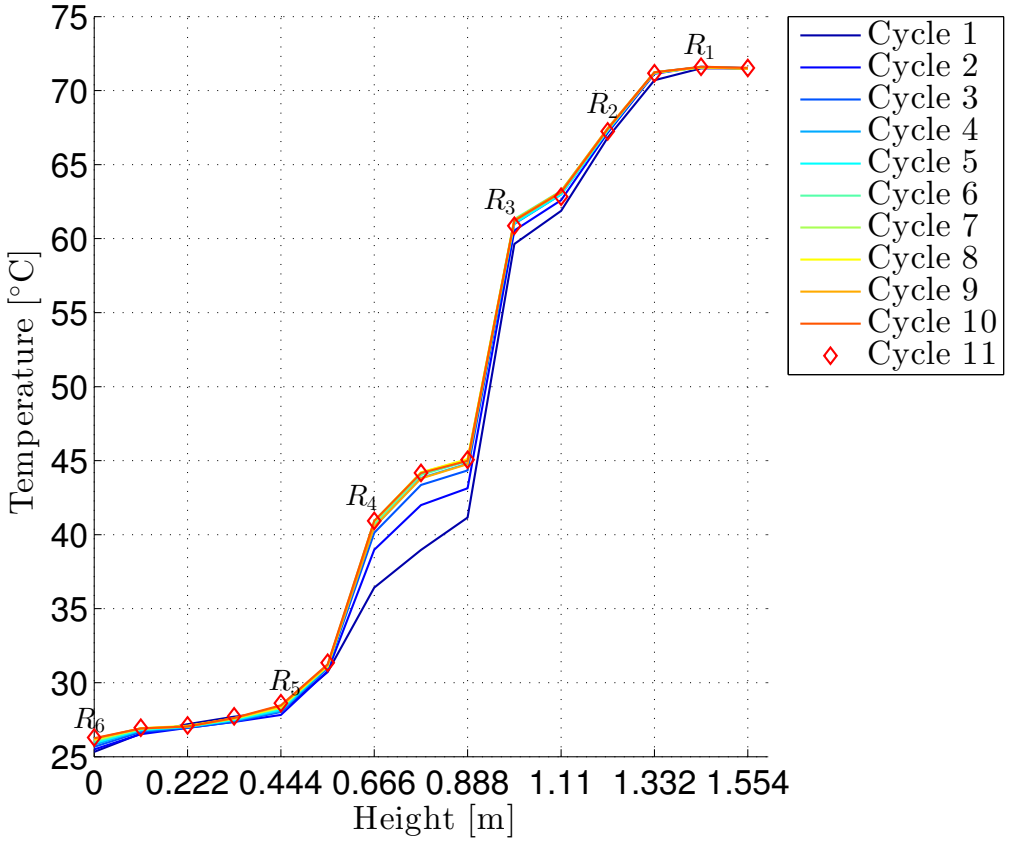

Figure 4.25: Tank temperature profile at the end of each cycle and the position of the rings

Fig.4.26 to Fig. 4.33 belong to the same experiment being discussed here. Fig. 4.26 depicts the last thermodynamic cycle of the adsorption chiller. A very low magnitude of ΔT_h and ΔT_c occur except for the times when adsorber extracts water from the top and the bottom zones, suggests that the top and the bottom zones of the tank were maintained at the respective required temperature. Distinct "jumps" in the supply temperature to the adsorber are observed both in the adsorption and the desorption half cycles. These jumps or steps in $T_{ad,o}$ occur as soon as the criterion for switching is reached and the next available extraction ring is selected.

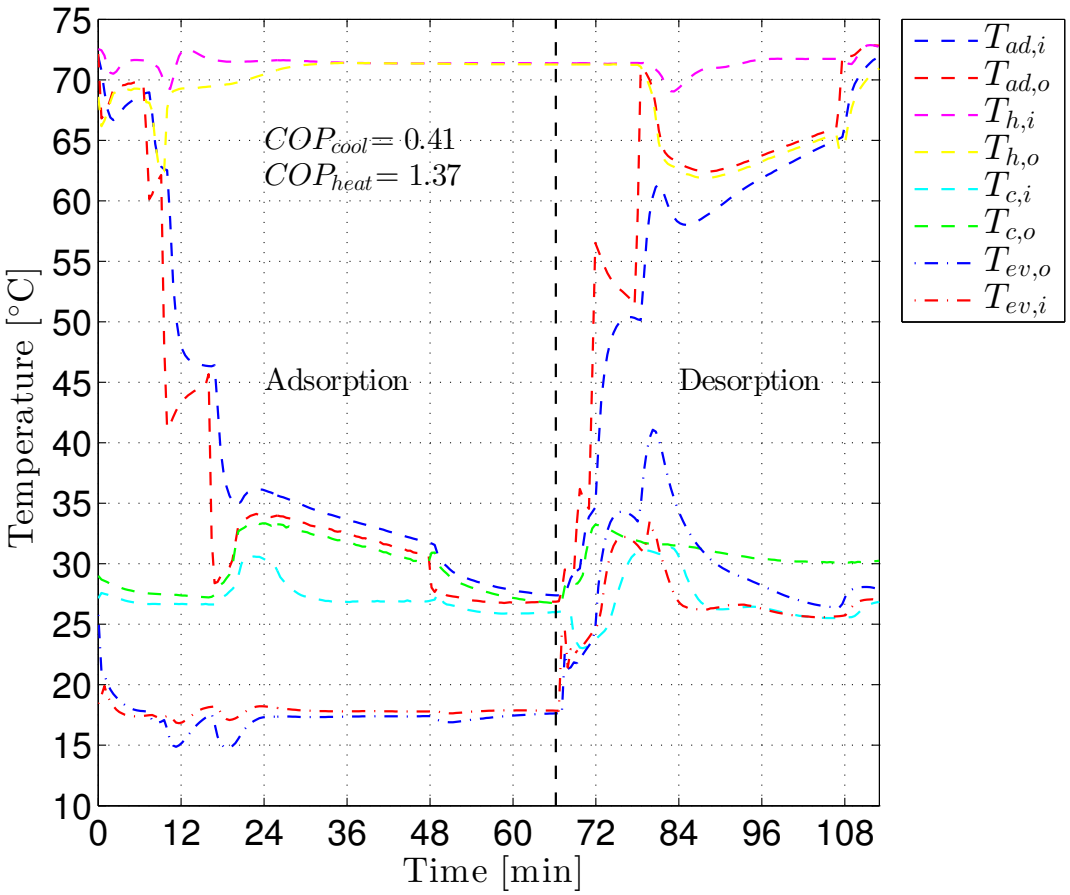

Figure 4.26: Temperature profile of the three hydraulic circuits of the adsorption chiller for the cycle condition 72/27/18 °C

As the top zone of the tank is at a uniform temperature a very flat temperature gradient exists across it. As a result at the start of the adsorption half cycle the return temperature to the adsorber is lower than the supply temperature (due to heat lost to the surroundings) and the adsorber goes through a short desorption phase. The return temperature from the evaporator is therefore warmer than the supply temperature and no cooling power is available. It can be seen that the first peak in $\dot{Q}_{ads}$ is on the negative side (owing to Eq. 4.5) due to the effect discussed here. This effect can be rectified by choosing a higher value of switching criterion ($|\Delta T_{ad}|$). Choosing a lower flow rate of the heating module can also rectify this effect. The lower values of $\dot{V}_h$ lead to a temperature gradient in the top zone of the tank. Hence cooling power would then be available even during the first adsorption step.
The adsorber starts to adsorb as soon as the cycle is switched to the second adsorption step

at around 10 minutes after the start. From this point onward until the end of adsorption continuous cooling power is available. A peak in $T_{ev,o}$ occurs as soon as the cycle switches to the next adsorption step. Similarly peaks in the condenser return temperature can be seen during desorption.

An interesting observation can be made about the second last adsorption step. The time required to switch is 45% of the half cycle time although the volume of water contained between the rings is the same as for the second adsorption step. The other adsorption steps are shorter. The reason for this effect is seen in Fig. 4.27. The plot shows the change in evaporator pressure (P_{evap}) and the saturation pressure ($P_{saturation}$) during the complete cycle. P_{evap} was measured by externally mounted pressure sensor. It was found that in spite of evacuating the adsorption chiller's vacuum chamber a small amount of inert gases were present which gave rise to the pressure offset of approximately 2 mbar. As there was no information about the surface temperature of the evaporator heat exchanger available, it was assumed that the return temperature from the evaporator very closely represents the surface temperature. Hence $P_{saturation}$ is computed based on $T_{ev,o}$.

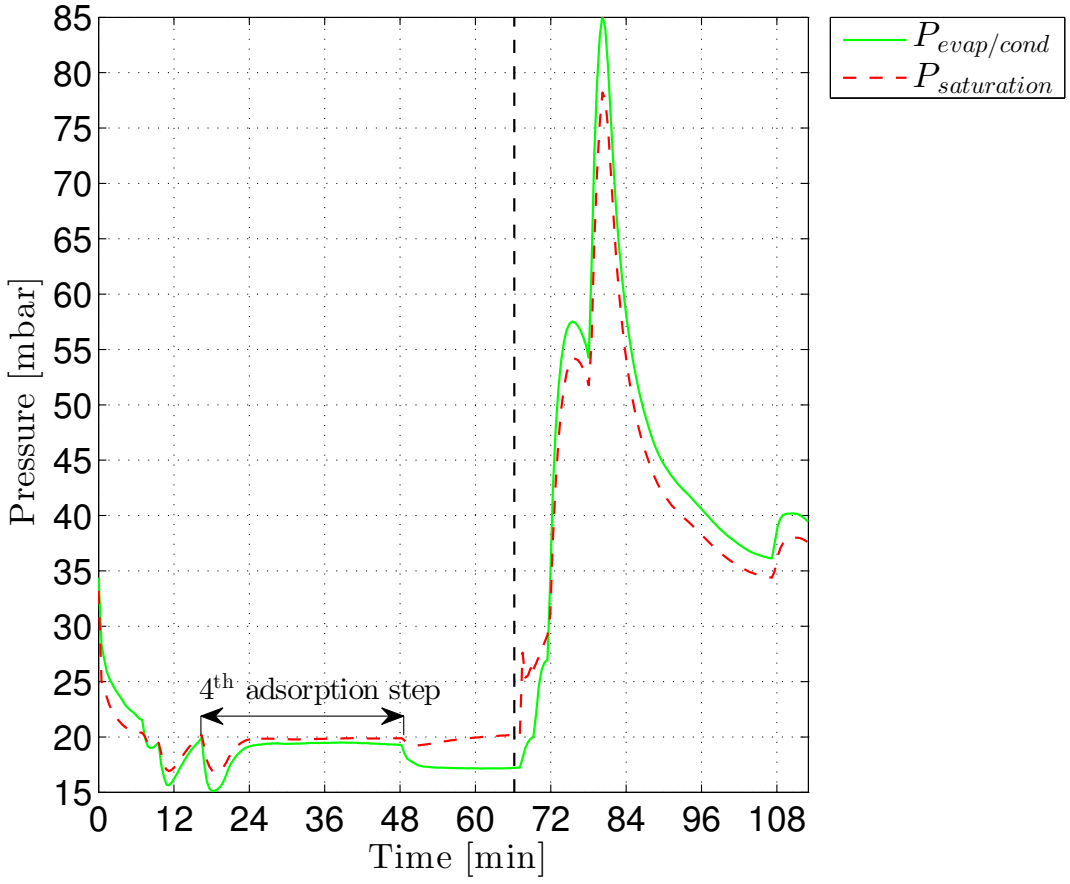

Figure 4.27: Evaporator/Condenser and saturation pressure

After initial rapid sinking in $T_{ad,o}$ at the start of the 4$^{\text{th}}$ adsorption step the rate of change in ΔT_{ad} is very low. The difference between P_{evap} and $P_{saturation}$ almost vanishes suggesting that the adsorber has nearly reached equilibrium loading corresponding to $T_{ad,i}$ and $P_{saturation}$. Only marginal heat of adsorption is released as the change in the adsorber loading would

be very low. Moreover, during this adsorption step, the flow rates of the chiller and the cooling module overlap. The warmer water being pushed from R_4 towards R_5 mixes with the cooler water being pushed towards R_5 from the cooler bottom zone of the tank. Hence the temperature spread across the adsorption chiller remains higher than the switching value for a longer time than the previous adsorption steps. Hence the switching to the next adsorption step is delayed as compared to the other steps.

Fig. 4.28 shows the plot of power of different components. The energy supplied and rejected was calculated using Eq. 4.5 except for Q_c. The heat rejected in the cooler in the complete cycle is considered for the calculation of COP_{heat}. Hence,

$$Q_c = \int_0^{t_{end}} dQ_c = \int_0^{t_{end}} \dot{m}_c \cdot c_p \cdot (T_{c,i} - T_{c,o}) \cdot dt \tag{4.11}$$

The peaks of the adsorber power during adsorption and in desorption half cycles are of equal heights as the flow rate of the adsorber was constant throughout the cycle as differed to the experiment without heat recovery. The occurrence of the peaks in adsorber power correspond to the events at which the next ring is selected for extraction.

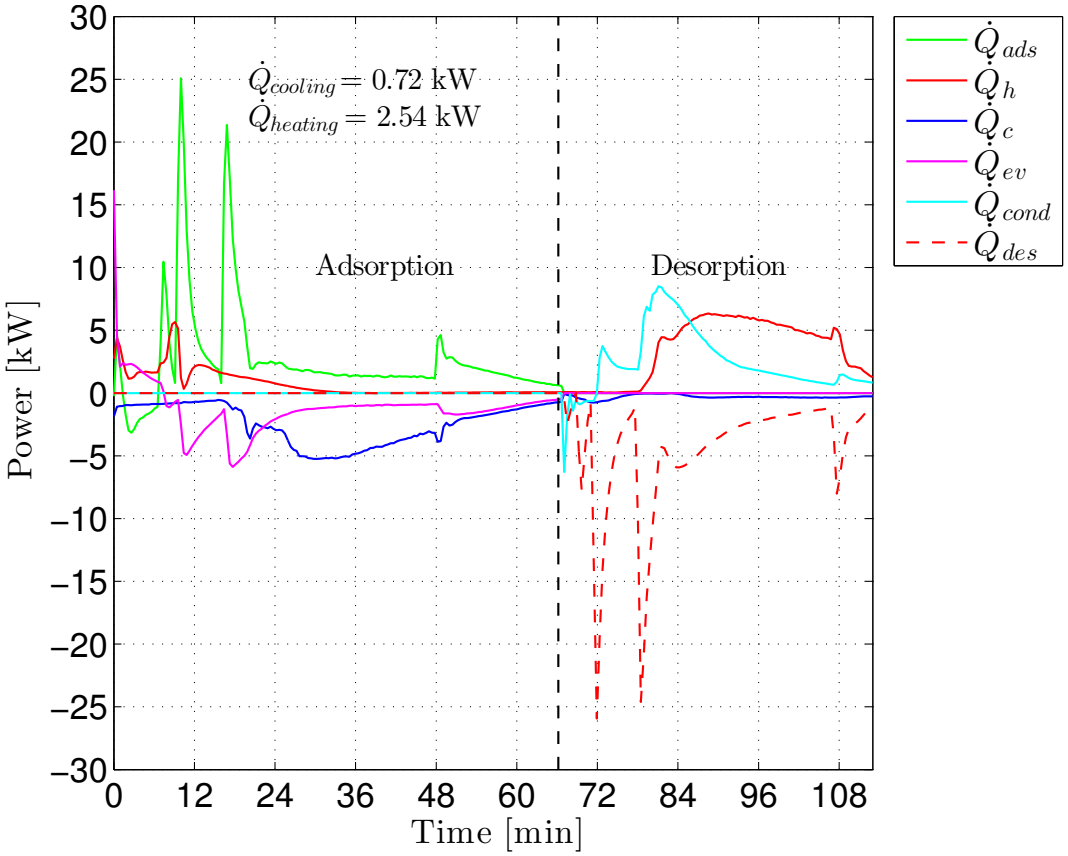

Figure 4.28: Power of different components during the stratisorp cycle for cycle condition 72/27/18 °C

Mixing in the top zone of the tank takes place at the start of adsorption half cycle and at the end of desorption half cycle. Hence water being extracted from the tank becomes

cooler. The heating module heats the extracted water. The heating operation of the heating module can be confirmed in this adsorption/desorption step from Fig. 4.28. ΔT_h drops close to zero for rest of the cycle and the heater operates with low power. Similarly mixing in the bottom zone of the tank occurs at the end of adsorption and at the start of desorption which increases the supply temperature to the cooler ($T_{c,o}$). The cooler operates during these phases in which the extracted warm water is cooled and reinserted into the tank through the lowest ring (R_6). The maximum cooling power required is 5 kW. During the desorption half cycle only a small amount of cooling power is required ($\dot{Q}_c < 1$ kW) as only the difference between $\dot{V}_{c_{tot}}$ and $\dot{V}_{cond}$ flows through the tank. Additionally, the bottom zone of the tank is already significantly cold.

The heater power momentarily drops to 0 at the start of the adsorption half cycle. It is due to switching from the second to the third adsorption step. The difference between $\dot{V}_{ad} - \dot{V}_h$ flows into the tank during the second adsorption step as seen in Fig. 4.29(a). Hence $T_{ad,i}$ and $T_{h,o}$ overlap during the second adsorption step as seen in Fig. 4.26.

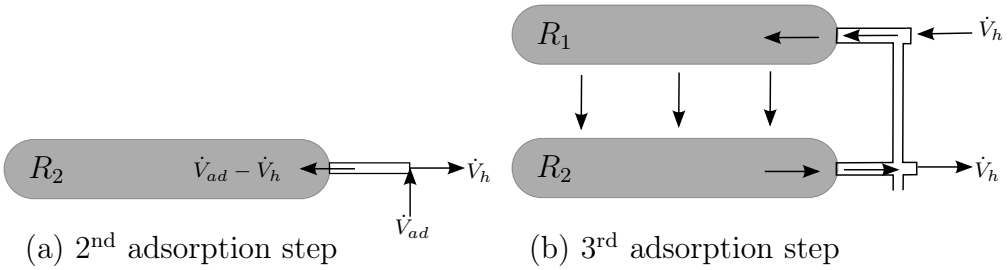

(a) 2nd adsorption step (b) 3rd adsorption step

Figure 4.29: Flow scenario during the second and the third adsorption step

Immediately after switching to the third adsorption step the heater extracts already preheated water from the top zone of the tank (Fig. 4.29(b)). ΔT_h becomes zero and consequently $\dot{Q}_h$ drops to zero (Fig. 4.28). As the supply temperature to the heater increases rapidly the supply temperature to the tank overshoots the set-point before the controller initiates the control action by switching off the electric heaters. Although the second adsorption step is finished after 10 minutes the heating module continues to heat the top zone of the tank for the next 20 minutes as seen from Fig. 4.28. It means that during the first two adsorption steps mixing had taken place in the top zone leading to significant drop in temperature of this zone.

Another interesting observation is made with regards to the stratification behaviour. Two representative scenarios are discussed here in order to shed light on the functioning of the stratification rings during a stationary stratisorp cycle. These two scenarios are shown in Fig. 4.30.

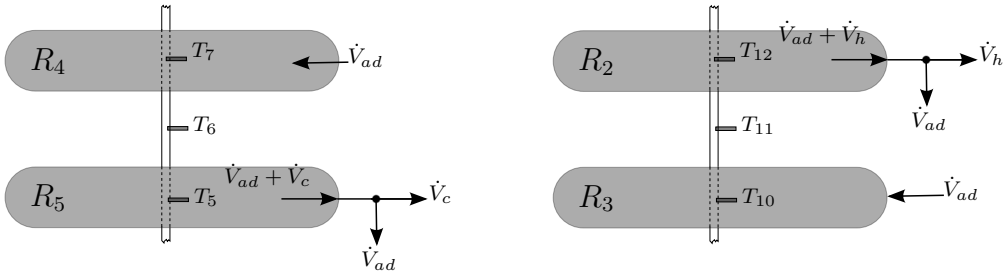

(a) 4th adsorption step (b) 4th desorption step

Figure 4.30: Flow scenario during the 4th adsorption and desorption step

The water being extracted by the cooler and by the adsorber leaves the tank from the stratification ring R_5 during the 4th adsorption step. Similarly the total flow leaving the tank from stratification ring R_2 during the 4th desorption step gets divided into $\dot{V}_{ad}$ and $\dot{V}_h$. The stratification rings handle a higher flow rate (1866 lph during adsorption and 1600 lph during desorption) during these steps. Fig. 4.31 shows the evolution of the tank temperature with focus on the scenarios shown in Fig. 4.30.

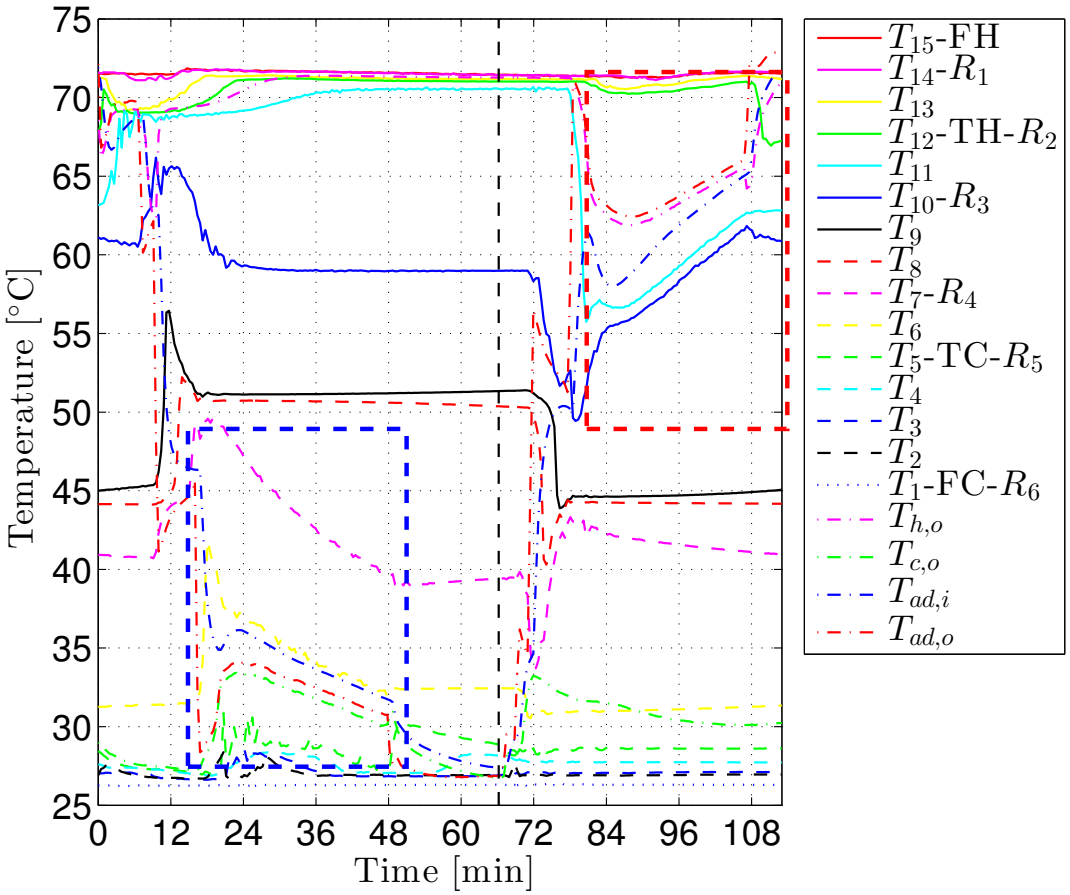

Figure 4.31: Change in the tank temperature during the stratisorp cycle. Blue and red dotted rectangle show the change in tank temperatures for the sensors between R_4-R_5 during 4th adsorption and between R_2-R_3 during 4th desorption step respectively

The flow entering the tank through R_4 at $T_{ad,i}$ is lower than the tank temperature T_7 at

the same level. $T_{ad,i}$ is rather closer to T_6 i.e. the next lower layer in the tank. The flow sinks to this fluid layer although causes mixing in the layer where it entered the tank as suggested by the drop in T_7. The flow veil effect is probably not predominant at this flow rate (1000 lph). If the flow veils are predominant in the flow then theoretically no change in T_7 would be observed.
Exactly opposite flow phenomenon takes place during the 4^{th} desorption step. The temperature of the return flow to the tank ($T_{ad,i}$) is higher than the surrounding water at T_{10}. The return flow to the tank mixes with the surrounding fluid in the tank causing rise in T_{10} and T_{11}. Here as well the absence of the flow veils can be confirmed. From this discussion it is evident that the ring stratification system would work efficiently at lower flow rates ($\dot{V}_{ad} < 1000$ lph). It is also evident that although T_{12} lies at the same level as R_2, no change in T_{12} is recorded. This shows that a sharp temperature gradient exists at the the level of R_2.
At the start of the adsorption half cycle the flow rates of the adsorber and heating module overlap. Hence R_2 handles 1600 lph flow in the first adsorption step causing mixing near the extraction zone in the tank. This strong mixing can be confirmed by rise in T_{11} and drop in T_{12} and T_{13}. It can also be seen that although the cooling module and the adsorber extract water from the same ring (R_5) during the fourth adsorption step, the temperatures $T_{ad,o}$ and $T_{c,o}$ differ from each other. The respective temperature sensors were located approximately 50 cm from each other as seen from Fig. 4.23 which was responsible for this difference.

Fig. 4.32 and Fig. 4.33 shown below elaborate the energy balance calculated for the stratified storage tank and the adsorption chiller for the stationary cycle (last cycle). The integral input and output energies over the cycle are shown in red and in blue, respectively. The fraction of the input energy lost to the environment is negligible.

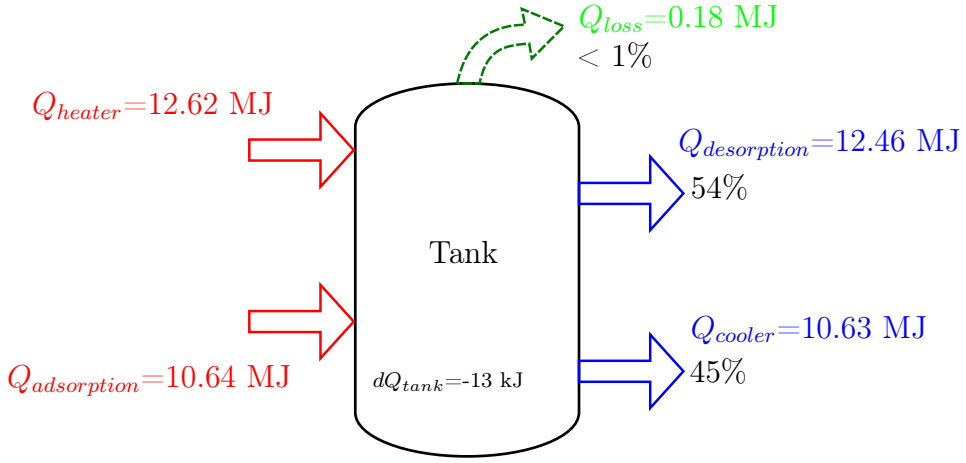

Figure 4.32: Energy balance of the tank for the stationary cycle

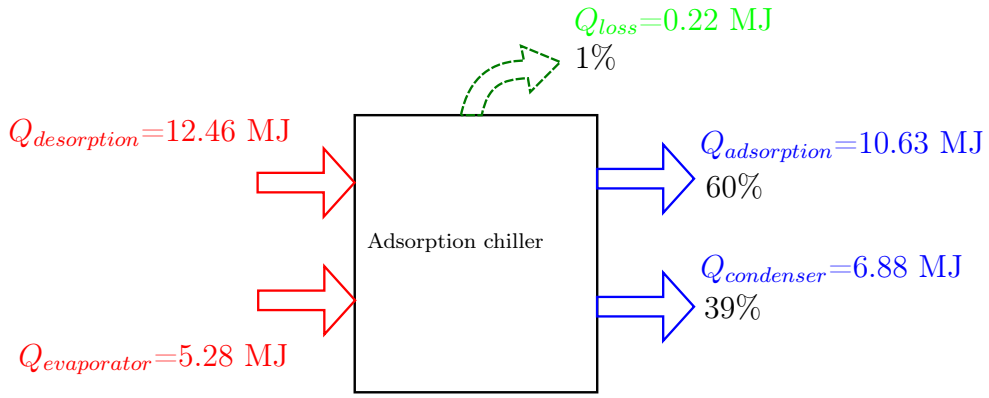

Figure 4.33: Energy balance of the adsorption chiller for the stationary cycle

The driving temperature (T_h) and the temperature of heat rejection (T_c) was varied keeping the other experimental settings unchanged and the trend of COP_{cool} Vs. T_h and $\dot{Q}_{cooling}$ Vs. T_h at different T_c was generated.

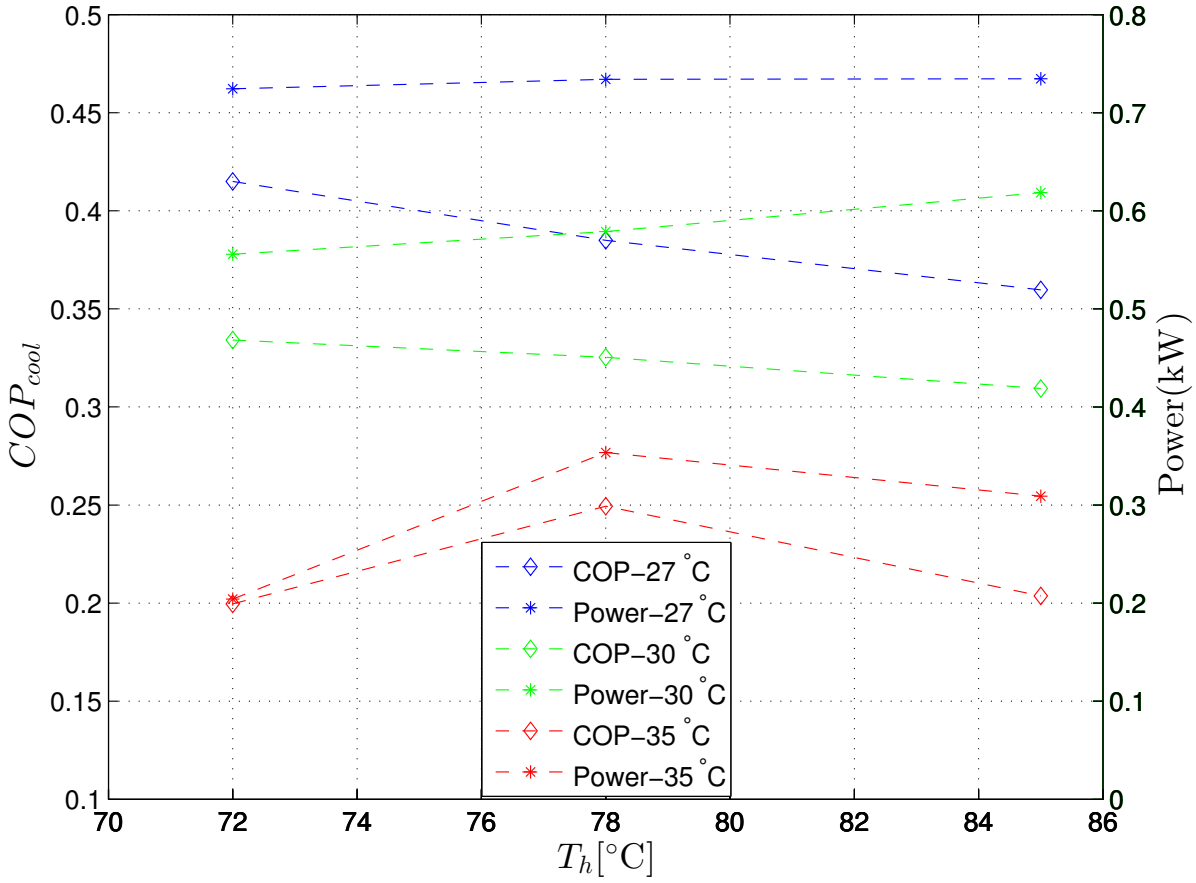

Figure 4.34: Plot of the COP_{cool} and cooling power of the stratisorp cycle with variations for different driving temperatures (T_h=72/78/85 °C) and different medium temperatures (T_c=27/30/35 °C) and keeping the temperature of low temperature heat source constant (T_e=18 °C). The flow rates were set according to Tab. 4.5

At least 10 consecutive cycles were measured and the average COP_{cool} and $\dot{Q}_{cooling}$ over the last 5 cycles were calculated to achieve each data point in the plot. Total duration of approx. 24 hours was required per experiment. Maximum $COP_{cool} \approx 0.42$ for the cycle with condition 72/27/18 °C was obtained. This cycle condition was chosen for further investigation. The reproducibility of the results is documented in appendix A.3.

4.3 Control strategies for stratisorp cycle

The basic stratisorp cycle discussed until now (72/27/18 °C) offered only 16% improvement in COP_{cool} as compared to the cycle without heat recovery. Two probable measures which have potential to increase the COP_{cool} and cooling power of the original stratisorp cycle are discussed in the following sections.

4.3.1 Variation in switching criteria

Detailed investigations based on the differential heat curves for water-silica gel 127B revealed that the overlap between the differential curves is large between the temperature range 40-65 °C (Fig. 2.5). When the stratisorp cycle is underway within this temperature range the potential for heat recovery is significantly higher than in other temperature ranges. This temperature range corresponds to the central section of the tank. It is also evident from the vertical temperature profile in the tank that between the stratification rings R_3 and R_4 a steep temperature gradient exists (Fig. 4.25). Such steep gradient means that while switching from R_3 to R_4 momentarily a peak in the adsorber power occurs. This effect is reversed during the desorption half cycle while switching back from R_4 to R_3.

Half cycle	Extraction	Insertion	while $\lvert\Delta T_{ad}\rvert$ is...	
			modified	original
Adsorption	R_2	R_1	> 3	1
	R_3	R_2	> 3	1
	R_4	R_3	> 0.75	1
	R_5	R_4	> 3	1
	R_6	R_5	> 1	0.5
Desorption	R_5	R_6	> 3	1
	R_4	R_5	> 3	1
	R_3	R_4	> 0.75	1
	R_2	R_1	> 3	1
	R_1	R_2	> 2	1

Table 4.7: Modified and original switching criteria

As a result the driving temperature difference at the adsorber increases which in turn decreases the overlap between the differential heat curves. Hence the fraction of recoverable portion of the sorption heat decreases and adversely affects the COP. This adverse effect can be rectified by either reducing flow rate for the adsorption/desorption step in discussion or by changing the switching criterion to a lower value thereby effectively extending the time to switch to the next step. In the current LabView code the adsorber flow could not be changed for the temperature based switching cycle. Therefore the second option was used. Moreover,

it was also intended to achieve a higher cooling power by reducing the cycle time. Hence the switching criterion was increased for the remaining steps (Tab. 4.7).

It is clear from the Fig. 4.35 that the third peak in the adsorption or desorption half cycle is reduced by 48% as compared to Fig. 4.28 as a result of this measure. The cooling power is increased by almost 39% by reducing the cycle time by 35%. The comparison of Fig. 4.28 and Fig. 4.35 shows a very important difference in both cycles. The cycle with variable switching criteria show hardly any negative peaks in the adsorber power during the first adsorption step. A steeper tank temperature profile across the top zone of the tank causes this effect. Due to such temperature profile, there exists a temperature spread across the adsorber even during the first adsorption step as differed to the standard cycle. Hence the cooling power is much earlier available than the standard cycle. A detailed comparison revealed that the energy required for the sensible cooling of the evaporator (area under the magenta curve on the positive side) is reduced by 21% which led to increase in the COP_{cool} by the same factor.

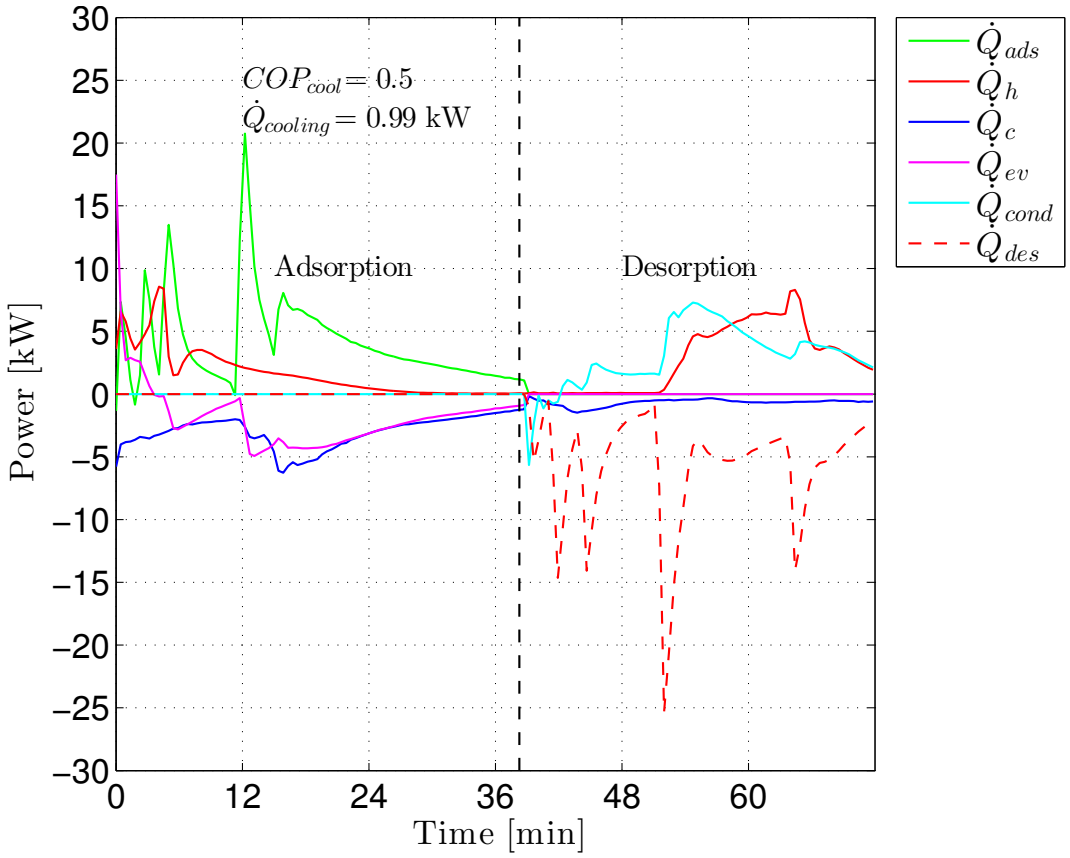

Figure 4.35: Power achieved during a stratisorp cycle with variable switching criteria

An interesting fact can be observed in Fig. 4.35 regarding $\dot{Q}_c$. The cooling module operates with a very low power towards the end of the desorption cycle (586 W). However, after switching to the adsorption half cycle it operates with a significantly higher power (5.78 kW) which is almost 10 times more. This happens due to the fact that the temperature profile in the bottom zone of the tank for the stationary cycle is steeper than the standard stratisorp cycle discussed before. Hence the power of the cooling module scales with $\dot{V}_c$ i.e. the flow rate being circulated by the cooling module through the tank. $\dot{V}_c$ is also approximately 10

times higher during adsorption half cycle than during the desorption half cycle owing to the construction of the test set-up (see page 94).
Fig. 4.36 shows the evolution of various temperatures during the stratisorp cycle with variable switching. Comparison with the standard stratisorp cycle based on Fig. 4.31 shows that for the cycle with variable switching the tank temperature profile matches better with the temperature spread across the adsorption chiller. This can be confirmed by the trend of different temperature sensors, especially the trends of T_7 and T_{10}.

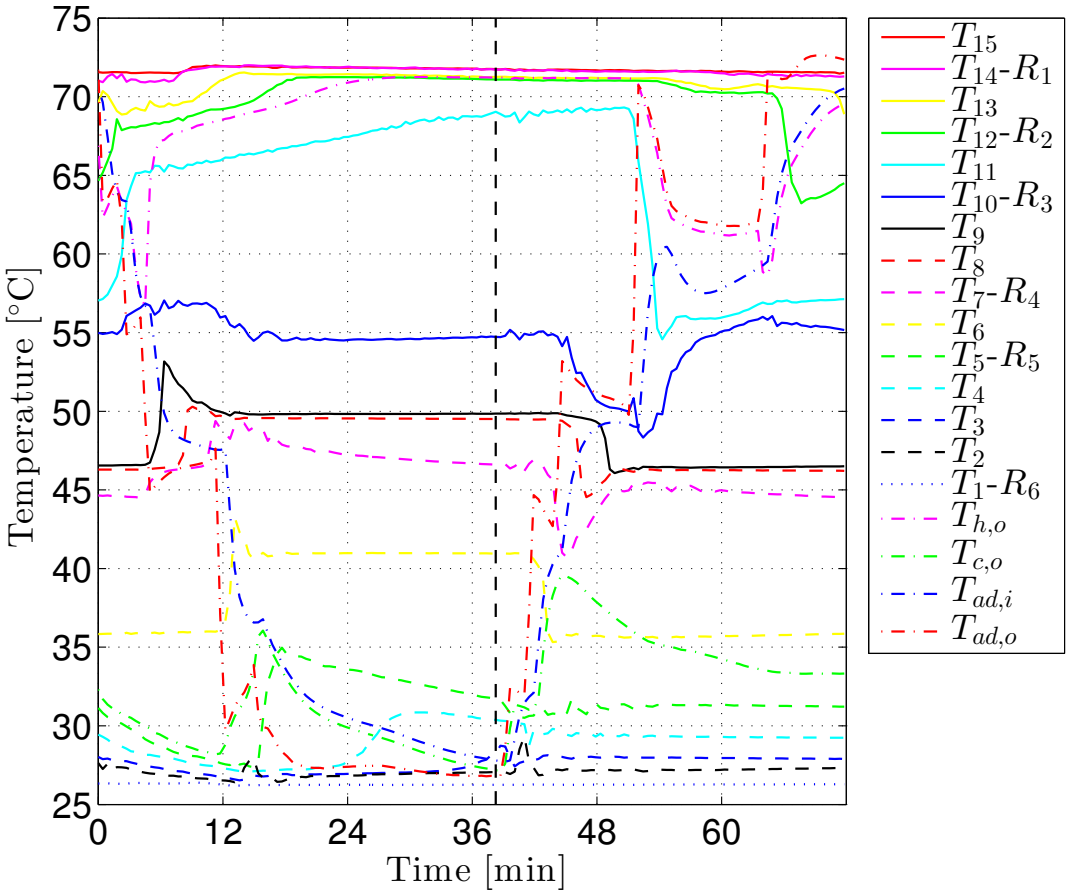

Figure 4.36: Plot of the tank temperatures at different heights of the storage for the stratisorp cycle with variable switching

The temperature of the return flow from the adsorption chiller to the tank ($T_{ad,i}$) during the fourth adsorption step and during the fourth desorption step is much closer to T_7 and T_{10}, respectively. It causes less mixing at the point of entry into the tank and hence the temperature change in T_7 and T_{10} is much lower than seen before in Fig. 4.31. Here it can also be seen that the duration of the relevant adsorption and desorption steps is shorter than before as higher value (Tab. 4.7) of switching criterion was chosen. This measure not only shortens the duration but also avoids the negative impact of cooler operation on the adsorption step. A faster cycle led to increase in the cooling power.

4.3.2 Intermittent heating and cooling

The modified stratisorp cycle with intermittent heat supply and heat rejection was originally proposed by Schmidt.*et at.* [51] in a simulation study but it had never been experimentally validated. From the previous experiment on the standard cycle it was observed that the heating and the cooling module caused significant mixing in the respective tank zones due to continuous operation. Hence is was important to investigate the performance of the cycle when these modules do not interfere with the stratified tank. When the driving heat is only intermittently available as in the case of CHP unit, solar hot water storage, the silica gel adsorption chiller with the control strategy discussed below can be used.
At the end of the desorption half cycle when the temperature of water being extracted becomes too low for continuing desorption, the heater is activated. On the other hand, when the adsorption half cycle approaches the end by taking water from the lowest section of the tank and if not enough cool water is available for further adsorption then the cooler is switched on. The heater and the cooler are thus intermittently active i.e. only at the end of each half cycle. For the rest of the cycle the bypass valve V_1 (Fig. 3.23) in the heater is open thereby assuring that the water at T_h is circulated in the heating module.

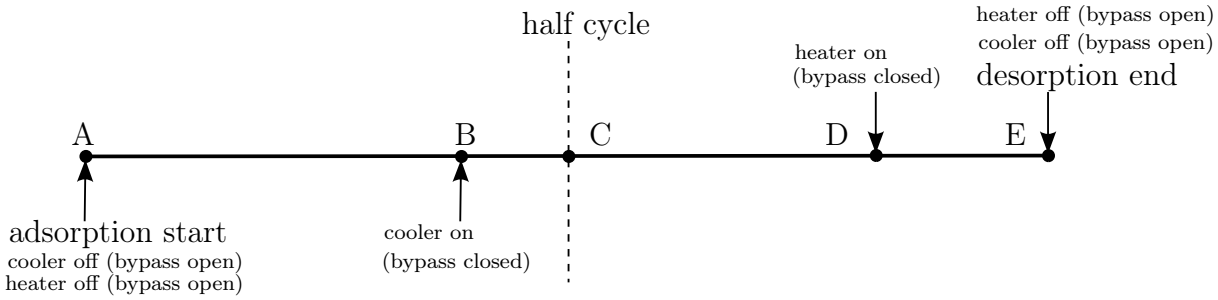

Figure 4.37: Sequence of operation of heater and cooler in the modified stratisorp cycle

The same operation can not be implemented for the cooler as the cooler needs to be operating during the complete desorption half cycle in order to reject the heat of condensation. Hence the cooler bypass is activated from the start of the adsorption half cycle till the cooling action is needed at the end of the adsorption half cycle. An external 3-way valve was hence connected between the inlet and outlet of the cooling module (Fig. 3.24). The operation of this cycle is shown on a qualitative timeline in Fig. 4.37.

The basic idea behind this type of the cycle operation is to utilise the tank solely for storing the sorption heat released during adsorption phase and utilising it for the desorption half cycle. The tank is decoupled from the heating and cooling module. Hence equal flow rates of the heating module, cooling module, condenser and adsorption chiller were chosen. The flow scenarios arising at the timestamps A,B,C,D,E due to equal flow rates in different hydraulic circuits are shown in Fig. 4.38. The flow rate was set to 800 lph in all hydraulic circuits connected to the tank. This lower flow rate would mean a lower power available and poor heat transfer properties in the adsorber heat exchanger. However, it also means that the temperature spread across the adsorption chiller would be higher. A higher temperature spread would match better to the stationary tank temperature profile and could lead to lower mixing in the tank. Accordingly the modified switching criteria are tabulated in Tab. 4.8.

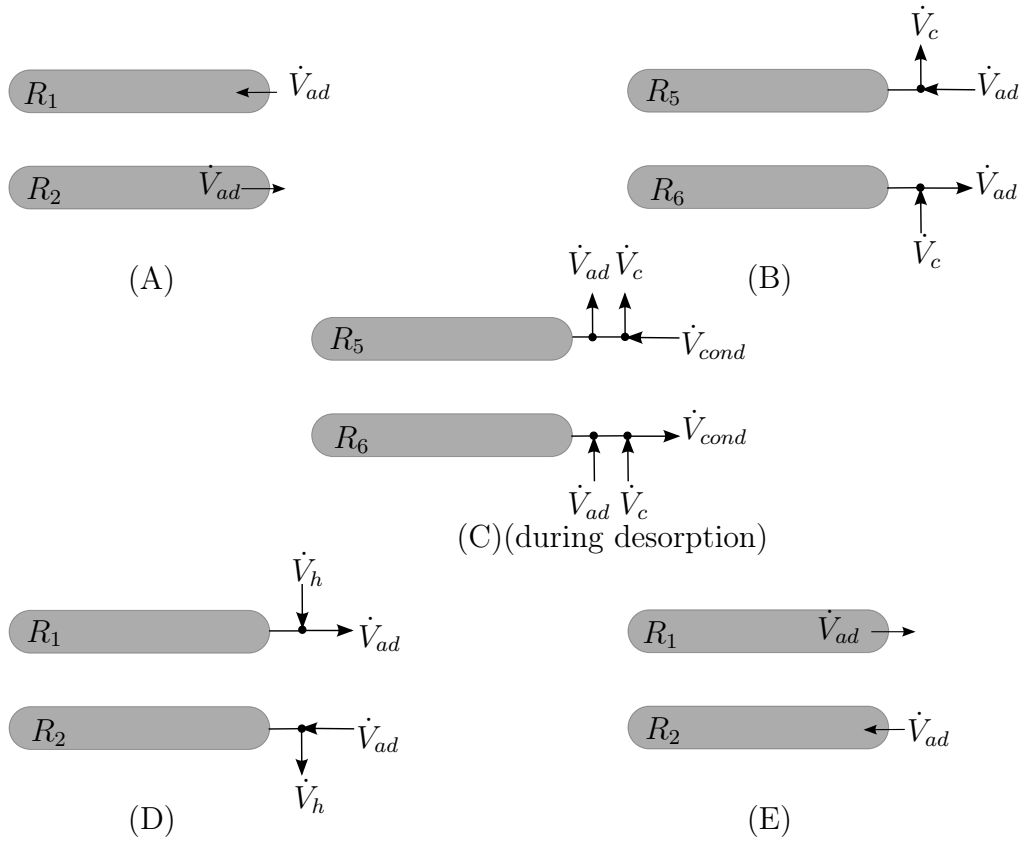

Figure 4.38: Flow scenarios at the occurrence of events A to E. The net flow through the tank in events B and D is zero

Half cycle	Extraction	Insertion	while $\lvert\Delta T_{ad}\rvert$ is...
Adsorption	R_2	R_1	> 1
	R_3	R_2	> 1
	R_4	R_3	> 1
	R_5	R_4	> 1
	R_6	R_5	> 2
	Scenario B (using cooler)		> 0.5
Desorption	R_5	R_6	> 1
	R_4	R_5	> 1
	R_3	R_4	> 1
	R_2	R_1	> 1
	R_1	R_2	> 3
	Scenario D (using heater)		> 1

Table 4.8: Switching criteria used for cycle with intermittent heating and cooling

The tank was preconditioned exactly as for the basic stratisorp cycle. As the heater had

been decoupled from the tank, the warm water contained in the top zone of the tank was exhausted for desorbing the adsorber in the 5th desorption step. This zone could now only be heated up by the heat of adsorption and not by the heater.

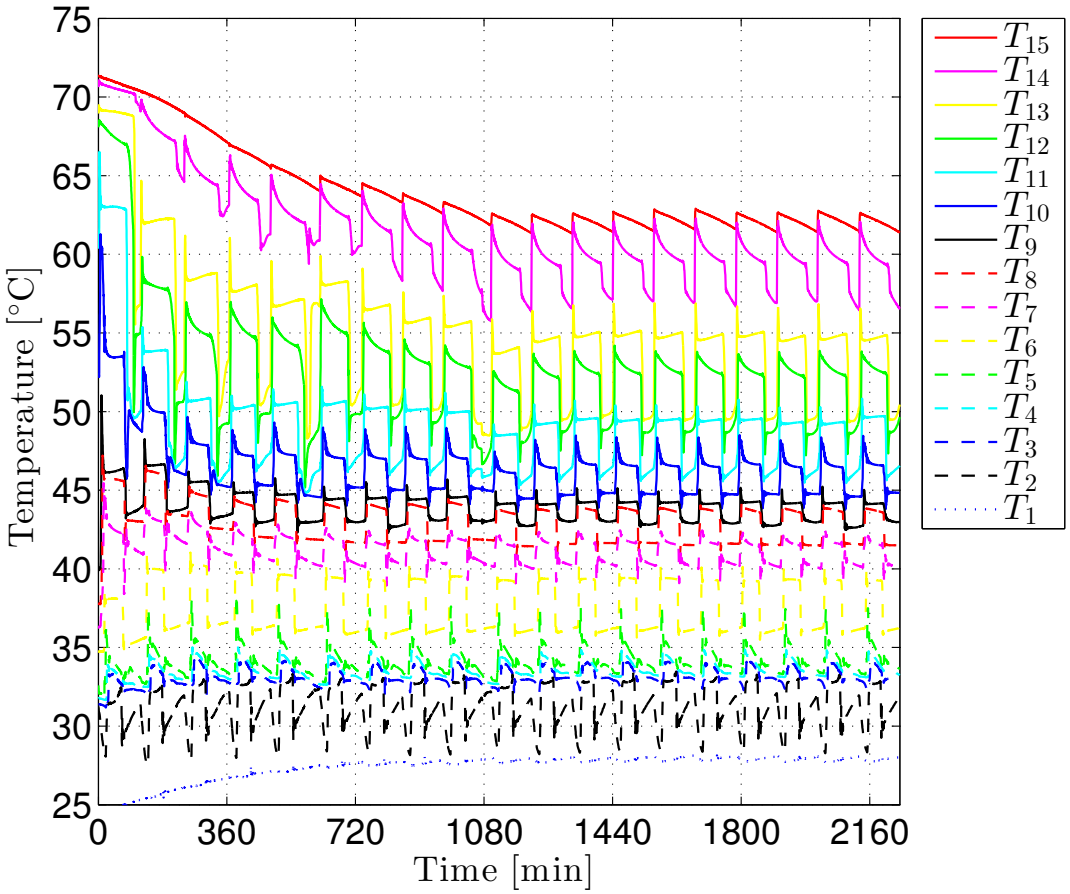

Figure 4.39: The tank temperature during the stratisorp cycle with intermittent heating and cooling

On the other hand, the cooled preconditioned bottom zone of the tank was almost completely exhausted for cooling the adsorber during the 5th adsorption step. The warm water returning to the tank carrying the heat of adsorption increases the temperature of this zone. This zone was not cooled down again to the medium temperature (T_c) of the cycle as the cooling module was decoupled from the tank. Fig. 4.39 shows how the tank temperature evolved over the cycles. Fig. 4.40 confirms that the bottom section of the tank warms up over initial 6 cycles. The starting temperature profile for this experiment was the temperature profile obtained at the end of the experiment with variable switching criteria explained earlier. Had the tank temperature been uniform (say at room temperature) it would have taken extremely long to achieve a stationary state. However, although after starting with linear temperature profile nearly 20 cycles were needed to reach to a stationary state.

The intermittent operation of the heater and cooler is easily identified in the plot of power (Fig. 4.41)[12]. Cooling power at the evaporator is much earlier available as compared to the standard stratisorp cycle (Fig. 4.28) owing to a steeper temperature gradient in the hot zone

[12]refer appendix A.3 for different flow rates

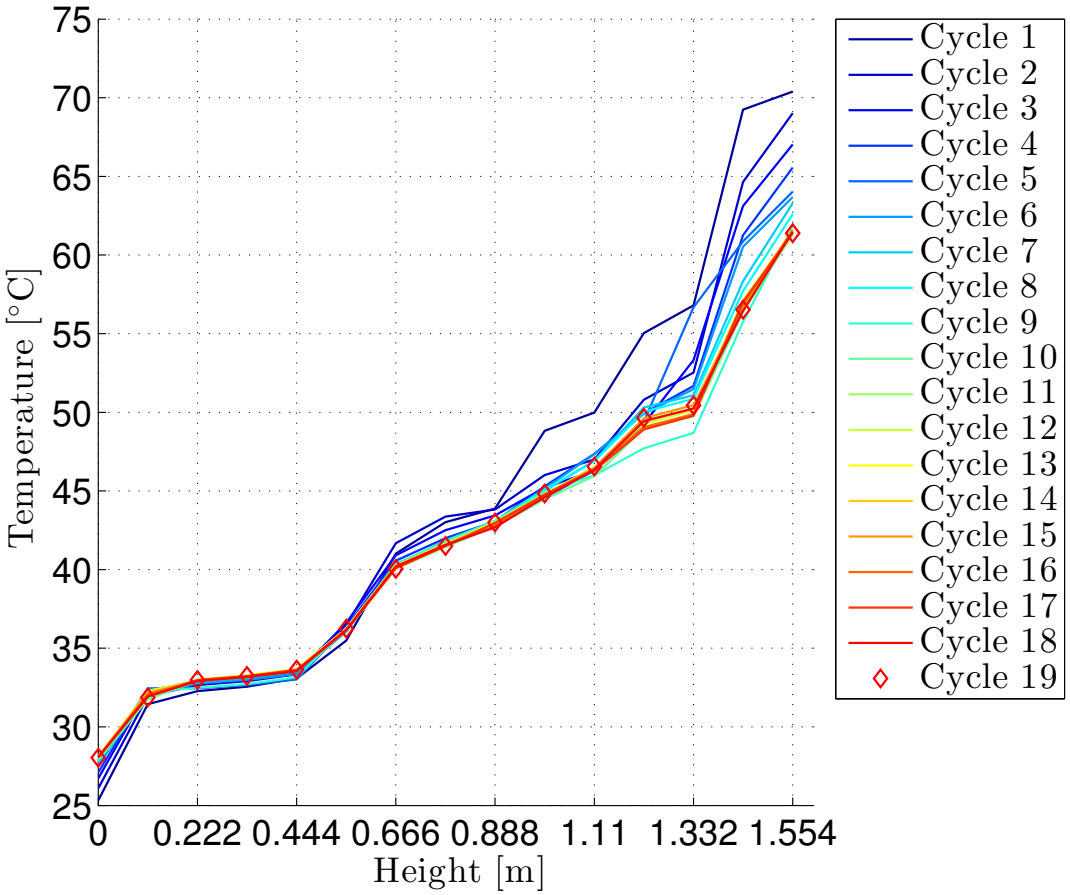

Figure 4.40: The tank temperature profile at the end of each cycle during the stratisorp cycle with intermittent heating and cooling

of the tank. The energy supplied or rejected during the cycle is computed as per Eq. 4.5 except for Q_h and Q_c as :

$$\begin{aligned} Q_h &= \int_{t_{heater'ON'}}^{t_{end}} dQ_h = \int_{t_{heater'ON'}}^{t_{end}} \dot{m}_h \cdot c_p \cdot (T_{h,i} - T_{h,o}) \cdot dt \\ Q_c &= \int_{t_{cooler'ON'}}^{t_{halfcycle}} dQ_c = \int_{t_{cooler'ON'}}^{t_{end}} \dot{m}_c \cdot c_p \cdot (T_{c,i} - T_{c,o}) \cdot dt \end{aligned} \tag{4.12}$$

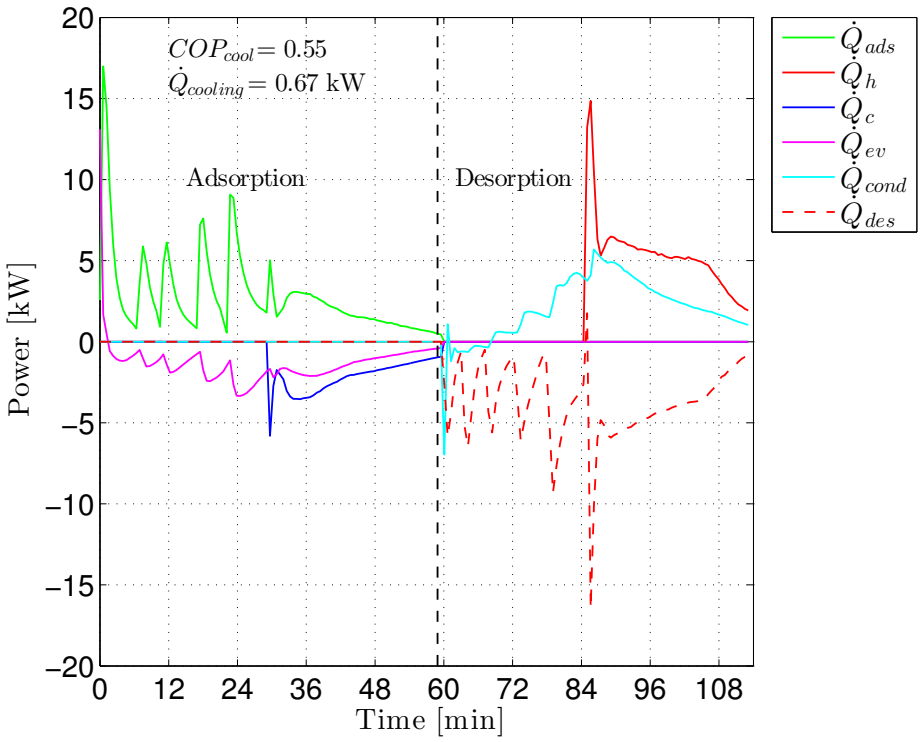

Figure 4.41: Plot of power obtained for the last cycle for the stratisorp cycle with intermittent heating and cooling

The driving heat required by the cycle is reduced by 30% leading to an increase by 34% in COP_{cool} as compared to the standard stratisorp cycle operating under the same temperature condition[13]. The stratisorp cycle with intermittent heating and cooling thus offers a significant increase in the COP_{cool} as compared to the standard stratisorp cycle (continuous operation of heater and cooler) in case of the silica gel adsorption chiller operating under these temperature conditions (72/27/18 °C). There are of course further possibilities of implementing efficient control strategies which could also lead to improvement in the COP_{cool}. e.g. combination of both approaches (variable switching criteria and intermittent heating and cooling), reduction of the adsorber flow rate during the valve switching interval (to reduce mixing during switching interval). These approaches are not investigated in this work.

4.4 Discussion

In the following discussions the stratisorp cycle with intermittent heating and cooling is compared with the standard cycle operating with $\dot{V}_{ad}$ = 800 lph on the basis of evolution of the tank temperature profile.

[13]additional experiment with $\dot{V}_{ad}$ = 800 lph was carried out in order to have a fair comparison with the experiment with intermittent heating and cooling which was also operated at the same flow rate

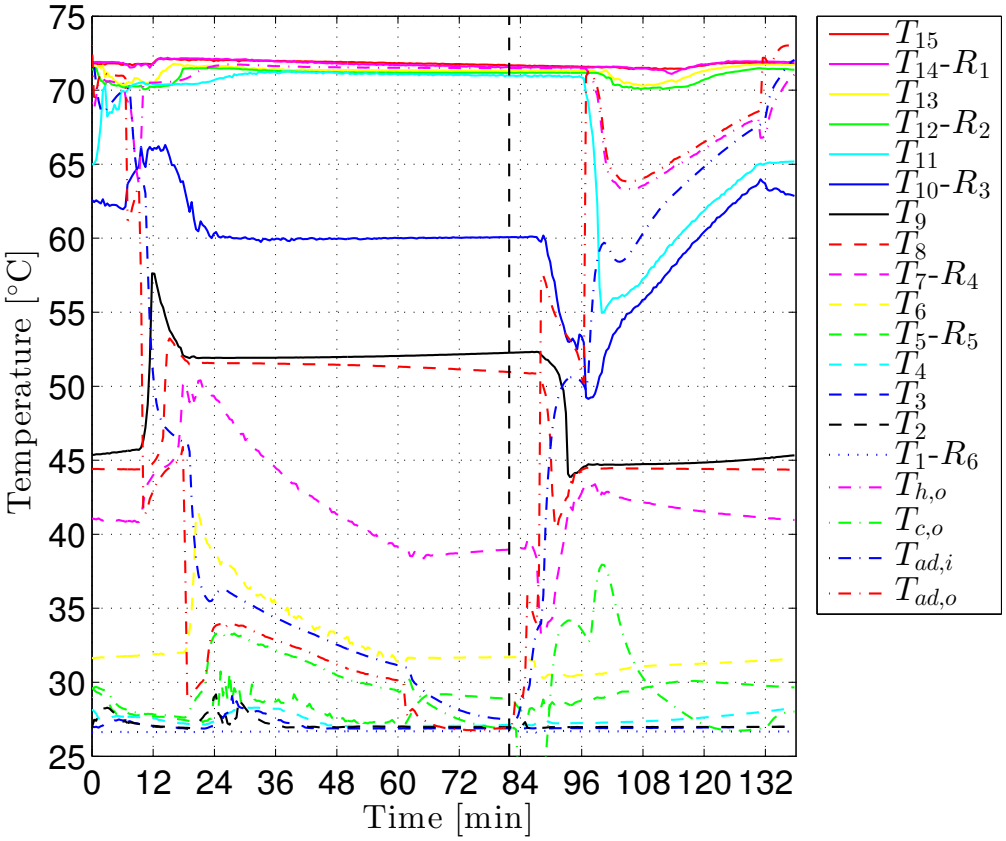

(a) Tank temperature for the standard stratisorp cycle ($\dot{V}_{ad}$ = 800 lph)

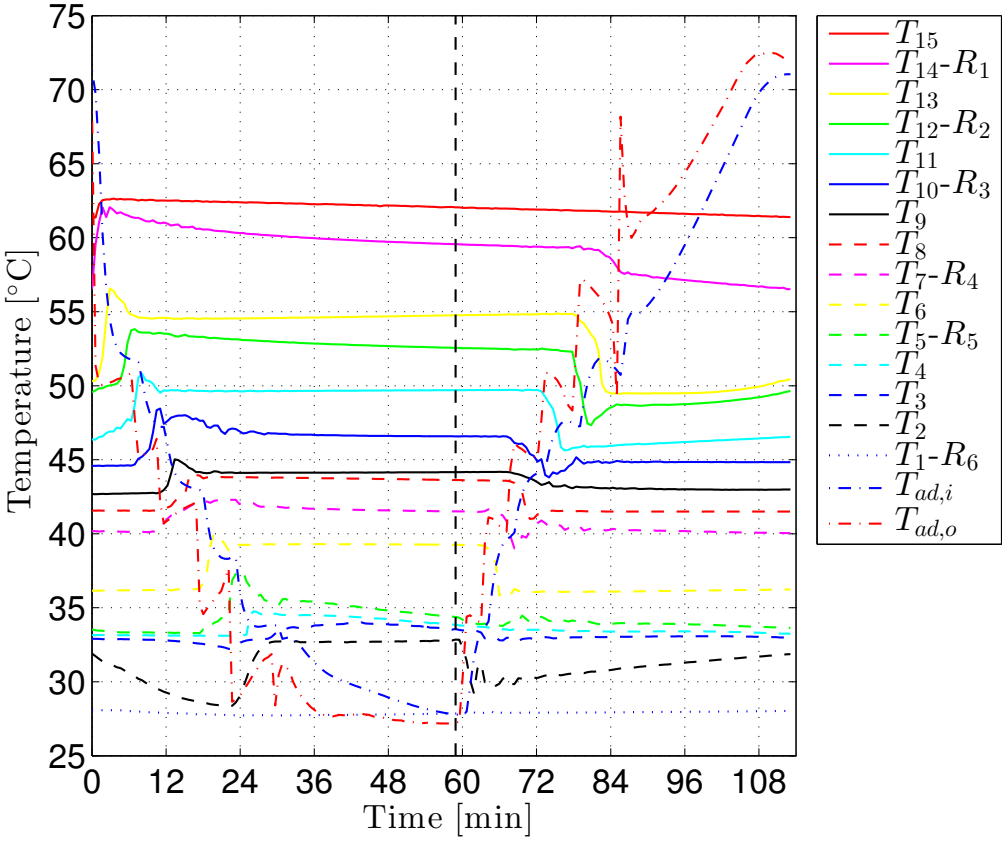

(b) Tank temperature for the stratisorp cycle with intermittent heating and cooling ($\dot{V}_{ad}$=800 lph)

Figure 4.42: Effect of intermittent heating and cooling the tank temperature

From Fig. 4.42(b) it is clear that the tank temperature profile suits better to the temperature spread across the adsorber if the heater and the cooler are operated intermittently. Here again the comparison of the trends of T_7 and T_{10} confirms that the mixing in the tank is drastically reduced as the temperature spread across the rings matches very good to the temperature spread across the adsorption chiller. The heights of the "jumps" in $T_{ad,o}$, caused due to extraction of water from the next lower ring or from the next upper ring, are significantly lower. This assures that the adsorption chiller is operated with a lower driving temperature difference and the overlap between the differential heat curves is higher (Fig. 2.5). The temperature of each zone in the tank increases during the adsorption half cycle as the warmer return flow to the tank stratifies at the position of the rings. The temperature of the zones does not change significantly until the desorption steps commence. This effect is attributed to lower mixing in the tank compared to the standard cycle (Fig. 4.42 (a)). Hence the degree of internal heat recovery for this modified cycle is higher which clearly is the reason for higher COP_{cool}. The decoupling of the cooling and the heating module from the tank also avoids mixing. Moreover, the fourth adsorption step and the fourth desorption step are faster than before causing faster cycle and higher power.
Tab. 4.9 compares the results of the experiments described until now.

	Experiment (72/27/18 °C)	COP_{cool}	Cooling power (kW)	Cycle time (min)
	Without heat recovery $\dot{V}_{ad_{adsorption}}$=1050 lph $\dot{V}_{ad_{desorption}}$=640 lph	0.36	1.35	48
Stratisorp	$\dot{V}_{ad}$=1000 lph	0.42	0.72	110
	Variable switching criterion $\dot{V}_{ad}$=1000 lph	0.50	1	72
	$\dot{V}_{ad}$=800 lph	0.41	0.61	137
	Int. heating and cooling $\dot{V}_{ad}$=800 lph	0.55	0.67	114

Table 4.9: Summary of all results obtained

Fig. 4.43 shows the tank temperature profile of the stationary cycles for different experiments discussed till now. As seen before the central section of the tank bears importance as far as the heat recovery is concerned. The temperature range of 40-65 °C is of much interest for the stratisorp cycle as the overlap between the heat curves is significant between these temperatures. The relevant temperature range lies across the span of 3 rings i.e. from R_2 to R_4. The tank temperature gradient is much flatter in the experiment with intermittent heating and cooling than in the other experiments. Clearly a flatter temperature gradient is beneficial to the cycle. The adsorber is cooled or heated with a smaller temperature difference (blue curve), especially between 40-65 °C, as compared to other experiments (red, magenta and green curve). A flatter temperature profile suits also well to the temperature spread across the adsorption chiller as seen before in Fig. 4.42(b). A trend between the tank temperature gradients, especially in the zone between R_3 and R_4, and improvement in the COP_{cool} is generally observed here.

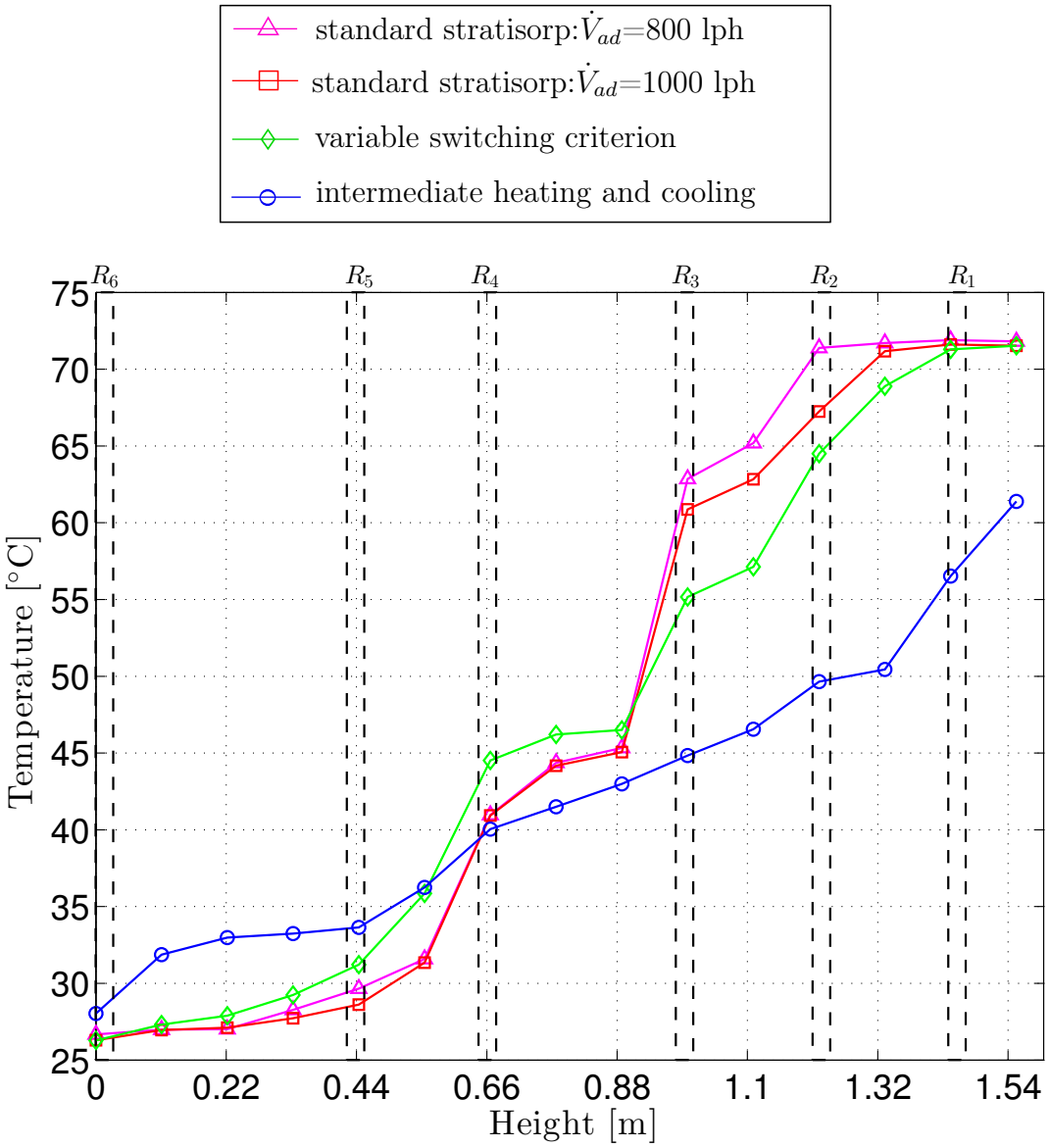

Figure 4.43: Comparison of final tank temperature profiles for a stationary cycle during different experiments with identical cycle conditions (72/27/18 °C) and the positions of the rings

Thus the stratified thermal storage fulfils its role of storing the heat of adsorption and utilising it for the desorption half cycle more efficiently than for the standard stratisorp cycle and cycle with variable switching criterion. This led to increase in COP_{cool} of the improved stratisorp cycle (intermittent heating and cooling). The tank temperature profiles for the standard stratisorp cycles (red and magenta curves) can also lead to improvement in COP_{cool} if the spatial resolution of the extraction rings in central section of the tank is increased. In that case the adsorber return flow into the tank would get stratified near to the correct height corresponding to the "matching" fluid layer and consequently the mixing would be reduced.

Chapter 5

Conclusion and future work

5.1 Conclusion

The experimental proof of concept for the stratisorp system concept was presented in this work. A silica gel module used for adsorption chiller eCOO 2.0 was successfully operated according to the stratisorp concept and the potential of improvement in the coefficient of performance for cooling applications was demonstrated in the course of this work. The experimental set-up which included a storage tank, a heating module, a re-cooler (cooling module), an adsorber emulator module and the adsorption chiller was built. The stratified thermal storage is a central component for the stratisorp system concept. The mixing in the storage tank seriously hampers performance of the cycle. In this work, a novel stratification system consisting of stratification rings placed at different heights of the tank was developed. It facilitated insertion and extraction of fluid from the tank while causing minimal mixing in the stored fluid provided that the temperature spread across the adsorption chiller matches close to the temperature spread across the adjacent rings. The fluid flow was controlled by opening or closing of two way valves attached to the supply and return flow sides. The stratification rings were manufactured during this work (see appendix A.3). These rings incorporated a number of holes drilled on the inside of the inner perimeter of the rings. The inertia of the flow was reduced by wrapping reticulated foam strips around the rings. The effectiveness of the foam towards reduction in mixing and flow inertia was tested using an ink test on short sections of pipes. The rings were deployed into a tank (volume $\approx$ 500 litres) that provided optical access. The insertion and extraction from the tank was carried out using a stratification system based on solenoid valves. The ink test could not be used for the characterisation of flow in the tank. Hence a non invasive flow visualisation technique, the Background Oriented Schlieren (BOS), was used. The BOS method used in this work can only be used for qualitative characterisation of the flow field and the stratification rings. A unique use of this method along with the temperature sensors in the tank meant that quantitative information about the flow field could be achieved. The method was first thoroughly studied and its applicability for the stratisorp cycle was scrutinised. The BOS method was successfully tested on a small plexiglas tank (volume $\approx$ 10 litres) with rotationally symmetric fluid entry. The BOS method was then implemented on the tank with optical access. Initially an emulated stratisorp cycle was executed by operating the emulator similar to the operation of an adsorption chiller. However, as only the supply temperature to the tank was controlled by the emulator and not the power, the cycle did not exactly replicate the real

cycle conditions. Moreover, only low flow rates and low T_h could be set ($\dot{V}_{ad}$ = 300 lph and T_h = 63 °C). This cycle condition was less interesting for the stratisorp system concept not only due to lower flow rate, but also due to the lower desorption temperature. Hence the sole aim of this test was to visualise the flow and qualitatively confirm the functional effectiveness of the stratification rings. From the flow visualisation tests it could be confirmed that the rings fulfilled their role of inlet flow distributors by inducing minimal mixing and assuring a rotationally symmetric flow. A stable thermocline region was formed giving rise to a plug flow. A much more realistic flow condition was later set ($\dot{V}_{ad} \approx$ 700 lph) using the adsorption chiller and operating the emulator as a cooling or heating load. Due to an unstable flow rate achieved in an unpressurised system the flow visualisation test was carried out during only one of the adsorption steps rather than for the whole cycle. In a linearly stratified thermal storage tank, it was observed that as soon as the fluid possessing higher temperature than the surrounding fluid entered the tank, it rose to the next layer in the tank whose temperature matched the inlet temperature. The flow formed veils before stratifying in that layer. Their existence was confirmed by the BOS method. However, the adsorption chiller flow rate used ($\dot{V}_{ad}$ = 1000 lph) in the stratisorp experiments had not been tested in a BOS experiment. It is hence unclear if the flow veils occur at this flow rate. It was also confirmed that the fluid in the central cylindrical section bordered by the inlet perimeter of the rings remained relatively undisturbed. It could be concluded that the stratification rings, developed in this work, insert and extract fluid from the tank causing minimal perturbations and also maintain rotational symmetry. This fact makes this stratification system easier to model (CFD or mathematical model) as compared to state of the art stratification systems readily available (SOLVIS lance). A stratification lance developed by a German manufacturer Sailer also facilitates the ease of modelling, however this lance tends to entrain the surrounding fluid into the main flow inside the lance. This effect has been proven to be detrimental to the thermal stratification [57].
The adsorption chiller was initially operated in a cycle without heat recovery by adapting the cycle conditions according to the available test set-up. The experimental results achieved by the adsorption chiller manufacturer were replicated with some deviation in COP_{cool} of the cycle. The differences in the adsorption chiller flow rate and presence of an inert gas in the vacuum chamber of the chiller were attributed to be the cause of the deviations in the results. The stratification rings were then mounted in another tank (volume $\approx$ 750 litres) and the stratification system was constructed. The adsorption chiller was then operated using the stratisorp system concept and a clear improvement in COP_{cool} was obtained. In this work a method of estimation of COP of the stratisorp cycle has been introduced and the experimental data was processed accordingly. It was observed that for the given size of the storage approximately 10-15 consecutive cycles were necessary in order to reach a stationary state. The stratisorp cycle was operated for different driving temperatures (T_h) and re-cooling temperatures (T_c) keeping the temperature of the low temperature heat source constant (T_e =18 °C) and the trend of COP_{cool} Vs. T_h and cooling power ($\dot{Q}_{cooling}$) at different T_c was generated. These curves are not to be confused with the characteristic curves of the module given by the manufacturer. The trend curves are only valid for the given silica gel adsorber module operated according to the stratisorp concept using the specific set of parameters. The basic stratisorp cycle was modified by changing the switching criterion for different adsorption and desorption steps, specifically by elongating the adsorption step within the temperature range 40-65 °C. The overlap between the differential heats of adsorption and desorption is found to be at a maximum in this temperature range for the silica gel-water

pair. It was found that the COP_{cool} increased by 21% while the cooling power increased by 39% as compared to the standard stratisorp cycle operating at the same flow rate ($\dot{V}_{ad}$ = 1000 lph). Another modification in the stratisorp cycle was demonstrated where the heater and the cooler are switched on only at the end of the desorption and the adsorption half cycles respectively (intermittent heating and cooling). This mode of operation offered the maximum improvement in COP_{cool} as compared to the previous two cycle modes (standard stratisorp and with variable switching criterion). The COP_{cool} was found to have increased by 34% as compared to the standard mode of operation where $\dot{V}_{ad}$ was set to 800 lph. These three different modes of operation were compared based on the tank temperature profile for the steady state condition. It was concluded that a flatter temperature gradient in the zones of the tank where the temperature range corresponded to the range in which maximum overlap of the differential heat curves exists, is beneficial to the stratisorp cycle. This works in favour of operating the cycle with lower driving temperature differences and thereby improving the overlap of the differential heat curves.
The theoretical investigations of the stratisorp cycle by the simulations has proven that significant improvement in the adsorption chiller's COP_{cool} by implementation of a stratified thermal storage tank is possible, provided that ideal insertion and extraction from the storage is available [53]. However, the experimental investigations in this work have identified that the mixing caused due to the limited number of rings available for fluid extraction and insertion is the most important factor affecting the COP_{cool} of the stratisorp cycle. This is the main reason why the stratisorp cycle although having a good potential for COP improvement has lower COP_{cool} than the state of the art heat recovery systems readily available on the market.e.g. the heat recovery system invented by SorTech (explained in Chapter 2). In this work it has also been shown that lower mixing in the central section of the tank lead to significant improvement in COP_{cool}. An improved stratification system can be realised by increasing the spatial resolution of the rings in the central section of the tank. This measure would assure that within the region of maximum overlap of the differential heat curves, the adsorption chiller is operated at very low driving temperatures and the COP_{cool} would improve. For the current system with the available number of rings (six rings) the adsorber heat exchanger design needs to be adapted. The temperature spread at the set flow rate across the adsorber heat exchanger used in this work does not match to the temperature spread across the adjacent rings. Lower temperature spread across the adsorber heat exchanger leads to severe mixing in the tank and the heat of adsorption is not efficiently stored. An adsorber heat exchanger with higher UA-value would be well suited to the current stratisorp system with six rings. The adsorption chiller from SorTech is a standard chiller used for cooling applications based on the heat recovery system invented by SorTech. The chiller had not been developed aiming at the dynamics of the stratisorp cycle. Hence any modifications on the current chiller are a matter of future projects. However, using two or even three chillers connected in series, a wider temperature spread across the first and the last chiller can be achieved. Such a temperature spread would then adapt to the temperature spread across adjacent rings and cause less mixing than a single adsorber stratisorp system.

5.2 Future work

For the current experimental set-up with the given number of the stratification rings, a combination of the proposed controlled strategies would be very beneficial to the cycle

performance. The jump in the temperature of fluid extracted for the adsorber during the adsorption half cycle clearly has an adverse effect on the COP. This can be rectified by introducing additional rings in those zones of the tank where the temperatures correspond to the temperature range with a maximum overlap of the heat curves. This would flatten the temperature gradient in this zone and could improve the cycle performance.
Delaying the return flow to the tank at the start of each adsorption and desorption step can also lead to a small improvement in COP_{cool} (analogous to the SorTech heat recovery cycle) as the mixing in the tank would be lowered by this measure. An additional 3-way valve operating as a bypass at the adsorber inlet would be needed for this measure.
It was also observed that lower heater or cooler flow rates are beneficial to the cycle as they cause a steeper gradient in the top and the bottom zones of the tank. The effect of varying these flow rates on the performance of the cycle would also be interesting to investigate.
The production of the stratification rings was complicated and time consuming. A far simpler design with less intricate details can be used to replace the present stratification rings. e.g. an octagonal inlet distributor made from short pipe sections with holes on the side facing the tank axis and connected by readily available bends.
The regeneration temperature corresponds also to the hot water temperature available from a medium scale CCHP unit. This makes the application of the stratisorp system very interesting. The tank can be conditioned to the maximum desorption temperature of 72 °C. The conditioned tank represents a fully charged buffer tank of a CCHP system. Using this tank some stratisorp cycles can be carried out. The initial cycles would be very fast and much less cooling power would be available. After a few cycles a vertical temperature gradient would develop in the tank and more cooling power for later cycles would be available.
In general the stratisorp system would be suited for cooling applications where heat is available close to the regeneration temperature of the adsorbent (e.g. waste heat, solar heat) and where the temperature spread across the low temperature heat source and the medium temperature heat sink is not significantly large. The stratified storage works not only as heat storage but also as means of coupling the external heat source to the adsorption chiller.e.g. warm return flow from the solar collector can be connected to the top zone of the tank. The stratisorp system concept can be extended to a zeolite adsorption chiller operating at higher desorption temperatures. The potential of improvement in COP can also be demonstrated for the zeolite chiller.

Appendix A

Appendices

A.1 Calibration of temperature sensors

Calibration of temperature sensors for plexiglas tank: The temperature was measured using Pt-1000 resistance temperature detectors (RTD) and recorded on the computer based data acquisition system. Data acquisition was carried out using NI USB Box 6211 , a signal converter for converting temperature dependent resistance into voltage signal (0-10 V) and LabView 2012 software installed on Win XP system. The corresponding LabView code can be found in appendix A.2. For achieving maximum precision and accuracy, all temperature sensors were calibrated by comparing against a precision reference sensor Pt-25. A circulation thermostat was used to prepare water at different temperatures. A copper block with drilled holes for adapting the sensors and the reference sensor Pt-25 was used in order to homogenise the temperature field and to assure high precision. The experimental arrangement can be seen in Fig. A.1.

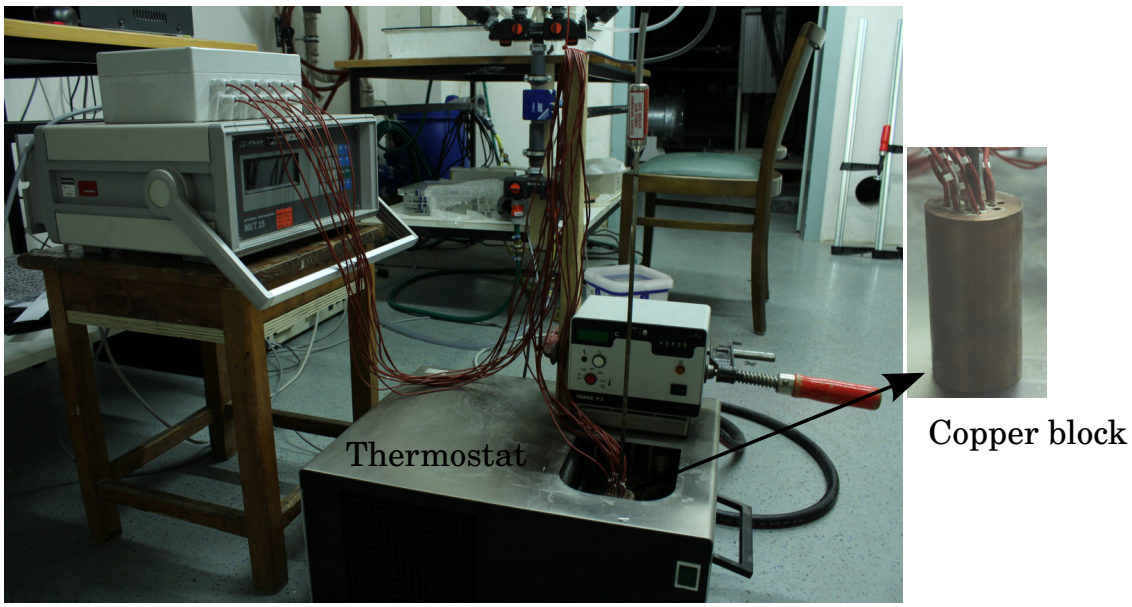

Figure A.1: Set-up for the calibration of Pt-1000 temperature sensors

The sensors along with the copper block were immersed into the circulation thermostat

and temperature recording commenced starting with 25 °C in the steps of 5 °C till 90 °C. The set point of the circulation thermostat was changed manually. The temperature of the reference sensor displayed, was carefully observed and noted down after it settled to a constant value. After reaching a steady temperature, it was maintained for at least 10 minutes before changing the set point of the thermostat. The absolute time for each reading was noted down. This procedure was continued till the last set point i.e. 90 °C. The temperature recorded by LabView was then processed. This temperature recorded by LabView was derived from the characteristic curve of temperature against resistance according to DIN EN 60751 shown in the Fig. A.2.

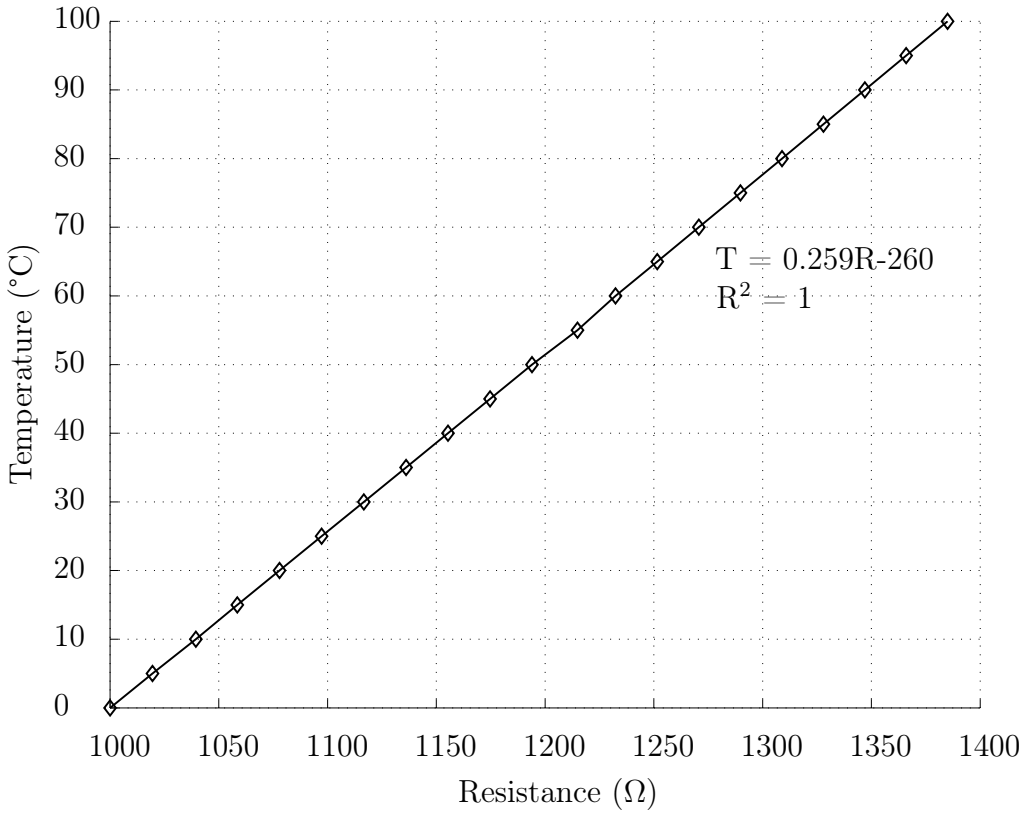

Figure A.2: Resistance characteristic for Pt-1000 sensors according to DIN EN 60751

The average value for each time interval for all the sensors has been tabulated in table A.1).

For the sake of depiction the values till second decimal places have been shown. The calibration procedure was carried out using values till four decimal places. A linear curve for each sensor was fit to the data tabulated above by the method of least-squares. The corrected measurements with their residual errors are shown in Fig. A.3

Temperature	S 0	S 1	S 2	S 3	S 4	S 5	S 6
20.035	20.28	20.38	20.34	20.37	20.45	20.48	20.31
25.025	25.34	25.43	25.36	25.34	25.43	25.50	25.33
30.015	30.27	30.32	30.28	30.34	30.38	30.43	30.37
35.084	35.37	35.39	35.33	35.39	35.48	35.47	35.37
40.043	40.32	40.32	40.26	40.31	40.43	40.44	40.31
45.022	45.26	45.24	45.18	45.30	45.39	45.44	45.28
50.088	50.36	50.34	50.29	50.39	50.47	50.48	50.31
55.063	55.32	55.31	55.24	55.31	55.47	55.48	55.31
60.042	60.31	60.24	60.17	60.27	60.38	60.41	60.22
65.005	65.21	65.34	65.36	65.29	65.22	65.28	65.29
70.077	70.38	70.28	70.25	70.35	70.51	70.48	70.28
75.053	75.31	75.20	75.15	75.26	75.39	75.38	75.20
80.025	80.27	80.14	80.11	80.24	80.37	80.35	80.13
85.085	85.38	85.20	85.20	85.32	85.47	85.43	85.20
90.155	90.40	90.21	90.18	90.29	90.45	90.44	90.21

Table A.1: Temperature recorded by Pt-25 and average values for each temperature sensor

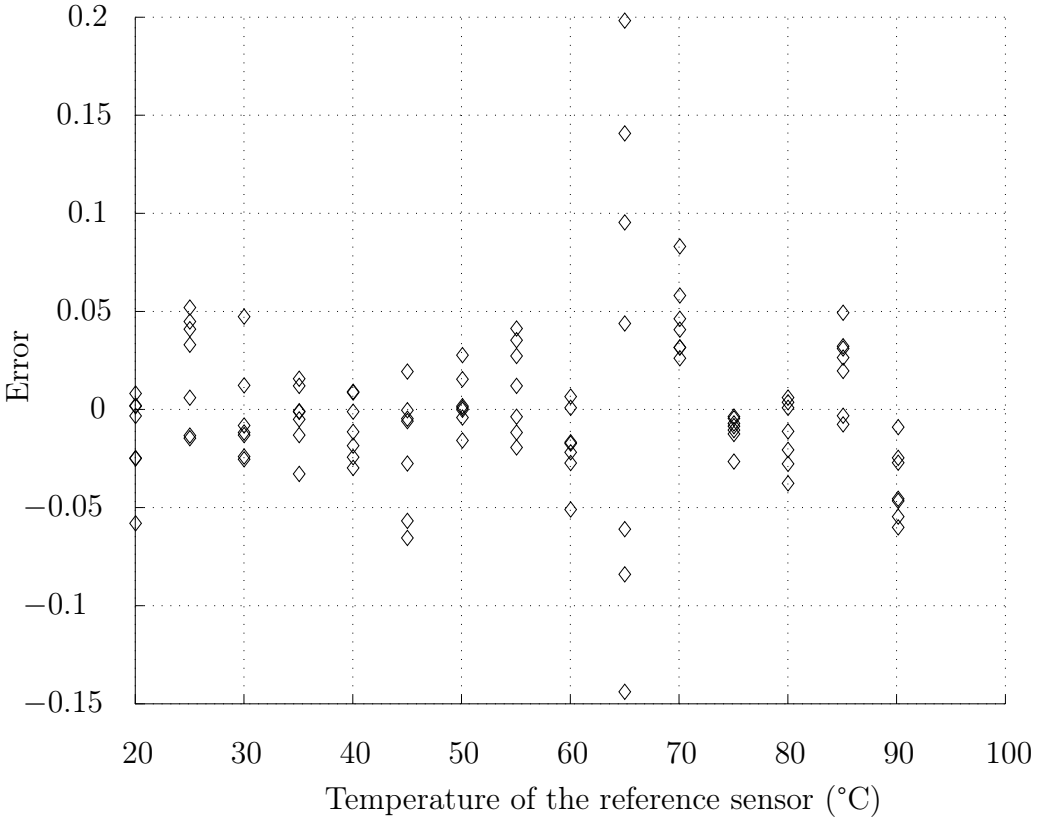

Figure A.3: Residual plot of corrected errors for the sensors used in the plexiglas tank

Calibration of temperature sensors for the stratisorp tank A data acquisition switch unit by Agilent (34972 A) along with 20 channels multiplexer (34901 A) were connected to a PC working on Windows 7 operating system using LAN connection.

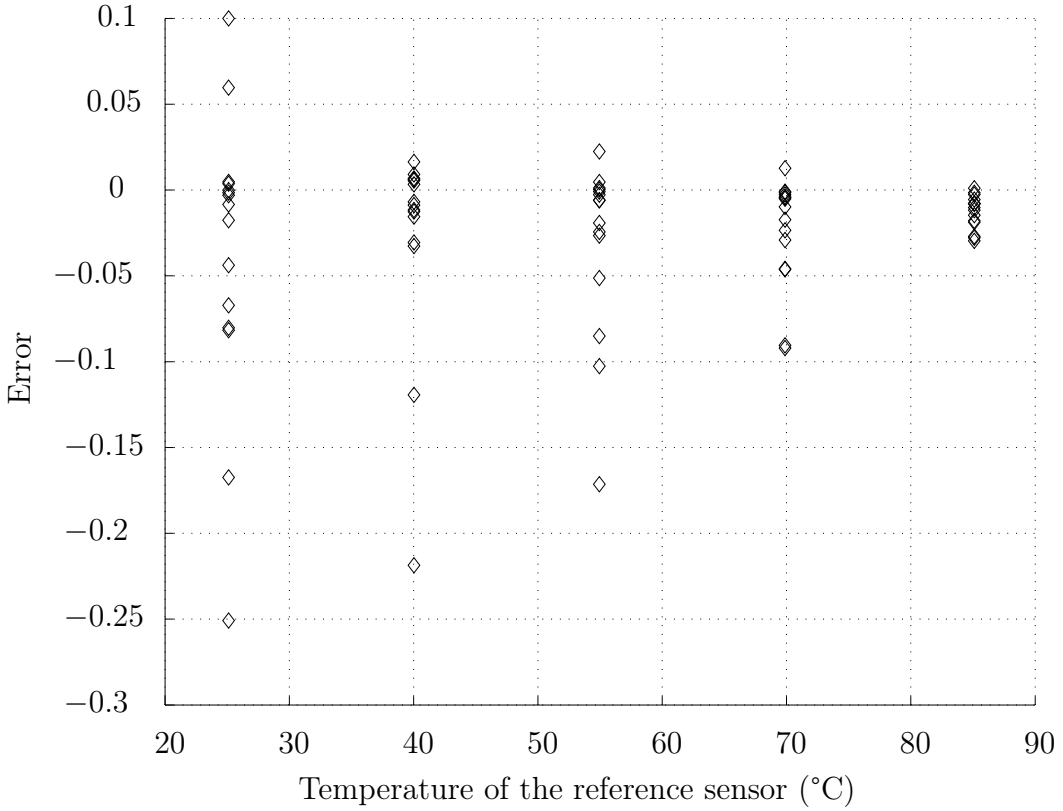

Figure A.4: Residual plot of corrected errors for sensors used in the tank

It can be noticed that the magnitude of the residual absolute error is strongly temperature dependent. Hence the measurement uncertainty expressed in standard deviation is plotted as function of temperature and a linear fit by the method of least-squares is used

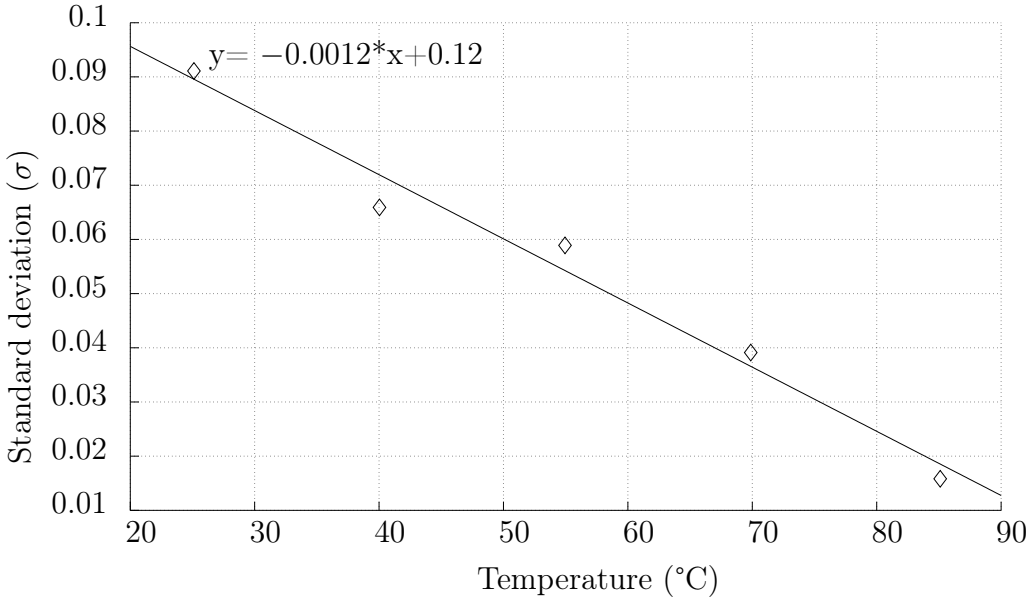

Figure A.5: Standard deviation as function of the reference sensor's temperature

The error in the tank temperature measurement is propagated to the calculation of energy contained in the tank.

Pt-100 sensors and flow meters: The following plots show the dependency of the residual errors in Pt-100 temperature sensors used in the experimental set-up. The calibration had been carried out at Forschungs- und Testzentrum für Solaranlagen in Stuttgart.

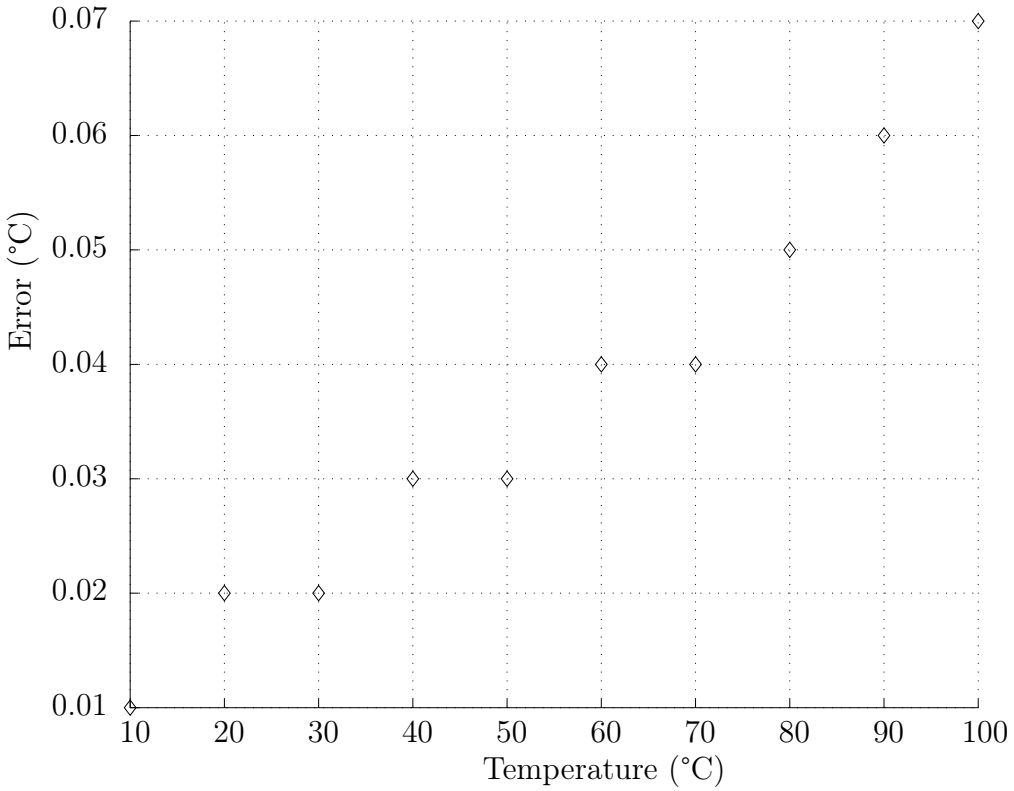

Figure A.6: Residual plot of corrected errors for Pt-100 sensors

	Flow meters				
	Adsorber	Heater	Cooler	Evaporator	Condenser
Relative error (%)	±1.25	±0.5	±1.25	±0.5	±1.25

Table A.2: Relative error in the flow rate measurement

Depending upon the inlet and outlet temperatures and the flow rate in each hydraulic circuit the values of δT_i, δT_o and $\delta \dot{m}$ are selected and inserted in the equations of propagation of uncertainty (such as Eq. A.4).

A.2 LabView VI for calibration procedure

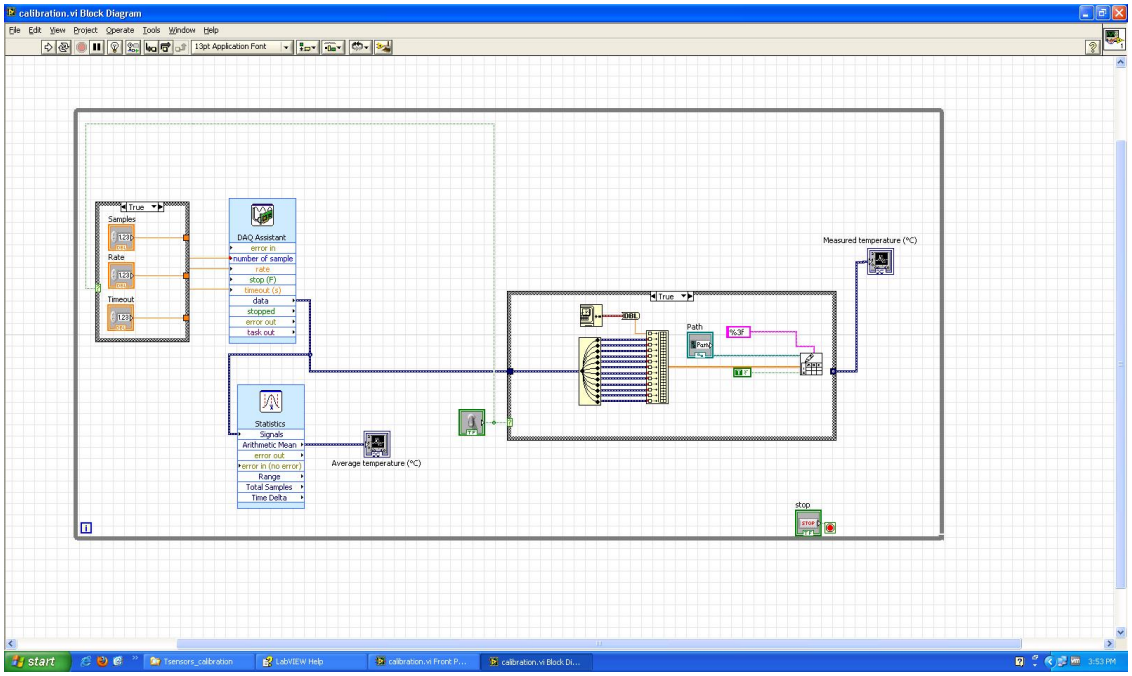

Figure A.7: LabView VI used for the calibration procedure and for the temperature data acquisition in the flow visualisation experiments

A.3 Miscellaneous results

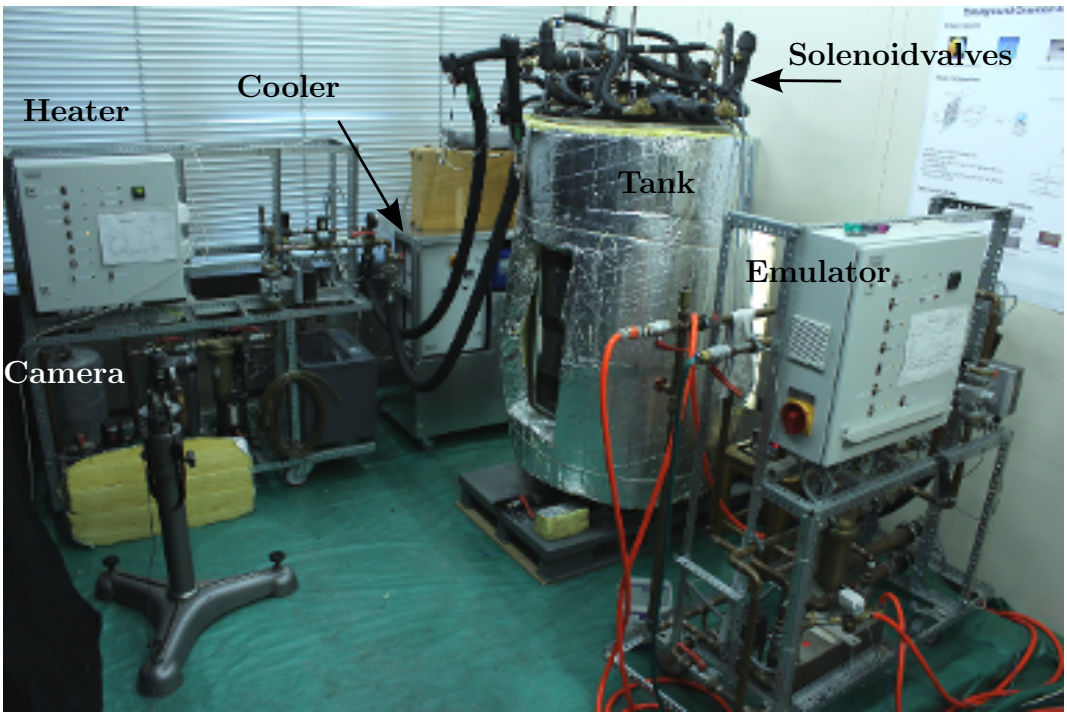

Figure A.8: Experimental arrangement for BOS measurements

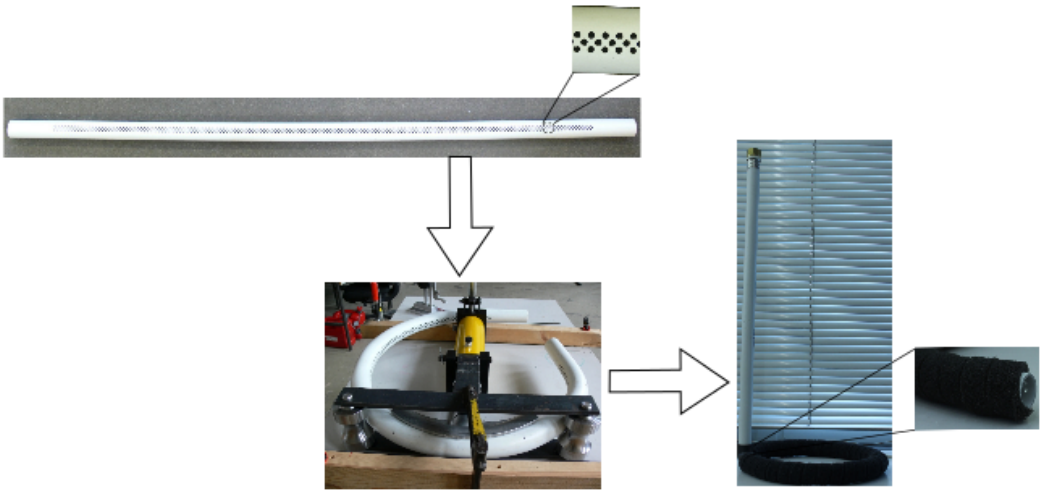

Figure A.9: Steps taken in the production of the flow diffuser rings-drilling holes, pipe bending, cladding with foam

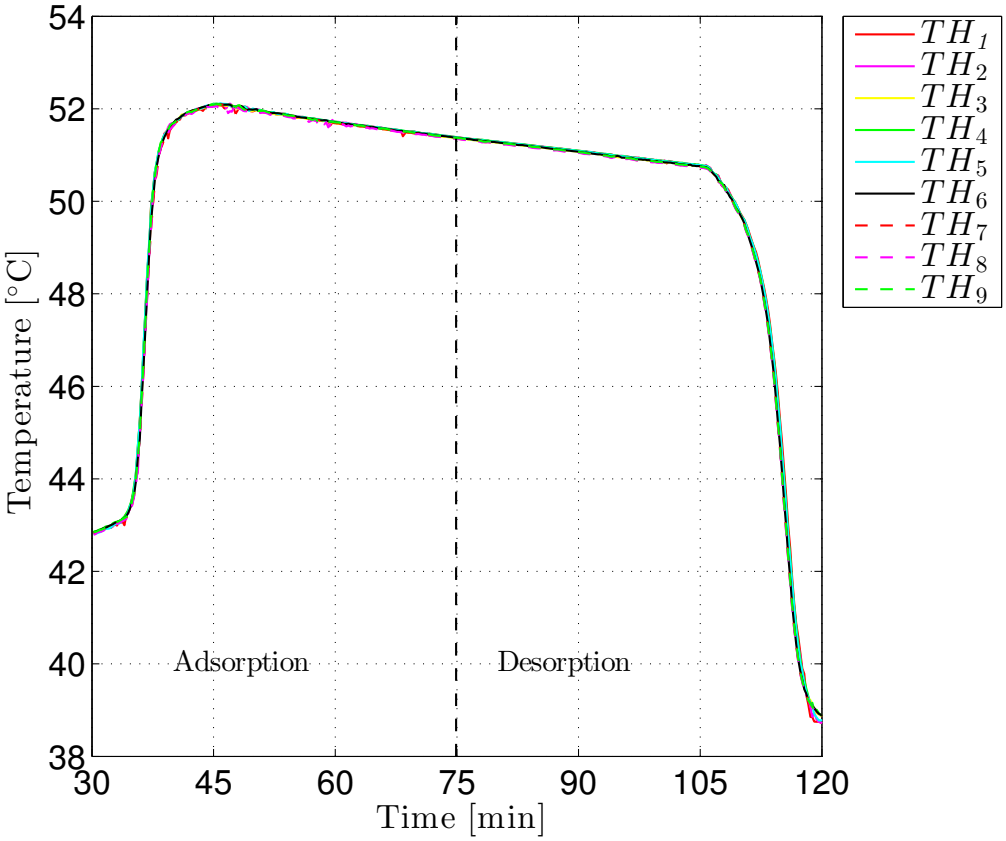

Figure A.10: Change in the temperatures in the zone Z_3 during both half cycles

Fig. A.10 shows the trend of the temperature recorded by the horizontal temperature lance which was mounted within Z_3. All temperature sensors show simultaneous rise and fall in the temperatures during the adsorption and the desorption half cycles. It can be inferred from Fig. A.11 that the temperature gradient inside the thermocline is mainly composed of vertical gradients. Negligible temperature gradient is seen in the X direction.

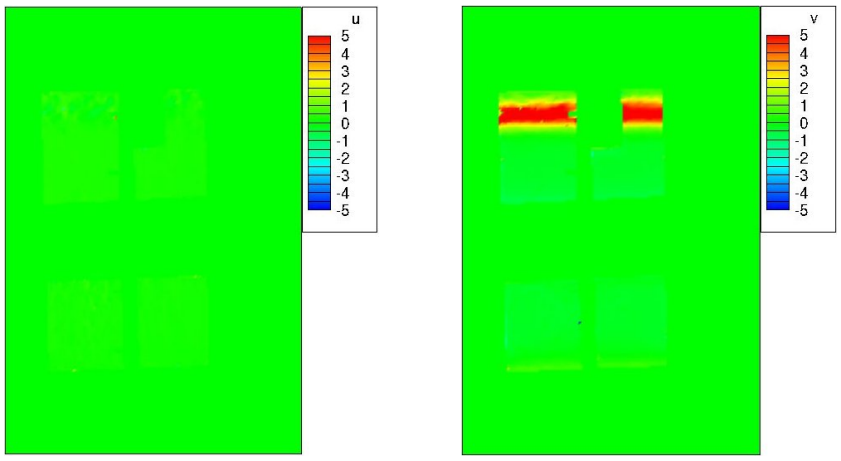

(a) X displacement (b) Y displacement

Figure A.11: Horizontal and vertical pixel displacement

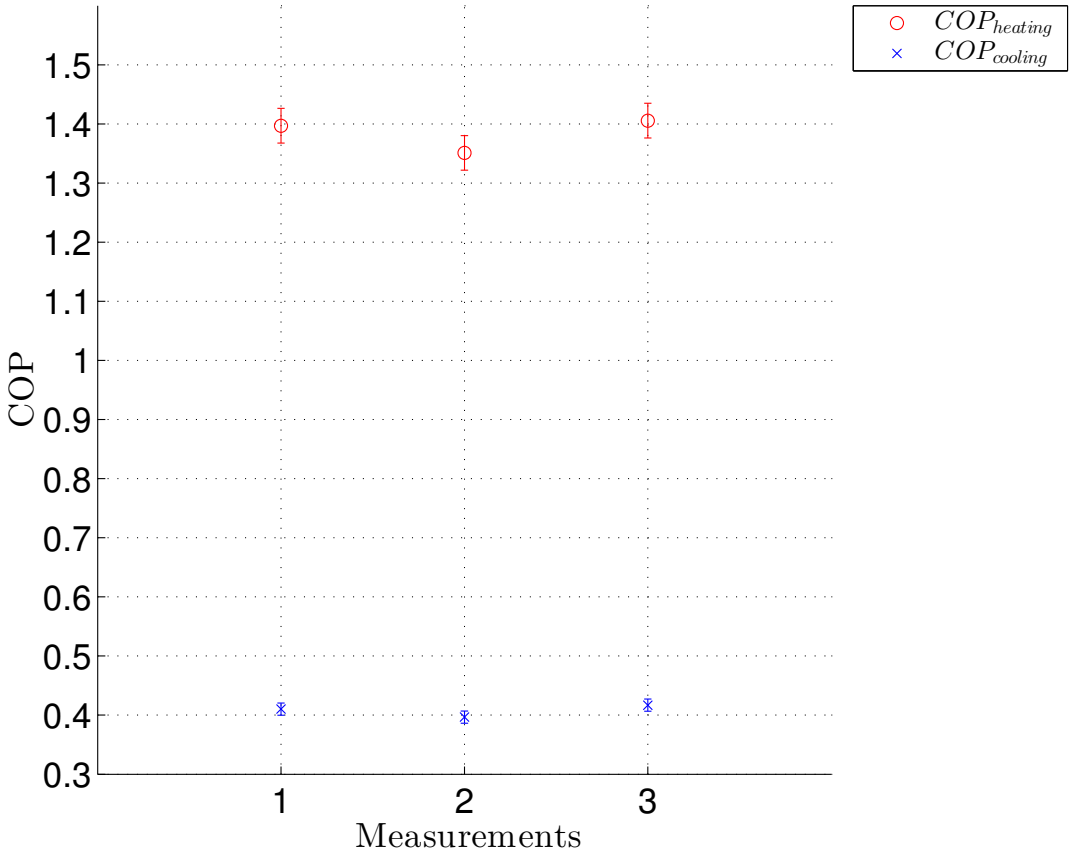

Figure A.12: Reproducibility of $COP_{cooling}$ and $COP_{heating}$ for the stratisorp cycle with condition 72/27/18 °C

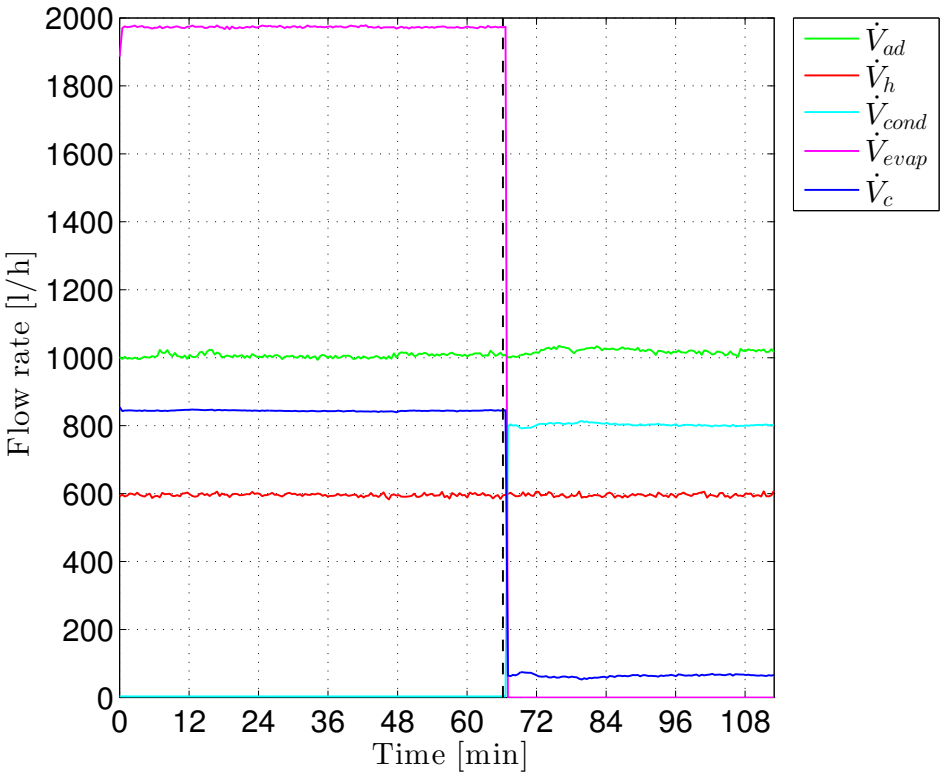

Figure A.13: Flow rate in various hydraulic circuits for the stratisorp cycle with condition 72/27/18 °C

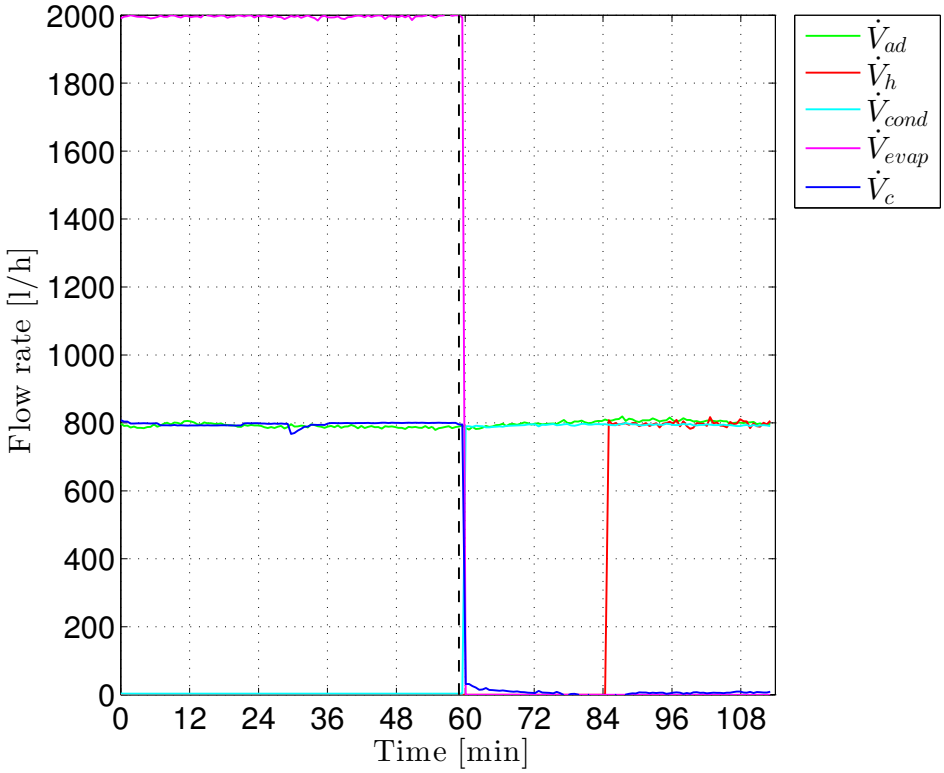

Figure A.14: Flow rate in various hydraulic circuits for the stratisorp cycle with intermittent heating and cooling with condition 72/27/18 °C

Although the cooler flow rate was recorded throughout the length of the cycle the cooler interacted with the adsorber place only at the end of the adsorption half cycle. The flow meter in the cooling module was built inside the module. Hence the flow rate was recorded irrespective of whether or not the bypass was open. In case of the heating module, the flow meter was mounted externally. As a result, no flow rate measurement was possible as soon as the bypass of the heating module was opened.

A.4 Technical drawings of the tanks

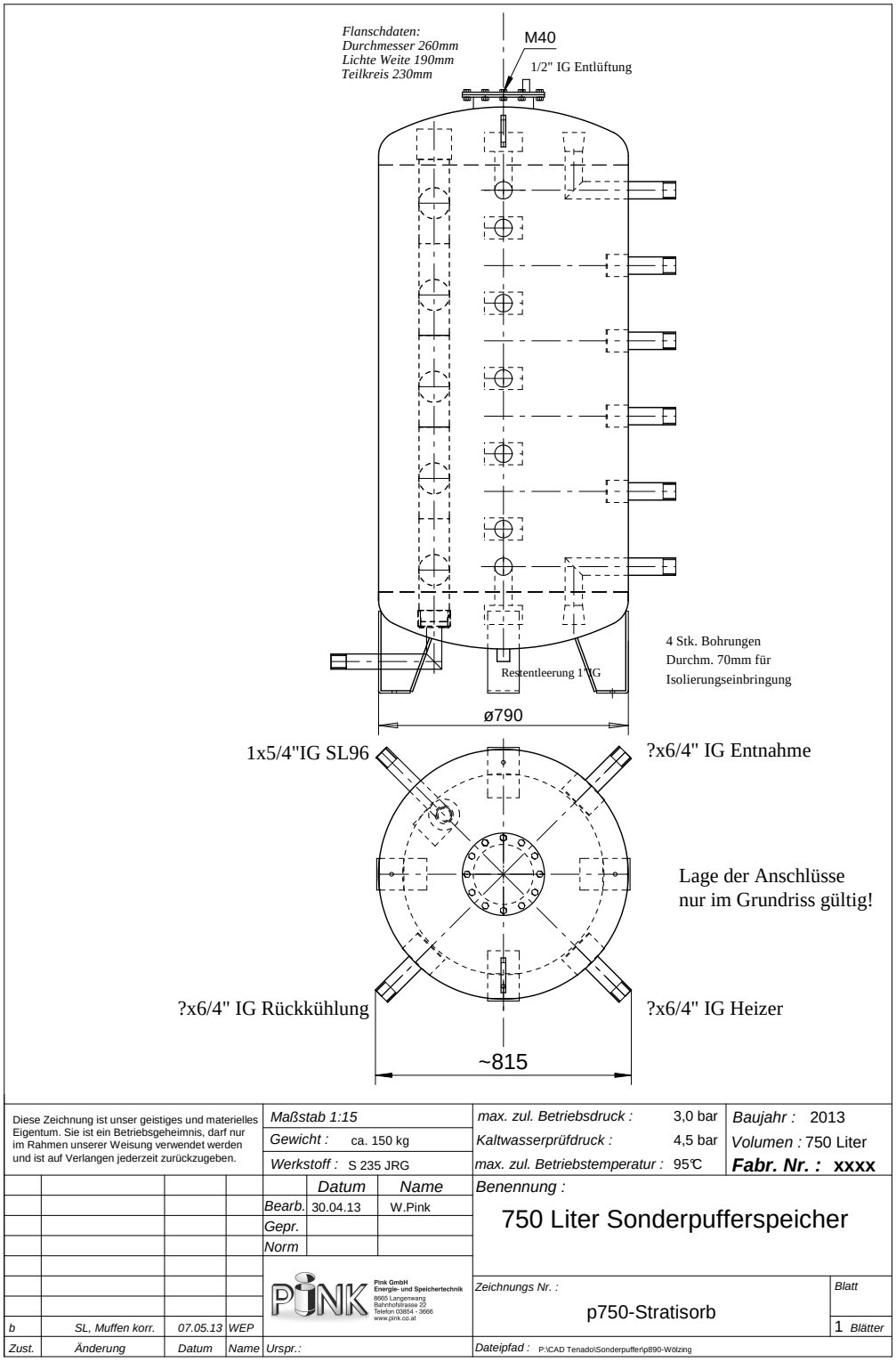

Figure A.15: Tank used for the experiments without heat recovery

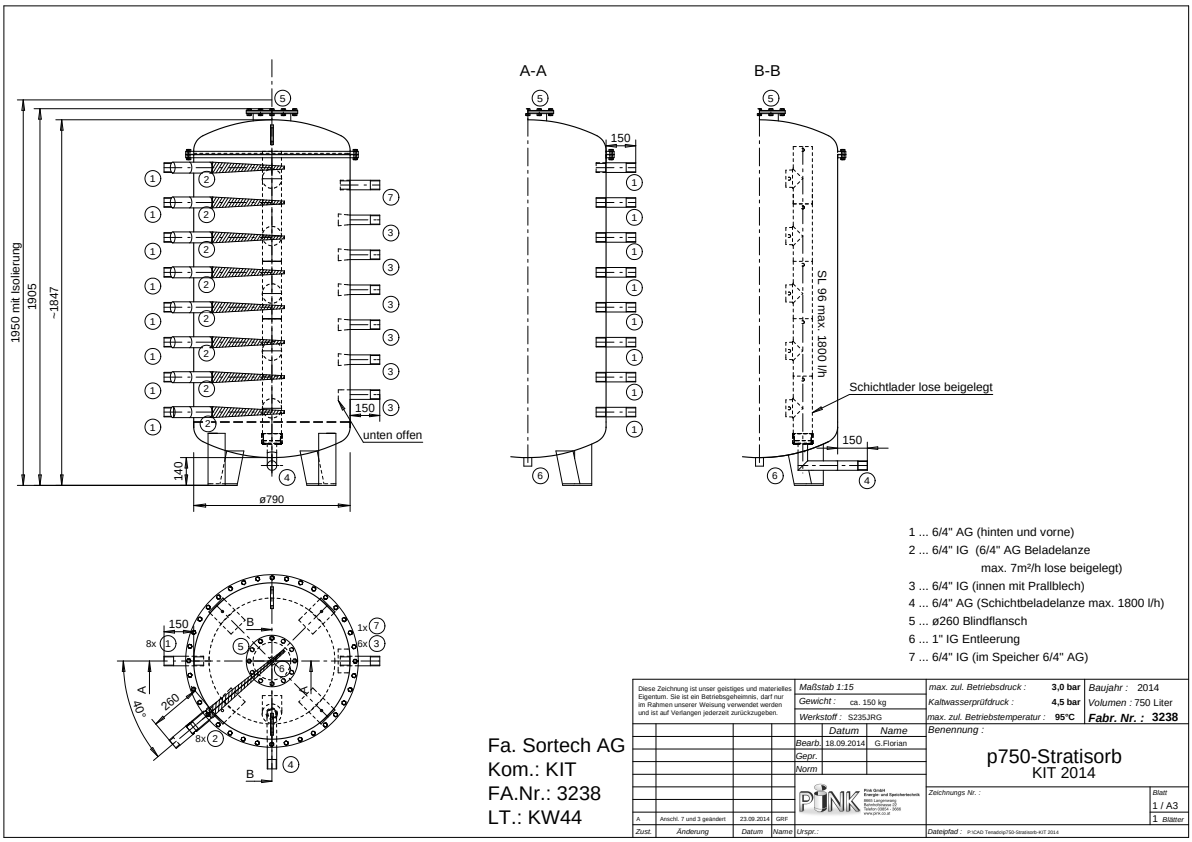

Figure A.16: Tank used for validation of the stratisorp concept

A.5 Eurotherm controller tuning

The Eurotherm controller tuning was carried out in order to optimise the controller parameters. During the adsorption half cycle, the cooler is connected only with the tank as the condenser flow rate is 0 (refer Fig. A.17).

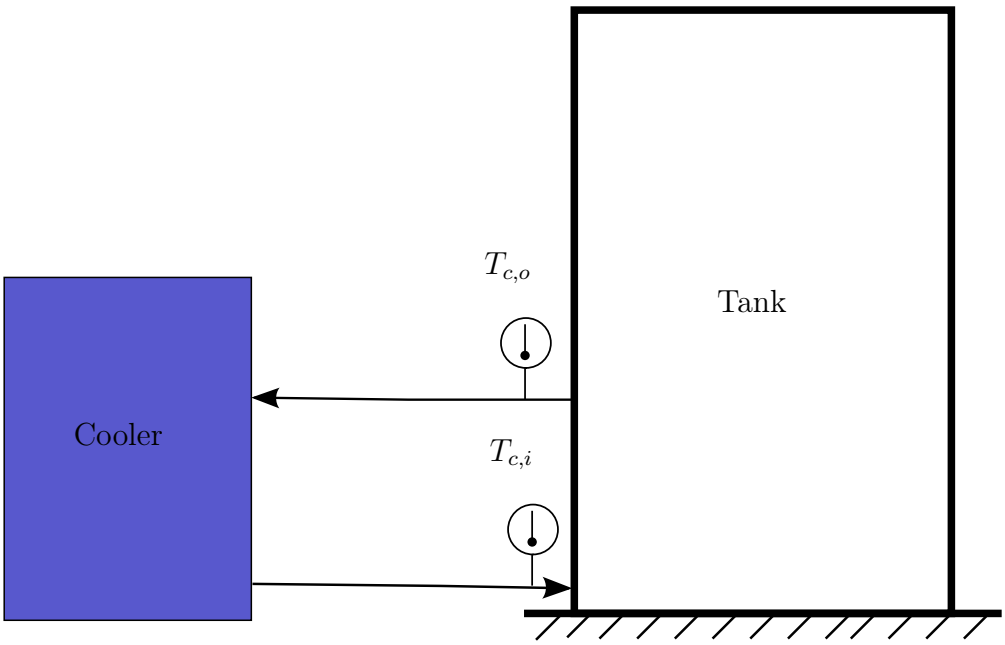

Figure A.17: Experimental arrangement during initial tuning with step change in the setpoint

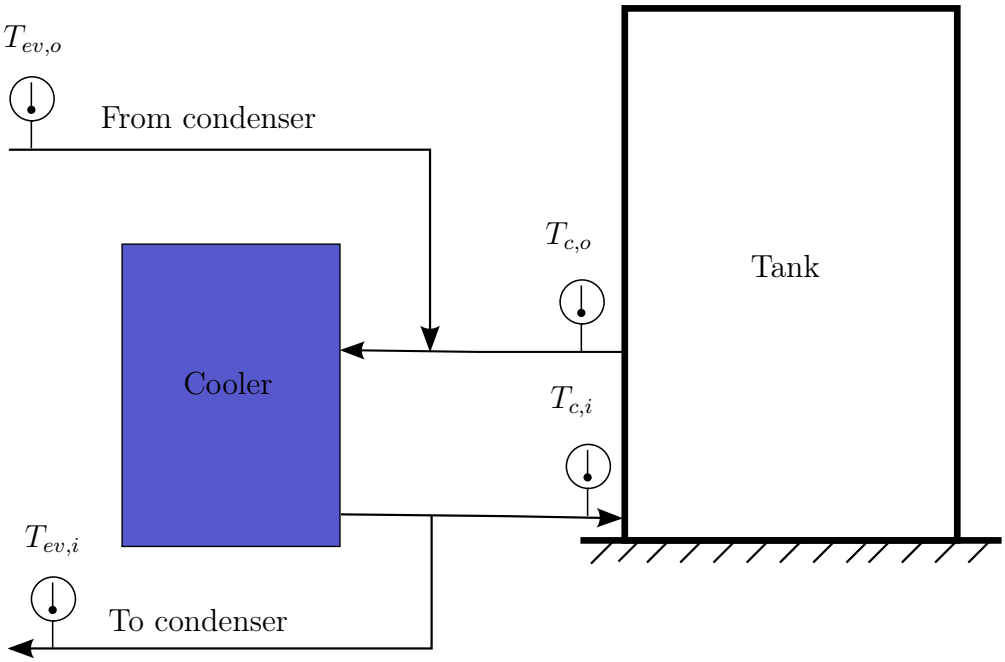

Figure A.18: Experimental arrangement during final tuning (desorption)

It cools the bottom part of the tank during which the cooling load does not change much. However, during the desorption half cycle, the cooler not only extracts water from the tank but also receives water from the condenser outlet(refer Fig. A.18).The condenser outlet water is relatively warmer than the water being extracted by the cooler from the tank. This warm water then mixes with the colder water extracted from tank and flows together to the cooler. The inlet temperature signal to the cooler is noisy as the cooler receives water at a mixed temperature. When the input signal is noisy, it is generally preferred to use PI controller instead of PID controller as the derivative action of the controller further enhances the disturbances. The tuning of the PI controller was carried out intuitively keeping in mind that :

- Too high proportional gain (K_p) leads to higher steady state error while too low proportional gain causes too small control action.

- Too high values of integral time (T_i) reduce oscillations in the process value (PV) while too low values of integral time offer faster control. However smaller values of integral time are linked with oscillations in the PV and hence overshooting from the target set point.

The integral time term eliminates offset in the output. Moreover, a dead band of 1% was chosen which means that the controller action is off when the PV is within 0.05% on either side of the set point. The controller tuning was carried out in 2 steps :

Step 1: Initially the auto-tuning of the controller was carried out which returned values of $K_p = 23$ and $T_i = 70$. During this initial tuning procedure the cooler circulated water only with the tank with 750 l/h. The performance of these parameters was checked by inducing step change in the set point of the cooler. The integral time seemed to be too high as the approach towards PV was slow. The integral time was reduced by 75% in two steps and it was observed that it offered better control of PV (i.e $T_{c,i}$). Moreover, it was found that the temperature sensor $T_{c,i}$ had an offset of 0.3 K with respect to the temperature sensor used as feedback for the controller. Fig. A.19 explains the initial tuning procedure.

Step 2: The controller parameters set in step 1 were tested for their performance during the desorption half cycle. Here, the PV was both $T_{ev,i}$ and $T_{c,o}$. However the change in $T_{ev,i}$ was faster owing to significantly higher flow rate of the condenser (600 lph) than the flow rate through the tank (150 lph). As explained before in Fig. A.18 the cooler receives mixture of warm and cool water. It can be seen from Fig. A.20 that the controller parameters from step 1 were no more efficient as the PV oscillated drastically about the set point of 27 °C. This was caused due to lower value of integral time. Hence the integral time was raised by 100% in two steps thereby increasing K_p by 50% in order to offer more control action. The effect of this change is clearly seen in Fig. A.20.

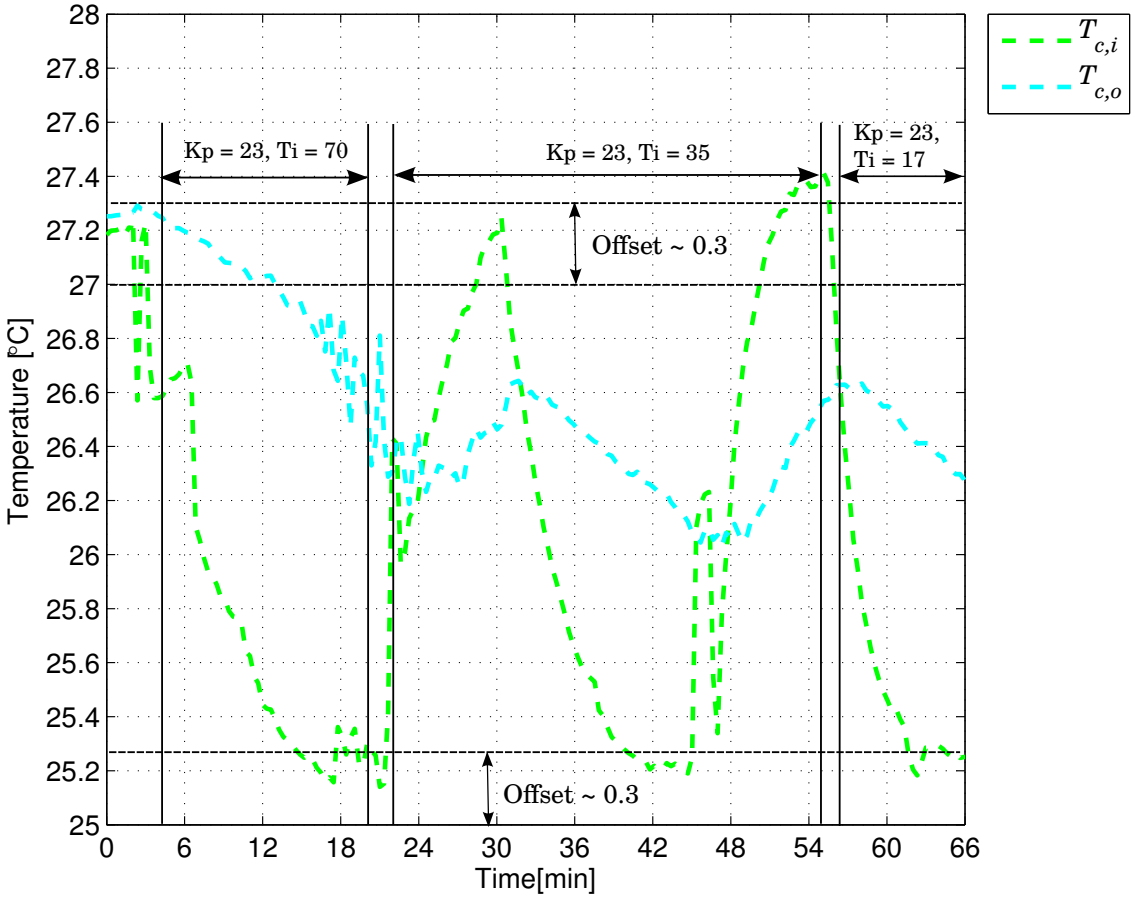

Figure A.19: Eurotherm 3216 temperature controller tuning - step change set point

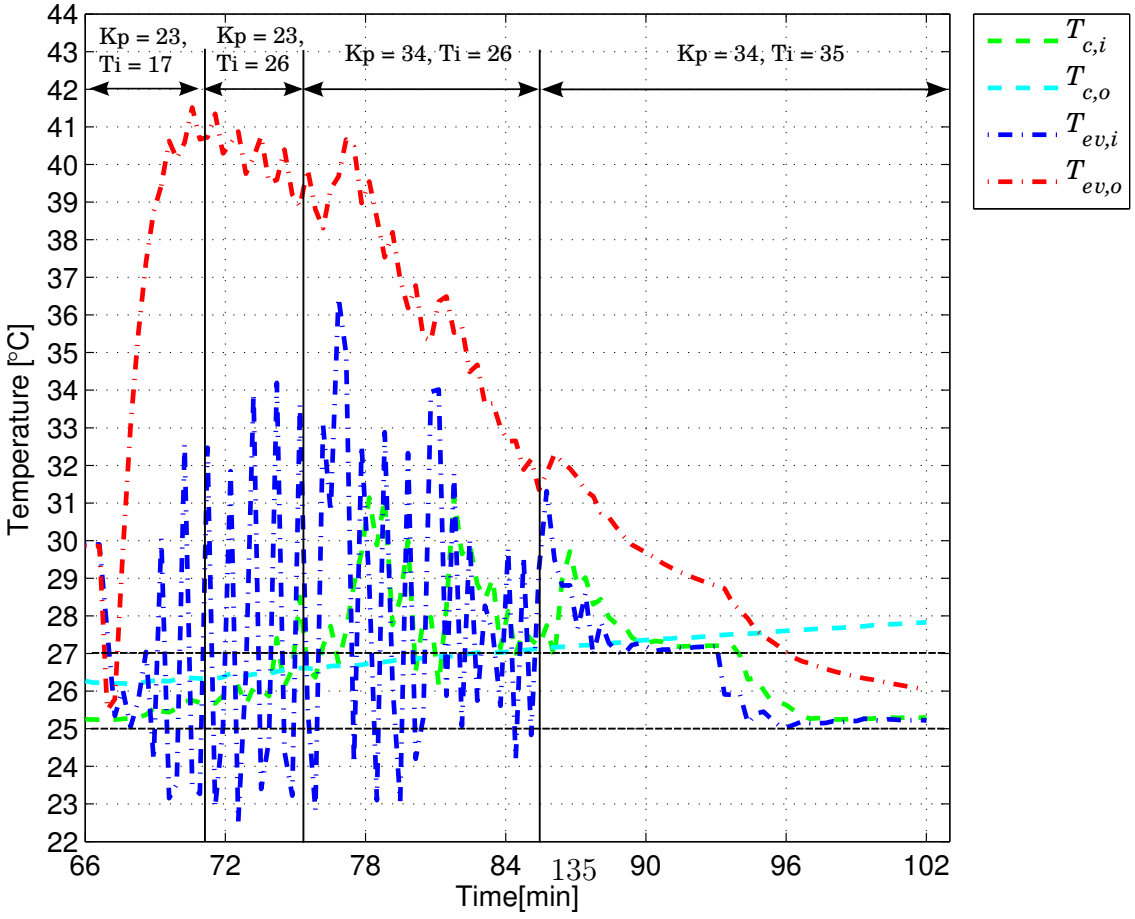

Figure A.20: Eurotherm 3216 temperature controller tuning during desorption

With the controller parameters $K_p = 34$ and $T_i = 35$, the setpoints of 27 °C and 25 °C were reached comfortably without much oscillation in the PV. However this was achieved towards the end of the desorption half cycle i.e. when $T_{ev,o}$ and $T_{c,o}$ were relatively close to each other. Further tests showed that these controller parameters were not efficient at the start of the desorption i.e. when $T_{ev,o}$ and $T_{c,o}$ differed significantly from each other. Oscillations similar to those seen in Fig. A.20 were observed. Further tuning of the controller parameters at the start of the desorption half cycle was carried out. It was found that with $K_p = 42$ and $T_i = 63$ very satisfactory controller performance was achieved. Figure A.21 shows the control action using these parameters.

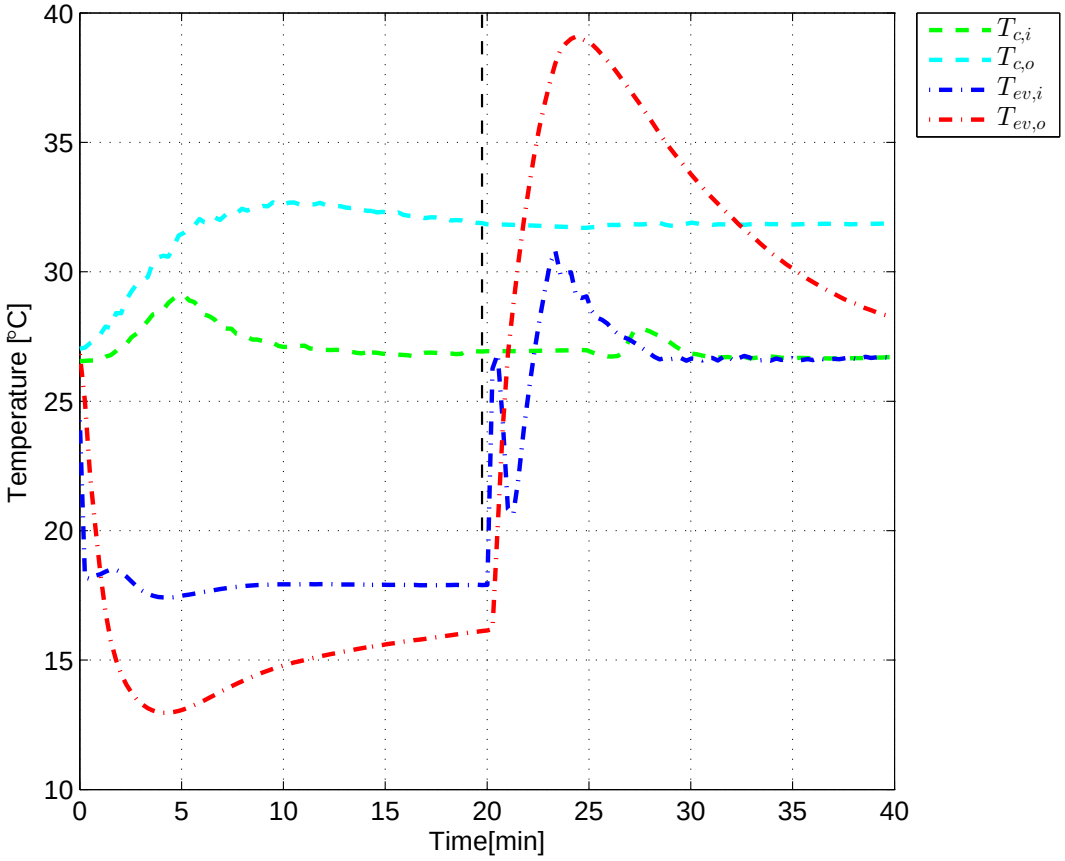

Figure A.21: Eurotherm 3216 temperature controller output after corrected tuning parameters ($K_p = 42$ and $T_i = 63$)

A.6 Properties of the reticulated foam

Datenblatt / Technical Data Sheet / Fiche Technique

Kunde / Customer / Client	
Material / Material / Matériel	Polyurethan-Weichschaumstoff Polyurethane Foam / Mousse Souple de Polyuréthanne
Type / Type / Type	PantaCell® - Qualitäten Polyether, retikuliert

Qualität	T 25 P 10 R PPI 10	T 25 P 20 R PPI 20	T 25 P 30 R PPI 30	T 25 P 45 R PPI 45
Rohdichte [kg/cbm] DIN EN ISO 845 Piece Density / Densité nette	23,0 +/- 2	23,0 +/- 2	23,0 +/- 2	23,0 +/- 2
Stauchhärte, CV40 [kPa] DIN EN ISO 3386-1 Compression load Deflection / Résistance à la Compression	6,8 +/- 1	5,0 +/- 0,8	3,9 +/- 0,6	3,8 +/- 0,6
Zugfestigkeit [kPa] DIN 53 571 Tensile Strength / Résistance à la Rupture	min. 70	min. 80	min. 80	min. 80
Bruchdehnung [%] DIN 53 571 Elongation at break / Allongement à la Rupture	min. 80	min. 100	min. 120	min. 160
Zellenzahl per lfcm Pores / Cellules au cm lin	2,0 - 3,2	3,3 - 5,2	5,8 - 7,5	12 +/- 2
Luftdurchlässigkeit [l/(m²sec)] DIN EN ISO 9237 Air Permeability / Perméabilité à l'air	6500 +/- 1500	6000 +/-1500	5500 +/-1000	4000 +/-500

Figure A.22: Properties of the reticulated foam used

A.7 MATLAB code for data evaluation

MATLAB code for evaluation of COP, power and plotting functions :

```
% Program to estimate the COP of the adsorption heat pump

mkdir Last_Cycle ;
main_path = pwd ;
plots_path=cat(2,main_path,'/Last_Cycle');

rho=1000;  % Density of water (kg/m^3)
c_p = 4200;     % Sp. heat of water (J/Kg.K)
D_sp = 0.790 ;       % Diameter of the tank (m)
A_sp = pi()* D_sp^2 /4 ;     % Area of cross section (m^2)
H = 1.56 ;     % Distance between the first and the last sensor (m)
z = 0.111 ;     % Distance between adjacent sensors (m)
sensor_pos = [0:z:H]';   % Vector for the position of the temperature ...
  sensors (m)

B = importdata('Stratisorp_72_27_18.txt');
Messergebnisse = B.data;
min = Messergebnisse(:,1)./60;        %Umrechnung von s in min

dt = zeros(length(min),1);
```

```
for i=2:length(dt)-1,
    dt(i)=(min(i+1)-min(i))*60;      % Vector of all delta time
end

V_cond = Messergebnisse(:,35);
Tank_Temp = Messergebnisse(:,11:25); % Vector of tank temperature for ...
 the complete measurement


ind_ads = find(V_cond < 5);   % Index of all measurement points during ...
 adsorption half cycles
ind_des = find(V_cond > 5);

adsorp_start = ind_ads(1); % This section of the code locates the starts ...
 and the ends of each cycle

for i=1:length(ind_ads)-1,
    if ind_ads(i+1)-ind_ads(i) > 1,
       adsorp_start=cat(1,adsorp_start,ind_ads(i+1));  % Index of all ...
        measurement points for start of adsorption
    end
end

desorp_end = adsorp_start(2:end)-1 ;
desorp_end=cat(1,desorp_end,ind_des(end));

desorp_start = ind_des(1);

for i=1:length(ind_des)-1,
    if ind_des(i+1)-ind_des(i) > 1,
       desorp_start=cat(1,desorp_start,ind_des(i+1));  % Index of all ...
        measurement points for end of desorption
    end
end


ts = adsorp_start(end) ; % Time stamp-start of the last cycle
tswitch = desorp_start(end)-1 ; %Time stamp-switch between the half cycles

last_cycle = Messergebnisse(ts:end,:); % Last cycle
cycle_timestamps = min(ts:end);
half_cycle = tswitch -ts ;

T_ev_out = last_cycle(:,33);
Psat = XSteam_m('psat_T',T_ev_out);

for i = 1:length(cycle_timestamps),
    if i==1,
        temp = 0;
    else
        temp = cycle_timestamps(i)-cycle_timestamps(1);
    end
    if i==1,
        cycle_time = temp;
    else
        cycle_time = cat(1,cycle_time,temp);
```

```
    end

end

t_cycles = zeros(adsorp_start,1);
for i=1:length(adsorp_start),
    t_cycles(i) = (min(desorp_end(i))-min(adsorp_start(i)))*60;
end

t_cycle =  (min(end)-min(ts))*60 ;% Duration of the last cycle (s)
Ttank_start_lc = last_cycle(1,11:25)';
Ttank_end_lc = last_cycle(end,11:25)';

m_ad = Messergebnisse(:,30)/3600; %Messergebnisse(:,30)=V_ad
m_h = Messergebnisse(:,5)/3600; %Messergebnisse(:,5)=V_h
m_c = Messergebnisse(:,34)/3600; %Messergebnisse(:,34)=V_c
m_ev =Messergebnisse(:,8)/3600;  %Messergebnisse(:,8)=V_ev
m_cond = Messergebnisse(:,35)/3600;

dT_ad = Messergebnisse(:,9) - Messergebnisse(:,10);   % (T_ad,i-T_ad,o)
dT_h = Messergebnisse(:,6) - Messergebnisse(:,7);  % (T_h,i-T_h,o)
dT_c = Messergebnisse(:,4) - Messergebnisse(:,3);  % (T_c,i-T_c,o)
dT_ev = Messergebnisse(:,33) - Messergebnisse(:,32);  % (T_ev,o-T_ev,i)

P_h = c_p * m_h .* dT_h;
P_c = c_p * m_c .* dT_c;


P_ev = zeros(length(min),1);
Q_evaporator = zeros(length(adsorp_start),1);

P_cond = zeros(length(min),1);
Q_condenser = zeros(length(adsorp_start),1);

P_ads = zeros(length(min),1);
Q_adsorption = zeros(length(adsorp_start),1);

P_des = zeros(length(min),1);
Q_desorption = zeros(length(desorp_start),1);

P_heat = zeros(length(min),1);
Q_heater =zeros(length(adsorp_start),1);

P_cool = zeros(length(min),1);
Q_cooler =zeros(length(adsorp_start),1);

cooling_power = zeros(length(adsorp_start),1);
heating_power = zeros(length(adsorp_start),1);
adsorption_power = zeros(length(adsorp_start),1);
desorption_power = zeros(length(adsorp_start),1);

for i=1:length(adsorp_start),

P_ev(adsorp_start(i):desorp_start(i)-1)=...
    c_p * m_ev(adsorp_start(i):desorp_start(i)-1)...
    .*dT_ev(adsorp_start(i):desorp_start(i)-1)   ;
```

```
Q_evaporator(i)=sum(P_ev(adsorp_start(i)+1:desorp_start(i)-1)...
    .*dt(adsorp_start(i)+1:desorp_start(i)-1));% Q_evap (J)
P_cond(desorp_start(i):desorp_end(i))=...
    c_p*m_cond(desorp_start(i):desorp_end(i))...
   .*dT_ev(desorp_start(i):desorp_end(i));
Q_condenser(i)=sum(P_cond(desorp_start(i)+1:desorp_end(i))...
   .*dt(desorp_start(i)+1:desorp_end(i)));  % Q_cond (J)
P_ads(adsorp_start(i):desorp_start(i)-1)=...
    c_p*m_ad(adsorp_start(i):desorp_start(i)-1)...
  .*dT_ad(adsorp_start(i):desorp_start(i)-1);
Q_adsorption(i)=sum(P_ads(adsorp_start(i)+1:desorp_start(i))...
   .*dt(adsorp_start(i)+1:desorp_start(i)));% Q_ads (J)
P_des(desorp_start(i):desorp_end(i))=...
    -1*c_p*m_ad(desorp_start(i):desorp_end(i))...
   .*dT_ad(desorp_start(i):desorp_end(i));
Q_desorption(i)=sum(P_des(desorp_start(i)+1:desorp_end(i))...
   .*dt(desorp_start(i)+1:desorp_end(i)));% Q_des (J)
P_heat(adsorp_start(i):desorp_end(i))=...
    c_p*m_h(adsorp_start(i):desorp_end(i))...
   .*dT_h(adsorp_start(i):desorp_end(i));
Q_heater(i)=sum(P_heat(adsorp_start(i)+1:desorp_end(i))...
   .*dt(adsorp_start(i)+1:desorp_end(i)));% Q_h (J)
P_cool(adsorp_start(i):desorp_end(i))=...
    c_p*m_c(adsorp_start(i):desorp_end(i))...
   .*dT_c(adsorp_start(i):desorp_end(i));
Q_cooler(i)=sum(P_cool(adsorp_start(i)+1:desorp_end(i))...
   .*dt(adsorp_start(i)+1:desorp_end(i)));% Q_c (J)

end

for i=1:length(adsorp_start),
cooling_power(i)=abs(mean((P_ev(adsorp_start(i):desorp_end(i)))))/1000;
heating_power(i)=(mean(P_cond(adsorp_start(i):desorp_end(i)))+...
  abs(mean((P_cool(adsorp_start(i):desorp_end(i))))))/1000;
adsorption_power(i)=mean(P_ads(adsorp_start(i):desorp_start(i)-1))/1000;
desorption_power(i)=mean(P_des(desorp_start(i):desorp_end(i)))/1000;

end

% Last Cycle
Q_start=(A_sp*z*rho*c_p).*trapz(sensor_pos,Ttank_start_lc);%Q_tank_start

Q_end=(A_sp*z*rho*c_p).*trapz(sensor_pos,Ttank_end_lc) ; %Q_tank_end

dQtank_lc=(Q_end-Q_start)

% Last Cycle

Q_tank_start = zeros(length(adsorp_start),1);

for i=1:length(Q_tank_start),
Q_tank_start(i)=(A_sp*z*rho*c_p)...
       .*trapz(sensor_pos,Tank_Temp(adsorp_start(i),:));
end

Q_tank_end = zeros(length(desorp_end),1);
```

```
for i=1:length(Q_tank_end),
Q_tank_end(i)=(A_sp*z*rho*c_p)...
      .*trapz(sensor_pos,Tank_Temp(desorp_end(i),:));
end

dQtank = zeros(length(adsorp_start),1);
for i=1:length(dQtank),
dQtank(i)=Q_tank_end(i)-Q_tank_start(i);
end

Q_balance = zeros(length(adsorp_start),1);
for i=1:length(Q_balance),
Q_balance(i)=(Q_heater(i)+Q_cooler(i)...
            +Q_adsorption(i)-Q_desorption(i))-dQtank(i) ;
end

Q_balance_module=Q_desorption(end)+abs(Q_evaporator(end))...
                -Q_condenser(end)-Q_adsorption(end);

E_module=cat(1,Q_desorption(end),abs(Q_evaporator(end))...
   ,Q_condenser(end),Q_adsorption(end),Q_balance_module);
%   Calculation of COP_heat and % COP_cool , avg. cooling and heating power

COP_heat=(Q_condenser + abs(Q_cooler))./(Q_heater-dQtank);
COP_cool=abs(Q_evaporator)./(Q_heater-dQtank);

COP_cycles=cat(2,COP_heat,COP_cool);

COP_heat_lc=COP_heat(end)
COP_cool_lc=COP_cool(end)

COP_avg=cat(2,...
mean(COP_heat(length(adsorp_start)-4:length(adsorp_start))),...
mean(COP_cool(length(adsorp_start)-4:length(adsorp_start))));

COP_cycles = cat(1,COP_cycles,COP_avg);
Power_cycles =cat(2,...
heating_power,cooling_power,adsorption_power,desorption_power);

Power_avg=cat(2,...
mean(heating_power(length(adsorp_start)-4:length(adsorp_start))),...
mean(cooling_power(length(adsorp_start)-4:length(adsorp_start))),...
mean(adsorption_power(length(adsorp_start)-4:length(adsorp_start))),...
mean(desorption_power(length(adsorp_start)-4:length(adsorp_start))));

heating_power_lc=heating_power(end)
cooling_power_lc=cooling_power(end)
adsorption_power_lc=adsorption_power(end)
desorption_power_lc=desorption_power(end)

Power_cycles = cat(1,Power_cycles,Power_avg);


save('Power','Power_cycles','-ascii');
save('COP','COP_cycles','-ascii');
```

```
save Wspace.mat
% Calculation of COP_heat and COP_cool
cycle_numbers=(linspace(1,length(adsorp_start),length(adsorp_start)));
E=cat(2,Q_heater,Q_cooler,Q_adsorption,-1*Q_desorption,dQtank,Q_balance);
cs=jet(length(adsorp_start));
figure()
h=bar(cycle_numbers,E/1e6,'grouped');
hold on
for i=1:length(adsorp_start),
    if i>length(E(1,:)),
    break
    end
set(h(i),'FaceColor',cs(length(adsorp_start)+1-i,:));
end
hold off
xlabel('Cycles','FontSize',12,'interpreter','latex');
ylabel('Energy [MJ]','FontSize',12,'interpreter','latex');
l = legend(gca, 'string', {'Heater','Cooler','Adsorption',...
    'Desorption','dQtank','Loss'},...
    'Location','NorthEastOutside','interpreter','latex');
print('-depsc', '-loose','energy_balance_Tank.eps');

%Pie Chart

figure()
h = pie(E_module);
hText = findobj(h,'Type','text');         % text handles
percentValues = get(hText,'String');     % percent values
labels = {'Desorption: ','Evaporator: ','Condenser: '...
            ,'Adsorption: ','Loss: '}';
combinedstrings = strcat(labels,percentValues);   % text and percent values
oldExtents_cell = get(hText,'Extent'); % cell array
oldExtents = cell2mat(oldExtents_cell); % numeric array
set(hText,{'String'},combinedstrings);
newExtents_cell = get(hText,'Extent'); % cell array
newExtents = cell2mat(newExtents_cell); % numeric array
width_change = newExtents(:,3)-oldExtents(:,3);
signValues = sign(oldExtents(:,1));
offset = signValues.*(width_change/2);
textPositions_cell = get(hText,{'Position'}); % cell array
textPositions = cell2mat(textPositions_cell); % numeric array
textPositions(:,1) = textPositions(:,1) + offset; % add offset
set(hText,{'Position'},num2cell(textPositions,[5,2])) % set new position
print('-depsc', '-loose','energy_balance_module_Last.eps');


figure();     %plot dQ_Tank
plot(dQtank(1:length(adsorp_start),1)/1e3,'bd');
grid('on');
xlabel('Cycles','FontSize',16,'interpreter','latex');
ylabel('$\Delta Q_{tank}$ [kJ]','FontSize',16,'interpreter','latex');
set(gca, 'XTick', 0:1:length(adsorp_start));
%set(gca, 'YTick', -1*Q_tank_start(end)/1e3:-1*1e2:0);
l = legend(gca, 'string', {'$\Delta Q_{tank}$'},'interpreter','latex');
set(l,'FontSize',16);
```

```
set(gca,'FontSize',16);
print('-depsc', '-loose','dQ_tank.eps');
figure();
hold on
for i=1:length(adsorp_start),
    if i==length(adsorp_start),
plot(sensor_pos,Tank_Temp(desorp_end(i),:),'rd','Linewidth',1);
    else
plot(sensor_pos,Tank_Temp(desorp_end(i),:),'Color',cs(i,:),'Linewidth',1);
    end
end
hold off
grid('on');
xlabel('Height [m]','FontSize',16,'interpreter','latex');
ylabel('Temperature [$^{\circ}$C]','FontSize',16,'interpreter','latex');
xlim([0,1.60])
set(gca, 'XTick', 0:2*z:H);
ylim([25,75])
set(gca, 'YTick', 25:5:75);
l1=legend(gca,'string',{'Cycle 1','Cycle 2','Cycle 3','Cycle 4',...
    'Cycle 5','Cycle 6','Cycle 7','Cycle 8','Cycle 9','Cycle 10',...
    'Cycle 11','Cycle 12','Cycle 13','Cycle 14','Cycle 15'},...
    'Location','NorthEastOutside','interpreter','latex');
set(l1,'FontSize',16);
set(gca,'FontSize',16);
print('-depsc', '-loose','Tank_temp_profiles.eps');


figure();                    %plot T_adi und T_ado
cooling_cop = ['$COP_{cool}$= ', num2str((COP_cycles(end,2)))];
heating_cop = ['$COP_{heat}$= ', num2str((COP_cycles(end,1)))];
plot(cycle_time,last_cycle(:,9),'--b','Linewidth',1);hold('on');
plot(cycle_time,last_cycle(:,10),'--r','Linewidth',1);hold('on');
plot(cycle_time,last_cycle(:,6),'--m','Linewidth',1);hold('on');
plot(cycle_time,last_cycle(:,7),'--y','Linewidth',1);hold('on');
plot(cycle_time,last_cycle(:,4),'--c','Linewidth',1);hold('on');
plot(cycle_time,last_cycle(:,3),'--g','Linewidth',1);hold('on');
plot(cycle_time,last_cycle(:,33),'-.b','Linewidth',1);hold('on');
plot(cycle_time,last_cycle(:,32),'-.r','Linewidth',1);hold('on');
plot([cycle_time(half_cycle,1),cycle_time(half_cycle,1)],[10,75],...
    '--k','LineWidth',1);
grid('on');
xlabel('Time [min]','FontSize',16,'interpreter','latex');
ylabel('Temperature [$^{\circ}$C]','FontSize',16,'interpreter','latex');
xlim([0,ceil(cycle_time(end))])
set(gca, 'XTick', 0:12:cycle_time(end));
ylim([10,75])
set(gca, 'YTick', 10:5:75);
l1 = legend(gca,'string',{'$T_{ad,i}$','$T_{ad,o}$','$T_{h,i}$',...
    '$T_{h,o}$','$T_{c,i}$','$T_{c,o}$','$T_{ev,o}$','$T_{ev,i}$'}...
   ,'Location','NorthEastOutside','interpreter','latex');
set(l1,'FontSize',16);
set(gca,'FontSize',16);
print('-depsc', '-loose','Thermal_Cycle_Last.eps');
```

```
figure();%plot V_ad, V_h, V_c, V_evap,, V_cond
plot(cycle_time,last_cycle(:,30),'g','Linewidth',1);hold('on');
plot(cycle_time,last_cycle(:,5),'r','Linewidth',1);hold('on');
plot(cycle_time,last_cycle(:,35),'c','Linewidth',1);hold('on');
plot(cycle_time,last_cycle(:,8),'m','Linewidth',1);hold('on');
plot(cycle_time,last_cycle(:,34),'b','Linewidth',1);hold('on');
plot([cycle_time(half_cycle,1),cycle_time(half_cycle,1)],[0,2000],...
    '--k','LineWidth',1);
grid('on');
xlabel('Time [min]','FontSize',16,'interpreter','latex');
ylabel('Flow rate [l/h]','FontSize',16,'interpreter','latex');
xlim([0,ceil(cycle_time(end))])
set(gca, 'XTick', 0:12:cycle_time(end));
ylim([0,2000])
set(gca, 'YTick', 0:200:2000);
l2=legend(gca,'string',{'$\dot V_{ad}$','$\dot V_{h}$','$\dot V_{cond}$',...
 '$\dot V_{evap}$','$\dot V_{c}$'},...
 'Location','NorthEastOutside','interpreter','latex');
set(l2,'FontSize',12);
set(gca,'FontSize',12);
print('-depsc', '-loose','Flow_rate_Last.eps');

figure();  %plot Q_ad
cooling_pow = ['$\dot{Q}_{cooling}$= ', num2str((Power_cycles(end,2))),' ...
 kW'];
heating_pow = ['$\dot{Q}_{heating}$= ', num2str((Power_cycles(end,1))),' ...
 kW'];
plot(cycle_time,P_ads(ts:end)/1000,'g','Linewidth',1);hold('on') ;
plot(cycle_time,P_h(ts:end)/1000,'r','Linewidth',1);hold('on')
plot(cycle_time,P_c(ts:end)/1000,'b','Linewidth',1);hold('on')
plot(cycle_time,P_ev(ts:end)/1000,'m','Linewidth',1);hold('on')
plot(cycle_time,P_cond(ts:end)/1000,'c','Linewidth',1);hold('on')
plot(cycle_time,-1*P_des(ts:end)/1000,'--r','Linewidth',1);hold('on')
plot([cycle_time(half_cycle,1),cycle_time(half_cycle,1)],[-30,30],...
        '--k','LineWidth',1);
grid('on');
xlim([0,ceil(cycle_time(end))])
set(gca, 'XTick', 0:12:cycle_time(end));
ylim([-30,30])
set(gca, 'YTick', -30:5:30);
xlabel('Time [min]','FontSize',16,'interpreter','latex');
ylabel('Power [kW]','FontSize',16,'interpreter','latex');
l = legend(gca, 'string', {'$\dot Q_{ads}$','$\dot Q_{h}$',...
 '$\dot Q_{c}$','$\dot Q_{ev}$','$\dot Q_{cond}$','$\dot Q_{des}$'},...
 'Location','NorthEastOutside','interpreter','latex');
set(l,'FontSize',16);
set(gca,'FontSize',16);
print('-depsc', '-loose','Power_Last.eps');

figure(); %plot T15 to T1
plot(cycle_time,last_cycle(:,25),'r','Linewidth',1);hold('on');
plot(cycle_time,last_cycle(:,24),'m','Linewidth',1);hold('on');
plot(cycle_time,last_cycle(:,23),'y','Linewidth',1);hold('on');
plot(cycle_time,last_cycle(:,22),'g','Linewidth',1);hold('on');
plot(cycle_time,last_cycle(:,21),'c','Linewidth',1);hold('on');
plot(cycle_time,last_cycle(:,20),'b','Linewidth',1);hold('on');
```

```
plot(cycle_time,last_cycle(:,19),'k','Linewidth',1);hold('on');
plot(cycle_time,last_cycle(:,18),'--r','Linewidth',1);hold('on')
plot(cycle_time,last_cycle(:,17),'--m','Linewidth',1);hold('on')
plot(cycle_time,last_cycle(:,16),'--y','Linewidth',1);hold('on')
plot(cycle_time,last_cycle(:,15),'--g','Linewidth',1);hold('on')
plot(cycle_time,last_cycle(:,14),'--c','Linewidth',1);hold('on')
plot(cycle_time,last_cycle(:,13),'--b','Linewidth',1);hold('on')
plot(cycle_time,last_cycle(:,12),'--k','Linewidth',1);hold('on')
plot(cycle_time,last_cycle(:,11),':b','Linewidth',1);hold('on')
plot(cycle_time,last_cycle(:,7),'-.m','Linewidth',1);hold('on')
plot(cycle_time,last_cycle(:,3),'-.g','Linewidth',1);hold('on')
plot(cycle_time,last_cycle(:,9),'-.b','Linewidth',1);hold('on')
plot(cycle_time,last_cycle(:,10),'-.r','Linewidth',1);hold('on');
plot([cycle_time(half_cycle,1),cycle_time(half_cycle,1)],[25,75],...
    '--k','LineWidth',1);
grid('on');
xlabel('Time [min]','FontSize',16,'interpreter','latex');
ylabel('Temperature [$^{\circ}$C]','FontSize',16,'interpreter','latex');
xlim([0,ceil(cycle_time(end))])
set(gca, 'XTick', 0:12:cycle_time(end));
ylim([25,75])
set(gca, 'YTick', 25:5:75);
l1 = legend(gca,'string',{'$T_{15}$-FH','$T_{14}$','$T_{13}$',...
   '$T_{12}$-TH','$T_{11}$','$T_{10}$','$T_{9}$','$T_{8}$','$T_{7}$',...
   '$T_{6}$','$T_{5}$-TC','$T_{4}$','$T_{3}$','$T_{2}$','$T_{1}$-FC',...
   '$T_{h,o}$','$T_{c,o}$','$T_{ad,i}$','$T_{ad,o}$'},...
'Location','NorthEastOutside','interpreter','latex');
set(l1,'FontSize',16);
set(gca,'FontSize',16);
print('-depsc', '-loose','Storage_temperature_vertical_Last.eps');

figure();                                                    %plot P_evap
plot(cycle_time,last_cycle(:,31)-2,'g','Linewidth',1);    hold('on');
plot(cycle_time,Psat*1e3,'r--','Linewidth',1);    hold('on');clear
plot([cycle_time(half_cycle,1),cycle_time(half_cycle,1)]...
    ,[15,85],'--k','LineWidth',1);
grid('on');
xlabel('Time [min]','FontSize',16,'interpreter','latex');
ylabel('Pressure [mbar]','FontSize',16,'interpreter','latex');
xlim([0,ceil(cycle_time(end))])
set(gca, 'XTick', 0:12:cycle_time(end));
ylim([15,85])
set(gca, 'YTick', 15:5:85);
l = legend(gca, 'string', {'$P_{evap/cond}$','$P_{saturation}$'},...
    'Location','NorthEastOutside','interpreter','latex');
set(l,'FontSize',16);
set(gca,'FontSize',16);
print('-depsc', '-loose','P_evap_Last.eps');


figure();
plot(sensor_pos,Ttank_start_lc,'bs-','Linewidth',2);hold('on');
plot(sensor_pos,Ttank_end_lc,'ro-','Linewidth',2);hold('on');
grid('on');
xlabel('Height [m]','FontSize',12,'interpreter','latex');
ylabel('Temperature [$^{\circ}$C]','FontSize',12,'interpreter','latex');
```

```
xlim([0,1.60])
set(gca, 'XTick', 0:z:H);
ylim([25,75])
set(gca, 'YTick', 25:5:75);
l1 = legend(gca,'string',{'Start','End'},...
    'Location','NorthEastOutside','interpreter','latex');
set(l1,'FontSize',12);
print('-depsc', '-loose','Tank_temp_profile_Last.eps');

movefile('*_Last.eps',plots_path);
```

A.8 Error estimation

Error estimation: The heat transferred to an incompressible flow within one measurement timestep Δt seconds flowing with mass flow rate $\dot{m}$, specific heat capacity C_p and undergoing temperature change ΔT can be written as [55] :

$$Q = \dot{m} \cdot C_p \cdot \Delta T \cdot \Delta t \tag{A.1}$$

The COP_{cool} and COP_{heat} of the adsorption heat pump cycle is given by Eq. 2.9. As seen from these equations, the COPs are dependent on Q_h, Q_c, Q_{ev}, Q_{cond}, ΔQ_{tank}. These different energy terms are determined by the temperature and the flow rate measured by the relevant sensors. Naturally the accuracy of these sensors affects the accuracy of calculation of the energy terms and there by affects the accuracy with which the COPs can be estimated. Consequently a detailed investigation of the propagation of uncertainty (systematic errors) to the calculated COP values is necessary. Using the rules of propagation of uncertainty, the uncertainly δCOP_{cool} can be calculated as [44],[1]:

$$\delta COP_{cool} = |COP_{cool}| \cdot \sqrt{(\frac{\delta Q_{ev}}{Q_{ev}})^2 + (\frac{\delta Q_h}{Q_h})^2 + (\frac{\delta \Delta Q_{tank}}{\Delta Q_{tank}})^2} \tag{A.2}$$

Moreover, the uncertainty in the calculation of Q_{ev} in Eq. A.2 can be written as :

$$\delta Q_{ev} = \sqrt{(\delta Q_{ev_{start}})^2 + \cdots (\delta Q_{ev_i})^2 \cdots + (\delta Q_{ev_{halfcycle}})^2} \tag{A.3}$$

Each term inside the square root is the square of error in the calculation of the energy absorbed by the evaporator per measurement timestep. δQ_{ev} is calculated from the measurement uncertainties of the flow sensor ($\delta \dot{m}_{ev}$), the inlet temperature sensor ($\delta T_{ev,i}$) and the outlet temperature sensor ($\delta T_{ev,o}$) using :

$$\delta Q_{ev_i} = |Q_{ev}| \cdot \sqrt{(\frac{\delta \dot{m}_{ev}}{\dot{m}_{ev}})^2 + (\frac{\delta T_{ev,i}}{\Delta T_{ev}})^2 + (\frac{\delta T_{ev,o}}{\Delta T_{ev}})^2} \tag{A.4}$$

The uncertainties of the sensors used in the Eq. A.4 have been documented in appendix A.1. Similar procedure can be used for the estimation of δQ_h and $\delta \Delta Q_{tank}$. The propagation of uncertainties in the flow and the temperature measurements to the calculated energy terms is depicted in Fig. A.23.

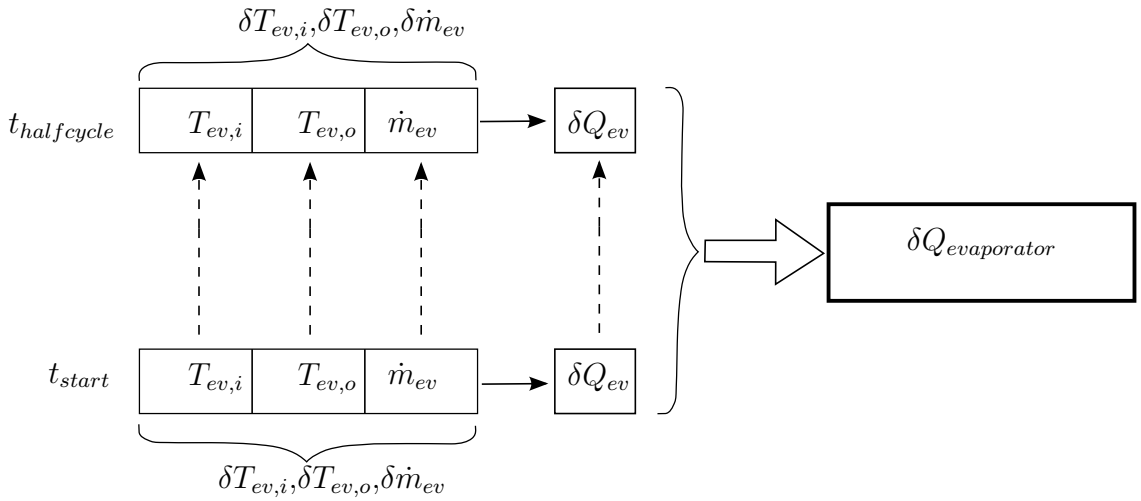

Figure A.23: Propagation of error in the calculation of Q_{ev}

Time used for the calculation of Q_{ev} corresponds to the half cycle time as Q_{ev} is absorbed only during the adsorption half cycle. On the contrary, for the calculation of Q_{cond}, the measurement timesteps during the desorption half cycle were considered.

This procedure was used to calculate the propagated uncertainty for all four experiments. The summary of this analysis is tabulated in Tab. A.3.

		Uncertainties (%)	
		COP_{heat}	COP_{cool}
Without internal heat recovery		±2.63	±2.33
With internal heat recovery (stratisorp)	Standard	±3.41	±4.43
	Variable switching	±2.95	±3.19
	Int. heating/cooling	±2.93	±3.73

Table A.3: Uncertainties in the calculation of COPs for different experiments

A.9 Entropy change rate

Fig. A.24 and Fig. A.25 shown below depict the rate of change of entropy of the relevant zones of the tank i.e. zones where rings are located and the zones where the supply and return flow of the heating and the cooling module is connected. These figures compare the experiments discussed in the section 4.4 on the basis of rate of change of entropy of the tank zones.

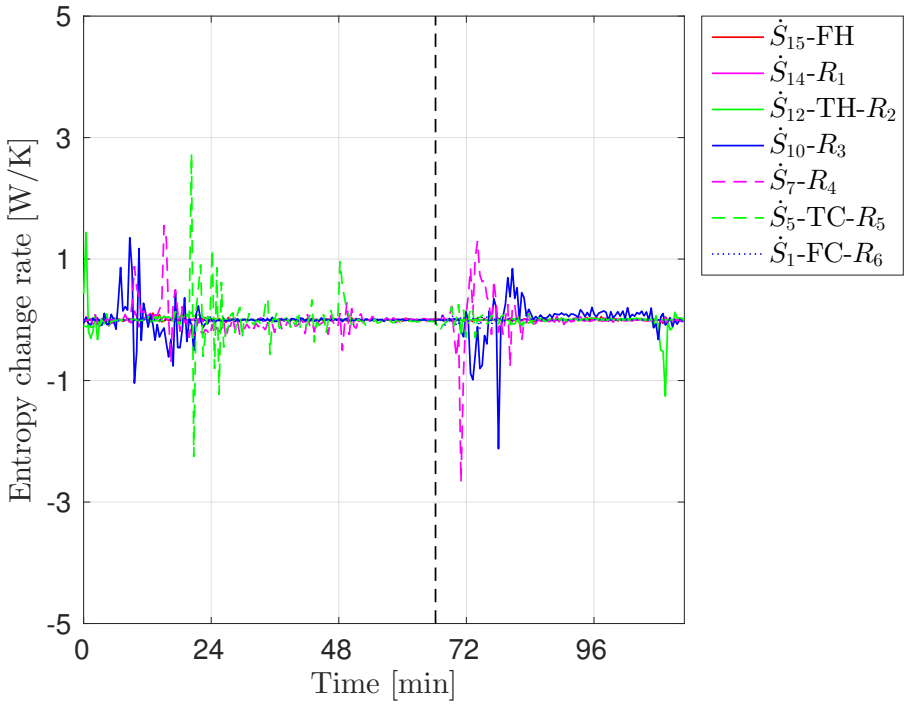

(a) Entropy change rate of the storage for the standard stratisorp cycle ($\dot{V}_{ad}$ = 1000 lph)

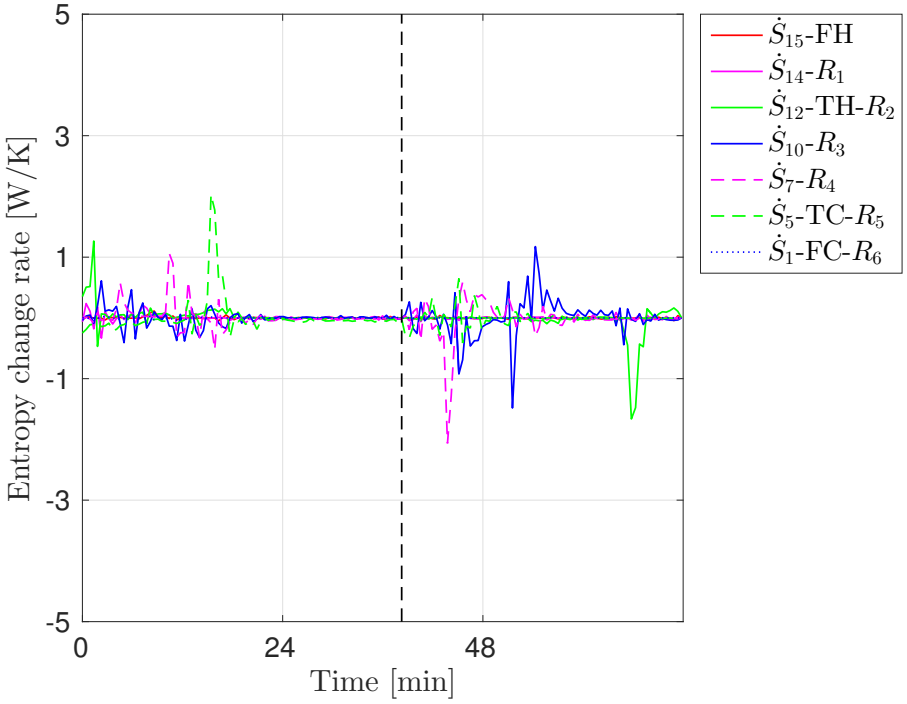

(b) Entropy change rate of the storage for the stratisorp cycle with variable switching criteria ($\dot{V}_{ad}$ = 1000 lph)

Figure A.24: Effect of variable switching on the entropy change rate in the tank

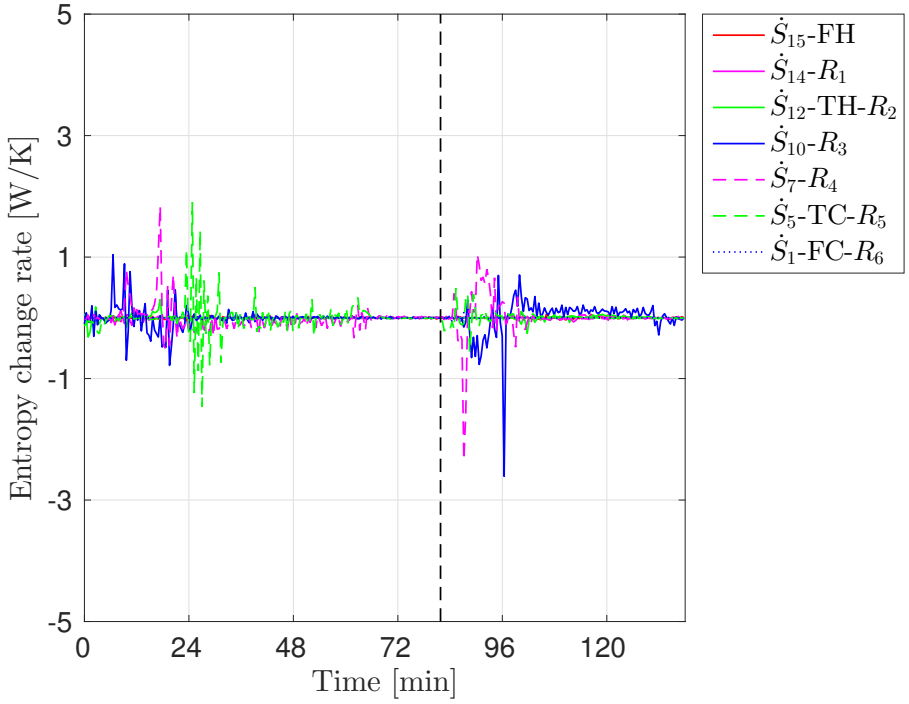

(a) Entropy change rate of the storage for the standard stratisorp cycle ($\dot{V}_{ad}$ = 800 lph)

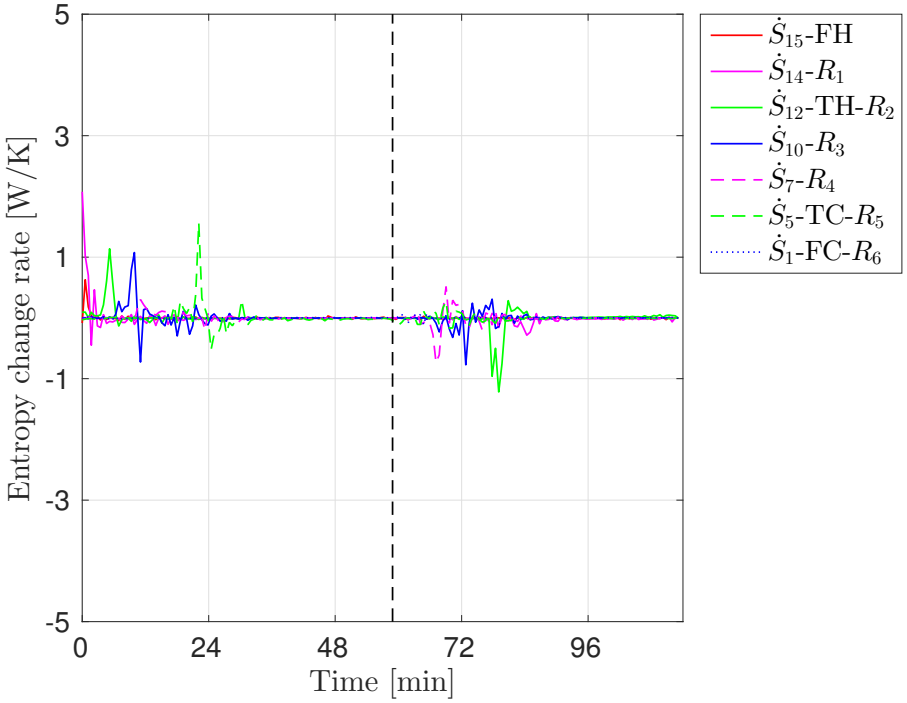

(b) Entropy change rate of the storage for the stratisorp cycle with intermittent heating and cooling ($\dot{V}_{ad}$ = 800 lph)

Figure A.25: Effect of intermittent heating and cooling on the entropy change rate in the tank

List of Figures

List of Tables

Bibliography

[1] *A summary of error propagation*, Lab handouts by Harvard University Physical Sciences 2 course. 2007.

[2] *Solar Domestic Water Heating Component Test and Analysis Protocol, Document TM-1*, December 2006.

[3] *Residential energy consumption survey (recs)*, Tech. report, U.S. Energy Information Administration, 2009.

[4] *Energie in Deutschland - Trends und Hintergründe zur Energieversorgung*, Tech. report, Bundesministerium für Wirtschaft und Technologie (BMWi), 2013.

[5] N. Ben Amar, L.M. Sun, and F. Meunier, *Numerical analysis of adsorptive temperature wave regenerative heat pump*, Applied Thermal Engineering **16** (1996), no. 5, pp. 405 – 418, Applications of Adsorption in Energy Transfer and Storage Symposium.

[6] Bradley Atcheson, Ivo Ihrke, Wolfgang Heidrich, Art Tevs, Derek Bradley, Marcus Magnor, and Hans-Peter Seidel, *Time-resolved 3d capture of non-stationary gas flows*, ACM Transactions on Graphics (2008).

[7] W.P. Bahnfleth and A. Musser, *Parametric study of charging inlet diffuser performance in stratified chilled water storage tanks with radial diffusers: Part 1–model development and validation*, HVAC&R Research **7** (2001), no. 1, pp. 31 – 50.

[8] A. Berg, *Numerical and experimental study of the fluid flow in porous medium in charging process of stratified thermal storage tank*, Master's thesis, Karlsruhe Institute of Technology, 2013.

[9] Sliwinski B.J., Mech A.R., and Shih T.S., *Stratification in thermal storage during charging*, 6th International Heat Transfer Conference, Volume 4, vol. 4, 1978, pp. 149–154.

[10] N.M. Brown and F.C. Lai, *Enhanced thermal stratification in a liquid storage tank with a porous manifold*, Solar Energy **85** (2011), no. 7, pp. 1409 – 1417.

[11] A. Cabelli, *Storage tanks—a numerical experiment*, Solar Energy **19** (1977), no. 1, pp. 45 – 54.

[12] G. Cacciola and G. Restuccia, *Progress on adsorption heat pumps*, Heat Recovery Systems and CHP **14** (1994), no. 4, pp. 409 – 420.

[13] L. Cai, W.E. Stewart Jr., and C.W. Sohn, *Turbulent buoyant flows into a two dimensional storage tank*, International Journal of Heat and Mass Transfer **36** (1993), no. 17, pp. 4247 – 4256.

[14] Biplab Choudhury, Bidyut Baran Saha, Pradip K. Chatterjee, and Jyoti Prakas Sarkar, *An overview of developments in adsorption refrigeration systems towards a sustainable way of cooling*, Applied Energy **104** (2013), pp. 554 – 567.

[15] Alfred Clark, *The theory of adsorption and catalysis*, Academic Press, 1970.

[16] R.E. Critoph, *Forced convection adsorption cycles*, Applied Thermal Engineering **18** (1998), no. 9–10, pp. 799 – 807.

[17] Cynthia A. Cruickshank, *Evaluation of a stratified multi-tank thermal storage for solar heating application*, Ph.D. thesis, Queen's university, Kingston, Ontario, Canada, 2009.

[18] Hasan Demir, Moghtada Mobedi, and Semra Ülkü, *A review on adsorption heat pump: Problems and solutions*, Renewable and Sustainable Energy Reviews **12** (2008), no. 9, pp. 2381 – 2403.

[19] N. Denecke, *Experimentelle Untersuchungen zur Emulation eines KWKK-Systems mit Schichtwärmespeicher*, Karlsruhe Institute of Technology, 2013, Bachelor Thesis.

[20] I. Dinçer and M. Rosen, *Thermal energy storage : Systems and applications*, John Wiley and Sons, LTD, 2002.

[21] C.E. Dorgan and J.S. Elleson, *Design guide for cool thermal storage*, ASHRAE (1994).

[22] N. Douss and F. Meunier, *Experimental study of cascading adsorption cycles*, Chemical Engineering Science **44** (1989), no. 2, pp. 225 – 235.

[23] F. Feuerstein, *Experimentelle Untersuchung von thermischen Schichtspeichern mittels optischer Strömungsvisulisierungsverfahren, Background Oriented Schlieren (BOS)*, Karlsruhe Institute of Technology, 2013, Diploma Thesis.

[24] E. Goldhahn and J. Seume, *The background oriented schlieren technique: sensitivity, accuracy, resolution and application to a three-dimensional density field*, Experiments in Fluids **43** (2007), no. 2-3, pp. 241 – 249.

[25] Erik Goldhahn, Olga Alhaj, Florian Herbst, and Jörg Seume, *Quantitavie Measurements of Three-Dimensional Density Fields Using the Background Oriented Schlieren Technique*, Springer, 2009, pp. 135 - 144.

[26] K.L. Guo and S.T. Wu, *Numerical study of flow and temperature stratification in a liquid storage tank*, Journal of Solar Energy Engineering **107** (1985), pp. 15 – 20.

[27] Michel Y. Haller, Cynthia A. Cruickshank, Wolfgang Streicher, Stephen J. Harrison, Elsa Andersen, and Simon Furbo, *Methods to determine stratification efficiency of thermal energy storage processes – review and theoretical comparison*, Solar Energy **83** (2009), no. 10, pp. 1847 – 1860.

[28] Michel Y. Haller, Eshagh Yazdanshenas, Elsa Andersen, Chris Bales, Wolfgang Streicher, and Simon Furbo, *A method to determine stratification efficiency of thermal energy storage processes independently from storage heat losses*, Solar Energy **84** (2010), no. 6, pp. 997 – 1007.

[29] M. Hampel, *Rechnerunterstützte Entwicklung von Warmwasser-Wärmespeichern für Solaranlagen*, Ph.D. thesis, University of Stuttgart, 2008.

[30] Michael J. Hargather and Gary S. Settles, *A comparison of three quantitative schlieren techniques*, Optics and Lasers in Engineering **50** (2012), no. 1, pp. 8 – 17, Advances in Flow Visualization.

[31] A.H. Harvey, J.S. Gallagher, and J.M.H. Levelt Sengers, *Revised Formulation for the Refractive Index of Water and Steam as a Function of Wavelength, Temperature and Density*, Physical and Chemical Reference Data **27** (1998), no. 4, pp. 761 – 774.

[32] K.O. Homan and S.L. Soo, *Model of the transient stratified flow into a chilled-water storage tank*, International Journal of Heat and Mass Transfer **40** (1997), no. 18, pp. 4367 – 4377.

[33] Klaus Huber, Elmar Bollin, Eva Scheck, Dainel Jödicke, Edo Wiemken, Jakub Wewior, Ursula Eicker, Dirk Pietruschka, Antoine Dalibard, Rolf Meißner, and Christiane Kettner, *Operation analysis and energy evaluation of a solar-thermal system assisting the air conditioning of an office/administration building*, Tech. report, 2010, Renewable Energies Knowledge – transfer network, Kassel 2010.

[34] R. Huhn, *Beitrag zur thermodynamischen Analyse und Bewertung von Wasserwärmespeichern in Energieumwandelungsketten*, Ph.D. thesis, Thechnische Universität Dresden, Germany, 2007.

[35] M.A. Karim, *Experimental investigation of a stratified chilled-water thermal storage system*, Applied Thermal Engineering **31** (2011), no. 11–12, pp. 1853 – 1860.

[36] E.M. Kleinbach, W.A. Beckman, and S.A. Klein, *Performance study of one-dimensional models for stratified thermal storage tanks*, Solar Energy **50** (1993), no. 2, pp. 155 – 166.

[37] Zalman Lavan and James Thompson, *Experimental study of thermally stratified hot water storage tanks*, Solar Energy **19** (1977), no. 5, pp. 519 – 524.

[38] F. Leopold, *The application of the colored background oriented schlieren technique (cbos) to free-flight and in-flight measurements*, 22nd International Congress on Instrumentation in Aerospace Simulation Facilities (ICIASF 2007), 2007, pp. 1–10.

[39] M.F. Lightstone, G.D. Raithby, and K.G.T. Hollands, *Numerical simulation of the charging of liquid storage tanks:comparion with experiment*, Journal of Solar Energy Engineering **111** (1989), pp. 225–231.

[40] W. Merzkirch, *Flow visualisation*, Academic Press, Inc., 1987.

[41] F Meunier, S.C Kaushik, P Neveu, and F Poyelle, *A comparative thermodynamic study of sorption systems: second law analysis*, International Journal of Refrigeration **19** (1996), no. 6, pp. 414 – 421.

[42] F. Meunier, F. Poyelle, and M.D. LeVan, *Entropic analysis of regenerative adsorptive refrigeration cycles*, Fundamentals of Adsorption **356** (1996), pp. 627 – 634.

[43] Y. Mo and O. Miyatake, *Numerical analysis of the transient turbulent flow field in a ththermal stratified thermal storage tank*, Numerical Heat Transfer **Part-A 30** (1996), pp. 649 – 667.

[44] R.J. Moffat, *Contribution to the theory of single-sample uncertainty analysis*, ASME Transactions **104** (1982), pp. 250 – 257.

[45] J.E.B. Nelson, A.R. Balakrishnan, and S. Srinivasa Murthy, *Experiments on stratified chilled-water tanks: Expériences menées avec des reservoirs d'accumulation d'eau glacée à stratification*, International Journal of Refrigeration **22** (1999), no. 3, pp. 216 – 234.

[46] Sören Paulussen, *Adsorption apparatus comprising a heat recovery system*, Patent no.: US 2011/0167842 A1, 2011.

[47] F.A. Peuser, K-H. Remmers, and M. Schnauss, *Solar thermal systems, successful planning and construction*, James & James, London, 2002.

[48] M. Pons, D. Laurent, and F. Meunier, *Experimental temperature fronts for adsorptive heat pump applications*, Applied Thermal Engineering **16** (1996), no. 5, pp. 395 – 404, Applications of Adsorption in Energy Transfer and Storage Symposium.

[49] H. Richard and M. Raffel, *Principle and application of the background oriented schlieren (BOS) method*, Measurement Science and Technology **12** (2001), pp. 1576 – 1585.

[50] Douglas M. Ruthven, *Principles of adsorption and adsorption processes*, John Wiley and Sons, 1984.

[51] Ferdinand P. Schmidt, Gerrit Füldner, Lena Schnabel, and Hans-Martin Henning, *Novel cycle concept for adsorption chiller with advanced heat recovery utilising a stratified storage*, OTTI solar air-conditioning conference, 2007, pp. 618 – 623.

[52] Valentin Schwamberger, *Thermodynamische und numerische Untersuchung eines neuartigen Sorptionszyklus zur Anwendung in Adsorptionswärmepumpen und -kältemaschinen*, Ph.D. thesis, Karlsruhe Institute of Technology (KIT), 2016.

[53] Valentin Schwamberger, Chirag Joshi, Hadi Taheri, and Ferdinand P. Schmidt, *Stratisorp: Neuartiges Schichtspeichersystem zur Effizienzsteigerung von Adsorptionswärmepumpen und -kältemaschinen*, Tech. report, Karlsruhe Institut für Technologie (KIT), 2010, Forschungsbericht BWPlus.

[54] Sam V. Shelton, William J. Wepfer, and Daniel J. Miles, *Square wave analysis of the solid-vapor adsorption heat pump*, Heat Recovery Systems and CHP **9** (1989), no. 3, pp. 233 – 247.

[55] P. Stephan, K.Schaber, K. Stephan, and F.Mayinger, *Thermodynamik, Band 1 : Einstoffsysteme*, 17 ed., Springer, 2006.

[56] S Szarzynski, Y Feng, and M Pons, *Study of different internal vapour transports for adsorption cycles with heat regeneration*, International Journal of Refrigeration **20** (1997), no. 6, pp. 390 – 401.

[57] Hadi Taheri, *Numerical investigation of stratified thermal storage tank applied in adsorption heat pump cycle*, Ph.D. thesis, Karlsruhe Institute of Technology (KIT), 2014.

[58] L. Venkatakrishnan and G. E. A. Meier, *Density measurements using the background oriented schlieren technique*, Experiments in Fluids **37** (2004), pp. 237 – 247.

[59] P.P. Votsis, S.A. Tasson, D.R. Wilson, and C.J. Marquand, *Experimental and theoretical investigation of mixed and stratified hot water storage tanks*, Journal of Mechanical Engineering Science **202** (1988), pp. 187 – 193.

[60] R.Z Wang, *Performance improvement of adsorption cooling by heat and mass recovery operation*, International Journal of Refrigeration **24** (2001), no. 7, pp. 602 – 611.

[61] M.W. Wildin and C.R. Truman, *Performance of stratified vertical cylindrical thermal storage tanks part 1: Scale model tank*, ASHRAE Transactions 95 (1989), pp. 1086 – 1095.

[62] W.P.Bahnfleth and A. Musser, *Evolution of temperature distributions in a full-scale stratified chilled-water storage tank with radial diffusers*, ASHRAE Transactions **104** (1998), no. 1, pp. 1 – 13.

[63] C.K. Yee and F.C. Lai, *Effects of a porous manifold on thermal stratification in a liquid storage tank*, Solar Energy **71** (2001), no. 4, pp. 241 – 254.

[64] J. Yoo, M. W. Wildin, and C. R. Truman, *Initial formation of a thermocline in stratified thermal storage tanks*, ASHRAE Transactions **92** (1986), no. 2A, pp. 280 – 292.

[65] Yousef H. Zurigat, Pedro R. Liche, and Afshin J. Ghajar, *Influence of inlet geometry on mixing in thermocline thermal energy storage*, International Journal of Heat and Mass Transfer **34** (1991), no. 1, pp. 115 – 125.

[66] Semra Ülkü, *Adsorption heat pumps*, Journal of Heat Recovery Systems **6** (1986), no. 4, pp. 277 – 284.

Selbstständigkeitserklärung

Hiermit erkläre ich, dass ich die vorliegende Arbeit selbständig angefertigt habe und keine anderen als die angegebenenen Quellen benutzt sowie die wörtlich und inhaltlich übergenommenen Stellen als solche kenntlich gemacht und die Satzung der Universität Karlsruhe (TH) zur Sicherung guter wissenschaftlicher Praxis in der jeweils gültigen Fassung beachtet habe.

Oktober 2015 Chirag Joshi